DEPARTMENT OF
CONSERVATION AND RESTORATION

AUTHENTICATION OF AMADEO DE SOUZA-CARDOSO PAINTINGS AND DRAWINGS WITH DEEP LEARNING

AILIN CHEN
MSc in Colour in Informatics and Media Technology

DOCTORATE IN CONSERVATION AND RESTORATION OF CULTURAL HERITAGE

NOVA University Lisbon
November, 2022

DEPARTMENT OF
CONSERVATION AND RESTORATION

AUTHENTICATION OF AMADEO DE SOUZA-CARDOSO PAINTINGS AND DRAWINGS WITH DEEP LEARNING

AILIN CHEN

MSc in Colour in Informatics and Media Technology

Adviser: Rui Manuel Feliciano de Jesus
Associate Professor, Instituto Superior de Engenharia de Lisboa (ISEL), IPL

Co-adviser: Márcia Gomes Vilarigues
Assistant Professor, Faculdade de Ciências e Tecnologia, Universidade Nova de Lisboa

Examination Committee

Chair: Nuno Manuel Robalo Correia
Full Professor, Faculdade de Ciências e Tecnologia, Universidade Nova de Lisboa

Rapporteurs: Pedro Miguel Torres Mendes Jorge
Coordinator Professor, Instituto Superior de Engenharia de Lisboa (ISEL), IPL

João Manuel Maciel Linhares
Assistant Professor, Escola de Ciências da Universidade do Minho

Adviser: Rui Manuel Feliciano de Jesus
Associate Professor, Instituto Superior de Engenharia de Lisboa (ISEL), IPL

Members: Nuno Manuel Robalo Correia
Full Professor, Faculdade de Ciências e Tecnologia, Universidade Nova de Lisboa

Vanessa Otero Matias
Assistant Researcher, Faculdade de Ciências e Tecnologia, Universidade Nova de Lisboa

Rui Filipe Xavier
Head of Preventive Conservation & Restoration, Fundação Calouste Gulbenkian

DOCTORATE IN CONSERVATION AND RESTORATION OF CULTURAL HERITAGE

NOVA University Lisbon
November, 2022

Authentication of Amadeo de Souza-Cardoso Paintings and Drawings With Deep Learning

This document was created with the (pdf/Xe/Lua)LaTeX processor and the NOVAthesis template (v6.9.14) [160].

To my family.

Acknowledgements

First of all, I would like to express my deepest gratitude and respect to my supervisors, Prof. Rui Jesus and Prof. Márcia Vilarigues. Without their invaluable advice, guidance and encouragement this research would not have been possible.

A special acknowledgement goes to all the lecturers from FCT, especially from DCR, including Prof. Maria João Melo and Prof. Ludwig Krippahl, to name a few, who assisted me during my PhD study and made possible this research.

Special thanks to all my friends that supported my study and research. Their invaluable friendship, encouragement and advice helped me to make the research successful.

Last, but not least, my love and gratitude go to my family: my parents Shijun Chen and Xuding Tong, my sister Yanni Chen and my brother Xiaoyong Chen. Thank you all for believing in me, for your sacrifice, support and love in every step of my life.

"Learning without thinking is useless, thinking without learning is perilous." (Confucius)

Abstract

Art forgery has a long-standing history that can be traced back to the Roman period and has become more rampant as the art market continues prospering. Reports disclosed that uncountable artworks circulating on the art market could be fake. Even some principal art museums and galleries could be exhibiting a good percentage of fake artworks. It is therefore substantially important to conserve cultural heritage, safeguard the interest of both the art market and the artists, as well as the integrity of artists' legacies. As a result, art authentication has been one of the most researched and well-documented fields due to the ever-growing commercial art market in the past decades. Over the past years, the employment of computer science in the art world has flourished as it continues to stimulate interest in both the art world and the artificial intelligence arena. In particular, the implementation of Artificial Intelligence, namely Deep Learning algorithms and Neural Networks, has proved to be of significance for specialised image analysis. This research encompassed multidisciplinary studies on chemistry, physics, art and computer science. More specifically, the work presents a solution to the problem of authentication of heritage artwork by Amadeo de Souza-Cardoso, namely paintings, through the use of artificial intelligence algorithms. First, an authenticity estimation is obtained based on processing of images through a deep learning model that analyses the brushstroke features of a painting. Iterative, multi-scale analysis of the images is used to cover the entire painting and produce an overall indication of authenticity. Second, a mixed input, deep learning model is proposed to analyse pigments in a painting. This solves the image colour segmentation and pigment classification problem using hyperspectral imagery. The result is used to provide an indication of authenticity based on pigment classification and correlation with chemical data obtained via XRF analysis. Further algorithms developed include a deep learning model that tackles the pigment unmixing problem based on hyperspectral data. Another algorithm is a deep learning model that estimates hyperspectral images from sRGB images. Based on the established algorithms and results obtained, two applications were developed. First, an Augmented Reality mobile application specifically for the visualisation of pigments in the artworks by Amadeo. The mobile application targets the general public, i.e., art enthusiasts, museum visitors, art lovers or art experts. And second, a desktop application with multiple purposes, such as the visualisation of pigments and hyperspectral data. This application is designed for art specialists, i.e., conservators and restorers. Due to the special circumstances of the pandemic, trials on the usage of these applications were only performed within the Department of Conservation and Restoration at NOVA University Lisbon, where both applications received positive feedback.

Keywords: Cultural Heritage, Authentication, Artificial Intelligence, Deep Learning, Hyperspectral Analysis, Visualisation, Amadeo de Souza-Cardoso

Resumo

A falsificação de arte tem uma história de longa data que remonta ao período romano e tornou-se mais desenfreada à medida que o mercado de arte continua a prosperar. Relatórios revelaram que inúmeras obras de arte que circulam no mercado de arte podem ser falsas. Mesmo alguns dos principais museus e galerias de arte poderiam estar exibindo uma boa porcentagem de obras de arte falsas. Por conseguinte, é extremamente importante conservar o património cultural, salvaguardar os interesses do mercado da arte e dos artistas, bem como a integridade dos legados dos artistas. Como resultado, a autenticação de arte tem sido um dos campos mais pesquisados e bem documentados devido ao crescente mercado de arte comercial nas últimas décadas.Nos últimos anos, o emprego da ciência da computação no mundo da arte floresceu à medida que continua a estimular o interesse no mundo da arte e na arena da inteligência artificial. Em particular, a implementação da Inteligência Artificial, nomeadamente algoritmos de aprendizagem profunda (ou Deep Learning) e Redes Neuronais, tem-se revelado importante para a análise especializada de imagens.Esta investigação abrangeu estudos multidisciplinares em química, física, arte e informática. Mais especificamente, o trabalho apresenta uma solução para o problema da autenticação de obras de arte patrimoniais de Amadeo de Souza-Cardoso, nomeadamente pinturas, através da utilização de algoritmos de inteligência artificial. Primeiro, uma estimativa de autenticidade é obtida com base no processamento de imagens através de um modelo de aprendizagem profunda que analisa as características de pincelada de uma pintura. A análise iterativa e multiescala das imagens é usada para cobrir toda a pintura e produzir uma indicação geral de autenticidade. Em segundo lugar, um modelo misto de entrada e aprendizagem profunda é proposto para analisar pigmentos em uma pintura. Isso resolve o problema de segmentação de cores de imagem e classificação de pigmentos usando imagens hiperespectrais. O resultado é usado para fornecer uma indicação de autenticidade com base na classificação do pigmento e correlação com dados químicos obtidos através da análise XRF. Outros algoritmos desenvolvidos incluem um modelo de aprendizagem profunda que aborda o problema da desmistura de pigmentos com base em dados hiperespectrais. Outro algoritmo é um modelo de aprendizagem profunda que estima imagens hiperespectrais a partir de imagens sRGB. Com base nos algoritmos

estabelecidos e nos resultados obtidos, foram desenvolvidas duas aplicações. Primeiro, uma aplicação móvel de Realidade Aumentada especificamente para a visualização de pigmentos nas obras de Amadeo. A aplicação móvel destina-se ao público em geral, ou seja, entusiastas da arte, visitantes de museus, amantes da arte ou especialistas em arte. E, em segundo lugar, uma aplicação de ambiente de trabalho com múltiplas finalidades, como a visualização de pigmentos e dados hiperespectrais. Esta aplicação é projetada para especialistas em arte, ou seja, conservadores e restauradores. Devido às circunstâncias especiais da pandemia, os ensaios sobre a utilização destas aplicações só foram realizados no âmbito do Departamento de Conservação e Restauro da Universidade NOVA de Lisboa, onde ambas as candidaturas receberam feedback positivo.

Palavras-chave: Património Cultural, Autenticação, Inteligência Artificial, Aprendizagem Profunda, Análise Hiperespectral, Visualização, Amadeo de Souza-Cardoso

Contents

List of Figures

List of Tables

Acronyms

μ-FTIR	Micro-Fourier Transform Infrared *(p. 8)*
μ-Raman	Micro-Raman Spectroscopy *(pp. 8, 18)*
μ-SPEX	Micro-spectrofluorimetry *(p. 8)*
μ-XANES	Micro-X-ray Absorption Near-Edge Spectroscopy *(p. 8)*
μEDXRF	Micro Energy Dispersive X-ray Fluorescence *(pp. 2, 8, 9, 61, 84, 99)*
2D	two-dimensional *(p. 24)*
3D	three-dimensional *(p. 10)*
Acc	Accuracy *(p. 53)*
ADDG	Art Due Diligence Group *(p. 21)*
AGI	Artificial General Intelligence *(p. 38)*
AI	Artificial Intelligence *(pp. 3, 38, 39, 46, 107)*
AiAF	Authentication in Art Foundation *(p. 21)*
ALR	Art Loss Register *(p. 1)*
ANI	Artificial Narrow Intelligence *(p. 38)*
ANN	Artificial Neural Network *(pp. 42, 44, 45)*
AR	Augmented Reality *(pp. 5, 6, 107, 108, 110, 111, 114, 122, 123, 126, 129)*
ASI	Artificial Super Intelligence *(p. 38)*
ATR-FTIR	Attenuated Total Reflectance Fourier Transform Infrared Spectroscopy *(p. 18)*
BoF	Bag of Features *(p. 25)*
CAM	Centre of Modern Art *(pp. 12, 54)*
CIELab	CIE 1976 L*a*b Colour Space *(pp. 85, 88, 101–104, 118, 152, 156)*
CNN	Convolutional Neural Network *(pp. xiv, 4, 6, 15, 16, 20, 42, 44–46, 48, 81, 125)*
CONV	Convolution *(pp. 45, 46, 48)*
CSV	Comma Separated Values *(p. 118)*

DCR	Department of Conservation and Restoration *(pp. 2–5, 13, 54, 74, 93, 102, 127)*
DL	Deep Learning *(pp. 38, 41, 44)*
DNN	Deep Neural Network *(pp. xvi, 15, 19, 20, 76, 100, 101, 106)*
ED	Euclidean Distance *(pp. 20, 104)*
EEG	Electroencephalogram *(pp. 127, 128)*
F1-S	F1-Score *(p. 53)*
FAEI	Fine Art Expert Institute *(p. 1)*
FC	Fully Connected *(pp. 45, 46)*
FCG	Calouste Gulbenkian Foundation *(p. 11)*
FCLS	Fully-Constrained Least Squares *(pp. xvi, 61, 73–75, 79–81, 83, 125)*
FFANN	Feedforward Artificial Neural Network *(pp. 42, 44, 46)*
FN	False Negatives *(pp. 41, 53)*
FORS	Fibre Optic Reflectance Spectroscopy *(pp. 155, 156)*
FP	False Positives *(pp. 41, 53)*
FTIR	Fourier Transform Infrared *(pp. 8, 9, 17)*
GAN	Generative Adversarial Network *(pp. 128, 129)*
GC-MS	Gas Chromatography-Mass Spectrometry *(pp. 9, 18)*
GIF	Graphics Interchange Format *(p. 117)*
HMM	Hidden Markov Model *(p. 14)*
HPLC-DAD	High Performance Liquid Chromatography - Diode Array Detector *(p. 8)*
HU	Hyperspectral Unmixing *(p. 19)*
IDF	Inverse Document Frequency *(p. 30)*
IFAR	International Foundation for Art Research *(p. 21)*
ILSVRC	ImageNet Large-Scale Visual Recognition Challenge *(p. 49)*
IoT	Internet of Things *(p. 107)*
IR	Infrared Radiation *(p. 2)*
IRR	Infrared Reflectography *(p. 8)*
IWPs	Ink Wash Paintings *(p. 16)*
KM	K-Means Clustering *(pp. 16, 25, 30, 39, 51, 53, 98, 173–175, 177–179)*
KM++	K-Means++ Clustering *(pp. 30, 174, 175, 177–179)*
KM||	K-Means|| Clustering *(p. 30)*
LSTM	Long Short-Term Memory Network *(pp. 42, 44)*

MaxPool	Maximum Pooling *(pp. 45, 48)*
ML	Machine Learning *(pp. 6, 38, 39, 41, 182)*
MLP	Multilayer Perceptron *(pp. 4, 42, 44, 63, 125)*
MNN	Modular Neural Network *(pp. 42, 44)*
MRAE	Mean Relative Absolute Error *(pp. 80, 93, 104)*
NIR	Near Infrared *(pp. 10, 20)*
NL	Normal Light *(p. 8)*
NN	Neural Network *(pp. 4, 41, 42, 44, 124)*
NOVA	NOVA University Lisbon *(pp. 2, 5, 102)*
POOL	Pooling *(p. 45)*
Prec	Precision *(p. 53)*
Raman	Raman Spectroscopy *(pp. 8, 9, 11, 17, 18)*
RBFNN	Radial Basis Function Neural Network *(pp. 42, 44)*
Rec	Recall *(p. 53)*
ReLU	Rectified Linear Unit *(pp. 45, 46, 48, 77)*
RFID	Radio Frequency Identification *(p. 24)*
RIS	Reflectance Imaging Spectroscopy *(p. 10)*
RLSC	Regularised Least-Squares Classifier *(pp. 25, 31, 39, 40, 53, 59)*
RMSE	Root Mean Square Error *(pp. 34, 35, 80, 86, 88, 89, 93, 94, 114, 126, 183)*
RNN	Recurrent Neural Network *(pp. 16, 42, 44)*
SAM	Spectral Angle Mapper *(pp. 20, 33–35, 61, 63, 73, 93, 94, 99, 104, 114, 126)*
SCM	Spectral Correlation Mapper *(pp. 63, 71, 114, 125)*
SEM	Scanning Electron Microscopy *(pp. 2, 17)*
SEM-EDS	Scanning Electron Microscopy and Energy Dispersive X-ray Spectrometry *(pp. 8, 17, 18)*
SERS	Surface-Enhanced Raman Spectroscopy *(p. 11)*
SIFT	Scale-Invariant Feature Transform *(pp. 16, 24, 25, 27–29, 31, 51, 173, 178, 179)*
SNN	Simulated Neural Network *(p. 42)*
SNR	Signal to Noise Ratio *(pp. 65, 78)*
SOP	Synthetic Organic Pigments *(p. 18)*
sRGB	Standard Red, Green and Blue *(pp. xv–xvii, 4, 6, 9, 34, 35, 49, 64, 68, 72, 75, 76, 78–81, 93, 96, 97, 100–106, 114, 118, 126, 152, 153, 160, 164)*
SVC	Support Vector Clustering *(p. 39)*
SVM	Support Vector Machine *(pp. 14–16, 39, 61, 183)*
SWIR	Shortwave Infrared *(p. 20)*

TF	Term Frequency *(p. 30)*
TF-IDF	Term Frequency-Inverse Document Frequency *(pp. 25, 30, 53)*
TLU	Threshold Logic Unit *(p. 42)*
TN	True Negatives *(pp. 41, 53)*
TP	True Positives *(pp. 41, 53)*
UNESCO	United Nations Educational, Scientific and Cultural Organization *(p. 7)*
UV	Ultra Violet *(pp. 8, 18)*
VIS-NIR	Visible-Near Infrared *(p. 10)*
VR	Virtual Reality *(pp. 107, 108)*
WAP	Wireless Application Protocol *(p. 24)*
XR	X-Radiography *(pp. 8, 9, 18)*
XRD-CT	X-ray Diffraction Computed Tomography *(pp. 8, 11)*
XRF	X-ray Fluorescence *(pp. 2, 9, 17, 18, 33, 83–90, 94, 126)*
XYZ	CIE 1931 XYZ Colour Space *(p. 118)*

1

Introduction

1.1 Background and Motivation

The world is developing rapidly and so is humankind who no longer seeks fulfilment of the most basic requirements for survival, but also seeks to improve its living standards through the acquisition of objects with spiritual and cultural value. Art collectors in particular play a significant philanthropist role, given the fact that supporting arts and thriving artists, as well as preserving historical legacy are on many occasions some of the important reasons behind their art collection [247]. This has driven the increase in the demand for valuable pieces of artwork which unfortunately has become the target of art forgers for their financial gain.

Art forgery can be traced back for at least two thousand years and as early as to the Roman period, when Roman sculptors reproduced Greek sculptures. Even the world-renowned sculptor Michelangelo started his career by forging and selling fake antiquity [46]. Art forgers not only perturbed the art market, some even made a name for their own artworks. Examples of these include the infamous Elmyr de Hory, Han van Meegeren, Wolfgang Beltracchi, Thomas Patrick Keating and John Myatt, who forged some of the world's most famous artists including Johannes Vermeer, Pablo Picasso, Max Ernst, van Gogh, Edgar Degas and Henri Matisse among others [120, 243, 246, 263]. It is estimated that about 20% of artworks in principal British museums were possibly fake [240]. A report in 2014 by Fine Art Expert Institute (FAEI) from Switzerland noted that at least half of the artworks circulating in the art market were fake [34, 190]. Another report recorded that the exhibitions with the largest number of faked and forged artworks occurred in 2018 [34]. A typical example is that more than half of the paintings in a French museum were found to be fake [95].

The Art Loss Register (ALR), established in 1991, is the primary private governance body based in London where the most extensive database of missing art and artefacts in the world is stored. Although it is challenged by the Art Recovery Group since 2014 due to multiple reasons, the ALR still holds a high record of 500,000 items that can be reviewed without much effort, unlike other databases such as National Police, where only a few thousand items are recorded [224]. The authentication of the art objects, especially the newly-emerged items without a clear track record, is quintessential prior to their entrance to the art market. This is required to avoid unnecessary financial loss by both the museums and art collectors. Museums, in particular, rely on both analytical techniques and connoisseurship. Even though connoisseurship has been widely used to resolve the authenticity problem of many artworks due to the experts' enormous experience, it is often disputed as being one of the most effective methods and often resulted in further feuds and controversies among art institutions. For example, regardless of the inclusion of a painting by Pierre-Auguste Renoir in the catalogue of Bernheim-Jeune Galerie, one of the oldest galleries in Paris, as well as several art experts' approval, Wildenstein Institute, the French art institute that publishes scholarly inventories and catalogues raisonnés, disapproved its authenticity of the painting, providing their own connoisseurship [9]. A similar event occurred to the Monet painting *Bords de la Seine à Argenteuil*, where even though extensive evidence was presented to Wildenstein Institute for its authenticity, the institute dismissed it as a real Monet [125]. Subsequently, scientific investigation tends to be more reliable. Such analysis includes both invasive approaches and non-destructive techniques. Exemplary invasive methods where a small sample is required for analysis, are Scanning Electron Microscopy (SEM) and Micro Energy Dispersive X-ray Fluorescence (μEDXRF) spectroscopy, although the latter is on many occasions considered a non-invasive technique since the sampling is at micro level [35, 36, 127, 193, 253]. Examples of non-invasive techniques include X-ray Fluorescence (XRF) spectroscopy, Infrared Radiation (IR) spectroscopy, Raman Spectroscopy and so on. The former approach is destructive and therefore not often recommended, particularly on legacies and heritages.

Computer science has been evolving rapidly over the years, and its employment in many fields including the identification, conservation and restoration of artworks has also advanced. The application of machine learning in the research of artworks is a non-destructive approach. Machine learning is applied by Montagner from the Department of Conservation and Restoration (DCR) of NOVA University Lisbon (NOVA) on the analysis of artworks by the late Portuguese artist Amadeo de Souza-Cardoso for the determination of the authenticity of his paintings. In Montagner's work, both brushstroke and material analysis were considered equally significant to authenticate an artwork by Souza-Cardoso [171, 172], and both analyses are investigated via implementing a series of conventional machine learning algorithms like image processing and feature extraction techniques.

Our research is motivated by Montagner's study, and intended to enhance the original method to be applied to a broader setting. To achieve this, our study focused on exploiting the use of artificial neural networks which imitate the human brain in order to assess the effects of both approaches on the data, i.e., different artists, styles and genres. Our research evaluates the proposed authentication and its generalisation on paintings and drawings by other artists and other genres and is deemed to contribute to the development of a more generic method for the non-destructive evaluation and identification of artwork.

Theoretically, further data on Souza-Cardoso's drawings as well as other artists would be obtained so that the holistic method could be generalised and evaluated potentially leading to the development of a unified software solution for the identification and authentication of a particular artist or genre. However, no further data were acquired and thus all work was performed with the available data at hand only collected by Montagner and provided by DCR.

1.2 Research Questions

Based on the problem and the challenges associated with the analysis of cultural heritage artwork discussed, this thesis aims to improve and provide a new set of algorithms based on Artificial Intelligence (AI) techniques. With this in mind, the thesis answers the following questions through the various chapters:

- **How can deep learning be used for the identification and ultimately the authentication of artwork through the analysis of brushstroke?** The brushstroke is the signature of an artist that typically changes through his/her career as the artist evolves and experiments with new materials and techniques. This work evaluates the use of deep learning models to determine the feasibility to determine the artist attribution and therefore contribute to the authentication prediction.

- **Can machine learning be used to identify pure and/or mixed colour pigments in artwork?** Artists use a finite number of pigments in a palette when creating paintings. These pigments can be used on their own as pure colours or mixed with other pigments to create an infinite variety of colours. Our research explores the use of machine learning techniques to identify potential areas of a painting as pure or mixed colours from a known set of pigments.

- **How can the knowledge and techniques developed be used for the dissemination of cultural heritage?** Although the ultimate goal of the research is to develop algorithms to tackle the challenges associated with artwork analysis, it is important to ensure that the knowledge and methodologies developed have a lasting impact on the art world and society. Our work also explores the potential practical applications of the methodologies developed to generate tools that can contribute to the dissemination of cultural heritage information for the benefit of society.

1.3 Contribution

The work described in this thesis covers the review of previous efforts to authenticate artwork from Amadeo de Souza-Cardoso using minimal, conventional machine learning algorithms. This has led to the development of methodologies for the analysis of artwork by means of more complex and suitable deep learning models. These included the analysis of brushstroke, the artist's signature, and the analytical analysis of pigments within a painting for identification.

Brushstroke analysis is performed by the feature analysis of sRGB images of paintings through a deep learning model based on 2-dimensional CNN architecture. The network highlights features of the images analysed at different levels which are then passed through a Multilayer Perceptron (MLP) for classification. A methodology for the analysis of large, high-quality images is proposed where multiple samples of a given image are used to obtain the probability of the artwork belonging to the artist in question. The method proposed has been successfully implemented to identify artwork by Amadeo de Souza-Cardoso. The solution proposed has also been tested with different datasets to verify the generalisation capability between the identification of other artists and genres.

For the analysis of pigments, hyperspectral imaging and processing were implemented in conjunction with deep learning methods. A methodology for pure pigment prediction was achieved by combining hyperspectral metric functions and 3-dimensional CNNs. A methodology to produce artificial colour mixtures and artificial imagery for training was also successfully developed. Colour mixing prediction on the other hand was achieved by the implementation of deep Neural Network (NN)s which reconstructed pigment reflectances based on a dictionary of reference reflectances. While the reconstruction was accurate, the practicalities of the results were better served by the use of standard hyperspectral metric functions. The resulting figures are used to estimate the probability of authenticity based on pigment analysis and for the potential use of colour matching for conservation and restoration purposes.

The algorithms developed and results obtained supersede and improved previous work leading to the implementation of tools and algorithms for the use of the DCR at the NOVA University of Lisbon and by curators and art specialists involved in analysis, conservation and restoration of heritage artwork.

1.3.1 Publications

The research work included in this thesis has successfully led to the dissemination and publication of achievements in the following peer-reviewed publications:

- A. Chen, R. Jesus, M. Vilarigues, "Using Deep Learning Techniques for Authentication of Amadeo de Souza Cardoso Paintings and Drawings", In: P. Moura Oliveira et al. (Eds.) Progress in Artificial Intelligence. EPIA 2019, Springer Nature Switzerland AG, LNAI 11805, 2019, 1–12.

- A. Chen, R. Jesus, M. Vilarigues, "Authentication of Art: assessing the performance of a machine learning based authentication method", ArtsIT 2019 – 8th EAI International Conference: ArtsIT, Interactivity & Game Creation, Aalborg, Denmark, 6-8 November 2019.

- A. Chen, R. Jesus, M. Vilarigues. "Identification of Pure Painting Pigment Using Machine Learning Algorithms", In Artificial Intelligence in Music, Sound, Art and Design: 10th International Conference, EvoMUSART 2021, Held as Part of EvoStar 2021, Virtual Event, April 7–9, 2021, Proceedings. Springer-Verlag, Berlin, Heidelberg, 52–64 (Best Paper Award).

- A. Chen, R. Jesus, M. Vilarigues. "Convolutional Neural Network-Based Pure Paint Pigment Identification Using Hyperspectral Images", In ACM Multimedia Asia (MMAsia '21), December 1-3, 2021. Association for Computing Machinery, New York, NY, USA, Article 64, 1–7.

- A. Chen, R. Jesus, M. Vilarigues. "Hyperspectral Image Reconstruction of Heritage Artwork Using RGB Images and Deep Neural Networks", In Proceedings of 19th International Conference on Content-based Multimedia Indexing (CBMI2022). ACM, New York, NY, USA, 6 pages

- A. Chen, R. Jesus, M. Vilarigues. "Identification and Visualisation of Pure and Mixed Pigments in Heritage Artwork Using Machine Learning", SN Computer Science. 4, 115 (2023).

1.3.2 Software

Some of the algorithms, models developed and results generated have been deployed in the following set of desktop and mobile applications. Further information regarding these applications is included in

- Amadeo AR. An Augmented Reality (AR), colour visualisation mobile application used to highlight pigments in paintings from Amadeo de Souza-Cardoso. Further details are included in Chapter 6.

- Amadeo Image Analysis Tool. A desktop application for analysis and visualisation of Amadeo de Souza-Cardoso paintings. Further details are included in Chapter 6.

1.4 Thesis Outline

The thesis structure is organised into 8 chapters.

Chapter 2 provides an introduction to the paradigm of artwork analysis and authentication. It presents the concepts and the literature review pertinent to work in similar fields of study including a review of the original set of algorithms for brushstroke and pigment analysis previously developed at NOVA DCR. A discussion on potential improvements is included along with results obtained from the evaluation of these. Finally, a brief overview of the concepts of machine learning relevant to this work is given.

Chapter 3 focuses on the solution proposed for brushstroke analysis used for artist identification. The deep learning model used is discussed and the methodology for training and evaluation of the model is described. Classification results obtained with the model are presented and compared against previous attempts of automatic classification using Machine Learning (ML) algorithms. The chapter concludes with a discussion of the results where limitations and possible improvements are included.

Chapter 4 describes the methodology proposed for the authentication of paintings using pigment identification via deep learning implementations. A CNN model is proposed for image segmentation and classification of pure pigments. The strategy for training and testing using artificial data and its limitations are examined. This chapter also includes a discussion of the techniques used for mixed pigment identification including requirements and constraints. Results of the pigment analysis are presented and compared against previous work. Finally, a summary of results obtained in sections 3 and 4 is presented. These are used in the final estimation of the indication of authenticity of artwork being authored by Amadeo de Souza-Cardoso.

Chapter 5 presents the results obtained from the work achieved on estimating hyperspectral images from sRGB images. This is a by-product of the work completed which uses deep neural networks in combination with colour science to estimate hyperspectral data that can be used for potential study and analysis of heritage artwork.

Chapter 6 includes a description of the implementation of some of the work achieved by means of two software applications. The first application, a desktop-based tool, uses the developed algorithms to analyse and visualise hyperspectral images including pigment prediction and data visualisation. The second tool, a mobile application, showcases the results of the pure pigment prediction method using an AR application. The results of the trial of these applications are also discussed.

Chapter 7 concludes by summarising the achievements and contributions obtained. The chapter also presents a discussion of the limitations, future work and possible applications for the authentication of artwork using different media.

2

Background

2.1 Introduction

In this section, the significance of cultural heritage preservation, and artwork analysis for the purpose of conservation and restoration are discussed.

2.1.1 The Importance of Cultural Heritage

United Nations Educational, Scientific and Cultural Organization (UNESCO) described heritage as the cultural legacy that is passed on from generation to generation from the past, to the present and into the future [63] and it can be categorised into different types of heritage depending on distinguishing characteristics. Based on whether the heritage can be moved or not, it is considered as movable and immovable heritage, where the meaning is self-identifiable. Based on the fact that the heritage can be touched or not, it is grouped as tangible and intangible heritage. History in different nations would be intangible, whereas clothing would be tangible. Different resources noted heritage could be classified into two types of heritage, i.e., cultural heritage and natural heritage, or it could be classified into three types of heritage, i.e., cultural, natural and constructive, or cultural, natural and mixed type. Regardless of how it is classified, it is understandable that preserving, conserving and protecting heritage and legacies is significant in terms of maintaining the particular characteristics and "*resilient communities*", i.e, the identity of local culture [200, 264, 268].

Historical works of art, for example, paintings, are a part of cultural heritage mostly done by people who are world-renowned artists but no longer exist. Such artworks are not replaceable and replicable and have historical significance, hence are priceless, and must be conserved [18]. Historical objects have endured the hardship of the time, which resulted in the inevitable decay and erosion, and on many occasions have been adversely affected by negligence or unscrupulous damage. Subsequently, art conservation or restoration must be performed so that the status of artworks can be maintained, preserved, restored and protected from future deterioration [14, 265].

2.1.2 Artwork Analysis

A comprehensive understanding concerning the material construction and composition of the painting by an artist is substantial in the heritage conservation field [154, 184]. For the purpose of restoring, conserving and preserving historical artwork, or identifying if an artwork is fake or authentic, a series of scientific analyses must be done. The reason being that most of the techniques can reveal features that are not visible to the human naked eye. Those techniques include, for example, Raman Spectroscopy (Raman), hyperspectral imaging, high-definition imaging in Normal Light (NL), Ultra Violet (UV) induced fluorescence, digital X-Radiography (XR), Infrared Reflectography (IRR), Polarizing Microscopy and Hirox Microscopy, High Performance Liquid Chromatography - Diode Array Detector (HPLC-DAD), μEDXRF, Fourier Transform Infrared (FTIR) spectroscopy, Micro-Fourier Transform Infrared (μ-FTIR) spectroscopy, Micro-Raman Spectroscopy (μ-Raman), Micro-spectrofluorimetry (μ-SPEX), Micro-X-ray Absorption Near-Edge Spectroscopy (μ-XANES), Scanning Electron Microscopy and Energy Dispersive X-ray Spectrometry (SEM-EDS), X-ray Diffraction Computed Tomography (XRD-CT), Synchrotron [13, 171, 201].

In terms of oil paintings, which are the principal objects for analysis in our research, are usually composed of the basic components of the support, the ground and preparatory layers, the paint layer and the varnish layer [135, 180]. The support varies, ranging from historically widely-used solid wood support, to plywood or hardboard support, to fabric support, depending on the expedient factor as well as reasons for artistic expression. The ground and preparation layer also differs depending on the surface being worked on. This can be textured grounds or absorbent grounds for example. Although white ground is mostly used, it can also be coloured ground. The ground layer not only serves as a physical function of adhering the paint to the support, but also functions aesthetically based on the painters' intent. The paint layer consists of elements like pigment, binder and fillers. Historically, paint pigments could be both organic compounds that were derived from natural sources like animal and vegetable dyes, or inorganic compounds that were derived from minerals and salts often with the basis of oxide, sulphate, sulphide, carbonate etcetera [135, 188]. Although painters' range of palettes depends on the availability, expense and purposes, modern synthesised pigments produced in the late eighteenth century expanded painters' palettes in general. Concerning historical oil paintings, binders are binding media that adhere the pigments together and hold them to the previous layer. These were typically egg tempera, distemper such as glue size (a gelatinous substance), and drying oils. Later on, acrylic paints introduced around the mid-twentieth century replaced such historical practice for paintings. Fillers or extenders are additives added for economic reasons, but mainly to improve the performance of the paint [27, 86, 110, 124]. Finally, the varnish layer serves as both protection of the paint layer and the aesthetic look of the painting.

In this work, for example, the paint layer is the primary component that is being investigated. In terms of the pigment of the paint, scientific techniques like Raman, XRF, XR can be used for the analysis of pigment for various purposes; further details can be found in section 2.4.2. Concerning binders, analytical techniques like FTIR and Gas Chromatography-Mass Spectrometry (GC-MS) can be used to determine the chemical content, for example, if it is natural or synthetic, or chemical structure in order to establish any deterioration problems [98, 168, 182]. With respect to fillers, together with other elements of a paint, can also be analysed and identified, for example, with μEDXRF or FTIR, so that information such as structure and formulation of a paint can be determined [12, 218].

In our research, different types of imaging techniques were used, including the most commonly applied three-channel sRGB images with an average size of 3365×3029 pixels, and hyperspectral images with 33 channels in the range of 400nm to 720nm. Hyperspectral imaging is a technique based on spectroscopy that allows analysing images at different wavelengths, this is, it analyses a wide spectrum of light instead of just using primary colours like red, green and blue. Typically, light is projected onto an object and the reflected light is recorded using a hyperspectral camera that breaks down the light measured into multiple bands producing a hyperspectral image. This is of high importance for cultural heritage because it is a non-destructive and non-invasive technique. This means that there is no need to obtain samples of the painting for analysis. Another advantage of hyperspectral imaging is that it allows highlighting hidden features by analysing certain wavelengths for example, or for visualisation, analysis, restoration and ultimately authentication of artwork. The problem with hyperspectral imaging is that it requires direct access to the artwork, it is time-consuming and therefore expensive. A more detailed explanation concerning hyperspectral imaging analysis can be found in section 2.4.2.

As mentioned previously, skilled forgers intentionally mimicked famous artists' styles and produced fake artworks of that artist for financial gain, especially under the circumstance that the art market has been flourishing rapidly in the past years. More and more unknown artworks are surfacing from every corner of the world and without a proper track record of provenance, it is not easy to identify a newly-emerged artwork to be authentically valuable or not, so that the interested art collectors can be protected financially. Fortunately, many of the analytical tools mentioned can be applied for art authentication purposes. Interesting examples concerning authentication of artworks by world masters would be: a portrait of a young woman originally believed to be by an unknown artist but later attributed to Rembrandt after meticulous and rigorous restoration and authentication process; and a portrait of a young woman, *La Belle Ferronnière*, that was thought to be by da Vinci, however, is still on dispute and is still uncertain till today whether it belongs to da Vinci's work, or one of his followers. It can be understood that determination of the authenticity of an artwork directly determines its value, whether it is a low-priced reproduction or an invaluable masterpiece [242].

Taking for example the analysis of artistic paintings, XRF is used for elemental analysis with microscopic cross-sections to study the stratigraphy of the paintings [13] and to reveal distinguishing chemical compositions with their specific characteristics [197]. *Underdrawings* and *pentimenti* are two of the most interesting topics in artwork analysis; both are concerning the early creation stage of drawings and paintings respectively. *Pentimenti* are in the form of hidden paintings under the current state of a painting. This is because they are the footprints or traces of prior work or changes conducted by the same or another artist on the same painting panel before the final product of a masterpiece [31, 104, 105]. These could be employed as documentation of an artist's revision [43], or an indication or a confirmation of an artist's genuine work [31]. While underdrawings are typically highlighted using Near Infrared (NIR), *pentimenti* are usually discovered with X-ray imaging techniques [104, 105]. For example, the existence of a Cupid in the painting *Girl Reading a Letter at an Open Window* by Johannes Vermeer has been known since 1979 via one of the most powerful X-ray sources: synchrotron radiation. It was originally believed that it was not Vermeer himself who covered the Cupid with paint in the 18th century, but this was restored recently by Staatliche Kunstsammlungen Dresden in Germany who considered that the Cupid should be present following the master's own interpretation. This restored masterpiece was on display as a centrepiece, from 10th September 2021 to 2nd January 2022, at the Gemäldegalerie Alte Meister in Dresden, Germany [209]. One of the most recent discoveries via X-ray imaging is a self-portrait of van Gogh on one of his most famous paintings, *Head of a Peasant Woman* (Figure 2.1), uncovered by conservators at the National Galleries of Scotland [114]. Another example is the discovery of three sketches hidden beneath one of the paintings by Amedeo Modigliani, *Nude with a Hat*, by curators at an Israeli museum [251].

(a) Original View

(b) X-Ray View

Figure 2.1: Hidden self-portrait by van Gogh. Images courtesy of [259, 269].

Although X-ray is the most common method for uncovering *pentimenti*, they can also be unearthed by implementing other analytical methods, such as Raking Angle Photography [55], Visible-Near Infrared (VIS-NIR) Reflectance Imaging Spectroscopy (RIS) synchronised with three-dimensional (3D) acquisition [234], multispectral techniques at different wave ranges [144], a combination of thermographic and reflectographic techniques at different wave ranges [49], and so on. For example, in the study by [201], XRD-CT was implemented and the chemical properties of Rembrandt's work were researched and its paint condition was analysed and diagnosed. The results of the analysis of the thin white crust cover of Rembrandt's 1663 painting, *Homer*, enabled the scientific team to apply the correct restoration and conservation process [201, 210].

Another example of the application of analytical methods is the analysis of *Craquelure*, i.e., distinguishing patterns or networks of cracks that are considered an old painting's fingerprint because they only develop over time. *Craquelure* is distinct from different periods and countries and thus can be used for authentication purposes [74, 102, 245]. Techniques involving microscopic analysis allow not only observation and analysis of *Craquelure*, but also, they can disclose detailed information concerning the stratigraphy of a painting. Other techniques like Raman are used for the identification of pigments, binding media as well as varnishes [164, 255]. For example, Mukhopadhyay [266] demonstrated the advantage of Surface-Enhanced Raman Spectroscopy (SERS) while detecting plant dye madder in an Egyptian painted quiver, and emphasised its capacity of discovering hidden secrets in artworks and national treasures.

In summary, different analytical technologies have distinguishing functions and play different roles in cultural heritage analysis. These techniques can be applied jointly or individually, and can identify and unearth distinct features in the artworks, be it to determine a specific pigment, to reveal hidden details, to expose fake information, or to uncover reasons behind certain characteristics of the artworks. All newly uncovered information is always helpful in deciding the precise and relevant measures to be taken for the restoration and conservation of artwork.

2.2 Amadeo de Souza-Cardoso

In this section, the major events in the life of the Portuguese artist Amadeo de Souza-Cardoso are briefly presented.

Amadeo de Souza-Cardoso (Figure 2.2) was born in Mancelos, Amarante in Portugal in 1887 and unfortunately perished of Spanish flu at the thriving age of 30 in Espinho in 1918. In 1905, he entered the Lisbon Academy of Fine Arts; the following year on his 19th birthday he went to Paris intending to study architecture, but opted to study painting instead. In Paris, he befriended a series of important contemporary artists, with both Portuguese origin and roots in other countries, including Thomaz Costa, Francis Smith, Acacio Lino, Alberto Nunes Cardoso, Eduardo Viana, Amedeo Modigliani, Picasso, Guillaume Apollinaire, Max Jacob, Ortiz de Zárate, Serge Diaghilev, Zadkine, Archipenko and Sonia Delaunay [94].

Amadeo was a relatively prolific Portuguese artist. His widow, Lucie Cardoso, and his friend Paulo Ferreira donated to the Calouste Gulbenkian Foundation (FCG) numerous documents in relation to Amadeo, which include a set of photographs. Conserved in the

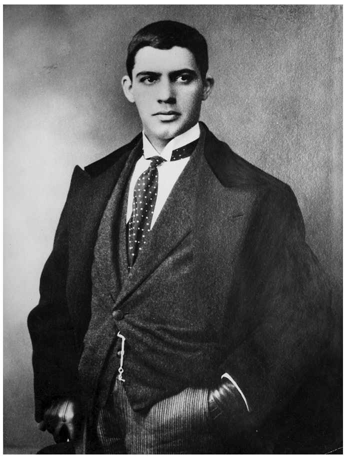

Figure 2.2: Amadeo de Souza-Cardoso (Biblioteca de Arte Fundação Calouste Gulbenkian).

Centre of Modern Art (CAM) are 200 pieces of artworks by Amadeo: 63 paintings, 136 drawings and watercolours and 1 illustrated manuscript.

Amadeo considered his work different from the academic and classic genre, claiming "*I do not follow any school. The schools died ... I'm an impressionist, cubist, futurist, or abstractionist? A bit of everything*" [9]. He enjoyed experimenting and expressing his artistic ideas mixing both antiquity and modernity [94]. Amadeo's Portuguese root as well as his experience in Europe left footprints in his artistic creations; he was appraised by his contemporary of the same Portuguese origin José de Almada Negreiros, as "*Portugal's first discovery in 20th century Europe*" [93]. José Augusto França, who dedicated the first monograph to Amadeo, defined him as "*reluctant Portuguese*"; Portuguese artist José Escada considered him as "*European painter*" [94].

Amadeo had the most productive years in 1911 and 1912 in terms of artworks creations and exhibition presentations, including the *Salon des Indépendants* in Paris in both years, the *Salon d'Automne* in Paris in 1912, *Der Sturm Gallery* exhibition in Berlin in 1912, the first exhibition of Modern Art in the United States in 1912, the Armony Show in New York in 1913. The *XX Dessins* album of drawings and *La Légende de Saint-Julien L'Hospitalier* were also created in 1912 [94]. It was believed by art historians that Amadeo achieved the most success during his career in the year 1917 [94, 225]. At least 6 untitled paintings were painted around 1916/1917, where elements like violins and lithographic letters and numbers were present in the paintings [92].

In 1914, Amadeo and his wife Lucie carried out a journey starting from Paris and continued following through Rocamadour, London, Barcelona and then back to Porto in Portugal, when the war was declared between France and Germany, which forced them to remain in Portugal longer than they expected [9]. During his stay in Portugal, he partook in a variety of artistic activities with his artist friends Sonia Delaunay, Robert Delaunay, Almada Negreiros, Eduardo Viana, José Pacheco, Guillaume Apollinaire and Blaise Cendrars. Amadeo exhibited his artworks for the first time in Portugal, in November 1916 in Porto, and in December 1916 in Lisbon. Both exhibitions received sensational success as well as controversial responses in Portugal [94]. Amadeo and Lucie planned to return to Paris as soon as they could but unfortunately, it was not possible due to the war and he died of the Spanish flu pandemic at the prime of his life at 30 in 1918.

Two volumes of Catálogo Raisonné dedicated to Amadeo de Souza-Cardoso have been published by Fundação Calouste Gulbenkian: Catálogo Raisonné Amadeo de Souza-Cardoso Fotobiografia [47] and Catálogo Raisonné Amadeo de Souza-Cardoso Pintura [48]. The two catalogues documented Amadeo's life and systematically collected Amadeo's photographs and paintings respectively. DCR is one of the leading participants in the compilation of these catalogues. In particular, the scientific research performed at DCR focused on the analysis of the colour palette used by Amadeo, the principal pigments used and the molecular analysis of these pigments [258]. The data obtained by the research in [258] are of special importance as it provides the basis for the pigment analysis included in this thesis.

2.3 Brushstroke: The Artist's Signature

In this section, the definition of brushstroke analysis and its applications in various fields implementing different algorithms are depicted.

2.3.1 What is Brushstroke?

Our research focuses mainly on the genre of paintings, therefore other artistic genres are not significantly discussed in this work. With regard to artistic paintings, the study and analysis of brushstroke have been attracting a lot of attention in recent years. Merriam-Webster [39] defines brushstroke as "*the configuration given to paint by contact with the bristles of a brush*", and "*the paint left on a surface by a single application of a brush or palette knife*", or figuratively "*to describe the quality especially of a narrative or description*". Herbert [113] also noted "*from the romantics through the impressionists and post-impressionists, the brushstroke bespoke autonomous artistic individuality and freedom from convention*", that is, specific painting brushstrokes can embody the artistic signature of a particular style. [96, 130, 165] also mentioned that brushstrokes are considered as artists' "*handwritings*". Many resources equally emphasised the significance of brushstrokes in terms of communicating distinguishing emotions, various states of mind, physics and environment [38, 40, 239, 241]. Research performed by [129] revealed that even a simple brush bristle can indicate a particular artist's style while analysing four different artists' brushstrokes after having applied identical brushes, paints and canvases to create an identical theme. [272] also emphasised that brushstroke plays the most important role in terms of classifying artistic style, out of so many other characteristics such as colour and objects in the paintings. Accordingly, it can be concluded that the brushstrokes of individual painters are like personal signatures. They have their own characteristic brushstroke patterns and styles and use their specific brushstroke style to convey their own sentiments, experiences, and views of the world surrounding them. Historically, one of the common ways for artist identification is via visual examination of the artist's brushstroke style by art experts, who have extensive experience with the artworks of the painters of their interest [165]; that is, art connoisseur - "*an expert on matters involving the judgement of beauty, quality or skill in art, food or music*" [61], and art connoisseurship - "*a specifically visual knowledge gained from looking at works of art*" [62] - such method is still widely used today as one of the most essential methods for artwork authentication. The analysis of brushstroke with the aim of identifying artistic styles is coined as "stylometry" [204], where brushstrokes are studied statistically and mathematically with extracted features from brushstrokes [122].

One typical example would be van Gogh's works, which can be differentiated without much effort by art enthusiasts because of his distinct brushstroke style. [146] described van Gogh's brushstrokes as "*abstract ornaments and threads of woven tapestries*". Art experts also observed his unique brushstroke style and research has been done to date to discern van Gogh's works from his contemporaries by analysing characteristics of his brushstrokes vs his contemporaries' [153]. Other renowned painters with idiosyncratic brushstrokes include for example, Paul Cézanne [113, 266], Rembrandt [181], Gustave Courbet, Édouard Manet, Claude Monet, Georges Seurat, and Pablo Picasso [113].

2.3.2 Brushstroke Analysis on van Gogh's Paintings

It appears that a considerable amount of research has been done to study van Gogh's brushstrokes due to his distinct brushstroke style but with different research objectives [3, 64, 91, 123, 147, 155, 260, 261]. These include for example [153], where conventional methods such as edge detection and segmentation were implemented to analyse van Gogh's brushstrokes. This concluded that there exists a strong rhythm in his brushstroke, that his brushstroke was consistent throughout periods of his artistic development and that it is distinguishable from that of his contemporaries. The work discussed by [130] was the first major project to collect and analyse a set of high-resolution painting data from both van Gogh and Kröller-Müller museums to be used across several different universities; the purpose was to study van Gogh's brushstrokes with the objective of artist attribution, that is, artwork identification and authentication. Since this work was one of the earliest attempts to study brushstrokes, the algorithms throughout the project were still typical and conventional; they concerned for example wavelet transform, Support Vector Machine (SVM) and Hidden Markov Model (HMM). Similarly, [165] reported the implementation of machine learning on the analysis of van Gogh's brushstrokes to identify van Gogh's works out of his contemporaries, which can also be used for artwork identification and authentication; the method applied was coined as "brushstroke textons", that is, brushstrokes characteristics were emphasised with the employment of a series of filters, and then translated as distinguishing spatial frequencies with different scales and orientations, that could formulate a bank of texton histograms for visualisation and classification of different artists. More recent research includes for example the work by [204, 205] that extracted and analysed the features, like texture and colour, that were obtained from van Gogh's brushstrokes region by region, to classify his artistic styles out of different artistic movements and differentiate his works from his peers' using CNNs. Likewise, [89] studied van Gogh's painting in comparison with his contemporaries, and applied CNN to extract discriminative features from brushstrokes, followed by machine learning classification algorithm SVM and a fusion process, which then used for decision making relating to the authorship of a painting while different fusion approaches were analysed and compared. In the work on [89], 27,000 images were collected out of 200 categories from Wikimedia Commons [267], and a dataset named "VGDB-2016" was created and is comprised of 207 van Gogh's works and 124 non-van Gogh; it was claimed to be the first public database, with high-quality digital images as well as density standardisation for tainting identification.

2.3.3 Brushstroke Analysis on Paintings of Other Artists

Excluding the studies that focus mainly on the examination of van Gogh's brushstrokes, the number of researchers that investigate artists' brushstrokes, in general, is also growing. For instance, in the work by [96], an automatic and rapid brushstroke extraction algorithm based on DNN and a foreground and background image matting technique was proposed; it was inspired by Pix2Pix network [126] and Soft Segmentation [8], and was coined as "Dstroke" which stands for Deep Network-based Brushstroke Extraction Method. "Dstroke" was proved to be more reliable and outperformed other methods; it was said to work effectively with most brush painting styles, such as oil paintings, acrylic paintings, Chinese paintings as well as watercolour. [140] provided an important argument and interesting application making use of the characteristics of brushstroke, that is, artistic style transfer, this is, the translation and reformulation of a real photographic image or a digitalised artistic work from one style to another style, for example, the style transformation from an ordinary contemporary digital image content to impressionism style. Unsurprisingly, one of the most widely-targeted styles in [140] is van Gogh's brushstroke style; the other interesting styles are also mentioned previously, for example, Pablo Picasso and Claude Monet. [140] stated that style transformation research was mainly centred around the studies within pixel domain in a majority of the cases. Nevertheless, such consideration was not natural for representations of paintings, because they are formulated with brushstrokes instead of pixels. Subsequently, [140] work implemented a series of image processing tools so that images could be rendered stylistically; the techniques involved optimisation of parameterised brushstrokes, followed by a rendering mechanism to differentiate the styles. The work by [82] introduced a different perspective by examining only the strokes in line drawings by artists, in lieu of the full-scale brushstrokes in the more frequently studied paintings; the objective was for artist attribution of unknown drawings. A collection of 80,000 strokes out of 300 digitalised drawings was created and experimented in this study; the database was comprised of primarily the drawings by

Pablo Picasso, Henry Matisse, Egon Schiele, Amedeo Modigliani and a small portion of representative drawings by other artists. Those line strokes were firstly segmented in order to quantify and classify the strokes accordingly; during the process, features were extracted with the application of one of the deep learning techniques, Recurrent Neural Network (RNN). Afterwards, the drawings then could be classified appropriately with the aggregated classification results of the line strokes. The proposed algorithm achieved a promising accuracy of over 80%, in the meanwhile was very robust while detecting fakes. Similarly, [57] also investigated line-based drawings implementing computer science with the aim of not solely determining artists of individual artworks, but also identifying the gender of the targeting audience; features such as angles between lines, line orientation, density of line segments and line strength were taken into consideration, and the drawing styles were classified efficiently. Notwithstanding the research done based on Manga artworks is still of important value for the exploration of brushstroke analysis. Not only western artworks benefited from the examination of brushstrokes, the brushstroke investigation on eastern artworks, for instance, Chinese Ink Wash Paintings (IWPs), also plays an important role in the identification of artwork authorship. Given as an example, [235] studied 120 IWPs of six renowned Chinese painters, a novel sparse hybrid CNN was devised to extract brushstroke features automatically; it was claimed to have produced promising results while being compared with two other algorithms.

In the study of [171, 172], of which a review is included in section 2.6, both brushstrokes and chemical analysis were deemed to be equally important in terms of authentication and identification of Amadeo's artwork. During the process of brushstroke analysis, image processing tools as well as conventional machine learning algorithms such as Gabor filter, SVM, Scale-Invariant Feature Transform (SIFT), K-Means Clustering (KM) were utilised. Four methods: simple Gabor, simple SIFT, Gabor in regular points, and Gabor in SIFT key points, namely SIFT+Gabor, were compared for the efficiency and accuracy of the classification results; it was claimed that SIFT+Gabor algorithm outperformed all the other three methods and achieved a very high accuracy of more than 95% in multiple cases. Although some issues were identified as described in section 2.6, the research by [171, 172] is still a significant milestone concerning several aspects in the analysis of artistic heritage artwork. This was not only one of the first works that explored brushstroke analysis as well as artwork authentication, but also it incorporated both image analysis from brushstroke analysis and material analysis together. Additionally, it was one of the few works that researched works by local and national artists that are not yet worldly well-known although it should have been the case.

The aforementioned examples are only a small part of the studies in relation to brushstroke analysis. Further works include for instance the report by [32, 33, 133, 169, 175, 177] among others. In summary, it can be concluded that a majority of investigations pertaining to brushstroke analysis are aimed at artist authorship, that is, artist identification and artwork authentication; more details will be discussed in the following section. In other cases, the research has purposes like image transformation, artistic style determination, and artwork audience categorisation.

2.4 Pigment Analysis

In this section, the techniques and algorithms concerning pigment analysis, and how they are implemented in cultural heritage are described.

2.4.1 What is Pigment Analysis?

Pigments are the materials whose molecules are responsible for the colour perceived due to the effects of absorption, reflection, scattering and diffusion of light. These pigments are typically applied in various materials, such as paints, dyes and inks for decorative purposes in archaeological and cultural settings. The colour perceived from pigments differ from each other depending on whether they are organic (e.g., dyes), inorganic mineral pigments, or compounds of both inorganic and organic materials [194, 196]. Pigment analysis is the execution of different scientific techniques to identify and analyse pigment for a variety of purposes in artistic contexts: dating the age of the artworks, artist authorship, artwork authentication, artwork conservation and restoration and so on [194, 196]. On many occasions, it is also called "elemental analysis", "material analysis" or "chemical analysis" and traditional investigation of pigments was performed mainly invasively with the removal of samples from the artwork [66]. These techniques for pigment analysis thus differ depending on the requirement for samples to be taken, and whether the test or measurement is of destructive or non-destructive nature to the samples or object analysed [194]. Examples of techniques in terms of pigment analysis are XRF, Raman, FTIR, hyperspectral imaging, SEM, SEM-EDS, to name a few [167].

The analysis of pigments has been widely implemented in various fields, for instance, in archaeology [196], in aquaculture [148, 149, 156, 216, 217], in biology and medicine [270], in chemistry and agriculture [191, 249], in geology and cartography [24], in sociology and heritage [24, 51] and so on. As a matter of fact, many of the areas are intertwined with each other, and the research outcome from any individual field often benefits another.

2.4.2 Pigment Analysis in Cultural Heritage

One of the most commonly-utilised areas for pigment analysis is in the cultural heritage context, more specifically, in the conservation and restoration field where it is particularly crucial for the purposes previously mentioned. The analysis of pigment on an artwork is deemed to be able to identify and determine specific pigments, which can then be used as a reference for conservators and restorers to conserve and restore historical heritage artwork. Moreover, they can be adopted as an important indication of the period, the region as well as the author of the artwork. In other words, pigment anachronism, in which the presence of certain pigments in an artwork, that shouldn't exist around the period of the creation of the artwork, can suggest that this artwork is forged, or due to past restoration process [41, 50, 87, 88, 118, 159]. For instance, with the help of non-invasive pigment analysis techniques of Raman and XRF, [51] examined the evolution of Bolognese illuminated manuscript around the thirteenth and fourteenth centuries and confirmed the evidence of the pigments usually-adopted during this period. Based on the definition of pigment anachronism, if a newly-discovered Bolognese manuscript purporting to be from this period while containing the pigments that were not generally used during this period, it is possible to deduce that this manuscript might be falsified. In the work by [50] applying Raman microscopy, a more concrete example related to an artwork claiming to be created by Russian-French artist Marc Chagall in the year 1910, was proved to be forged and thus was destroyed by requirement, due to the presence of phthalocyanine pigments, since such blue and green organic pigments did not yet exist until 1928 [50, 56, 100]. Similarly, the research by [233] employed a series of techniques with regards to pigment analysis to determine the authenticity of a painting asserting to be attributed to Russian artist Vassily Kandinsky around the year 1932; the technical approaches implemented were μ-Raman, UV and XR. Cross-examination of the samples applying all three methods concluded that this painting cannot be a work by Kandinsky. One of the reasons is the existence of the Synthetic Organic Pigments (SOP) in this painting, that were still rarely present prior to 1945. Another factor being the presence in several samples of the Synthetic Inorganic Pigment, titanium white, which was first available only in 1921 [42, 100]. Indeed, the group of inorganic pigment whites, that is, lead white, zinc white, and titanium white is one of the most typical examples for dating cultural heritage like artistic paintings with the purpose of artwork authentication or artist authorship, thanks to their prevailing production and usage periods in each case. Lead white is said to be the oldest white synthetic pigment for centuries until around the 1930s when legislation surrounding health concerns started to take place, zinc white began its prominent production around the 18th century while titanium white around the 20th century [83, 103, 121]. The research by [159] claimed to be the first work attempting to apply multiple analytical techniques to examine an artwork pertaining to world-renowned Spanish artist Pablo Picasso because it bears the signature of "Picasso"; a variety of spectroscopic and chromatographic techniques were employed to investigate both pigments and binders; they included μ-Raman, SEM-EDS, Attenuated Total Reflectance Fourier Transform Infrared Spectroscopy (ATR-FTIR) and GC-MS. Cross-examination and cross-reference proved that all identified materials from the painting were chronologically consistent with the references and documentation available for the period when the painting was executed.

Evidently, the aforementioned few examples demonstrated that pigment analysis is substantially important for art conservation and restoration; more specifically, pigment dating is one of the essential tools for artwork authentication.

2.4.3 Pigment Identification in Cultural Heritage

The examples regarding pigment analysis or identification applying various analytical techniques are a plethora; the cases referenced above are for exemplification purposes only. It can be found that they are mostly related to the determination of chemical components and composition with the application of different analytical techniques. Nevertheless, there also exists the perspective of pigment analysis, where the implementation of computer science is involved. In this situation, the scientific technique frequently applied is hyperspectral imaging. The pigment unmixing problem is often implicated, where data are collected along different wavelengths, image-wise or pixel-wise. The former acquisition process records spectral data for all pixels on the image at once while the latter process records spectral data from selected individual pixels on the image (e.g., line scanning). In a majority of the cases, pigments present on artworks, for example on paintings, are mixed pigments instead of pure pigments, therefore, pigment unmixing is necessary and important for various reasons, such as painting conservation and restoration [69]. As a matter of fact, operations like pigment mapping, pigment identification, pigment classification, image segmentation, etc., on many occasions relate to one another and involve the same or similar objective of pigment unmixing, or namely, spectral unmixing, given the fact that such task is performed in spectral space [84].

Pigment unmixing refers to the decomposition of a spectrum to quantitative values and proportions of individual pure pigments [84, 213], usually with the exploitation of a variety of machine learning algorithms and it is one of the most-discussed and actively-researched areas in terms of hyperspectral imaging analysis of pigments. For example, the work published in [69] studied the painting *Old Man in Warnemünde* by Norwegian painter Edvard Munch; the author made use of the mixing law of colourants, Kubelka-Munk theory, and applied a simple linear unmixing model, fully constrained least squares unmixing, for Hyperspectral Unmixing (HU), which resulted in promising results. A similar model was explored by the same author in the study of another painting, *The Scream*, also by Edvard Munch with the objectives of pigment unmixing and pigment mapping [66, 67]. Similarly, in [26] it was studied the Gough Map of Britain (c.1400) and the Selden Map of China (c.1619) with the application of the Grand Matrix and MaxD to extract endmembers, followed by non-negative linear least square and the K-Means algorithm as well as spectral angle spatial patterns method to classify and map pigments. Other examples include the work published in [271] and [162] where analysis on a laboratory-prepared sample and both laboratory-prepared samples and the real Chinese painting data from Qing Dynasty respectively were used to devise an effective model utilising the derivative of ratio spectroscopy.

On the other hand, while studying a 15th-century folio, the approaches proposed in [212, 213] employed an automatic non-linear unmixing model of one DNN to first decompose the given spectra to pure pigments, then another DNN to identify them to achieve the final objective of pigment unmixing. Likewise, in the work published in

[199], a study was done on a Buddhist painting in the Shortwave Infrared (SWIR) range or extended NIR while implementing DNNs. The comparison of the results obtained via both conventional mathematical model Spectral Angle Mapper (SAM) and DNNs was made, with the latter outperforming the former while dealing with the intrinsically-complex SWIR data range. Another example includes four paintings around the year 1340 that were analysed and used to build a large database so that a spectral CNN could be constructed [138]. The outcome was robust and promising when tested on paintings of similar styles.

It can be observed that the major difference between different pigment unmixing algorithms is whether they involve conventional mathematical and machine learning models, or state-of-art artificial neural networks. Investigations in the cultural heritage field for the first situation include for example work published in [2, 25, 28, 68, 85, 108, 137, 152, 158, 166, 189, 202, 211, 237, 254, 273], and for the second situation include for instance in [136, 161, 236]. It is noticeable that the conventional models in terms of pigment unmixing problem in the art field are still prevalent, whilst artificial neural network methods are still relatively scarce. Nevertheless, there is a plethora of research taking place in remote sensing areas with regard to pigment unmixing in both cases, since it was one of the areas where hyperspectral imaging was first introduced, and spectral unmixing was one of the most researched topics in remote sensing field [68, 109].

The study in [171, 172] might be the first work that incorporates spectral data of the painting pigments from the original tubes that the artist used during his lifetime, with spectral data of the paintings by the artist, as well as the elemental data of the pigments from the artist's paintings acquired applying some of the pigment analysis techniques mentioned previously. It works step by step to achieve primarily pigment identification and then artwork authentication objective: firstly, the spectral data of the tube pigments were compared with the spectral data of individual pixels of the paintings using Euclidean Distance (ED) to determine the presence of pure black and white pigments, followed by the determination of the presence of the same or similar pigments as the tube pigments employing SAM, where when the distance applying SAM was small enough within a defined threshold, the analysed pigment was considered as pure; all the pure pigments that were confirmed to be present in the paintings then were compared against the chemical data to define eventually whether an artwork is an authentic work by the artist or not. Although the process does not involve machine learning algorithms, it is novel in this field in the sense that it not solely considered the spectral data from the paintings, like all the other research, more importantly, it consolidated spectral pigment data from original tubes and chemical data of those pigments on the paintings.

All in all, pigment analysis is significantly important in various fields for multiple purposes; one of the most applied areas is in cultural heritage for conservation and restoration purposes. Usually, pigment identification can be achieved through a variety of scientific techniques implementing different pigment analytical devices; in the case of spectral imaging for pigment analysis, computer science is implicated, where both traditional machine learning algorithms and artificial neural networks are employed by numerous researchers, with the former currently still outnumbering the latter.

2.5 Artwork Authentication

In this section, following the background information provided in the previous sections, further detailed knowledge regarding art authentication is delivered.

2.5.1 What is Artwork Authentication?

The work published in [65] proposed that authenticity in art comes in different forms for a work of art when it is considered authentic and it distinguishes between nominal authenticity and expressive authenticity [80]. Artwork authentication appears to fall in the category of nominal authenticity; as the name suggests, is a process of using specialised techniques or expertise to authenticate if an artwork is authentic or forged, usually with reference to world-renowned artists. Artwork authentication is not just limited to works of art in the genre of artistic paintings; any works of art, including music, performance, cinema, sculpture, and architecture among others, can all implicate procedures of artwork authentication. Since the current research specifically involves artistic paintings, therefore, artwork authentication discussed in this dissertation only covers the genre of paintings. Artwork authentication is significantly important and imperative to safeguard the interest of both the art market and the artists, as well as the integrity of artists' legacies [174, 229]. For this ideal, there exists a network of international authentication research organisations, consisting of members for example, Authentication in Art Foundation (AiAF) in the Netherlands, International Foundation for Art Research (IFAR) in New York, and the Art Due Diligence Group (ADDG) in London, where cultural heritage forgery is primarily dealt with within the domain of the West although art forgery is severe also in the East [185].

The preceding discussions brought to light that there are multitudinous techniques in relation to art authentication. Approaches published in [229, 230] determined three fundamental channels for artwork authentication: firstly, artwork evaluation via art connoisseurship, secondly artwork provenance and thirdly, scientific examination. It can be noticed that all three items have been mentioned briefly or in detail in the previous sections.

2.5.1.1 "Connoisseur" and "Connoisseurship"

The words "*connoisseur*" and "*connoisseurship*" originated from the French language. The French verb "*connaître*" means "*to know, to be acquainted with*", hence the original meaning of "*connoisseur*" in French means "*the person who knows*" and "*connoisseurship*" "*the state or act of being a connoisseur*". They are in fact not merely restricted to the usual perspective of fine arts; aspects in gastronomy like cuisines and fine wines also implicate such profession. In the art world, connoisseur is defined as experts who "*have 'the eye' or instinct to pronounce* *whether an object is 'consistent' with the style of the artist or period*" because of their substantial knowledge and experience in said topic [119, 224, 229]. "*connoisseurship*" is "*The ability to tell almost instinctively who painted a picture*" [186], or "*the determination of similarity and difference and assessment of quality in works of art and material culture*" [52], or "*the endeavour to identify artworks by time, culture and authorship*" [79]. Historically, it is closely related to the expertise of knowledgeable art experts, i.e. "*the eye*"; in recent years, as technology advances, connoisseurship appears to encompass further domain, just like the definitions noted in [52, 79], which did not merely limit such concept to the territory of art art-historical connoisseurship, but simultaneously embraced the scientific investigation of physical materials in artworks, that is, scientific connoisseurship, which in fact corresponds to the third possible channel of artwork authentication defined in [229, 230]. Indeed, studies like those published in [52, 183, 206, 207, 256, 274] also mentioned the new art connoisseur, i.e., scientific connoisseurship in their studies. A connoisseur differs from an art historian, in the way "*The connoisseur might be defined as a laconic art historian, and the art historian as a loquacious connoisseur*" [192]. In fact, connoisseurship has been historically popular and has been considered one of the most credible and rudimentary techniques for artwork authentication and identification. Art historians are not content with such a profession due to various reasons, for example, the subjectivity of connoisseurship, thus scepticism for its credibility was raised considerably [81, 187]. Indeed, errors can occur with some of the most authoritative connoisseurs and art historians [151, 224]. For example, *Supper at Emmaus*, by the world-infamous art forger Han van Meegeren, who specialised in faking the works by old masters Johannes Vermeer, Frans Hals, Gerard ter Borch and Pieter de Hooch, was faked in the style of Johannes Vermeer, and was recognised as a genuine Vermeer masterpiece, by one of the most influential art historians and art experts like Abraham Bredius as well as Nazi field marshal Hermann Göring [78, 111, 170]. Furthermore, the views and decisions of the connoisseurs can be affected by many external factors [81, 101, 224]. Hence, a more objective approach and scientific methods with higher confidence and greater certitude are needed [81, 206, 207].

2.5.1.2 Artwork Provenance

The word "*provenance*" also originated from the French language. The French verb "*provenir*" derived came from Latin "*provenio*", meaning "*come forth, come from*", and "*provenance*" means "*the origin of someone or something*". In the art world, one of the most reliable and most utilised art authentication measures is provenance, that is, ownership history, which often involves exhibition history and publication history [195, 208]. It is usually defined as historical documentation concerning for instance the artist identification, the period and the historical whereabouts of the artworks [198]. A comprehensive provenance documents the history of the locations of the artwork that facilitate artist attribution and artwork authentication; nevertheless, it can be very problematic and challenging due to illegitimate acquisition or loss of artwork during the war period, especially Nazi era [208, 252].

Ownership of artwork takes into account a wide spectrum of forms: a label from an exhibition or gallery displayed on the artwork, an original sales receipt directly from the artist, or from a gallery knowledgeable about the artwork, or both, names of previous owners of the artwork that can be corroborated, catalogues for sales at auction, collections inventories, a film or recording of the artist speaking about the artwork, or a photograph of the artist with the art, an illustration or a discussion in an exhibition catalogue or in a book, and so on and so forth [17, 203]. In the meanwhile, the authenticity of provenance could also be questionable and necessitates verification [16, 34, 90, 99, 115, 176, 195, 262]. One of the most notorious art forgers John Myatt and his partner-in-crime John Drewe not only faked artworks but also falsified documents of provenance by infiltrating some of the most influential museums and galleries in the world [176]. A more recent example was Michigan art dealer Eric Ian Hornak Spoutz originating from a family of artists, who also owned a legitimate art gallery, but was selling artworks with fake provenance documentation he himself forged [90]. The work published by [198] proposed four ways of establishing the authenticity of provenance: the artist's signature on the artwork confirmed to be authentic, historical documents proving the history of artwork to be authentic; confirmation via scientific analysis, confirmation via connoisseurship. Ultimately, just like art connoisseurship, art provenance stand-alone cannot be relied on to prove an artwork is authentic or not [16], and further scientific investigation and confirmation are preferred, sometimes required.

2.5.1.3 Forgery as a Work of Art

It has been mentioned before that some of the most prolific art forgers had made a name for themselves due to their own inherent artistic talents; many of them also converted to collaborate alongside law enforcement and to assist in tackling art fraud [15]. There exists a debate surrounding "*forgery as a work of art*", where multiple authoritative critics argued that if a forged artwork was so adept, and was able to provide the same aesthetic gratification, to the extent that its authenticity was left open with ambiguity even after having undergone the most meticulous inspection, why and how it could not be acknowledged as a genuine work of art, and could not be placed together in the same exhibitions of the works of the plagiarised artist [29, 58, 107, 139, 150]. The work proposed in [29] contended that the conception of authenticity is implied within the conception of forgery because one cannot happen without the other; it is irrelevant to aesthetic perception whether an artwork is of aesthetically high calibre because it is authentic or of low-calibre because it is forged [150]. It is ultimately conditioned by the manner in which art is viewed by us [58].

2.5.2 Artwork Authentication Applying New Technology and Computer Science

The implementation of computer science with regard to art authentication has been flourishing rapidly over the past years. The issues surrounding artwork authentication by applying various technologies have been discussed in the previous sections. Some of them involve solely the examination of the data acquired via different analytical instruments while others involve further investigation and computation of the data obtained. A few examples that are slightly different from the aforementioned methods are introduced herein. In the work by [275], a decision tree model was trained using 55 artworks, including 12 forged artworks with determined attribution markers; although the preliminary results produced promising results, artworks with larger databases and known provenance are necessary to construct robust classification models. In [228] it is proposed a stand-alone solution and an internet-based solution that is established upon mobile architecture with random intrinsic object characteristics; it connects the certificate of authenticity and the relevant artwork. A Radio Frequency Identification (RFID) Tag and a two-dimensional (2D) barcode, along with an online Authentication Archive was applied. An approach proposed in [157] introduced an effective anti-counterfeiting and authentication method for ceramic artworks based on 2D code and Wireless Application Protocol (WAP) technology; the method proved to be practical, safe and easy to implement and manoeuvre after performance analysis. In [163], it is demonstrated a statistical model comprising first and higher-order wavelets; tests on the determination of paintings by Pieter Bruegel the Elder and Pietro Perugino showed promising results.

All the examples given above and before established that art authentication comes in different forms, either manually involving human intervention like connoisseurship, provenance or artwork analysis, or automatically implementing computer science and high technologies. Either way, artwork authentication is significantly important to guarantee that an artwork is an authentic artwork by famous artists and that art enthusiasts can appreciate a genuine piece of artistic creation.

2.6 Previous Work Review

This section presents a review of the previous work completed and documented by Montagner in [171]. An overview of the algorithms proposed, the issues identified, corrections, improvements made and updated results are discussed.

2.6.1 Brushstroke Algorithm

The work completed by Montagner aimed to develop an algorithm to predict the probability of a bitmap image belonging to a particular class. More specifically, the probability of a painting being the work from Amadeo de Souza-Cardoso. To do this, the algorithm proposed the use of image processing techniques, numerical statistics and unsupervised/supervised machine learning methods. The summary of the process is described below.

Montagner conducted the brushstroke investigation based on four computation methods: Gabor on the full image (simple Gabor), SIFT on the full image (simple SIFT), Gabor on cropped blocks (Gabor Regular) and Gabor on cropped blocks around SIFT keypoints (SIFT+Gabor). A total of 24 Gabor filters with 4 scales and 6 orientations are applied for all methods. Montagner reported results that suggested that the combination of SIFT+Gabor produced the highest classification accuracy making it the preferred algorithm for the authentication of paintings and the one reviewed in this work. The flowchart of the original method proposed by Montagner and derived from this review can be found in Figure 2.3 where blue and orange colours are used to highlight data used for training and testing respectively.

The SIFT+Gabor algorithm start with feature extraction by assessing images from both positive and negative training sets with keypoints and descriptors highlighted by SIFT. Blocks centred around the keypoints are then excerpted from the original training images and rotated accordingly based on the angle of the keypoint vectors.

The KM algorithm is then used to group features and find centroids that are thought to be the representations of a particular style of the artist during his career life. These centroids are referred to as visual words.

Next, the technique known as Bag of Features (BoF), originally designed for analysis of text and known as Bag of Words, is used to represent the data in terms of the number of occurrences of each of the visual words. Then, the Term Frequency-Inverse Document Frequency (TF-IDF) function is used to balance the weight of the visual words. This is, visual words that occur multiple times are assigned a low weight while visual words that are found with a lower frequency are assigned a high weight as these might be more useful to make distinctions.

The data are split into training and testing data sets. The training set is used for training a Regularised Least-Squares Classifier (RLSC) while the test data are used for evaluation of the method. The output of the classifier is assigned one of two labels: positive or negative. Positive classifications are indications that the data belong to a true and authentic painting while a negative classification suggests the painting does not match the requirements of the process and is therefore considered fake or not attributed to Souza-Cardoso.

The algorithm proposed by Montagner reported accuracies over 90% that seemed to increase as the number of visual words was increased with the SIFT+Gabor combination. However, the review of the implementation revealed a series of issues during the processing of the data. These included: the exclusion of keypoints identified by SIFT near the edge of the images, inconsistent rescaling of images, incorrect handling of the TF-IDF values for new data, unbalanced positive and negative datasets. However, the primary concern identified with the original method is found in the inclusion of the test data during the identification of centroids estimated with the KM algorithm. The idea behind clustering the features is to identify centroids that represent key features or visual words of the dataset allowing defining any painting in the dataset in terms of the presence of these visual words. The inclusion of the test dataset and other images to be evaluated in the clustering process thus results in the centroids being biased towards the test data. This is, the algorithm will describe the test data based on features that were known to the

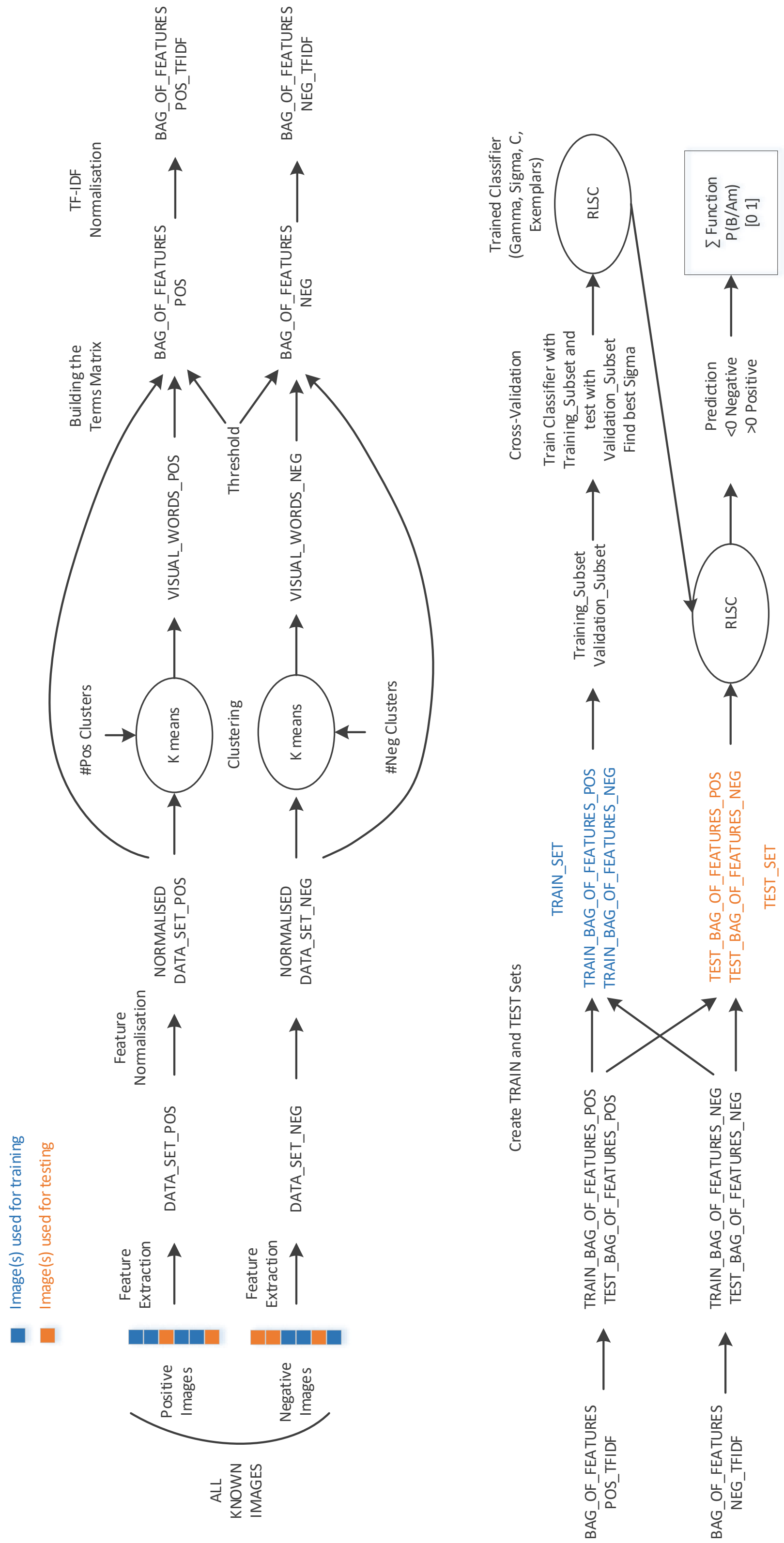

Figure 2.3: Flowchart of the brushstroke algorithm proposed in [171].

algorithm. The biasing error found is propagated through to the classifier which results in calculated accuracies over 90%.

To illustrate the effect of the biasing error identified, the algorithm was run a number of times for all four processing methods with the number of visual words set to those used by Montagner. Table 2.1 and Figure 2.4 show the results when the test data are included in the clustering step.

Updating the four implementations of the algorithm to exclude the test data from the clustering process generates the results shown in Table 2.2 and Figure 2.5. As observed, when the test data are included in the clustering process, the produced results are close to the ones reported in [171]. Additionally, the results produced from SIFT, Gabor and Gabor Regular methods show even better accuracies than reported. Nevertheless, SIFT+Gabor method appears to be less accurate than the Gabor Regular and SIFT methods in general where the latter is the most computation-intensive method. Note that for the standalone Gabor method, the number of words does not apply as no clustering was used.

Table 2.1: Accuracy obtained when testing data are included in KM clustering.

Number of Words	SIFT	Gabor	Gabor Regular	SIFT+Gabor
100	76.39%	80.56%	75.00%	72.22%
200	77.78%	80.56%	79.86%	75.69%
400	85.42%	80.56%	87.50%	75.69%
1000	93.06%	80.56%	91.67%	85.42%
1200	93.06%	80.56%	90.97%	87.50%
1400	95.14%	80.56%	91.67%	86.81%
1600	94.44%	80.56%	90.97%	90.97%
2000	95.83%	80.56%	93.75%	90.28%

Table 2.2: Accuracy obtained when testing data are excluded in KM clustering.

Number of Words	SIFT	Gabor	Gabor Regular	SIFT+Gabor
100	74.31%	80.56%	71.53%	76.39%
200	70.83%	80.56%	70.83%	78.47%
400	74.31%	80.56%	70.83%	81.94%
1000	75.00%	80.56%	75.69%	84.72%

Continued on next page

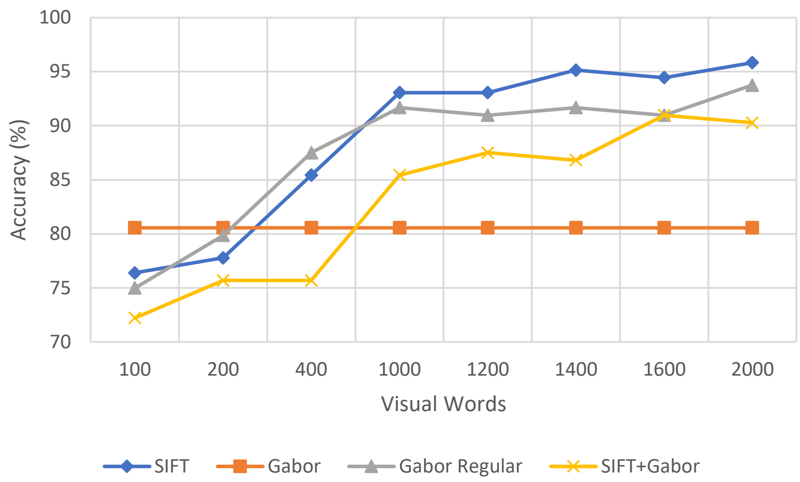

Figure 2.4: Accuracy obtained when testing data are included in KM clustering.

Table 2.2: Accuracy obtained when testing data are excluded in KM clustering. (Continued)

Number of Words	SIFT	Gabor	Gabor Regular	SIFT+Gabor
1200	75.69%	80.56%	76.39%	86.81%
1400	75.69%	80.56%	75.00%	86.81%
1600	72.92%	80.56%	73.61%	87.50%
2000	74.31%	80.56%	74.31%	87.50%

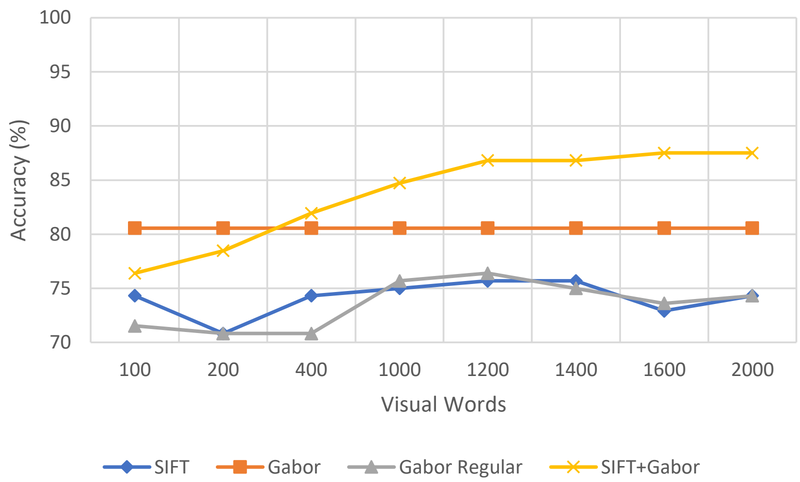

Figure 2.5: Accuracy obtained when testing data are excluded in KM clustering.

In the algorithm by Montagner, small cropped areas at the keypoints identified with SIFT were rotated in accordance with the angle detected by SIFT. A comparison was made to evaluate the performance of the method when the rotation is excluded from the process. The results show that differences are much larger than the 3% that was initially suggested in [171]. The results in Table 2.3 and Figure 2.6 were generated when the test set is excluded from clustering since the objective of our research and this review will move forward with an unbiased algorithm for a true representative classification.

Table 2.3: Comparison of accuracy obtained with SIFT-Gabor with and without rotation of SIFT keypoints.

Number of Words	Without Rotation	With Rotation	Numerical Difference
100	69.44%	76.39%	6.95%
200	70.14%	78.47%	8.33%
400	64.58%	81.94%	17.36%
1000	70.83%	84.72%	13.89%
1200	70.83%	86.81%	15.98%
1400	72.22%	86.81%	14.59%
1600	71.53%	87.50%	15.97%
2000	70.83%	87.50%	16.67%

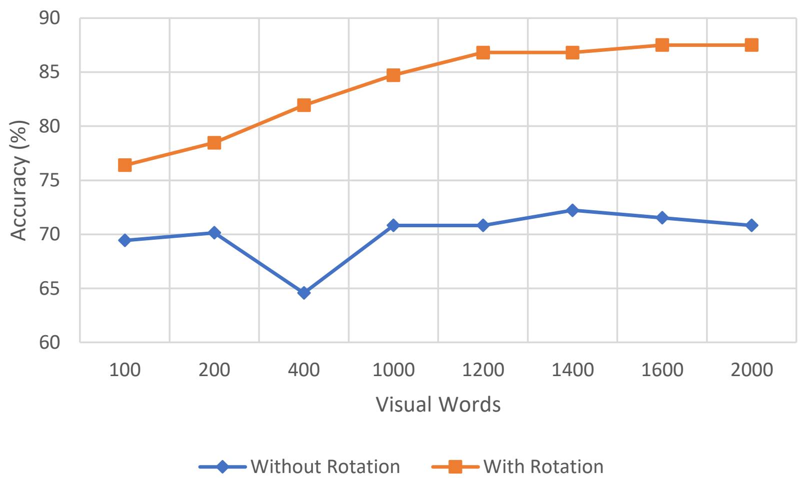

Figure 2.6: Comparison of accuracy obtained with SIFT-Gabor with and without rotation of SIFT keypoints.

The rotation of data is used only for the areas around the keypoints in the SIFT+Gabor method and therefore only results for comparison are available for this implementation. The general explanation is that the Gabor filter analyses frequency in a given direction. In order to make it independent of the orientation of the features that are trying to be identified, the features have to be oriented in the right way, otherwise, the same Gabor filter for the same feature will generate different results.

Two modified KM algorithms, K-Means++ Clustering (KM++) [19] and K-Means| | Clustering (KM| |) [23], which are designed to reduce the computation load while generating better, optimised centroids, were considered as a way to improve the selection of centroids or visual words. KM works on a trial-on-error approach. A seed is the first value chosen as a centroid, the error is calculated and the centroid moves. The process is then repeated until the error is very small. Since the seed in KM is completely random each time, it will not always yield the same result. KM++ on the other hand uses seeds that are initialised and estimated based on the data provided, where the seeds are optimised, hence not random. Subsequently, the algorithm converges faster and more accurately. Although all three types of KM methods have both pros and cons, the overall superiority level is considered as KM| | > KM++ > KM. Although KM| | uses fewer iterations than the other two methods, the seeding process is slower and its efficiency is small for small data sets, thus this was excluded from the evaluation of potential improvements.

To compare the performance of KM++ as an improvement, the algorithm was executed 10 times and the final classification accuracy was recorded and averaged. Similarly, the original KM method was executed but with random seeds as opposed to the original method used in [171] where seeds were set to the first points in the dataset. The results of this test are shown in Figure 2.7. Although the results of KM with random seeds are similar to those of KM++ the latter was found to be over 100 times faster making it the preferred clustering method.

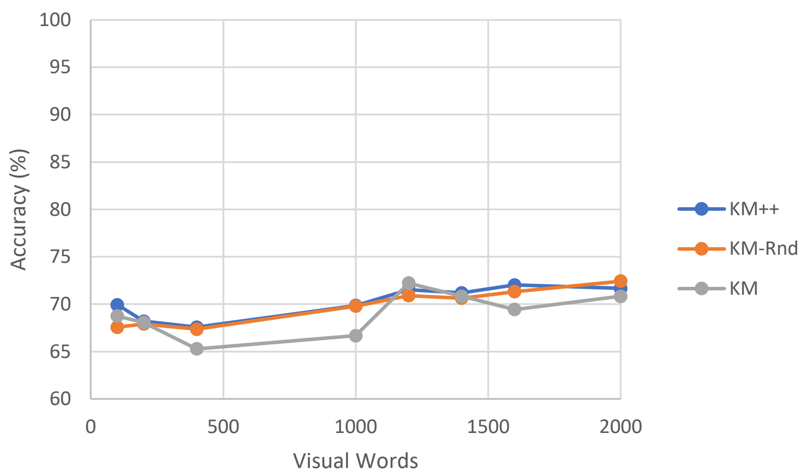

Figure 2.7: Comparison of accuracy obtained with SIFT-Gabor using KM, KM with random seeds and KM++.

The final updated algorithm based on Montagner's is shown in the flow diagram of Figure 2.8. This excludes the test dataset, highlighted in orange, entirely from all steps that produce data used in the training of the classifier. As a result of the exclusion and in the interest of evaluating new, unseen data, the centroids must be saved as well. Similarly, the Inverse Document Frequency (IDF) values of the TF-IDF process must be saved; the Term Frequency (TF) values are always computed on the data at hand but the IDF values are only those of the original corpus.

Regarding authentication, Montagner proposed calculating the probability of an image being the work of Amadeo given the result of brushstroke analysis based on the class discriminant function of the RLSC classifier $f(x)$. The proposed calculation is shown in Eq. 2.1 where $I_a(B/Am)$ is the probability of an image being the work of Amadeo given the result of brushstroke analysis. In Eq. 2.1, a sigmoid function is applied to the output of the classifier effectively rescaling the output value to the $[0, 1]$ range with slope parameter A set to 8 [171]. The resulting indicator of authenticity values using brushstroke reported in [171] are shown in Table 2.4. In [171] it is suggested that the value obtained for painting 77P9 might be low due to missing features related to text which are not identified by SIFT.

$$I_a(B/Am) = \frac{1}{1 + e^{-Af(x)}} \tag{2.1}$$

Table 2.4: Indicator of authenticity in [171] using brushstroke analysis.

Painting	$I_a(B/Am)$
68P11	89.00%
77P2	80.00%
77P5	95.00%
77P8	82.00%
77P9	35.00%
77P16	99.00%
77P20	71.00%
86P19	73.00%
86P21	70.00%
86P23	98.00%
92P209	98.00%
Fake	42.00%

2.6.2 Material Analysis

The material analysis part of the algorithm proposed by Montagner in [171] is based on the examination and correlation of a painting against a known database of reference pigments whose chemical properties are known. Such a database of reference pigments consists of paint tubes that were used by the painter in known artworks and therefore their authenticity is indubitable.

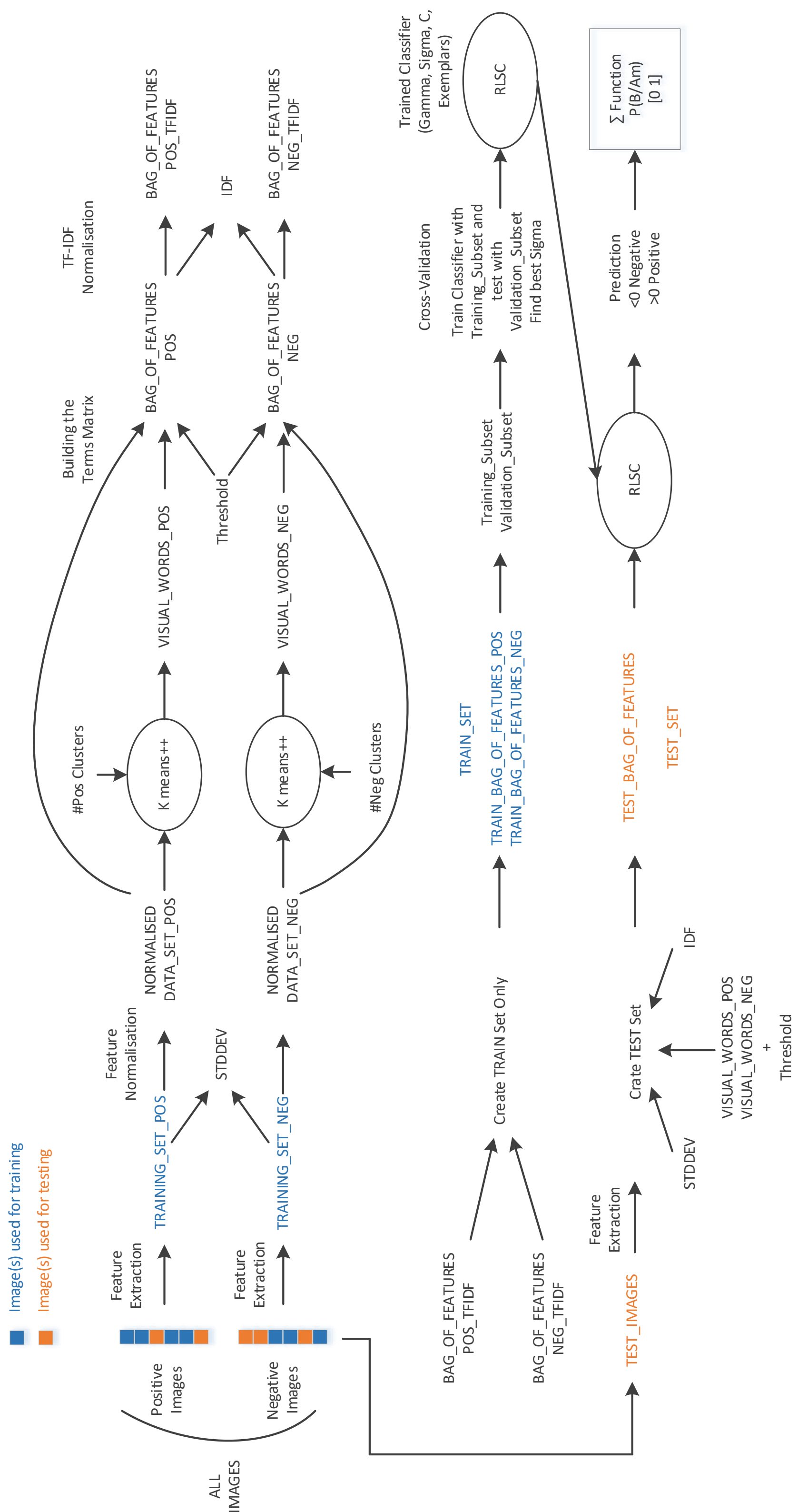

Figure 2.8: Flowchart of the brushstroke algorithm proposed in [171] updated to prevent biasing of results.

The correlation of reference pigments against a particular painting is done in five essential checks:

- Pre-processing
- Pure pigment identification
- Mixed pigment identification
- Authentication

The first stage of the material analysis method consists in creating artificial mixtures of 2 and 3 reference pigments using the pigment reflectance and additive colour mixing. Mixtures exclude the use of white and black colours. For each artificial mixture, the corresponding colour components are also obtained. The second stage of pre-processing consists in evaluating the colour from each point in the hyperspectral image against the colour of each sample in the collection of previously analysed points of the painting using XRF and referred to as the XRF database. If the colour difference between the point and the XRF samples is small (below a given threshold), the point in the painting is assumed to be identical to the point of the XRF sample. On the other hand, if the colour difference exceeds the minimum threshold for all samples the in the XRF database then the point is categorised as *Not Analysed*. This allows identifying areas in the painting for which no XRF data exist. These areas will not be analysed further.

Identification of pure pigments consists of finding points that closely resemble a pigment in the reference database. To achieve this, the reflectance difference from each point is measured against the pigment reference database. This is done using the SAM function which is considered invariant to illumination. The closest pigment in the reference database is marked as the potential match. Next, to check if the chemical composition of the reference pigment matches the pixel, the closest XRF sample to the point being analysed is used. As previously described, this XRF sample is assumed to be identical to the point and therefore a chemical element match between the XRF sample and the pigment on the reference database suggests the point analysed is *Pure*. Points that do not fall in this category are assumed to be a potential mixture of pigments and are analysed further.

A similar matching process as in pure pigment identification is performed in this stage. The reflectance of each point is matched against the artificial mixture of 2 pigments using SAM. The closest XRF sample to the point analysed is then assumed identical to the point and its chemical composition is checked against the two reference pigments in the mixture. If all chemical elements match, the point is classified as *Mixed* and corresponds to a mixture of 2 pigments. Otherwise, the point is further analysed.

For those points that did not match a mixture of two pigments, the process is repeated but using a three-pigment combination. Points that satisfy the conditions above described are marked as a three-pigment mixture. Otherwise, the point is marked as a *Negative* pixel, this is, the pixel has a different chemical composition to that found in the reference database.

The final step consists in quantifying the areas or number of points that are marked as pure or a mixture of pigments. The proportion of these areas is proportional to the probability of the painting under evaluation being positive or authentic, this is, authored by Amadeo de Souza-Cardoso.

For visualisation purposes, the algorithm in [171] recolours each point of the hyperspectral image analysed with approximated sRGB values of the point reflectance. Points classified as *Not Analysed* and *Negative* are coloured using pink and purple colours respectively. Using the software supplied by [171] which contains 17 pigments in the reference database, it is produced the recoloured image of Figure 2.9 for the hyperspectral image of the painting 68P11 (refer to Appendix B for details of the paintings).

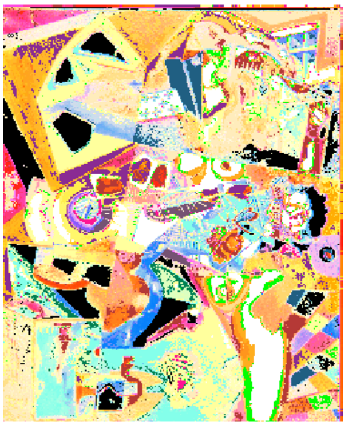

Figure 2.9: Results produced by the pigment analysis algorithm in [171] for painting 68P11 using 17 pigments in the reference database and recoloured using approximated sRGB values.

The primary issues with the algorithm proposed in [171] are the use of additive colour mixing for the generation of artificial colour mixtures, the exclusion of black and white colours in the artificial colour mixtures, and the use SAM as the metric function for spectral matching. Additive colour mixing is suitable when using light sources only as the sum of all reflectances yields white (white light). For paint pigments however colour mixing is of a subtractive nature and thus subtractive mixing should have been used in the algorithm proposed. Similarly, the inclusion of black and white in the artificial colour mixtures should have been considered as these would more accurately represent the mixtures created by Souza-Cardoso. Further details are available in chapter 4.

Finally, the use of alternative metric functions other than SAM should have been evaluated. SAM can be used as the metric function to evaluate the matching of reflectances that might exhibit a certain degree of illumination variance. This is, SAM is relatively insensitive to scaling of the spectra due to changes in pixel illumination [4, 132]. However, this is also a disadvantage as it is unable to accurately identify base colours that are brighter or darker, this is, pigments that have been mixed with white or black colours. On the other hand, Root Mean Square Error (RMSE) evaluates the true difference in amplitudes between reflectances allowing the method to distinguish mixtures that contain white and black colours. To exemplify this, hypothetical mixtures of up to 3 pigments including black and white were created. Then, the reflectance of each pixel in the hyperspectral image was matched using SAM and RMSE for comparison. The resulting matched hypercube was then converted to sRGB using the D65 illuminant and the resulting images are shown in Figure 2.10.

(a) SAM (b) RMSE

Figure 2.10: sRGB representation of hyperspectral matching results of painting 68P11 using SAM and RMSE.

Evidently, RMSE produces an accurate colour reconstruction of the image when black and white are used in the artificial mixture while SAM struggles to distinguish between dark and light colours. While RMSE shows a promising result, its implementation requires careful use as consistent illumination between the reference database and the hyperspectral images analysed is required. Yet, RMSE for colour matching has the potential to be used to highlight all areas in a painting that contain a certain pigment including black and white colours as shown in Figure 2.11 where certain pigments are highlighted.

Improvements made to the algorithm proposed in [171] are included in chapter 4 where the use of subtractive colour mixing, the inclusion of white and black colours and the use of alternative methods to predict pure and mixed pigments are presented.

Authentication of paintings using the pigment analysis method proposed by Montagner is calculated based on the area identified as positive Am, relative to the area where no analysis was made $NotAn$, as shown in Eq. 2.2. The resulting values as indicated in [171] are shown in Table 2.5.

$$I_a(M/Am) = Am * (1 - NotAn) \tag{2.2}$$

The final indicator of authenticity proposed in [171] is a linear combination of the indicator of authenticity obtained with brushstroke $p(B/Am)$ and pigment analysis $I_a(M/Am)$ as shown in Eq. 2.3. Here, the contribution from each indicator of authenticity has been

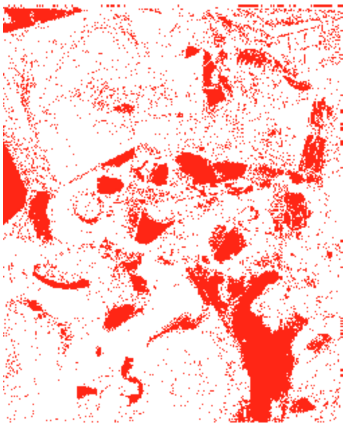

(a) Chinese Vermilion

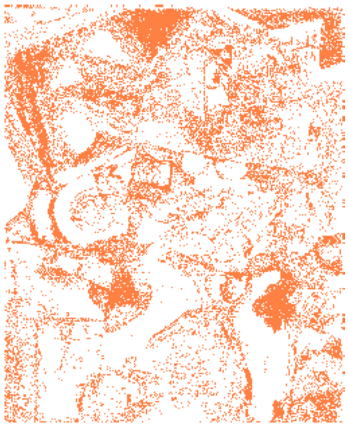

(b) Terra Rosa

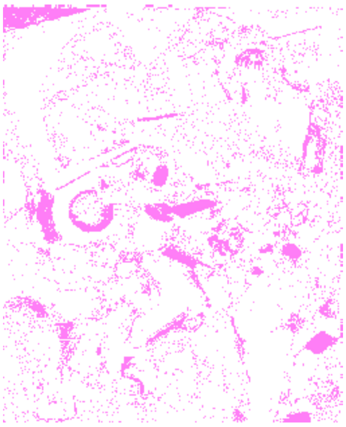

(c) Cobalt Violet

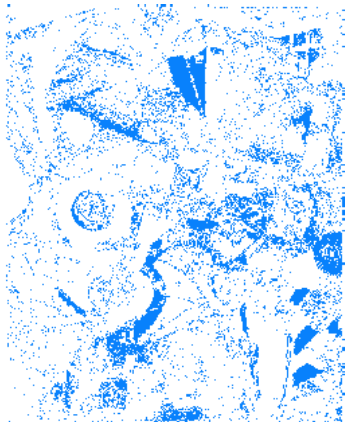

(d) Cerulean Blue

(e) White

(f) Black

Figure 2.11: Areas where the presence of colours in pure or mixed pigments was identified using RMSE for painting 68P11.

evenly distributed by setting the value of the weight $alpha = 0.5$ suggesting both methods are equally important for the authentication process.

$$I_a(Am) = \alpha p(B/Am) + (1 - \alpha)I_a(M/Am) \tag{2.3}$$

Table 2.6 summarises the authentication results obtained in [171], using both brush-stroke and pigment analysis.

Table 2.5: Indicator of authenticity in [171] using pigment analysis.

Painting	$I_a(M/Am)$
68P11	91.00%
77P2	99.00%
77P5	100.00%
77P8	99.00%
77P9	100.00%
77P16	100.00%
77P20	100.00%
86P19	74.00%
86P21	91.00%
86P23	84.00%
92P209	97.00%
Fake	49.00%

Table 2.6: Indicator of authenticity in [171].

Painting	$p(B/Am)$	$I_a(M/Am)$	$I_a(Am)$
68P11	89.00%	91.00%	90.00%
77P2	80.00%	99.00%	89.50%
77P5	95.00%	100.00%	97.50%
77P8	82.00%	99.00%	90.50%
77P9	35.00%	100.00%	67.50%
77P16	99.00%	100.00%	99.50%
77P20	71.00%	100.00%	85.50%

Continued on next page

Table 2.6: Indicator of authenticity in [171]. (Continued)

Painting	$p(B/Am)$	$I_a(M/Am)$	$I_a(Am)$
68P11	89.00%	91.00%	90.00%
86P19	73.00%	74.00%	73.50%
86P21	70.00%	91.00%	80.50%
86P23	98.00%	84.00%	91.00%
92P209	98.00%	97.00%	97.50%
Fake	42.00%	49.00%	45.50%

2.7 Deep Learning Concepts

In this section, background information concerning Deep Learning (DL) will be briefly introduced. This includes some of the DL concepts and methods that are used in this research.

2.7.1 Artificial Intelligence

The concept of AI is often confused with ML and DL and is frequently considered interchangeable with the other two terms. As a matter of fact, the terms differ and do not exactly refer to the same thing. According to [6, 7, 20, 59, 70, 72, 76], AI, as the name suggests, incorporates human intelligence with machines, so that characteristics of human intelligence can be mimicked through processing by machines. ML is a subset of AI, and DL is a subset of ML (Figure 2.12).

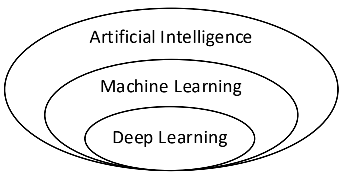

Figure 2.12: Hierarchy of AI, ML and DL [72].

AI is generally categorised as: Artificial Narrow Intelligence (ANI), that is, *Weak* AI with narrow capability; Artificial General Intelligence (AGI), that is, *Strong* AI with general capability; and Artificial Super Intelligence (ASI), that is, *Strong* AI with transcendent capability [7, 21]. American philosopher John Searle noted that *Strong* AI seeks to create artificial persons; machines that have all the mental powers we have, including phenomenal consciousness. *Weak* AI, on the other hand, seeks to build information-processing machines that appear to have the full mental repertoire of human persons [219]. The applications of *Weak* AI, with the ability to perform specific tasks, include for example chess playing and identification of individuals in photos while the applications of *Strong*

AI, with the ability to understand sentiments and interpret emotions, should be able to behave like how human behave, and it is when machines become human-like, as depicted in movies such as *I, Robot* and *Ex Machina*.

2.7.2 Machine Learning

The concept and implementation of ML have existed for many years. They not only involve robotics, which we often and immediately think of, but also the applications that are closely related to our daily lives, like spam filters or advertising optimisation [11, 214]. Machine learning is the implementation of a series of uniquely designed algorithms to solve specific problems; it is generally identified as the following types of systems depending on the amount of human supervision and intervention: supervised learning, unsupervised learning, semi-supervised learning and reinforcement learning [11, 214]. Other examples of machine learning applications include: learning associations, whose typical application is basket analysis, that is, the determination of the association between the products purchased by customers; classification, as the name suggests, the determination of the classes among different categories with distinguishing properties or characteristics; regression, the prediction of an output based on a series of characteristics of the studied subject. Both classification and regression are identified as supervised learning problems, where the output is subject to the learned patterns in relation to the input determined by the supervisor, that is, through input-output examples. On the other hand, unsupervised learning is when the supervisor does not exist and the patterns are learned through unlabelled input data and through mimicry. Finally, semi-supervised learning is when a small portion of the data is labelled and a large portion of the data is unlabelled during training [11, 116, 215].

Some of the typical machine learning algorithms include SVM, KM and RLSC, which are used and discussed in this dissertation. SVM is a type of supervised learning algorithm and aims at classification and regression analysis as well as detection of outliers [232].

SVM works by plotting data with a series of features in a n-dimensional space, where the value of each feature corresponds to the value of a particular coordinate, followed by the implementation of classification, regression, or outliers detection in the hyper-plane space [250]. The basic SVM is linear SVM with hard and soft margins with its extensions including for example Support Vector Clustering (SVC), multiclass SVM, transductive SVM, structured SVM, regression SVM, Bayesian SVM.

K-Means (KM) is a type of unsupervised learning algorithm and works for the purpose of clustering. There are various types of clustering: hierarchical clustering and partitioning clustering, where the former is subdivided into agglomerative clustering and divisive clustering, and the latter is subdivided into KM clustering and fuzzy C-Means clustering [131]. KM divides the samples into K clusters with similar characteristics in each cluster and it is initiated with randomly assigned centroids. The number of centroids K needs to be allocated and can be defined optimally for a given set of data. The initiation process is followed by the determination of the shortest distance between the randomly allocated centroids and other data points in the starting clusters respectively so that the centroid can be reassigned to that data point where the shortest distance is found in each cluster. Such a process is repeated until the re-allocation of the centroid stops, which means the K cluster is determined.

RLSC is a group of methods to solve the least squares problem while using regularisation to constrain further the resulting outcome. This is a type of supervised learning for classification purposes. Its principle is to minimise the sums of squares by finding the smallest sum of squared residuals through the calculation of the distance between the observed data value and the projected value of the proposed function, hence it is coined as "least squares". While applying for example least squares method, problems like overfitting and underfitting might occur. The implementation of techniques such as regularisation, cross-validation and pruning make sure the resulting solution is further constrained, penalised or evaluated so that the algorithmic model can fit optimally to the new unseen data.

The work proposed in [214] describes overfitting as an over-generalisation of the data. It happens when the problem is over-complicated than necessary to fit the training data so that the predicted outcome fits and performs too well on the training set. This is, the predictive model is overly dependent on the training data, hence it will very likely produce a higher error rate when encountering new unseen data. Figure 2.13(b) shows an example of overfitting where a 50-degree polynomial is used to fit a given set of data. Whilst overfitting over-complicates the problem, underfitting is the opposite of overfitting; that is, the problem is over-simplified while there is a high bias within the training data. Figure 2.13(a) shows an example where a 1-degree polynomial is used to fit the same data as in Figure 2.13(b). As [11] noted "*If there is bias, this indicates that our model class does not contain the solution; this is underfitting. If there is variance, the model class is too general and also learns the noise; this is overfitting*".

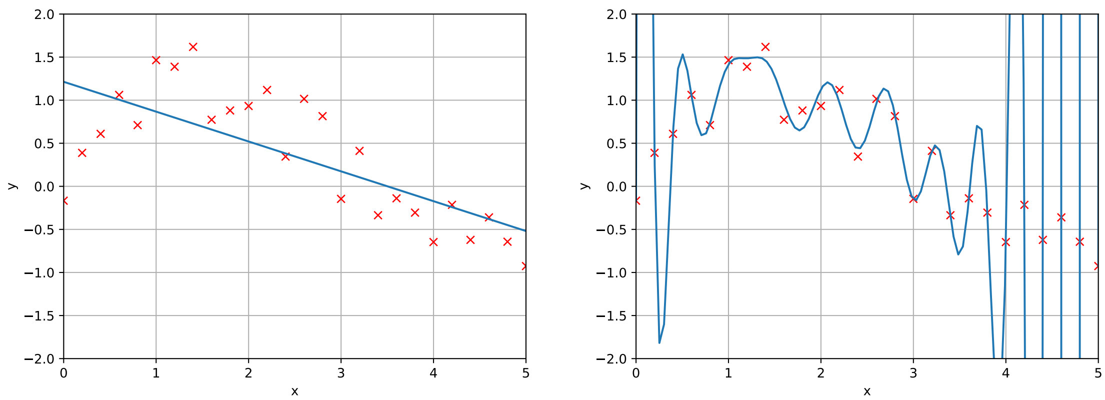

(a) (b)

Figure 2.13: Examples of (a) underfitting and (b) overfitting.

One important concept in ML is scoring which is used to measure the performance of a method. For example, to measure the accuracy of a binary classifier where two classes exist it is required to calculate the following outcome possibilities [141]:

- True Negatives (TN): the number of elements correctly classified as belonging to the negative class.
- True Positives (TP): the number of elements correctly classified as belonging to the positive class.
- False Negatives (FN): the number of elements incorrectly classified as belonging to the negative class.
- False Positives (FP): the number of elements incorrectly classified as belonging to the positive class.

The classification accuracy of a binary classifier evaluating N elements is therefore the proportion of correctly classified elements as defined in Eq. 2.4.

$$Accuracy = \frac{TN + TP}{N} \tag{2.4}$$

The precision of the binary classifier is defined as the fraction of correctly classified positive elements relative to the total number of positive predictions (Eq. 2.5).

$$Precision = \frac{TP}{TP + FP} \tag{2.5}$$

Another metric used for a binary classifier is recall defined as the fraction of correctly classified elements relative to the total number of positive elements (Eq. 2.6).

$$Recall = \frac{TP}{TP + FN} \tag{2.6}$$

Finally, the F1 score is defined as the harmonic mean of precision and recall (Eq. 2.7).

$$F1 = 2 \times \frac{precision \times recall}{precision + recall} \tag{2.7}$$

2.7.3 Deep Learning

DL is said to simulate the structure of a human brain with more complex and multi-layered neural networks, hence it involves more accuracy, more mathematics and more computation. It often refers to deep artificial Neural Networks (NN) [6, 20] and therefore, it is a subset of NNs, as illustrated metaphorically in the form of Matryoshka dolls in Figure 2.14 [7, 21].

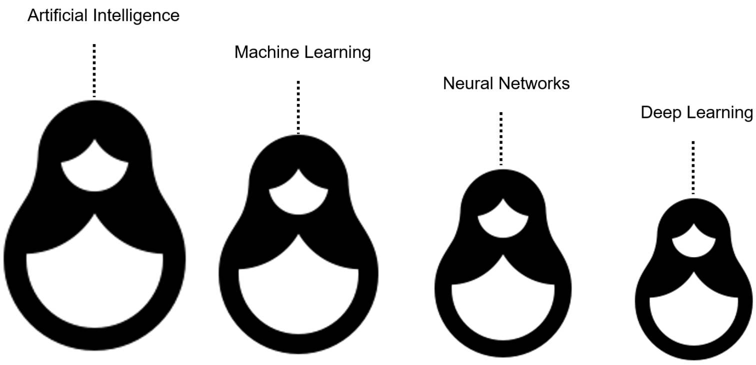

Figure 2.14: Metaphorical representation of the hierarchy of deep learning (image from [7])
.

2.7.3.1 Neural Networks

In computer science, Neural Networks are the implementation of a set of algorithms resembling how the human brain functions and performs a learning process by examples like how the human brain learns. The term is often interchangeable with Artificial Neural Network (ANN) or Simulated Neural Network (SNN) [7, 178, 179], as opposed to natural human or biological neural networks. Nevertheless, debate exists as certain data science experts consider ANNs standalone as a type of NN, that is, Feedforward Artificial Neural Network (FFANN) [5, 106].

Different types of NNs serve for specific data types and applications. Types or architectures of NNs are noted differently by different data science experts, in general, it appears that most agreed with the following major categories: Perceptron, MLP NN, FFANNs, Radial Basis Function Neural Network (RBFNN), RNN, Modular Neural Network (MNN), Long Short-Term Memory Network (LSTM), CNNs, Sequence-to-Sequence models and Autoencoders [1, 5, 60, 71, 106, 178, 179, 248]. A comprehensive guide to the types and architectures of NNs is compiled and illustrated by Fjodor van Veen from Asimov institute in Figure 2.15.

A NN usually consists of three basic components: an input layer, hidden layer(s), and an output layer [7, 179]. More specifically, inputs x, weights w, a bias or threshold b, and an output $F(x)$ for a given number of inputs m, and resembles the mathematical formula in Eq. 2.8.

$$F(x) = \sum_{i=1}^{m} w_i x_i + b \tag{2.8}$$

Similar to a single neuron, a Perceptron model, also known as Threshold Logic Unit (TLU) or McCullough-Pitts neuron, is a Single Layer Neural Network, and was first implemented by Frank Rosenblatt [179, 248]. It is the most fundamental and ancient form of NN and applies only the activation function on the input via the single neuron to produce a binary output. Therefore, it does not have any hidden layers and is only used for binary classification and is useful for logic functions like AND, OR, and NAND. In

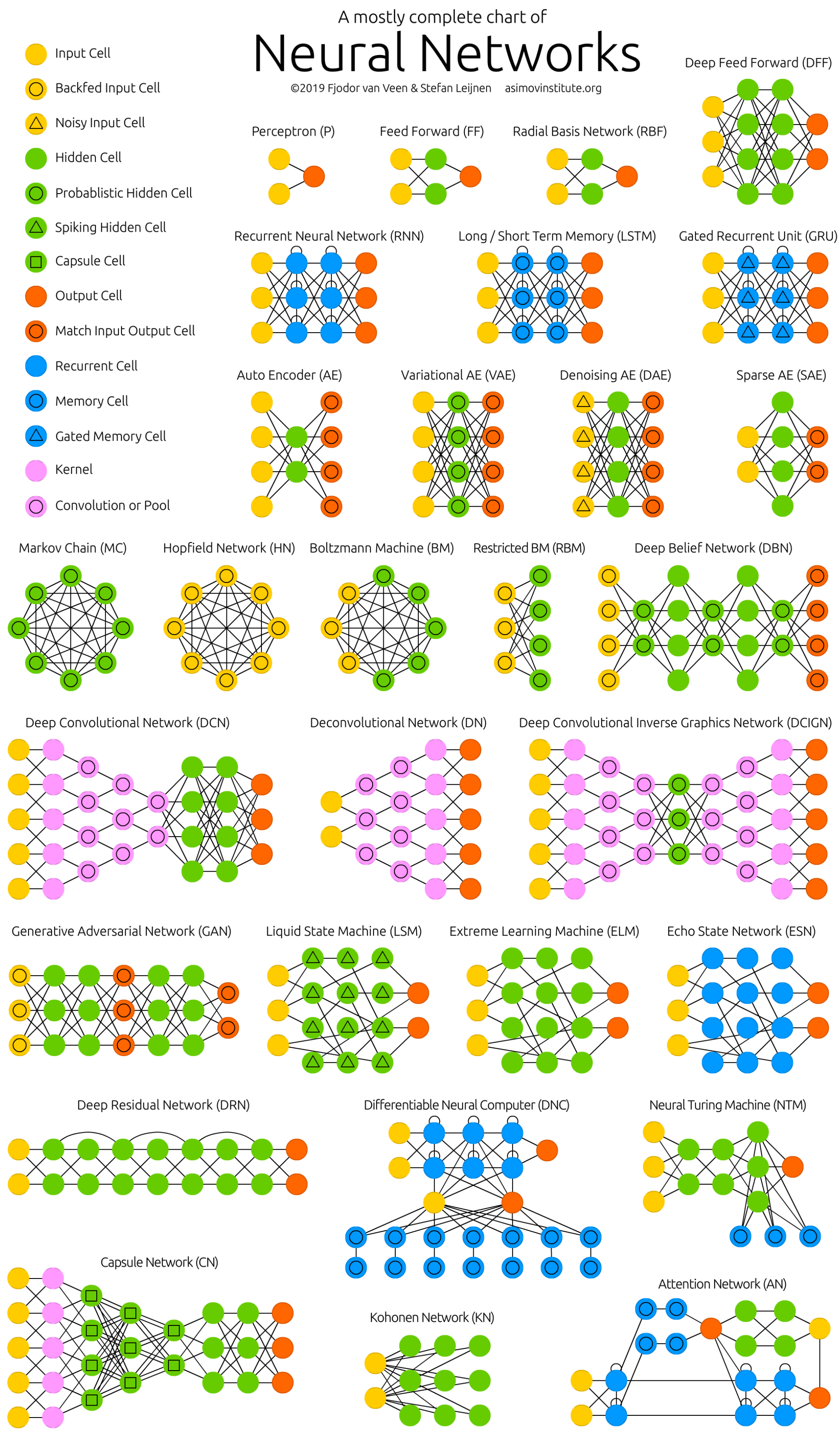

Figure 2.15: The Neural Network Zoo: https://www.asimovinstitute.org.

terms of MLP NNs, as the name implies, the input will be passed through more layers and is applied for complex classification. Its applications include, for example, speech recognition [1, 248]. FFANN, is sometimes referred to as ANN [60] or MLP NN [179] and as the name suggests, the processing flows merely in the forward direction and there is no backpropagation, therefore, the weights are not updated. Its applications include for example face recognition and speech recognition. Although it performs beyond the scope of traditional machine learning models, it does not achieve the complexity that exists in deep learning models [5, 106, 178, 248]. RBFNNs are different from traditional MLP NNs: the hidden layer uses Radial Basis Function neurons (RBFs) like Gaussian, thin plate spline, multi-quadratic with different parameters, as an activation function. Its major application is power restoration [1, 5, 106, 178]. Similarly, in RNNs, as the name "recurrent" implies, the operation occurs multiples times and repeatedly using sequential data [5, 106] and it resembles the structure of FFANNs, except that the memory from previous words influences the next prediction [1, 5, 106]. Its applications include for example sentiment analysis and text-to-speech processing. LSTM is the improved version of RNN and implements designated memory units along with the standard units used in RNN that preserves information for a prolonged period of time [1, 5, 106, 248]. Its applications include, for example, gesture recognition, speech recognition and text prediction [5, 106]. On the other hand, a Sequence-to-Sequence model is composed of two RNNs, with an encoder to process the input and a decoder to process the output, which works simultaneously. It differentiates itself from an actual RNN in its same length of input and output data [1, 248]. Its applications include, for instance, machine translation and chatbots. Autoencoders are a particular type of NN composed of three major parts: encoder, code, and decoder, where both the encoder and decoder possess a structure similar to FFANNs mirroring each other [5, 106] and it is mostly applied for image processing [244]. MNNs are a sequence of individual networks, each performing an independent sub-task without interacting with each other yet working towards achieving the final outcome. Therefore, the processing is broken down into independent and smaller components, resulting in the reduction of the computation complexity and computation load, that is, more rapid processing. Its applications include for example stock market prediction and character recognition [1, 5, 106, 248]. Last, but not least, CNNs are one of the most popular DL methods [60] and apply typically the mathematical principles, more specifically, matrix multiplication from linear algebra, and are said to be similar to FFANNs [179]. Its applications include for example image, video and natural language processing [1, 5, 60, 71, 106, 179, 248].

2.7.3.2 Convolutional Neural Networks

CNNs involve mathematical calculation, and convolution, which is an important imaging processing operation to extract features from images. Therefore, CNNs technique is particularly acclaimed and prevalent in image and video processing applications, although its implementation is multifaceted in other fields as well. The basic principle of convolution in image processing is the implementation of kernels, i.e., filters, to highlight discernible features in images. CNNs work in a similar manner through kernels in the hidden layers and intend to comprehend both spatial and temporal information via a series of relevant kernels [106].

As a type of ANNs, CNNs also share the three fundamental elements: an input layer, hidden layer(s), and an output layer. In general, the hidden layer is comprised of one or multiple sequences of three types of layers: Convolution (CONV) Layer, Pooling (POOL) Layer and Fully Connected (FC) Layer. Subject to the depth or the architecture of the CNN, additional layers of the same or further operations can be added accordingly in the hidden layers. Other operations include for instance padding, flatten, activation function or Rectified Linear Unit (ReLU), Maximum Pooling (MaxPool), Softmax and normalisation, to name a few. The CONV layer is the convolution processing applying a pre-designated stride on the kernel passing through an image from left to right and from top to bottom until the complete analysis of the image in both directions of height and width. As mentioned previously, the purpose of CONV operation is to extract features, for instance, edges and colour at lower-level layers, and more specific depiction and information of images at higher-level layers [5, 106]. For example, Figure 2.16 shows the features or activations of the first convolution layer of the model in section 3 using painting 86P21.

Figure 2.16: Example of output from the first convolution layer of the brushstroke model in section 3 using painting 86P21.

The POOL layer follows suit to extract dominant features, in the meanwhile minimises the number of parameters so that computation load can be reduced; it also helps to minimise overfitting. The FC layer is an ordinary FFANN and connects the outcome from the previous layers so that classification can be made at the output layer. CNNs can contain both forward propagation and backward propagation, where the former, mainly in CONV layer, processes the information, and the latter, in both FC and CONV layer, gauge the error and update the parameters [73]. CNNs have been popular in the AI field, with most applications in image and video processing [1, 5, 60, 71, 106, 179, 248]. One of the most well-known CNNs is AlexNet [143] which consists of five layers of CONV with more kernels in comparison with other CNNs as well as three layers of FC. Following each CONV and FC layer, ReLU activation function is implemented. AlexNet is an inspiration to many CNN structures concerning the application of artist attribution; nearly all research demonstrated their superiority over the conventional image classification projects [143]. In this PhD research, not only the AlexNet architecture was used for examination, but also other CNNs structures were applied for analysis producing optimistic and promising results.

To design or analyse a CNN, the size of the data before (input) and after (output) a layer is typically calculated to ensure compatibility between layers. The output size or number of output features n_{out} of a convolution layer is calculated using Eq. 2.9 where n_{in} is the input size or number of input features, k is the filter kernel size, p is the padding size and s is the stride [77].

$$n_{out} = \frac{n_{in} + 2p - k}{s} + 1 \tag{2.9}$$

Similarly, the output size of a pooling layer is calculated using Eq. 2.10. Other arithmetic variations of these two equations exist for other layers with convolution and pooling being the primary layers.

$$n_{out} = \frac{n_{in} - k}{s} + 1 \tag{2.10}$$

3

Brushstroke Analysis

This chapter describes brushstroke classification using convolutional neural networks, data augmentation for deep learning training and the application of the trained model for artwork authentication. Comparative results using the methodology proposed in [171] are discussed.

3.1 Deep Learning Approach

As discussed, brushstroke can be considered the artist's signature as it tends to be unique and representative of each artist, as shown in the exemplary images of Figure 3.1. This however changes through the career of an artist as the style matures and the artist experiments with different techniques and materials. Yet, it is believed that the core style of the artist can be distinguished from others by analysing the intricate features like brush pressure, stroke length, brush flow and colour among others. It is thus important to make use of analysis techniques to enhance these features for the easy identification and classification of results.

(a) (b) (c)

Figure 3.1: Brushstroke examples.

One of the main techniques used for brushstroke analysis is the enhancement of edges, also known as edge detection. This image processing technique enhances edges by differentiating (filtering) the colour content of a painting in a given direction. For example, horizontal pixel differentiation or filtering can be used to enhance vertical edges (Figure 3.2(a)). Similarly, vertical filtering can be used to detect horizontal edges (Figure 3.2(b)). A combination of these or more complex filters like Gabor or Sobel for example can be used to detect edges in multiple directions making it easier for the human eye and for machines to distinguish the features of a single brushstroke.

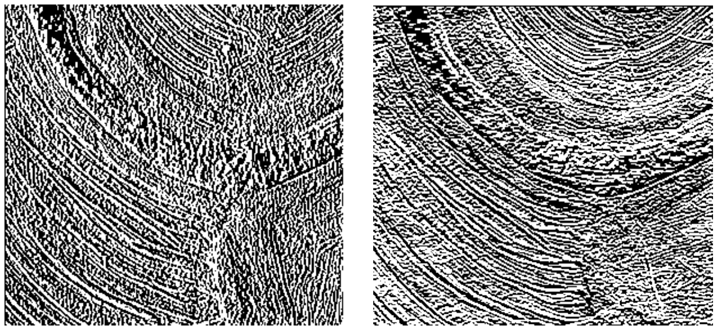

(a) Horizontal Filtering (b) Vertical Filtering

Figure 3.2: Edge detection of brushstroke using filtering.

In this work, we propose the use of a deep learning model for the automatic detection of edges or features and the final classification of the object analysed. The model proposed is based on the AlexNet architecture developed by Alex Krizhevsky [142] originally used for the automatic classification of objects in raster images. The original AlexNet model, shown in Figure 3.3, contains up to five levels of CONV - ReLU - MaxPool layers which create feature maps that summarise the important features that define the images. The feature maps are then used to classify the input image into one of 1000 different sets of data or classes via three fully-connected layers.

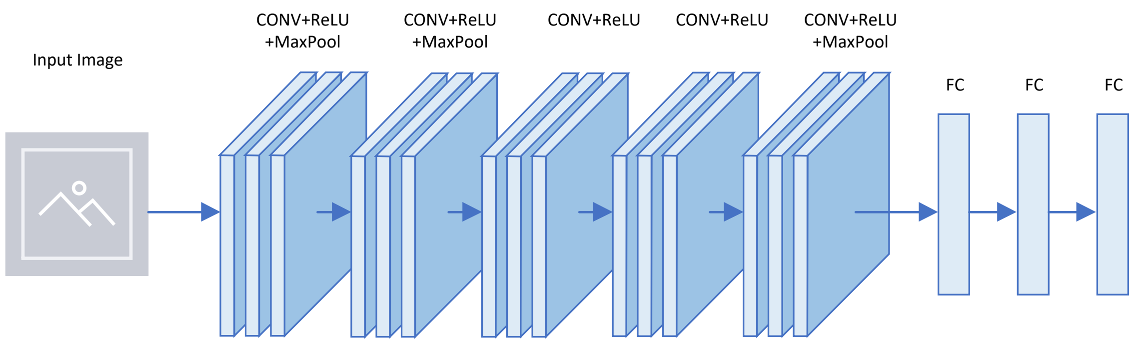

Figure 3.3: Block diagram of AlexNet CNN.

The proposed model for the classification of Souza-Cardoso paintings shown in Figure 3.4 contains two primary class outputs: positive and negative. The former class label is used to attribute an input image to Souza-Cardoso while the latter class label is used to attribute the image to a different artist or artists. The classification of a sample image into one of these two classes is done by finding the maximum value of the two outputs. In the network proposed, an input image size of 227×227 pixels is used. This input size image has been kept small to reduce the computational requirements for the training and classification process. Furthermore, the input size was found to be adequate given the average image size of the entire dataset of 3365×3029 pixels and the data augmentation process described in 3.3.

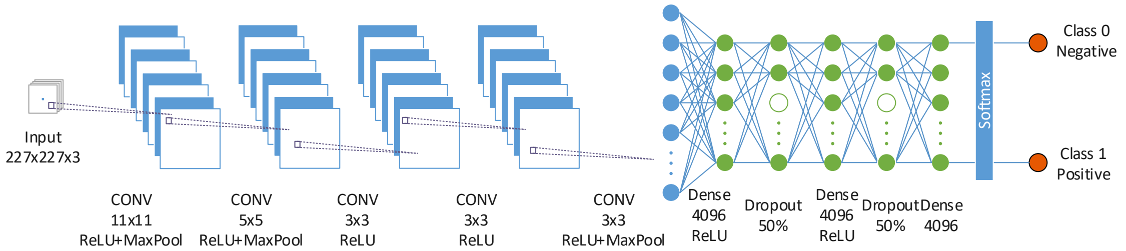

Figure 3.4: Block diagram of AlexNet-based model used for brushstroke classification.

3.2 Data Selection

Deep learning models require large datasets for correct training, for example, the original AlexNet model was trained with 1.2 million samples from the ImageNet Large-Scale Visual Recognition Challenge (ILSVRC) yielding overall classification error rates of 39.7% and 18.9% for the datasets tested [142]. A second requirement that affects the classification results is the balance of the training datasets, this is, how equally distributed between classes are the datasets used. Training data imbalance can lead to results that are biased towards a particular class and therefore it is important to carefully balance the training datasets.

To aid comparison with the method proposed in [171], the same datasets used for training and validation have been used; 200 positive sRGB images and 109 negative images with a combined average image size of 3365×3029 pixels. Exemplary images in the positive and negative datasets are shown in Figure 3.5 and Figure 3.6 respectively.

Figure 3.5: Exemplary images from the positive dataset containing images of paintings by Souza-Cardoso.

The datasets have been split into training and validation sets where the quantities and selected images have been kept identical to those used in [171] for direct comparison. These quantities are shown in Table 3.1 below.

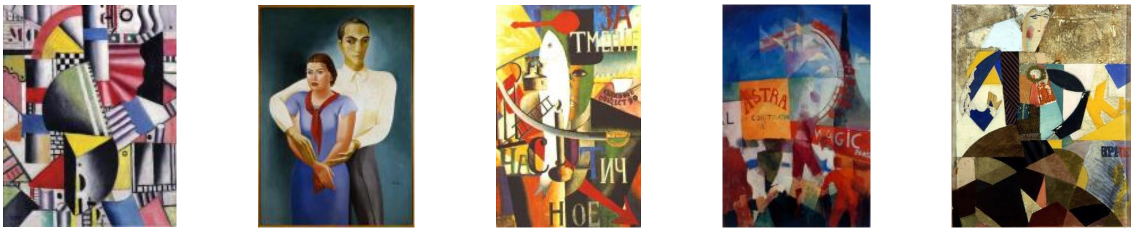

Figure 3.6: Exemplary images from the negative dataset containing images of paintings by Fernand Leger, Jose de Almada, Kazimir Malevich, Robert Delaunay and Eduardo Viana.

Table 3.1: Reference training and testing sets of Souza-Cardoso paintings.

Reference Set	Positive Paintings	Negative Paintings
Training Set	105	60
Validation Set	95	49

3.3 Pre-Processing and Data Augmentation

To tackle the problem described in Section 3.2 regarding the need for large datasets and to reduce the imbalance of data, a method to generate sample images from the original datasets is required. The proposed method is based on data augmentation whereby training samples are generated from the original full-sized images. The augmentation methodology proposed includes the following pre-processing steps which are used simultaneously:

- Random rotation between 0 and 360 degrees
- Random scaling between 10% and 100%
- Random vertical and horizontal reflection
- Random cropping with final size of 227×227 pixels

Using the above methodology, a large number of new sub-samples can be created from a single painting as required; for example, new sub-samples can be created for each training loop. The data augmentation process also helps the model proposed with the learning process by reducing overfitting to a certain degree due to the transformations applied to the images [223]. The scaling factor in particular allows the model to learn to recognise the brushstroke and other painted features at different scales or sizes. While the values of the rotation angle and randomness of the reflection are important, the selected values of the scaling range to be used are critical as must be set based on the overall average size of the training and validation images; low-resolution images would be unsuitable as the features of the painting at the scales provided would be too small or too large for the model.

Examples of the images generated using the data augmentation process proposed for Souza-Cardoso's painting P192 (Figure 3.7) are shown in Figure 3.8. As observed, multiple sections of the painting can be used for either training or validation.

Figure 3.7: Amadeo de Souza-Cardoso exemplary painting P192.

3.4 Test Results

The model proposed with two classification outputs was trained using the training and validation set of images described in Table 3.1 with random data augmentation on each epoch and with a maximum of 1000 epochs. Figure 3.9 shows the accuracy and loss of the training process.

As observed in Figure 3.9, the accuracy and loss seem to settle after 1000 iterations with an overall final classification accuracy of 75%. The results obtained suggested the trained model is suitable for the classification of the Souza-Cardoso paintings.

For comparison, the same set of paintings was analysed using the method proposed in [171] where a combination of techniques including SIFT, Gabor filtering, KM clustering,

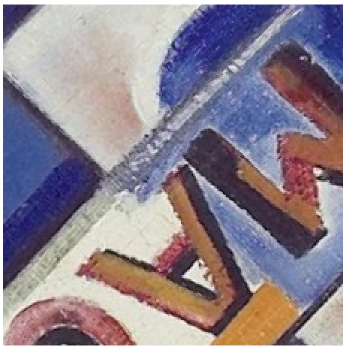
(a)


(b)


(c)

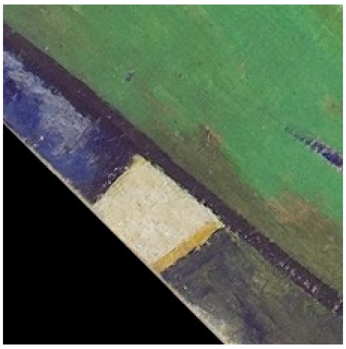
(d)


(e)


(f)

Figure 3.8: Exemplary data augmentation samples from panting P192 (Figure 3.7) used to train the proposed model.

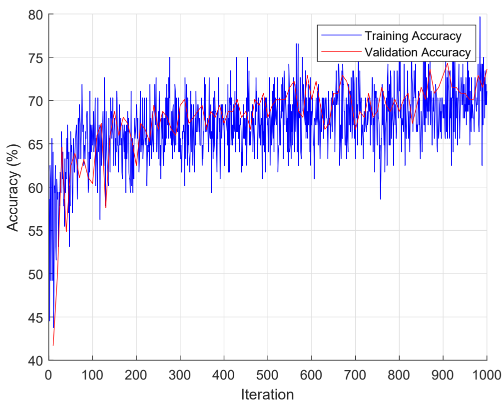

(a) Training Accuracy

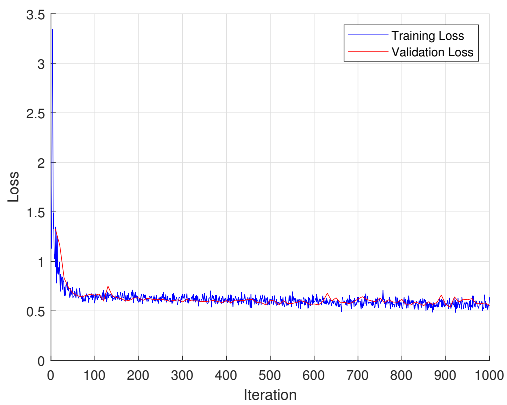

(b) Training Loss

Figure 3.9: Training accuracy and loss using the AlexNet-based model proposed.

TF-IDF processing and RLSC were used. The results of the classification process are shown in Table 3.2. Note that the method proposed in [171] was found to be biased due to the manner in which the training and validation sets were combined in the KM clustering step as described in section 2.6. The results reported herein for the method in [171] contain the correct, unbiased values obtained.

Table 3.2: Reference accuracy of the algorithm in [171] and the proposed method.

	Method from [171]								Method Proposed
No. of Words	100	200	400	1000	1200	1400	1600	2000	N/A
Accuracy	70.83	66.67	65.97	70.14	70.83	70.83	73.61	71.53	75.00

As the model used contains a spatial input size of 227×227 pixels the classification of paintings could be done using a single sub-sample of the painting, for example, a centrally cropped sample of the painting [54]. However, the approach proposed is to analyse multiple random samples of a painting that have been subjected to the same data augmentation process used during the training process. In this case, the approach proposed consists in calculating the fraction of samples predicted for that class as defined in Eq. 3.1:

$$P_{c_1} = \frac{1}{n}\sum_{i=1}^{n} x_i \quad \text{where} \quad x_i = \begin{cases} 1, & c_1 \\ 0, & \text{otherwise} \end{cases} \tag{3.1}$$

where P_{c_1} is the probability of the painting belonging to class 1 (positive class = Souza-Cardoso class), n is the total number of samples taken from the painting analysed, and x_i is a value of 1 if the i_{th} sample was predicted as c_1 (class 1, positive), or 0 otherwise.

The test dataset was analysed using the methodology proposed and using 100 samples per image. The probability of each image analysed belonging to Souza-Cardoso was then calculated using 3.1. Image classification was evaluated by thresholding the estimated probabilities in the range of 0.55 to 1.00 in steps of 0.05. The results are shown in Table 3.3 where the TP, TN, FP, FN, Accuracy (Acc), Precision (Prec), Recall (Rec) and F1-Score (F1-S) values have been calculated.

Figure 3.10 shows the values from Table 3.3 where a probability threshold of 0.8 was found to produce the best-balanced results between precision and recall. This is, the highest F1-S value is achieved. Classification of further images is therefore recommended using this threshold when using at least 100 augmented samples per image tested.

Table 3.3: Effect of thresholding the estimated probability using 100 samples per image.

Thold.	0.55	0.60	0.65	0.70	0.75	0.80	0.85	0.90	0.95	1.00
TP	95	95	95	95	95	94	87	78	64	28
TN	7	9	11	13	16	18	25	35	38	47
FP	42	40	38	36	33	31	24	14	11	2
FN	0	0	0	0	0	1	8	17	31	67
Acc.	0.708	0.722	0.736	0.750	0.771	0.778	0.778	0.785	0.708	0.521
Prec.	0.693	0.704	0.714	0.725	0.742	0.752	0.784	0.848	0.853	0.933
Rec.	1.000	1.000	1.000	1.000	1.000	0.989	0.916	0.821	0.674	0.295
F1-S	0.819	0.826	0.833	0.841	0.852	0.855	0.845	0.834	0.753	0.448

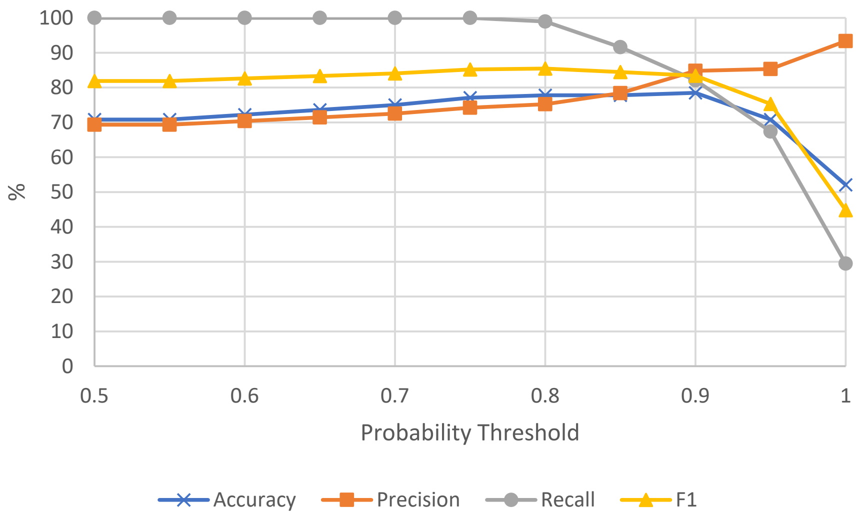

Figure 3.10: Accuracy, Precision, Recall and F1-Score of model proposed for the test set.

3.5 Authentication Through Brushstroke Analysis

To evaluate the suitability of the proposed method for authentication of Souza-Cardoso artwork, the same 11 images of paintings belonging to Souza-Cardoso plus a *Fake* image created at DCR and used in [171] were evaluated using the trained deep learning model. An overview of the test images is shown in Figure 3.11 (numbering corresponding to inventory code at CAM [47, 48, 171]).

For authentication, the numeric probability of each of the 12 images being authentic is required. Thus, 1000 samples per image were evaluated and the probability was calculated using Eq. 3.1. The results are summarised in Table 3.4 where high values were obtained for the authentic images. Using the threshold of 0.8 proposed in section 3.4 would result

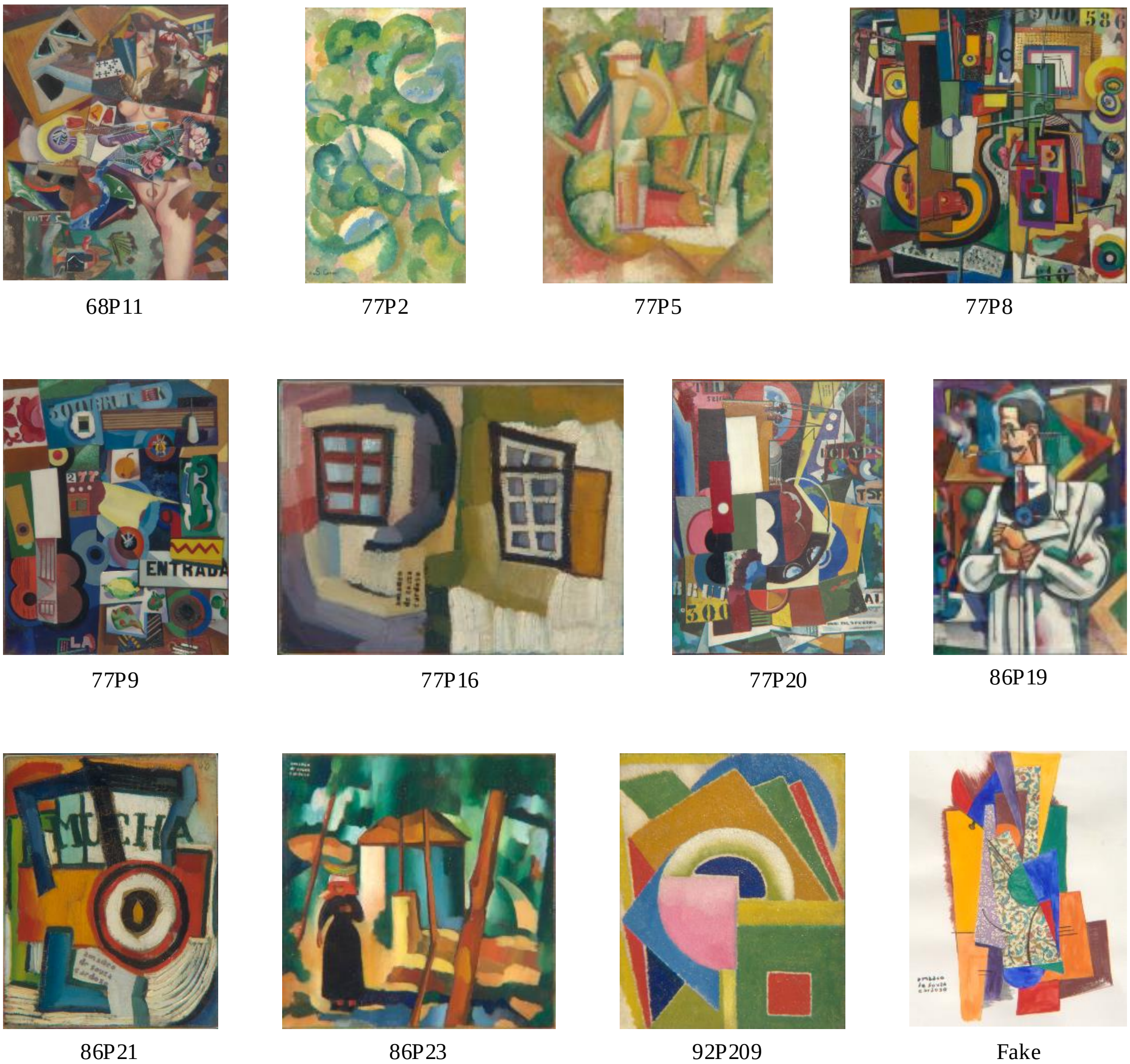

Figure 3.11: Test images used for evaluation.

in correct classification of all 12 images analysed. The results are thus encouraging and support the use of deep learning techniques as a tool for the authentication of artwork.

Table 3.4: Probability of authenticity using brushstroke analysis.

Painting	Probability of Authenticity
68P11	89.20%
77P2	100.00%
77P5	100.00%
77P8	95.10%

Continued on next page

Table 3.4: Probability of authenticity using brushstroke analysis. (Continued)

Painting	Probability of Authenticity
77P9	86.90%
77P16	97.00%
77P20	91.00%
86P19	93.50%
86P21	99.40%
86P23	95.60%
92P209	99.90%
Fake	53.60%

3.6 Further Testing

The suitability of the proposed deep learning model only using a single sample for artist identification was evaluated by means of training and testing the network with a variety of datasets [54]. The first additional dataset included a collection of 39 drawings by Amadeo de Souza-Cardoso obtained from the Calouste Gulbenkian Museum; 29 loose watercolour drawings (Figure 3.12) and 10 drawings from the manuscript *La Légende de Saint-Julien L'hospitalier* (Figure 3.13). These drawings were added to the test set only and evaluated with the proposed model and the algorithm in [171]. The classification results shown in Table 3.5 show an overall higher accuracy obtained with the model proposed while the algorithm in [171] did not produce better results with the increasing number of visual words.

(a) (b) (c) (d)

Figure 3.12: Sample drawings by Souza-Cardoso.

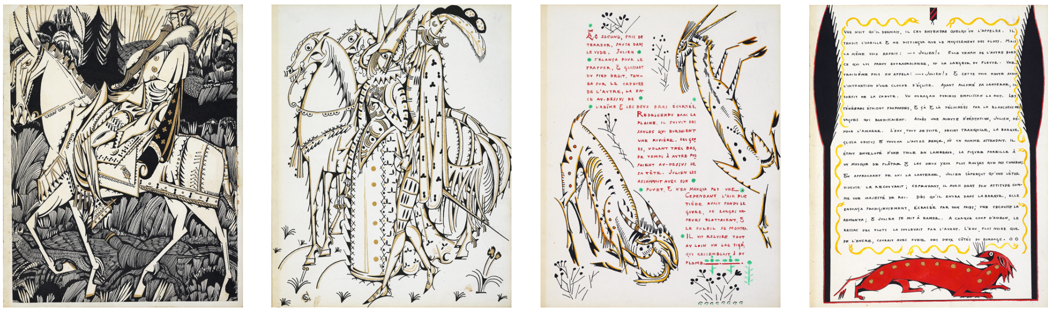

(a) (b) (c) (d)

Figure 3.13: Sample drawings by Souza-Cardoso from *La Légende de Saint-Julien L'hospitalier*.

Table 3.5: Classification accuracy of the algorithm in [171] and the proposed model using paintings + 39 drawings.

	Method from [171]								Method Proposed
No. of Words	100	200	400	1000	1200	1400	1600	2000	N/A
Accuracy	64.48	61.75	62.84	65.03	66.67	65.57	68.31	66.67	73.77

The second additional set of data included 91 paintings from the Chinese artist Daqian Zhang [1]. Samples of the images analysed are shown in Figure 3.14. Adding these to the negative test set produced significantly lower accuracies for the model proposed than for the algorithm in [171] as shown in Table 3.6. This is highly likely due to our model not being trained with examples of any paintings other than Souza-Cardoso's and his contemporaries.

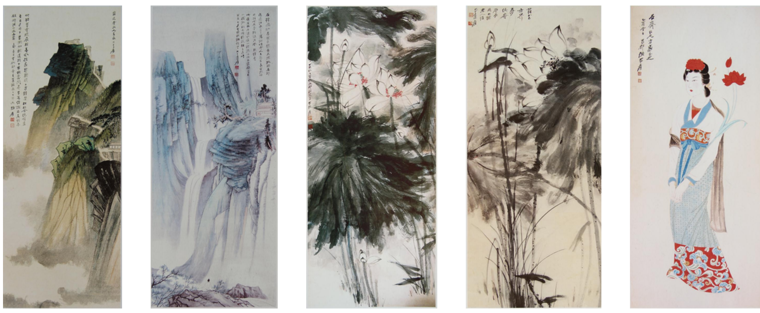

(a) (b) (c) (d) (e)

Figure 3.14: Sample Chinese drawings.

[1] Images courtesy of Pennsylvania State University.

Table 3.6: Classification accuracy of the algorithm in [171] and the proposed model using paintings by Souza-Cardoso and Chinese artist Daqian Zhang.

	Method from [171]								**Method Proposed**
No. of Words	100	200	400	1000	1200	1400	1600	2000	N/A
Accuracy	75.32	78.30	75.32	78.30	79.15	78.30	81.70	79.15	51.06

The third dataset included 210 paintings by the Dutch painter Vincent van Gogh [2] (Figure 3.15). These were added to the test set and evaluated using both methods. The classification results are shown in Table 3.7 where the accuracy of both methods was found to be low as many of the newly introduced test paintings were misclassified as positive, i.e., belonging to Souza-Cardoso.

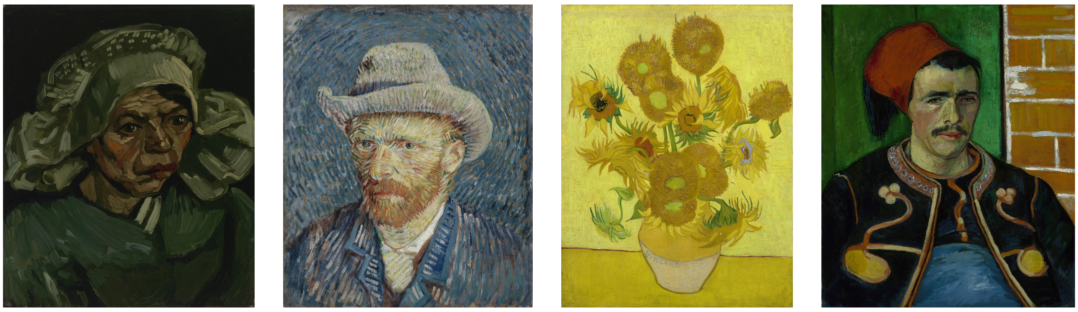

(a) (b) (c) (d)

Figure 3.15: Sample Vincent van Gogh drawings.

Table 3.7: Classification accuracy of the methodology in [171] and the proposed method using paintings by Souza-Cardoso and Dutch artist Vincent van Gogh.

	Method from [171]								**Method Proposed**
No. of Words	100	200	400	1000	1200	1400	1600	2000	N/A
Accuracy	57.34	57.34	53.67	50.00	52.54	52.26	50.28	52.82	46.61

To further evaluate the network proposed and to understand if it can be used to distinguish artists other than Souza-Cardoso and his contemporaries, the training set was updated to include only Chinese artwork. This is, the positive dataset was updated to include 46 paintings from Daqian Zhang only with the negative dataset set to include 49 paintings of his contemporaries. The test dataset was updated to include 45 and 49

[2] Images courtesy of the van Gogh Museum.

paintings respectively to keep the training and test set as balanced as possible. Table 3.8 shows the results of the classification process which shows higher classification accuracy than the algorithm in [171].

Table 3.8: Classification accuracy of the methodology in [171] and the proposed method using paintings by Daqian Zhang and his contemporaries.

	Method from [171]								Method Proposed
No. of Words	100	200	400	1000	1200	1400	1600	2000	N/A
Accuracy	68.09	70.21	70.21	69.15	70.21	68.09	69.15	70.21	86.17

Finally, a similar assessment was performed using 105 paintings from Vincent van Gogh and 37 from his contemporaries for training and with 105 and 36 paintings for testing respectively. The classification results are shown in Table 3.9.

Table 3.9: Classification accuracy of the methodology in [171] and the proposed method using paintings by Vincent van Gogh and his contemporaries.

	Method from [171]								Method Proposed
No. of Words	100	200	400	1000	1200	1400	1600	2000	N/A
Accuracy	72.34	75.18	74.47	78.01	75.89	76.60	76.60	77.30	77.30

3.7 Discussion

The original method designed in [171] was found to produce biased results as discussed in section 2.6. The unbiased results, where the validation/test set is fully segregated from the training process, produced low-accuracy classification results. The method proposed here, on the other hand, resulted in significantly higher classification accuracy of both the training and validation/test sets. The improvement is attributed to the more complex feature extraction produced by the convolution layers and the higher number of features produced and learnable parameters of the model compared to a standard RLSC model as used in [171].

In both cases, the method proposed in [171] and the method proposed in this work, training requires a significant amount of data for the feature learning process to be successful. This aspect however is very challenging in the art world given the limited number of artworks of a single artist. As proposed here, a large number of samples can be generated via data augmentation. This process was proven to be useful to achieve a high classification accuracy. The number of augmented samples generated however must be kept low enough to prevent overfitting but large enough to generate a variance in the features learned.

The size of the images to evaluate must be consistent with the average size of the images used for training. This is, the quality and size of any image to be analysed must be sufficiently large to ensure the data augmentation process generates images whose features are suitable for analysis; augmented images of size 227×227 pixels must contain sufficient detail for analysis. In the case of the images used for training and validation, the average image size of the sets used is 3365×3029 pixels. The use of significantly different size images will likely result in features not being identified correctly by the convolution process ultimately leading to incorrect classification.

Finally, the method proposed was found to be suitable for the classification of genres and other artists. The results obtained support the use of the model in other settings where art attribution or author identification is required. Although the classification process was limited to 2 classes per test, multiple classes can be added to the final classification layer of the model to increase the number of outputs and use the model in multi-author classification applications.

4

Pigment Analysis

This chapter discusses the methodology proposed for pigment analysis. The methodology focuses on the identification of pure pigments and pigment mixtures used in artwork by Amadeo de Souza-Cardoso. Results obtained are compared against the reference method proposed in [171].

4.1 Pure Pigment Identification

The identification of pure pigments is a task that can be achieved using a variety of tools including mathematical approaches like FCLS, spectral matching functions like SAM, or machine learning methods like SVM or other classifiers. These typically involve the correlation of colour components or spectral reflectances to a predetermined reference database considered as ground truth. Where mathematical analyses are used, the spectral or colour similarity is usually quantified followed by a thresholding function that discriminates those points that exhibit a significant difference in either colour or spectral components. Machine learning methods, on the other hand, classify the points analysed into a finite number of classes and thus require exemplary data of non-pure pigments.

Other methods to identify pure pigments include analytical techniques like μEDXRF that provide qualitative and quantitative information of points analysed. The data obtained can then be used to match the analysed point against a reference set of data for classification. The disadvantage of such techniques is that these are typically point-based, this is, they provide information of a small sample area only making analysis of a full painting a laborious and expensive process. In [171], an image segmentation method was proposed using the spectral metric function SAM and a thresholding function. SAM, defined in Eq. 4.1, is calculated for all points of the reference reflectance z and the reflectance evaluated $\hat{z}$. This method proposed extending the results of a point-based analysis of a segmented area to all points within the segmented area. The segmentation process, thresholding function and spectral metric function used are therefore critical and require fine-tuning to achieve optimal results. The use of the SAM function, while widely used, has been shown to be sub-optimal in certain cases and therefore other approaches are recommended.

$$SAM = \cos^{-1} \frac{\sum_{i=1}^{n} \hat{z}_i z_i}{\sqrt{\sum_{i=1}^{n} \hat{z}_i^2 \sum_{i=1}^{n} z_i^2}} \tag{4.1}$$

4.1.1 Pure Pigment Deep Learning Model

In this research, we propose the use of a deep learning model for image segmentation based on the analysis of colour reflectance. To achieve this, we propose the analysis of a hyperspectral image $\mathbf{Z} \in \mathbb{R}^{W \times H \times B}$ with width W, height H and B spectral bands of a painting of interest for classification using the reflectances of the reference database $\mathbf{S} \in \mathbb{R}^{B}$.

The deep learning model proposed [53], shown in Figure 4.1, includes a three-branch, mixed-input network for the analysis of hyperspectral data.

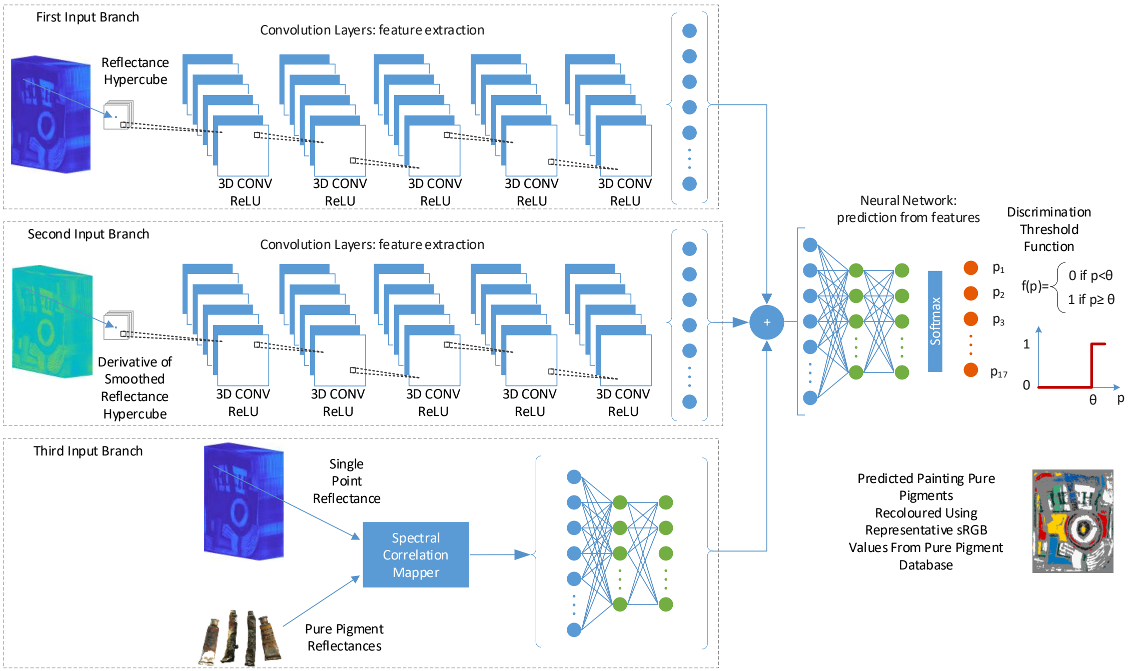

Figure 4.1: Block diagram of the three-branch, mixed-input deep learning model proposed for pure pigment classification.

The first input branch of the model implements a convolutional neural network that analyses a hypercube centred around a point of interest of the hyperspectral image $\mathbf{Z}$ being analysed. This analysis highlights features in the hypercube at different wavelengths. The spatial nature of the data on the other hand allows the identification of the transitions between the central and adjacent points. The second input branch of the network processes the derivative of the hypercube reflectances after smoothing using a Savitzky-Golay filter of size 9 and degree 2. This pre-processing step de-noises the hypercube reflectances while enhancing points of inflexion in the reflectance and removing any offset caused by differences in illumination during the acquisition process.

The size of the hypercube around a pixel of interest has been set to $9 \times 9 \times 33$. The spatial size was chosen to be small enough to ensure sufficient details of adjacent points are included, but not too large to not include too much data that would be detrimental to the performance of the classification process.

The third input branch of the model contains the measured error of the central point reflectance and each of the reflectances in the reference database. For this model the error is calculated using the Spectral Correlation Mapper (SCM) metric function which estimates the correlation between two spectral signatures [44, 45]. Unlike SAM, SCM allows distinction of negative correlation and tends to perform better in the presence of a larger number of reference reflectances [222]. SCM is defined in Eq. 4.2 where z is the reference reflectance $\hat{z}$ the reflectance evaluated.

$$SCM = \frac{\sum(\hat{z}_i - \overline{\hat{z}})(z_i - \overline{z})}{\sqrt{\sum(\hat{z}_i - \overline{\hat{z}})^2 \sum(z_i - \overline{z})^2}} \tag{4.2}$$

The output of the three parts of the model is flattened and concatenated. Then, the data are analysed by a series of MLP layers that reduce the dimensionality of the data before being passed through to a Softmax activation function. This computes the probability of the input data belonging to one of the pigments in the reference database. To further improve the classification, a thresholding function is used on the computed probabilities to discard borderline predictions.

4.1.2 Reference Pigments

To train the model proposed, a set of ground truth data is required. This includes a dictionary of reference reflectances and, most importantly, hyperspectral imagery with ground truth labels. For the dictionary of reference pigments, a set of 16 pure pigment reflectances have been selected from a hyperspectral image of samples provided in [171]. The reflectances have a range of 400nm to 720nm in steps of 10nm and include the pigments listed below. Further information is available in Appendix A:

- Cobalt Violet
- Chinese Vermilion
- Carmine Lake
- Terra Rosa
- Raw Sienna
- Yellow Ochre
- Chrome Yellow
- Cadmium Orange

- Cobalt Blue
- Cerulean Blue
- Prussian Blue
- Ultramarine
- Viridian
- Emerald Green
- Lead White
- Ivory Black

An overview of the reflectances in the pure pigment database is shown in Figure 4.2.

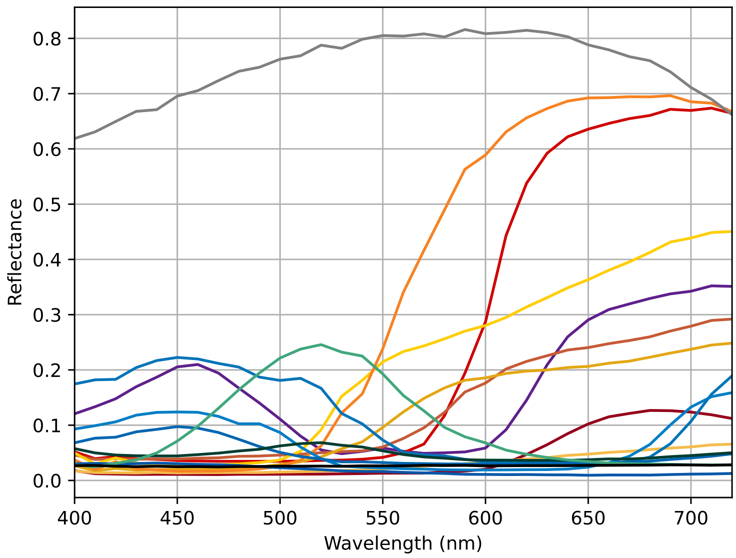

Figure 4.2: Reflectances in the reference pigment database. The colour of the reflectances is set to a representative sRGB colour with white shown in grey.

4.1.3 Data Augmentation: Pure Pigments

To train the model to classify correctly a sample reflectance into any of the 16 pure pigments of the reference database or a non-pure pigment, a large number of ground truth samples is required for each of these 17 classes. Data however are limited so to overcome this problem the use of the following data augmentation processes is proposed.

Data augmentation for the generation of pure pigment samples can be achieved by generating samples of a pure pigment with additive white Gaussian noise as in Eq.4.3 where P_λ is the noise-free reflectance, N_λ is the noise and $P_{\lambda N}$ the noisy reflectance. This is random noise with a probability distribution with zero mean and finite variance σ^2.

$$\begin{aligned} P_{\lambda N} &= P_\lambda + N_\lambda \\ N_\lambda &\sim N(0, \sigma^2) \end{aligned} \tag{4.3}$$

In this task, a Signal to Noise Ratio (SNR) value of 30dB was used to generate pure pigment samples. This value is low enough to ensure the data are still statistically representative of the pure pigment reflectance. In addition to this, a random reflectance intensity offset drawn from a normal distribution centred at 0 and with a standard deviation of 0.005 was added to the new sample. This simulates changes in the acquisition process (e.g., changes in illumination). Figure 4.3 shows an example of augmented reflectances of Cerulean Blue using the methodology proposed.

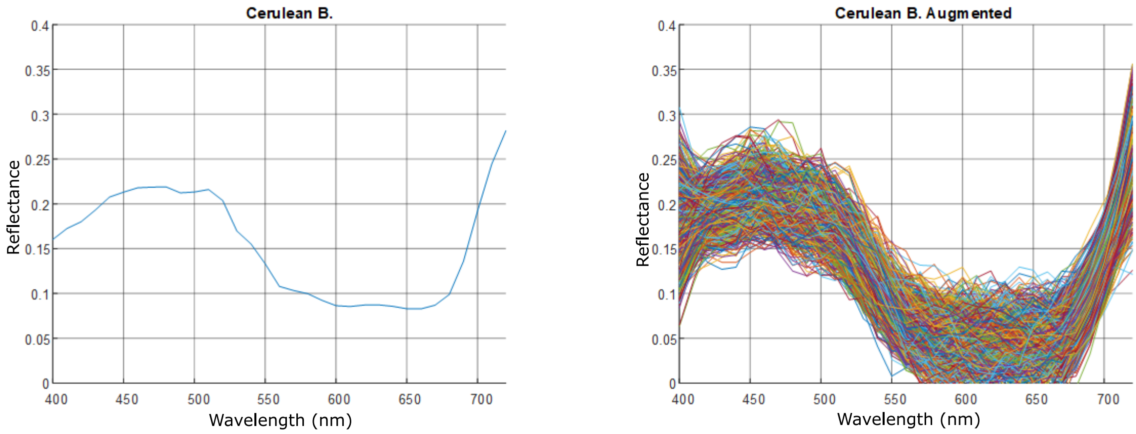

Figure 4.3: Reflectance of Cerulean Blue (left) and augmented reflectances using the method proposed (right).

4.1.4 Data Augmentation: Artificial Mixtures

For non-pure pigment identification, reflectances representative of mixed pigments or pigments not included in the reference database are required. To achieve this, a new expanded dataset can be generated by artificially mixing the reflectances of pigments in the reference database using colour mixing theory. In [171], artificial mixtures were generated using the linear mixing model in Eq. 4.4, where c_i is the proportion of the i^{th} pigment reflectance $P_{i,\lambda}$ and P_λ is the resulting mix pigment reflectance.

$$P_\lambda = \sum_{i=1}^{n} P_{i,\lambda} c_i \tag{4.4}$$

In colour mixing theory, additive mixing is suitable for mixing colours in lighting applications where the superposition of all colours yields white as shown in Figure 4.4. However, colour mixing of paints produces a different result where a darker colour is generated which makes additive mixing an unsuitable model for the generation of artificial colour mixtures of oil paint pigments.

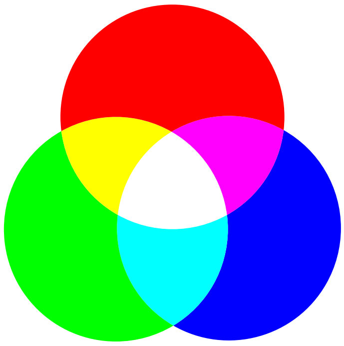

(a) (b)

Figure 4.4: Effect of additive (a) vs. subtractive (b) colour mixing.

In this research, we propose the use of the more suitable subtractive colour mixing model defined in Eq. 4.5 [226] where c_i is the proportion of the i^{th} pigment reflectance $P_{i,\lambda}$ and P_λ is the resulting mix pigment reflectance with the sum of all proportions equal to 1. Alternative colour mixing models like the Kubelka-Munk model [145] can produce improved results if parameters like the absorption and backscattering coefficients of the base pigments are known.

$$P_\lambda = \prod_{i=1}^{n} P_{i,\lambda}^{c_i} \tag{4.5}$$

The effect of applying Eq. 4.5 can be observed in Figure 4.5; additive mixing increases the reflectances linearly without correctly handling the amplitude mix. This effect distorts the colour as it increases the overall amplitude of the mix at all wavelengths.

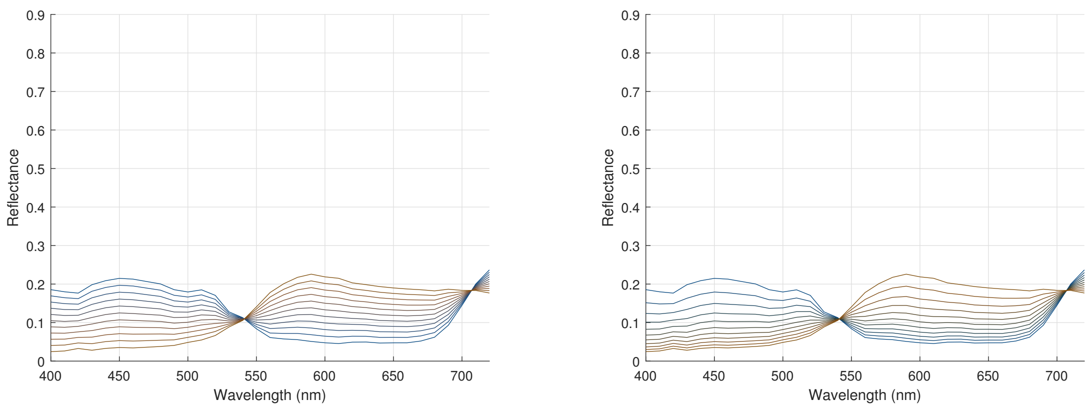

(a) (b)

Figure 4.5: Effect of additive (a) vs. subtractive (b) colour mixing using Cerulean Blue and Yellow Ochre pigments.

Another example is shown in Figure 4.6 where the effect is more visible when Black and White are used in the mix with Cerulean Blue. For subtractive mixing, the blue tone and reflectance shape are preserved for mixes as low as 10% of blue and 90% white. On the other hand, additive mixing changes the blue tone to white at a much faster rate. This confirms the suitability of the subtractive mixing model for the generation of all hypothetical mixing of paint pigments.

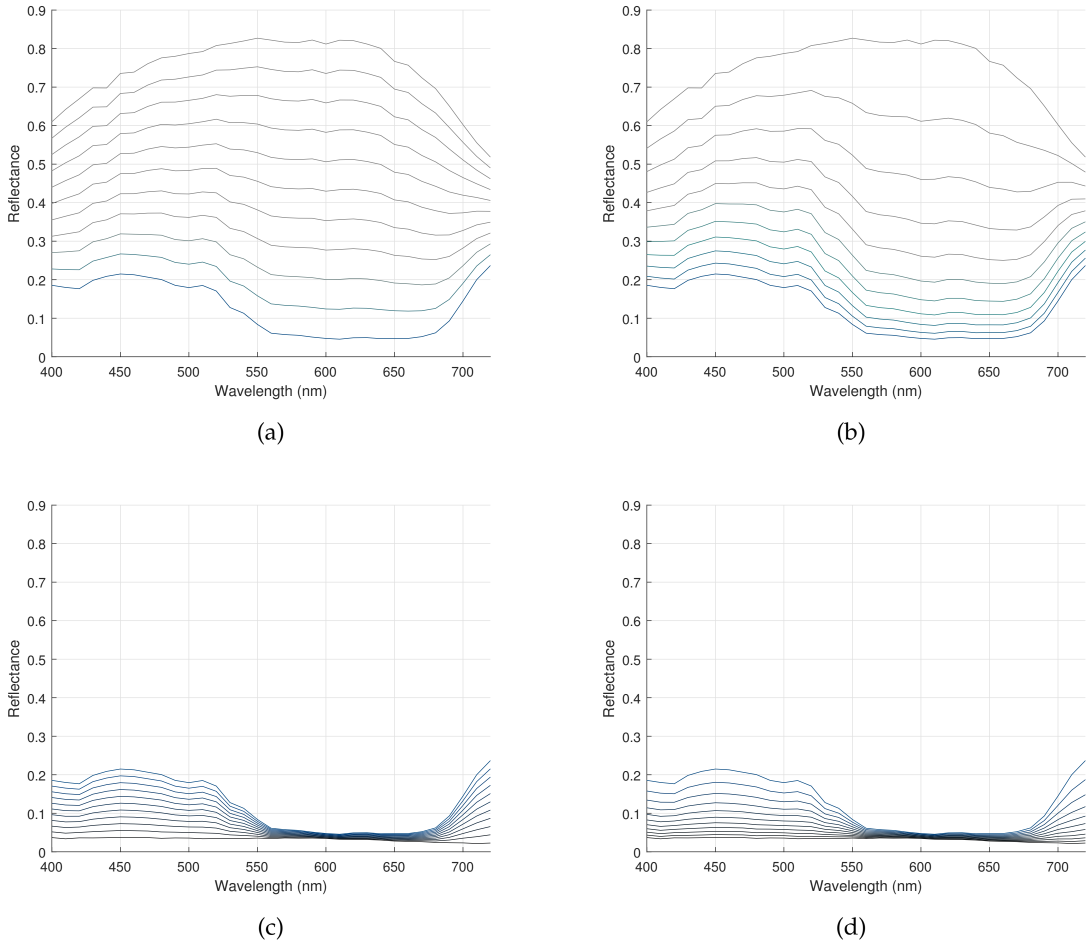

Figure 4.6: Additive (a,c) vs. subtractive (b,d) mixing of Cerulean Blue and White/Black.

To generate artificial pigment mixtures, the number of combinations $C_{(n,r)}$ choosing the number of pigments r from the total number of pigments n is calculated using Eq. 4.6, corresponding to a combination without repetition.

$$C_{(n,r)} = \frac{n!}{r!(n-r)!} \tag{4.6}$$

For each combination of pigments, artificial mixtures are generated using increments of 10%. Thus, the number of artificial mixtures for 2 out of 16 pigments and 3 out of 16 pigments is 1080 and 20160 respectively, this is, a total of 21240 unique artificial reflectances. These are shown in Figure 4.7 and are used in the training image described in Section 4.1.5.

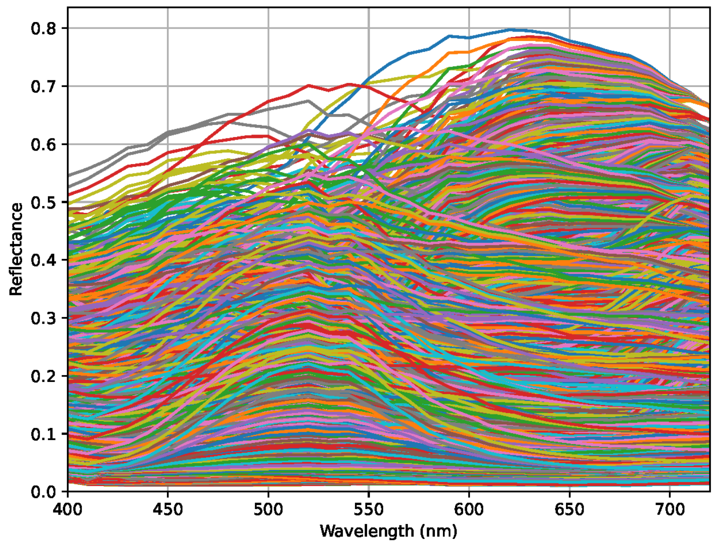

Figure 4.7: Artificially generated mixed pigment reflectances using subtractive mixing of 3 out of 16 pigments.

4.1.5 Training Image

To train the model described in Section 4.1.1, a ground truth hypercube is required, this is, a hyperspectral image where the label of each pixel is known. Obtaining such data can be impossible since the number of artworks produced by an artist, in our case Souza-Cardoso, is very limited. Furthermore, a well-preserved painting where the label of each and all points is known is not available. To solve this problem, we propose the generation of a hyperspectral training image using augmented data synthesised using the methods described in sections 4.1.3 and 4.1.4. The hyperspectral image must contain augmented samples of each reflectance in the reference database (16 in total), plus a collection of mixed pigments to represent the non-pure class.

To understand the effect of the training image during the design and evaluation of the model, preliminary results were obtained where a training image was constructed using vertical bars filled with reflectances of the pigments in the reference database and artificial mixture reflectances. The labels of the points in the generated image correspond to the zero-based index of the pure pigment (0-15) with artificial mixtures set to 16. The sRGB representation artificial image generated using the D65 illuminant is shown in Figure 4.8.

The model was trained with the training image for 5 epochs and using a sample patch of size $25 \times 25 \times 33$. The sample patches were then split into 70% for training and 30% for testing. The final probability thresholding function was not used in this evaluation.

The training image was evaluated with the trained model to determine its suitability. Figure 4.9 illustrates the classification results where the training, Figure 4.9(a), and predicted, Figure 4.9(b), images were recoloured with sRGB colours representative of each pure pigment in the database plus grey for mixtures. A greyscale version of the training image is shown in Figure 4.9(c) where pixels classified incorrectly are coloured in red. Note however that in this case all pixels were classified correctly so no red pixels are visible.

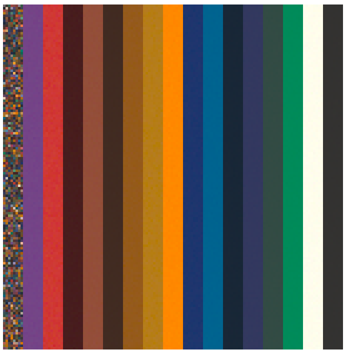

Figure 4.8: Artificially generated training image with vertical bars containing pure and mixed pigment reflectances.

(a) (b) (c)

Figure 4.9: Training image built using vertical bars: (a) ground truth and (b) predicted. Greyscale image highlighting misclassified pixels in red (c).

Although no misclassifications were observed, evaluating an actual hyperspectral painting with the trained model produced images where vertical artefacts were observed as shown in Figure 4.10. These were thought to be a result of the geometrical content of the training image, this is, colour transitions are present in the horizontal access only.

The training image was rotated to generate horizontal bars as shown in Figure 4.11. The model was trained with the updated image which was then evaluated with the trained model. The resulting classification results of the training image are shown in Figure 4.12 where no misclassifications were observed.

Evaluating a hyperspectral image of a painting by Souza-Cardoso produced horizontal artefacts as shown in Figure 4.13 confirming that the geometrical content of the training image affects the performance of the model.

To address the effect of the training image on the performance of the model, we propose the use of a hyperspectral training image containing 50×50 squares of size 10×10 pixels each. Each square contains either augmented pure pigment reflectances or artificial mix

Figure 4.10: Classification results of painting 86P21 when using vertical bars in the training image.

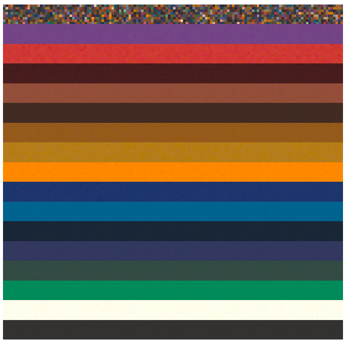

Figure 4.11: Artificially generated training image with vertical bars containing pure and mixed pigment reflectances.

(a) (b) (c)

Figure 4.12: Training image built using horizontal bars: (a) ground truth and (b) predicted. Greyscale image highlighting misclassified pixels in red (c).

Figure 4.13: Classification results of painting 86P21 when using horizontal bars in the training image.

pigment reflectances and is arranged in an alternating manner in both horizontal and vertical directions as shown in Figure 4.14.

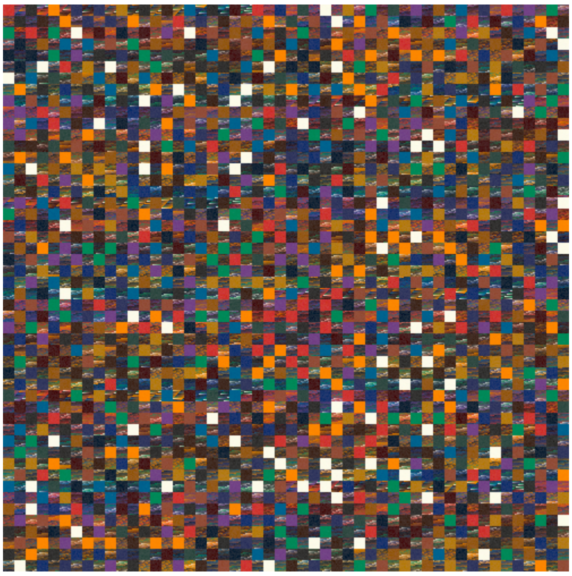

Figure 4.14: sRGB representation of the artificially generated training image.

4.1.6 Predicted Pure Pigments

The three-input model was trained using the training image generated following the process described in Section 4.1.5. From this artificial image, 250000 hypercubes of size $9 \times 9 \times 33$ were created. Hypercubes extending beyond the edge of the training image were padded with zeros. These hypercubes were used for the first input. For the second input, the derivative of each reflectance was calculated along the wavelength direction. Finally, for the third input, the SCM value of the central point of each hypercube and each entry in the pure pigment reference database was calculated. The training data were split using 70% of the values for training and 30% for validation. Training of the model was stopped after 20 epochs to prevent overfitting.

The final classification of each hypercube was achieved by applying a threshold of 0.90 to the predicted output of the model. This value was found experimentally and proved to be adequate to reject borderline predictions. The result of the training process and classification of the training image is shown in Figure 4.15(b) where predicted pure pigment points have been coloured using representative sRGB colour components of the predicted pigment. Points classified as non-pure are recoloured in grey.

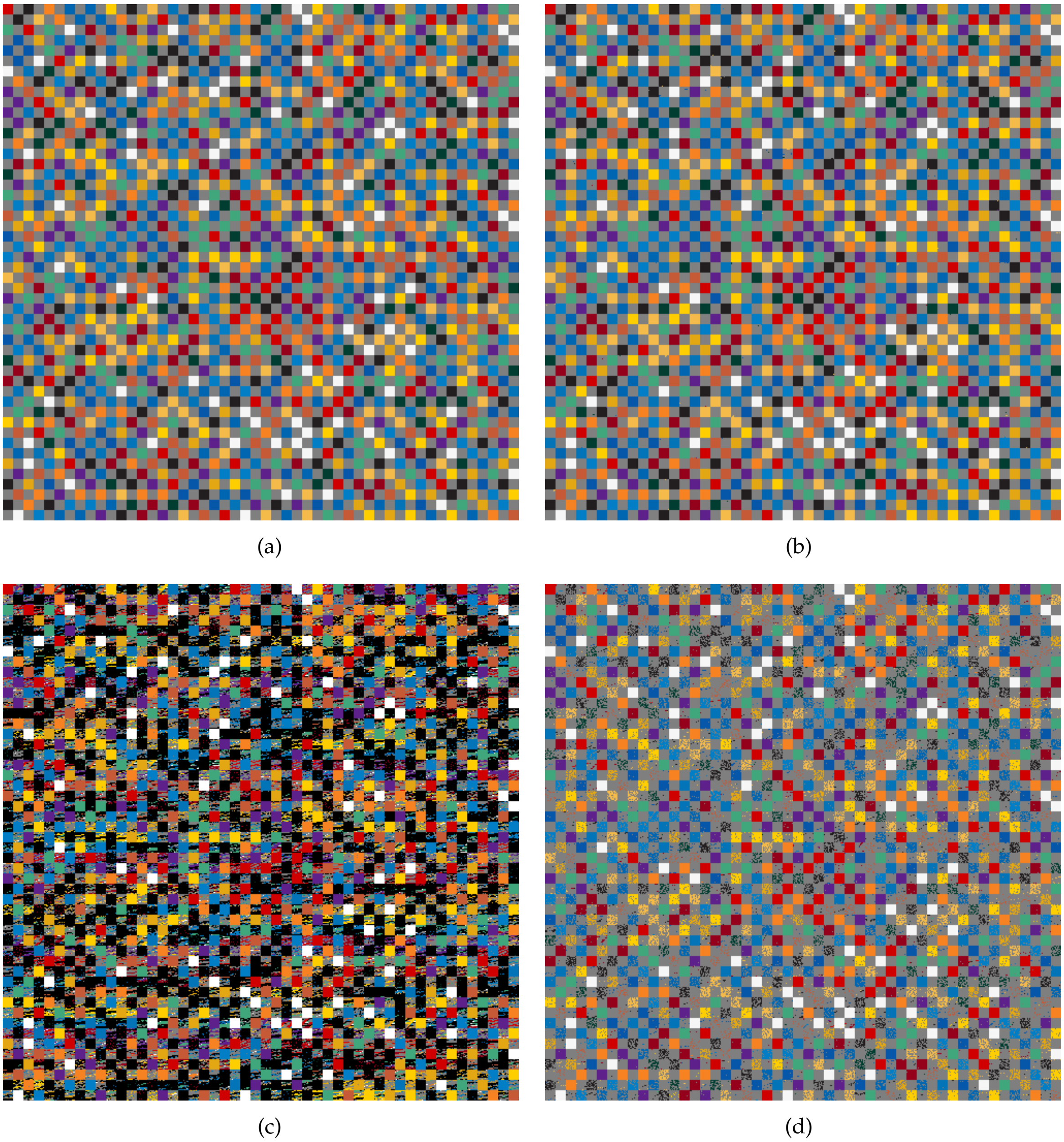

Figure 4.15: Training image results: (a) ground truth, (b) predicted using the proposed model, (c) predicted using the validated method in [171] and (d) using FCLS.

To compare the performance of the proposed method, the same hyperspectral training image was analysed with the algorithm in [171] which is summarised as:

- Measuring the Euclidean distance of the reflectance of the point analysed and the reflectance of the Ivory Black pigment
- Measuring the Euclidean distance of the reflectance of the point analysed and the reflectance of the Lead White pigment
- If the distance to the Lead White reflectance is greater than a threshold of 4.0 and the distance to the Ivory Black reflectance is less than 0.29 then mark the point as Ivory Black
- If the distance to Lead White reflectance is less than 2.06 then mark the point as Lead White
- Find the smallest SAM value of the derivative of the smoothed point reflectance and the derivative of the reflectance of each pigment in the database
- If the smallest value is less than 0.75 times the second smallest value then mark the point as pure pigment

The result of classifying each point in the hyperspectral training image is shown in Figure 4.15(c). As observed, a large number of mixed pigments were misclassified as Ivory Black resulting in low accuracy as observed in Table 4.1.

Table 4.1: Classification accuracy of the artificially generated hyperspectral image.

Classification Method	**Classification Accuracy**
Method Proposed	99.93%
Method in [171]	54.59%
FCLS	88.67%

In addition to the algorithm in [171], the FCLS linear unmixing method defined in [112] was evaluated for comparative purposes. FCLS solves the linear mixing model in Eq. 4.7 where r is the reflectance of a given pixel, $\mathbf{M}$ is the endmembers matrix, α the abundance matrix and n noise.

$$r = \mathbf{M}\alpha + n \tag{4.7}$$

FCLS approximates a given reflectance by linearly mixing a subset of reflectances and minimising the error. This results in reflectances that typically contain a large number of base reflectances albeit in small proportions or abundances, some more than others.

However, using a high threshold on these abundances can be used to determine the purity of a given reflectance. This is, if the i^{th} abundance is higher than a high threshold, e.g. 90%, then the reflectance analysed can be considered "pure" and belonging to the i^{th} pigment in the reference database. All points of the training image were classified using this approach with the result shown in Figure 4.15(d) where a good correlation of the ground truth to the predicted pigments is observed. The classification accuracy with FCLS, Table 4.1, was found to be higher than the one obtained with the method in [171] but lower than the classification accuracy of the method proposed in this work.

To evaluate the algorithm, 12 hyperspectral images used by [171] were used. These images include 11 off images corresponding to paintings from Souza-Cardoso plus 1 *Fake* image created DCR. These test images were evaluated with the three algorithms for comparison. The results of the classification process are summarised in Table 4.2 with Figure 4.16 showing the classification outcome for painting 86P21. A good visual correlation can be observed between the original painting and the predicted pure pigment areas using our method and the algorithm in [171]. FCLS on the other hand did not predict large pure pigment areas; FCLS synthesised most points as a linear combination of multiple reflectances.

Table 4.2: Pure pigment area prediction of each painting in the test dataset.

Painting	**Proposed Model**	**Method in [171]**	**FCLS**
68P11	39.26%	43.60%	1.85%
77P2	50.95%	26.94%	0.76%
77P5	61.31%	32.00%	1.90%
77P8	36.89%	56.41%	6.36%
77P9	51.91%	59.87%	5.81%
77P16	52.52%	48.09%	2.18%
77P20	41.35%	51.29%	3.51%
86P19	49.49%	60.92%	3.04%
86P21	46.53%	58.28%	7.79%
86P23	54.63%	56.65%	9.11%
92P209	43.70%	42.17%	4.44%
Fake	78.34%	75.36%	57.58%

The proposed methodology to generate an artificial hyperspectral image was successfully used to train the model for pure pigment identification. The results obtained show a good visual correlation with areas in the paintings that, to the human eye, closely resemble

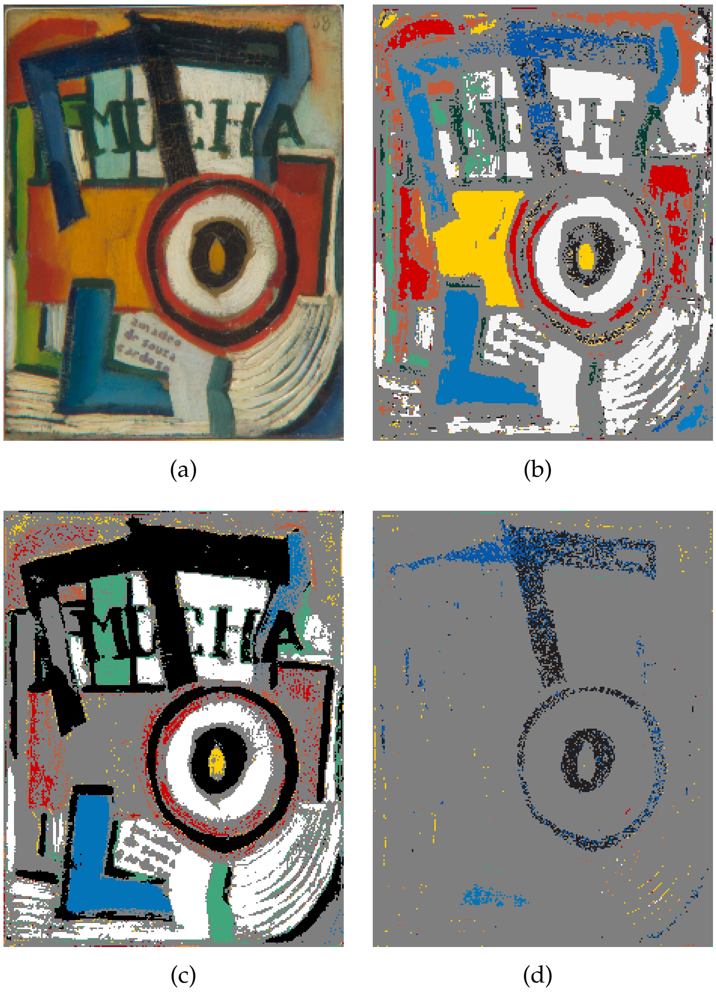

Figure 4.16: (a) sRGB representation of the hyperspectral image 86P21, predicted pure pigments using (b) the proposed method, (c) the method in [171] and (d) FCLS.

the pure pigments in the reference database. Similarly, the algorithm proposed in [171] shows a good correlation of pigment colours. The former method however required less manual tuning than the latter method which, using the values provided in the source code supplied, did not generate significantly better results. FCLS on the other hand failed to produce high levels of single pigment purity using a thresholding function. This is probably due to the error minimisation algorithm and the discrepancies in amplitudes between the reflectances of the reference database and those of the hyperspectral images. The overall image segmentation result using deep learning is satisfactory and paves the path for further development. In particular, improved connectivity between the multiple inputs of the network could be explored to increase the weight given to the third numerical input. Similarly, improvements can be made on the training image where the use of geometrical features other than squares could lead to better detection of pure areas.

4.2 Mixed Pigment Identification

Identification of mixed pigments using hyperspectral imaging and machine learning can be pursued through various options. In classification where a given test reflectance is assigned to a predetermined set of mixtures, requires a large number of possible mixtures or classes. However, the possible number of mixtures that an artist can generate by manually mixing pigments can be infinite which makes this approach not feasible. An alternative to this approach is the estimation of the abundances or fraction of the required reference pigments to approximate the reflectance analysed as a mixture of these pigments. This task could be achieved if a model is designed such that the inputs to this are the discrete points that form a given reflectance and the outputs or labels, the associated fraction of the pigments that when combined, approximate the input reflectance.

Prediction of pigment mixture fractions was evaluated where a 5-layer deep network of fully-connected layers with 33, 35, 33, 25 and 20 neurons respectively was trained. 44880 artificial mixtures were generated using subtractive mixing of up to 3 pigments in steps of 10% with the pigment database used in [171] and including Green Cd. The reflectance of each point in the hypercube of painting 68P11 was evaluated with the trained network to predict the fraction of each pigment required to reconstruct the reflectance. The estimated reflectance was then back-calculated using the subtractive mixing model in Eq. 4.5 and the equivalent sRGB image estimated assuming the D65 illuminant. The resulting sRGB image is shown in Figure 4.17 along with the sRGB image estimated from the original hyperspectral image. Although the visual results were encouraging, they required an increase in brightness. This might be due to fractions generated including negative values as the output of the model was unconstrained.

(a) (b)

Figure 4.17: sRGB representation of 68P11 from (a) the original hyperspectral image and (b) from an unconstrained 5-layer DNN.

4.2.1 Mixed Pigment Deep Learning Model

To overcome the hyperspectral unmixing problem, we propose the deep learning model shown in Figure 4.18 which provides multiple regression outputs from a single input. This is, for a given input reflectance, different numerical outputs are generated where each output corresponds to the fraction of a given pigment in the reference database. In this case, the input size is a vector of 33 points corresponding to the reflectance amplitude in the range of 400nm to 720nm in steps of 10nm. The number of outputs is set to 16 corresponding to the number of pigments in the reference database as described in Appendix A.

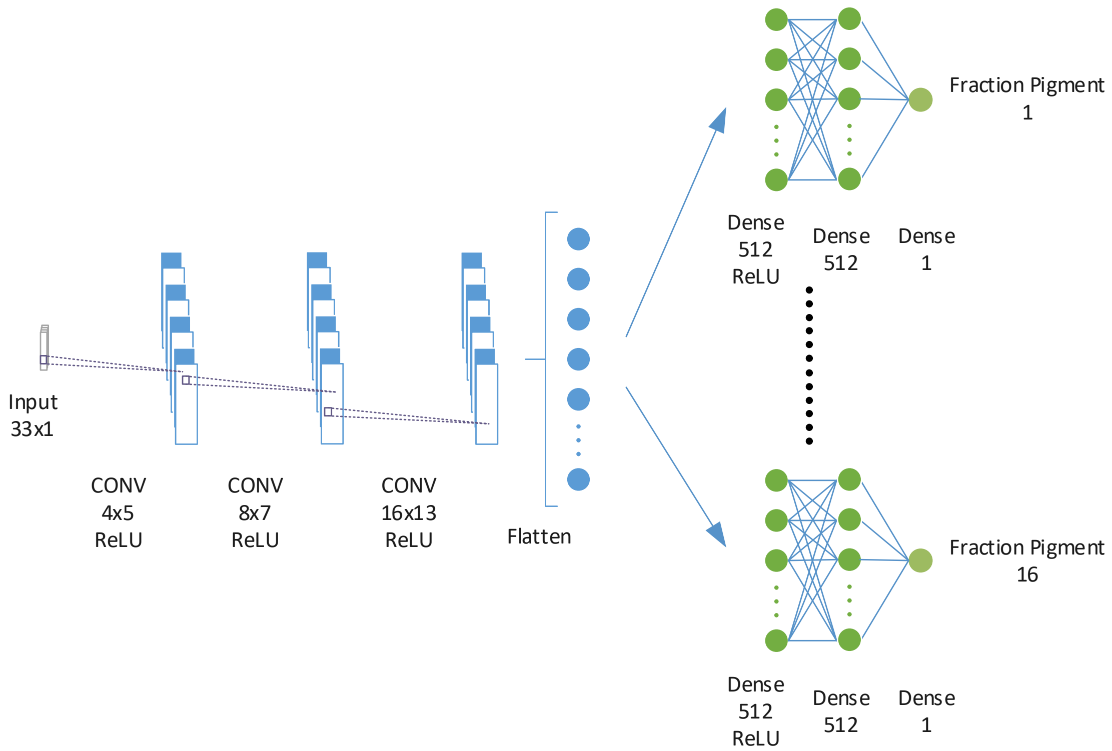

Figure 4.18: Block diagram model used for mix pigment prediction.

The input reflectance vector is passed through a first convolution layer with 4 filters of size 5, stride 1, padding of 2 and ReLU activation. The output size of this layer is 33×4. The second convolution layer contains 8 filters of size 7, stride 1, no padding and ReLU activation producing an output of size 27×8. The final convolution layer contains 16 filters of size 13, stride 1, no padding and ReLU activation generating an output of size 15×16. The increasing filter size analyses the reflectance first at small intervals for localised changes and finally at large intervals for large inflexion points in the reflectance. The output of the convolution layers is flattened and then split into 16 branches. Each branch contains two fully-connected layers of size 512 each with a final fully connected layer of size 1 which generates the predicted fraction in the range of 0 to 1 of the associated pigment. This last layer uses a sigmoid activation function to ensure non-negative output values are predicted for any given input reflectance.

4.2.2 Model Training

To train the proposed model described in section 4.2.1, artificial reflectances of up to 3 pigments out of 16 in steps of 10% were produced using the subtractive mixing model in Eq. 4.5. A total of 21256 artificial mixtures were generated as seen in Figure 4.19.

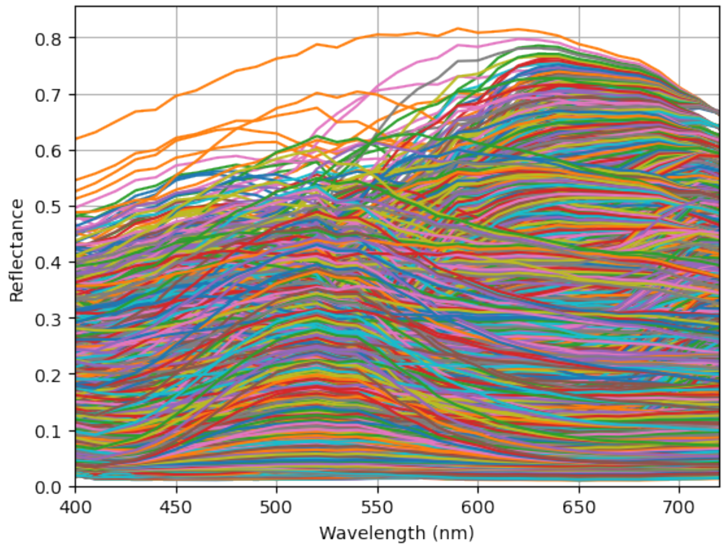

Figure 4.19: Artificially generated mixed pigment reflectances of up to 3 pigments out of 16.

The proposed model was trained with the 21256 reflectances as input data and the 16 fractions per pigment as labels. The model was then tested with the hyperspectral image of painting 86P21 producing estimated fractions per pigment which were rescaled such that the sum of all fractions was equal to 100%. Each reflectance was then reconstructed using the predicted fractions using the subtractive colour mixing model of Eq. 4.5 and the reference pigment reflectances. Finally, the sRGB representation of the predicted results was calculated using the D65 illuminant. The resulting image is shown in Figure 4.20 where a significant visual correlation error is observable. The error is likely related to the lack of training data with sufficient samples representative of true data which exhibits noise inherent to the acquisition process.

To increase the number of training samples and improve the performance of the model, these artificial reflectances were augmented using additive white Gaussian noise (Eq. 4.3) with a SNR of 30dB. A total of 10 noisy samples per artificial mixture were generated yielding 212560 artificial reflectances (Figure 4.21) for training and validation.

Training the model with the 212560 augmented reflectances significantly increased the visual correlation of the reconstructed sRGB image built using the predicted pigment fractions as seen in Figure 4.22. This confirms the importance of the quality and quantity of the training data in the performance of a deep learning model; the larger the training dataset with representative samples of the data the more accurate the prediction.

(a) (b)

Figure 4.20: sRGB representation of 68P11 from (a) the original hyperspectral image and (b) from the proposed mixed pigment deep learning model trained using 21256 reflectances.

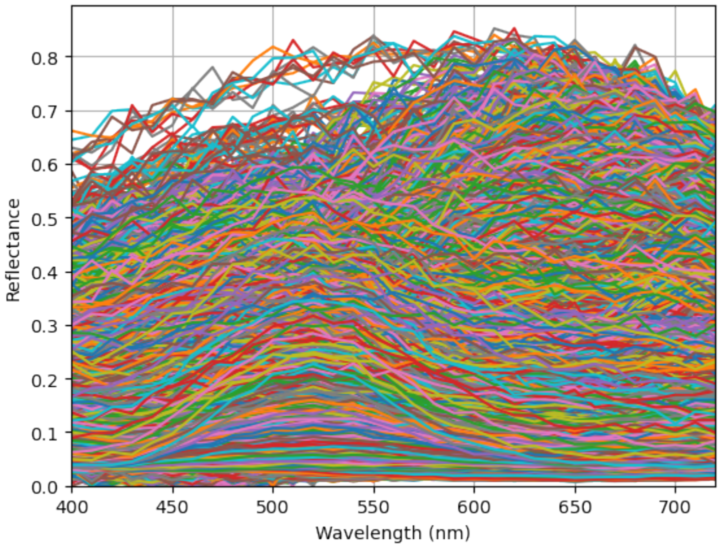

Figure 4.21: Artificially generated mixed pigment reflectances of up to 3 pigments out of 16 augmented with random noise.

4.2.3 Predicted Mix Pigments

The proposed deep learning model was trained with the 212560 augmented reflectances using 3 epochs and with a 70/30 split for training and validation with all reflectances shuffled at the start of each epoch. All 11 hyperspectral images were then analysed using the trained model and their corresponding sRGB images where all 16 pigment fractions are used were computed. The resulting images for the exemplary painting 68P21 are shown in Figure 4.23. Finally, the reconstructed sRGB image using the abundances calculated with FCLS where all 16 pigments are used is also shown.

The sRGB images resulting from taking the mixtures of the 2 and 3 highest fractions using the proposed model were also calculated by zeroing all other fractions and making the sum of the top 2 and 3 fractions respectively equal to 100%. The resulting images are

(a) (b)

Figure 4.22: sRGB representation of 68P11 from (a) the original hyperspectral image and (b) from the proposed mixed pigment deep learning model trained using 212560 augmented reflectances.

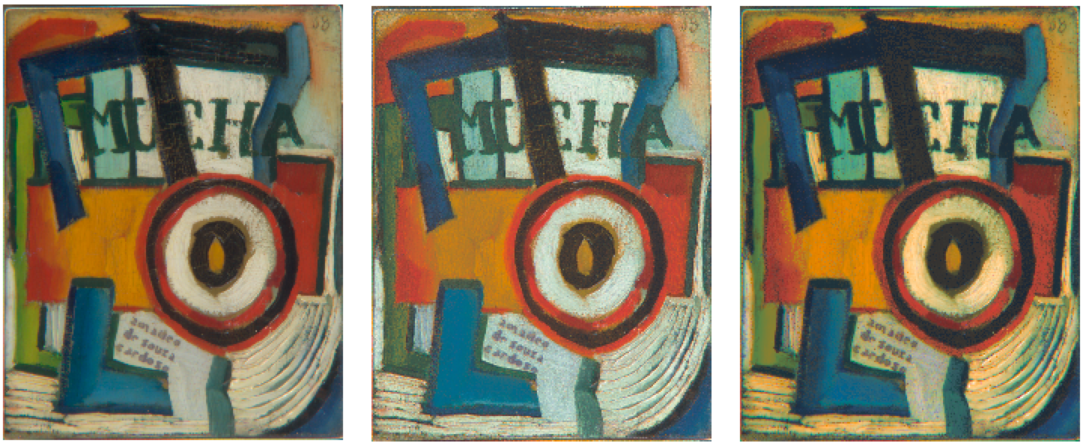

(a) Original (b) Predicted (c) FCLS

Figure 4.23: sRGB representation of the hyperspectral image 86P21 and predicted results.

shown in Figure 4.24 where it can be observed that the higher the number of pigments used, the better the approximated reconstruction is. This is confirmed in Table 4.3 where the RMSE and Mean Relative Absolute Error (MRAE) (Eq. 4.8) calculated values between the original reflectances z_{ij} and reconstructed reflectances $\hat{z}_{ij}$ are listed.

$$MRAE = \frac{1}{n} \sum_{i=1}^{n} \frac{\mid \hat{z}_{ij} - z_{ij} \mid}{z_{ij}} \tag{4.8}$$

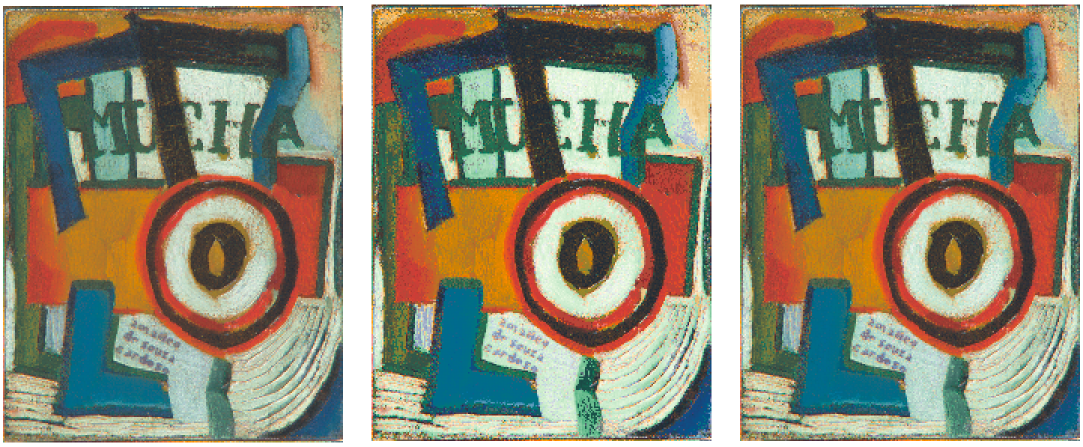

(a) All 16 fractions (b) Top 2 fractions (c) Top 3 fractions

Figure 4.24: sRGB image of painting 86P21 estimated using all 16 pigment fractions predicted, using the top 2 fractions and the top 3 fractions.

Table 4.3: Error measured between original and predicted/reconstructed hyperspectral image.

Painting	16 Fractions		Top 2 Fractions		Top 3 Fractions		FCLS	
	RMSE	MRAE	RMSE	MRAE	RMSE	MRAE	RMSE	MRAE
68P11	0.0618	0.1964	0.1115	0.4517	0.0705	0.2751	0.0971	0.4060
77P2	0.0995	0.3495	0.1164	0.4565	0.0948	0.3638	0.1079	0.4045
77P5	0.0824	0.2308	0.1145	0.4039	0.0798	0.2656	0.0994	0.3570
77P8	0.0716	0.2586	0.0998	0.4026	0.0761	0.3000	0.0882	0.3602
77P9	0.0766	0.2491	0.0964	0.3716	0.0768	0.2824	0.0940	0.3448
77P16	0.0507	0.1742	0.1224	0.4438	0.0666	0.2550	0.1045	0.3766
77P20	0.0664	0.2190	0.1104	0.4308	0.0753	0.2875	0.0978	0.4034
86P19	0.0631	0.2401	0.0933	0.4045	0.0628	0.2853	0.1043	0.3884
86P21	0.0828	0.3051	0.0934	0.3940	0.0767	0.3180	0.1021	0.3472
86P23	0.0536	0.4221	0.0701	0.5042	0.0545	0.4439	0.0678	0.3518
92P209	0.0984	0.2653	0.0968	0.2976	0.0891	0.2601	0.1028	0.3366
Fake	0.1923	0.3015	0.1852	0.3217	0.1894	0.3088	0.1509	0.2720

Figure 4.25 shows the location of points selected in painting 68P21 where the reflectance of the original hyperspectral image as well as the reconstructed reflectances with the CNN prediction using all 16 pigments, the top 3 pigments, the top 2 pigments and the FCLS abundances are plotted in Figure 4.26.

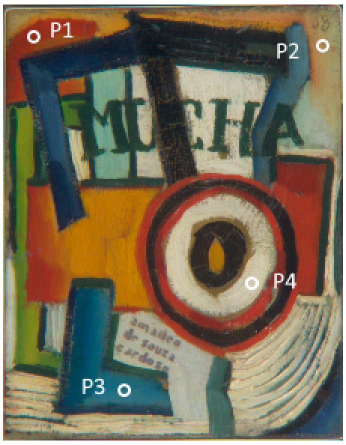

Figure 4.25: Selected points in painting 86P21 for comparison of reconstructed reflectances: P1=[20,20], P2=[27,212], P3=[255,80], P4=[184,165].

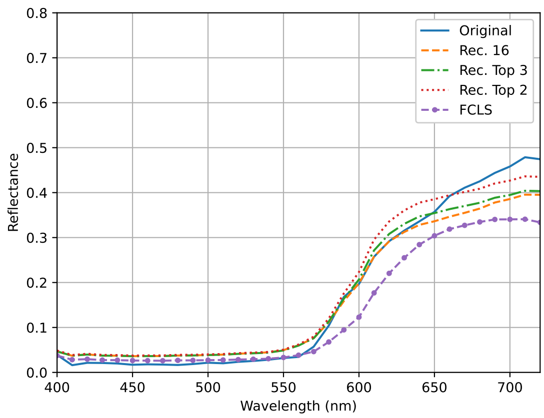

(a) P1

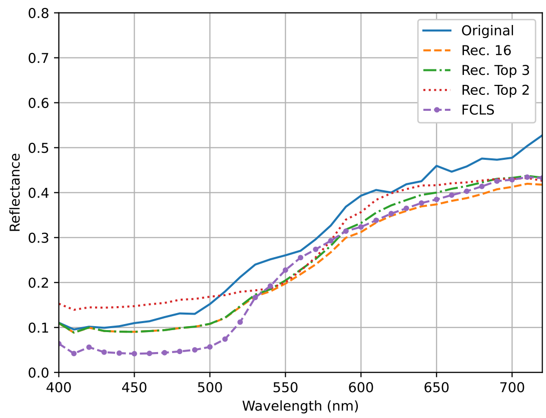

(b) P2

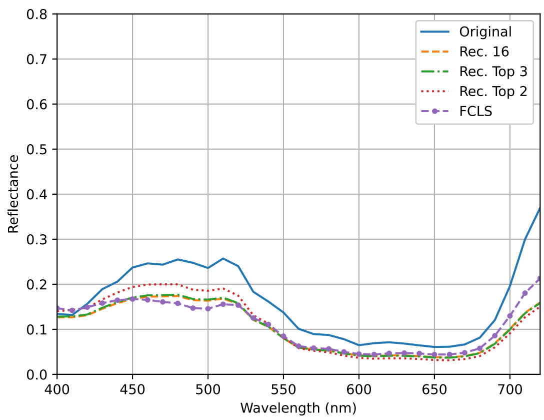

(c) P3

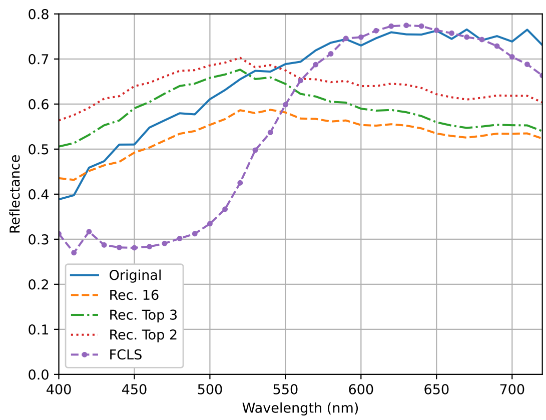

(d) P4

Figure 4.26: Reconstructed reflectances at the points selected of painting 68P21 in Figure 4.25.

As noted in the results obtained, the deep learning model proposed and the post-processing algorithm to normalise the output to 100% generated better mixed pigment fraction estimates than the standard FCLS method when all pigments were used. Reducing the number of pigments and rescaling the percentages also generated better estimates than FCLS when 3 pigments were used in the mixture. The use of 2 pigments however increased the discrepancy between the estimated mixture and the actual test reflectance. Yet, the errors were marginally higher than FCLS. This indicates that the proposed method using all predicted percentages is a suitable solution to the pigment unmixing problem at hand as it produces smaller approximation errors than FCLS.

4.3 Authentication Through Pigment Analysis

As proposed in [171], a method for the authentication of artwork through pigment analysis includes the quantification, qualification and cross-referencing of areas of a painting with reference to a ground truth database of pigments. This is, areas of a painting with similar colour and spectral characteristics can be assumed to be *True* if their physical and chemical characteristics match an entry of the pigment reference database. Chemical analysis is however a time-consuming and expensive process which makes analysing all areas of the painting a prohibitive process. Image segmentation to group similar coloured areas is advantageous if the assumption is that all points within that area are identical, thus requiring a single point to be analysed for cross-referencing.

The process proposed to achieve authentication via pigment analysis is based on the one proposed in [171] and follows the steps below.

- For a given point in the hyperspectral image, determine if the point matches the reflectance of the white or black paint in the reference database. If it does, mark the point as *Black* or *White* and analyse the next point, otherwise, continue.

- Determine if the point closely matches the colour of at least one of the samples in the XRF database. If the point does not match any XRF sample then the point is marked as *Not Analysed* and analyse the next point, otherwise, continue.

- Determine if the matching XRF samples are possible single pigment or mixtures of 2 or 3 pigments of the reference database. If no possible mixture is found, mark the point as *Negative* and analyse the next point, otherwise, continue.

- Determine if the point is a potential pure pigment by analysing the point reflectance. If a colour matching XRF sample exists and contains the same chemical elements as the potential pure pigment then mark the point as *Pure* and analyse the next point, otherwise, continue.

- Determine the mixture of 2 pigments whose reflectance is the closest to the point analysed. If a colour matching XRF sample exists and contains the same chemical elements as the potential mixture then mark the point as *Mixed* and analyse the next point, otherwise, continue.

- Determine the mixture of 3 pigments whose reflectance is the closest to the point analysed. If a colour matching XRF sample exists and contains the same chemical elements as the potential mixture then mark the point as *Mixed* and analyse the next point, otherwise, mark the point as *Negative*.

- Quantify the number of *Negative*, *Not Analysed*, *White*, *Black*, *Pure* and *Mixed* points and calculate the indicator of authenticity as the proportion of the area analysed and confirmed by XRF analysis.

4.3.1 XRF Data

The validity and accuracy of the results obtained are linked to the accuracy of the data used for processing the hyperspectral images. In particular, the accuracy of the chemical elements associated with each pigment and to each XRF entry in the painting sample database point is of high importance, as this directly affects the chemical matching process as described below. The assignment of the most representative chemical elements responsible for the colour of a pigment is a manual process that requires an accurate and expert interpretation of the XRF data measured. An incomplete or inaccurate selection of elements will indubitably result in chemical element mismatch when comparing pigments. In the XRF data supplied by [171] the only chemical element associated with the white pigment is Pb. The entries of the XRF database files supplied do not include Pb in most samples despite this appearing to be present in the μEDXRF spectrum of samples, for example, those shown in Figure 4.27 for samples *Bl1a* and *Y8a*. The chemical elements included in the respective XRF sample file include Fe, S for sample *Bl1a* and Cd for sample *Y8a*.

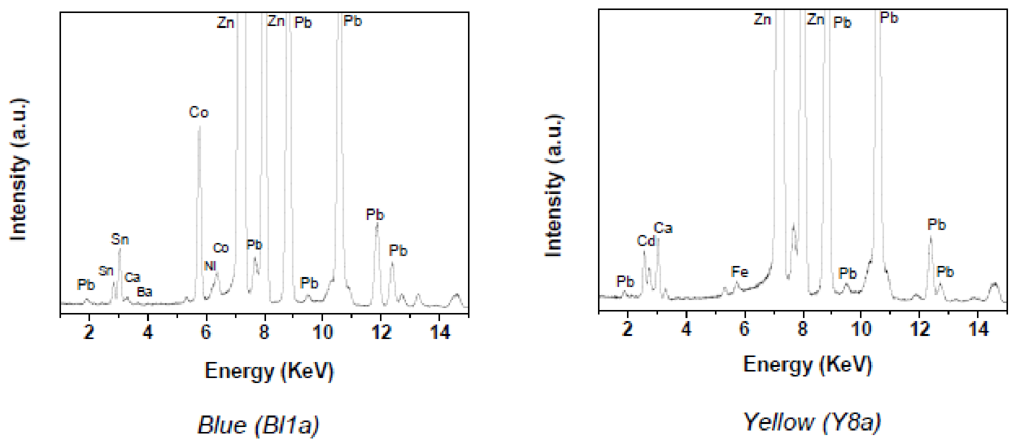

(a) Original (b) Preliminary Result

Figure 4.27: μEDXRF spectra of samples *Bl1a* and *Y8a* of painting 77P9 (p.205-206 [171]).

An artificial mixture of Lead White and Cadmium Orange would contain, by superposition, the chemical elements Pb and Cd. If this mixture produces the closest reflectance match to a given point, then that mixture is temporarily assigned to the point. At the same time, if the colour of the point analysed is similar to XRF sample Y8a, then the point is assumed to be identical to that sample. However, the chemical elements of the assigned mixture will not match the chemical elements of the XRF sample, resulting in this point being marked as either *Negative* or incorrectly being assigned an artificial mixture that does not closely match the point.

In summary, the exclusion of Pb in the XRF database samples limits the use of the white pigment in the artificial mixtures resulting in untested mixtures and ultimately, degraded performance. This does not apply to the Ivory Black pigment which has not been assigned any representative chemical element allowing correct generation mixtures and matching of these to XRF samples. The possible solutions include the review and inclusion of Pb in the XRF sample database for all paintings or the temporary removal of Pb from the white pigment. While the former could be the recommended approach its implementation is outside the scope of this research and therefore the latter is the practical approach to be used in this work and the results obtained.

4.3.2 XRF Colour Matching

To determine the colour difference between two points, namely an XRF sample and a point in the painting, CIE 1976 L*a*b Colour Space (CIELab) colour components are used. The colour difference ΔE^*_{ab} in this space between two points (L^*_1, a^*_1, b^*_1) and (L^*_2, a^*_2, b^*_2) is calculated using the CIE76 colour difference formula as defined in Eq. 4.9 [221].

$$\Delta E^*_{ab} = \sqrt{(L^*_2 - L^*_1)^2 + (a^*_2 - a^*_1)^2 + (b^*_2 - b^*_1)^2} \tag{4.9}$$

The selection of the ΔE^*_{ab} threshold for matching XRF samples and points in the painting is of high importance as this will have a significant impact on various stages of the method proposed. A low threshold imposes a constraint where a pixel analysed can only be assumed to be identical to an XRF sample if the colour is very similar. This will result in a large number of pixels not meeting this condition thus immediately increasing the number of pixels marked as *Not Analysed* or *Negative*. Similarly, a very relaxed threshold will result in a large number of points marked as *Pure* or *Mixed*. Thus, it is important to find the correct balance of the threshold. To determine the best suitable value of the threshold ΔE^*_{ab}, it is necessary to evaluate the detection of ground truth areas. This is, areas that can be attributed to a certain pigment with absolute certainty. One way this can be achieved is by using the CIELab values of the Cerulean Blue pigment from the reference database which are $L = 37.47$ $a = -9.62$ $b = -33.73$ and comparing these against the painting pixels and using multiple values for the threshold ΔE^*_{ab} as shown in Figure 4.28, where thresholds of 12 to 24 in steps of 3 are used. Based on this analysis for multiple pigments, the proposed value for the threshold ΔE^*_{ab} to be used for colour matching is 18.

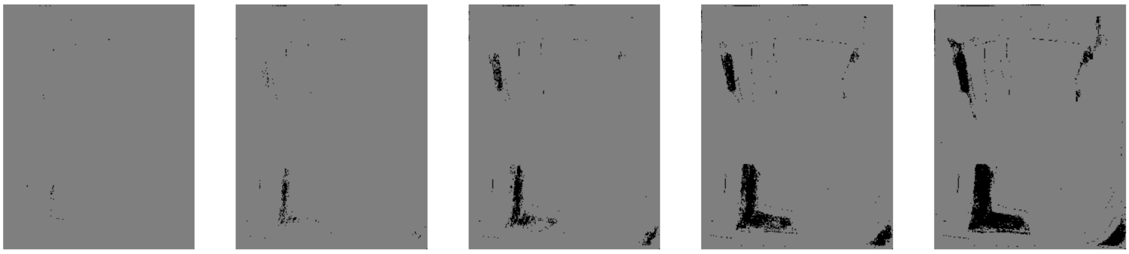

(a) ΔE^*_{ab} = 12 (b) ΔE^*_{ab} = 15 (c) ΔE^*_{ab} = 18 (d) ΔE^*_{ab} = 21 (e) ΔE^*_{ab} = 24

Figure 4.28: Evaluation of ΔE^*_{ab} values using Cerulean Blue in painting 86P21.

4.3.3 Preliminary Results

The process described was implemented using the deep learning model proposed in section 4.1.1 for pure pigment prediction with confirmation of pure pigments using the XRF database files supplied in [171]. Similarly, mixed pigments were predicted using the model proposed in section 4.2.1. The top 2 and top 3 fractions were used to estimate the pigment mixture and reconstructed reflectance. To determine the closest mixture between the top 2 and top 3 reconstructed reflectances, the error was measured using RMSE. The mixture with the lowest error was assigned and used for the chemical element check. The visual results of the classification process for painting 86P21 are shown in Figure 4.29, where bright pink colour has been used to highlight *Not Analysed* areas and bright purple to highlight *Negative* areas. All other colours including white and black are representative of estimated pure pigments predicted using the pure pigment model of section 4.1.1.

(a) Original (b) Preliminary Result

Figure 4.29: sRGB representation of 86P21 from the original hyperspectral image and from the preliminary classification results using deep learning models for pure and mixed pigment prediction. Pixels classified as *Negative* shown in bright purple and pixels classified as *Not Analysed* in bright pink.

The preliminary classification results for all 12 hyperspectral images are summarised in Table 4.4. As observed, the use of the deep learning model for mixed pigment prediction resulted in large areas being classified as *Negative*. This is the result of the 2 and 3 mixed pigment prediction not producing the correct mixture as identified by the XRF samples. This is, the deep learning model produces mixtures with a reflectance that, although close to the real-world value as previously shown in section 4.2.3, do not necessarily match the actual pigment mixture. This can be attributed to a combination of the inherent reflectance noise from the hyperspectral image acquisition process and the prediction from the deep learning model; the deep learning model produces predictions where the error of the approximation was minimised during training and thus produces mixtures that approximate a reflectance as a combination of the reflectances in the base pigment database.

Table 4.4: Preliminary results of area classification using the proposed method with 2 deep learning models for pure and mixed pigment prediction.

Painting	Not An.	Black	White	Pure	2-Mix	3-Mix	Negative
68P11	0.38%	1.38%	7.72%	2.72%	19.57%	8.60%	59.63%
77P2	2.25%	0.00%	4.94%	3.34%	17.14%	20.50%	20.66%
77P5	0.11%	0.00%	11.92%	18.40%	27.79%	9.36%	98.11%
77P8	9.51%	5.77%	4.11%	4.60%	3.97%	2.24%	44.79%
77P9	0.18%	3.02%	12.18%	10.27%	10.76%	3.97%	59.30%
77P16	1.05%	2.14%	10.27%	5.64%	2.72%	2.08%	33.21%
77P20	5.41%	0.43%	10.87%	11.11%	15.56%	4.78%	51.90%
86P19	24.46%	2.11%	15.85%	4.23%	2.55%	0.61%	48.10%
86P21	1.65%	5.73%	14.30%	3.10%	4.47%	0.48%	53.84%
86P23	10.28%	4.83%	1.21%	0.01%	1.62%	0.93%	48.57%
92P209	4.13%	0.00%	9.59%	22.51%	3.74%	2.67%	56.32%
Fake	2.26%	0.00%	40.46%	3.13%	0.97%	0.01%	25.88%

As a result of the low performance in accurately determining the correct mixture, the deep learning model for mixed pigment prediction cannot be used in the authentication method proposed. However, this deep learning model remains useful to determine the required pigment fractions to match a colour for restoration purposes.

4.3.4 Authentication Results

As discussed in the previous section, the deep learning model for mixed pigment prediction although it produces good results approximating the hyperspectral image $\mathbf{Z} \in \mathbb{R}^{W \times H \times B}$ from the dictionary of pigments in the reference database, it does not generate the expected results that can be confirmed via XRF matching. Thus, its use in the proposed method should be replaced by a hyperspectral metric function for matching any reflectance against the set of artificial mixtures generated using subtractive mixing. This, along with the removal of Pb from the white pigment as described in section 4.3.1 results in the updated method described below.

First, the artificial pigment mixtures using 2, 3 and 4 pigments out of the 16 pigments in the reference database in steps of 10% using the subtractive mixing model from Eq. 4.5 and the combination of pigments without repetition as defined in Eq. 4.6 must be calculated. Only entries where non-zero percentages exist are used. Then, evaluate each point in the hyperspectral image using the following algorithm steps:

1. Reduce the noise caused by the acquisition process by smoothing the reflectance point using a Savitzky–Golay filter with 5 samples and order 3.

2. Predict the pure pigment assignment using the deep learning model for pure pigment identification.

3. Confirm if the point matches white or black by calculating the error between the associated reflectances in the reference database entry and the point reflectance using RMSE. If it does, mark the point as *Black* or *White* and move to the next point, otherwise, continue.

4. Using a threshold $\Delta E^*_{ab} = 18$ identify if the CIELab colour components match any of the samples in the XRF database. If the point does not match any XRF sample then marked the point as *Not Analysed* and move to the next point, otherwise, continue.

5. If the point analysed matches the colour of at least one XRF sample, but no XRF sample exists that can be generated as a mixture of 1, 2, 3 or 4 pigments in the reference database, i.e., the combination of chemical elements of the mixture do not match the XRF chemical elements, then mark the pigment as *Negative* and move to the next point, otherwise, continue.

6. Check if the point is pure by checking if the pure pigment prediction matches an XRF sample that has similar colour and that matches the colour and chemical elements of the pigment in the reference database. If it does, mark the point as *Pure* and move to the next point, otherwise, continue.

7. Determine if the point is a potential mixture of 2 pigments by checking if at least an XRF sample exists that contains a valid 2-pigment chemical element combination and that matches the colour of the point analysed. If two or more samples exist, select the one with the smallest RMSE value.

8. Determine if the point is a potential mixture of 3 pigments by checking if at least an XRF sample exists that contains a valid 3-pigment chemical element combination and that matches the colour of the point analysed. If two or more samples exist, select the one with the smallest RMSE value.

9. Determine if the point is a potential mixture of 4 pigments by checking if at least an XRF sample exists that contains a valid 4-pigment chemical element combination and that matches the colour of the point analysed. If two or more samples exist, select the one with the smallest RMSE value.

10. If the point is a potential mixture of either 2, 3 or 4 pigments exclusively, i.e., it matches one but not the other, then mark the point as *Mixed* and analyse the next point, otherwise continue.

11. If the point is a potential mixture of more than one combination of pigments, e.g., a potential mixture of 2 pigments but also a potential mixture of 3 pigments, then mark the point as *Mixed* but assign to the point the combination with the smallest RMSE value and move to the next point, otherwise continue.

12. Any point that did not meet any of the previous conditions must be marked as *Negative*.

Finally, the number of *Negative*, *Not Analysed*, *White*, *Black*, *Pure* and *Mixed* points must be quantified and the corresponding areas calculated. The numerical result of analysing the 12 off hyperspectral test images with the proposed pigment authentication method is shown in Table 4.5.

Table 4.5: Final results of area classification using the proposed method.

Painting	**Not An.**	**Black**	**White**	**Pure**	**2-Mix**	**3-Mix**	**4-Mix**	**Neg.**
68P11	0.38%	1.39%	7.73%	2.80%	4.89%	32.72%	50.01%	0.09%
77P2	2.25%	0.00%	4.94%	3.19%	1.20%	17.78%	38.22%	1.25%
77P5	0.11%	0.00%	11.92%	17.84%	4.44%	46.38%	85.00%	0.00%
77P8	9.33%	5.96%	4.11%	4.57%	2.81%	26.80%	21.40%	0.00%
77P9	0.18%	3.10%	12.19%	10.07%	5.60%	33.69%	34.86%	0.00%
77P16	1.05%	2.21%	10.27%	5.56%	0.18%	10.09%	27.75%	0.00%
77P20	5.41%	0.44%	10.87%	11.04%	5.30%	28.07%	38.93%	0.00%
86P19	24.46%	2.21%	15.85%	4.25%	10.39%	25.20%	15.55%	0.00%
86P21	1.65%	5.82%	14.31%	2.67%	6.24%	30.25%	22.44%	0.18%
86P23	10.28%	5.05%	1.21%	0.05%	1.50%	20.99%	28.38%	0.00%
92P209	4.13%	0.00%	9.60%	22.04%	13.30%	46.36%	3.53%	0.00%
Fake	2.25%	0.00%	40.48%	3.29%	16.72%	0.30%	0.04%	9.63%

Using the quantified areas, the indicator of authenticity $I_a(M/Am)$ can be calculated as the proportion of the area analysed and confirmed as Amadeo, Am, via the algorithm proposed relative to the area not analysed, $NotAn$, using Eq. 4.10 [171].

$$I_a(M/Am) = Am \times (1 - NotAn) \tag{4.10}$$

The tabulated results are shown in Table 4.6. As expected, the results show a high probability of authenticity for most paintings analysed. Paintings 77P8, 86P19 and 86P23 show a lower probability of authenticity dictated primarily by the large number of pixels marked as *Not Analysed*. This is, large areas of the painting where no XRF samples are available. It must be noted however that, as previously discussed, the accuracy of the results is dictated by the accuracy of the data used and as provided by [171].

Table 4.6: Probability authenticity using pigment analysis.

Painting	**Probability of Authenticity**
68P11	90.06%
77P2	84.83%
77P5	92.68%
77P8	64.91%
77P9	84.33%
77P16	74.89%
77P20	78.78%
86P19	42.43%
86P21	72.27%
86P23	63.99%
92P209	82.54%
Fake	21.11%

The method proposed facilitates the generation and matching of mixtures that can contain up to 4 different pigments. This feature enables better matching and identification of the mixtures per area. Table 4.7 shows the area breakdown per pigment mixture identified in painting 86P21. As expected, most of the areas analysed have been confirmed to be mixtures of pigments.

Table 4.7: Area identified per pigment mixture for painting 86P21.

Pigment 1	Pigment 2	Pigment 3	Pigment 4	Area
Chrome Yellow				0.790%
Cerulean Blue				2.403%
Prussian Blue				0.005%
Lead White				17.119%
Ivory Black				6.970%
Chinese Vermilion	Chrome Yellow			1.633%
Chinese Vermilion	Viridian			1.431%
Yellow Ochre	Cerulean Blue			0.146%
Yellow Ochre	Viridian			1.192%
Yellow Ochre	Lead White			0.511%
Chrome Yellow	Prussian Blue			0.539%
Chrome Yellow	Lead White			0.002%
Cerulean Blue	Lead White			0.055%
Cerulean Blue	Ivory Black			0.095%
Prussian Blue	Viridian			1.211%
Prussian Blue	Lead White			0.655%
Viridian	Lead White			0.002%
Chinese Vermilion	Yellow Ochre	Chrome Yellow		0.063%
Chinese Vermilion	Yellow Ochre	Viridian		0.034%
Chinese Vermilion	Chrome Yellow	Viridian		2.325%
Chinese Vermilion	Chrome Yellow	Lead White		6.173%
Chinese Vermilion	Chrome Yellow	Ivory Black		2.743%
Chinese Vermilion	Viridian	Lead White		0.589%
Chinese Vermilion	Viridian	Ivory Black		0.430%
Yellow Ochre	Chrome Yellow	Prussian Blue		0.034%
Yellow Ochre	Chrome Yellow	Viridian		0.102%
Yellow Ochre	Chrome Yellow	Lead White		0.037%
Yellow Ochre	Chrome Yellow	Ivory Black		0.180%
Yellow Ochre	Cobalt Blue	Cerulean Blue		0.038%

Continued on next page

Table 4.7: Area identified per pigment mixture for painting 86P21. (Continued)

Pigment 1	Pigment 2	Pigment 3	Pigment 4	Area
Yellow Ochre	Cerulean Blue	Lead White		0.876%
Yellow Ochre	Cerulean Blue	Ivory Black		0.046%
Yellow Ochre	Prussian Blue	Viridian		0.400%
Yellow Ochre	Prussian Blue	Lead White		0.061%
Yellow Ochre	Viridian	Lead White		4.780%
Yellow Ochre	Viridian	Ivory Black		5.343%
Yellow Ochre	Lead White	Ivory Black		4.153%
Chrome Yellow	Prussian Blue	Viridian		0.014%
Chrome Yellow	Prussian Blue	Lead White		0.006%
Chrome Yellow	Prussian Blue	Ivory Black		0.040%
Chrome Yellow	Viridian	Lead White		1.489%
Cobalt Blue	Cerulean Blue	Lead White		0.002%
Cobalt Blue	Cerulean Blue	Ivory Black		0.706%
Cerulean Blue	Lead White	Ivory Black		1.791%
Prussian Blue	Viridian	Lead White		2.284%
Prussian Blue	Viridian	Ivory Black		0.327%
Prussian Blue	Lead White	Ivory Black		1.131%
Chinese Vermilion	Yellow Ochre	Chrome Yellow	Cobalt Blue	0.519%
Chinese Vermilion	Yellow Ochre	Chrome Yellow	Viridian	0.504%
Chinese Vermilion	Yellow Ochre	Chrome Yellow	Lead White	2.534%
Chinese Vermilion	Yellow Ochre	Chrome Yellow	Ivory Black	0.023%
Chinese Vermilion	Yellow Ochre	Cobalt Blue	Viridian	4.455%
Chinese Vermilion	Yellow Ochre	Viridian	Lead White	3.804%
Chinese Vermilion	Yellow Ochre	Viridian	Ivory Black	0.014%
Chinese Vermilion	Chrome Yellow	Viridian	Lead White	3.789%
Chinese Vermilion	Chrome Yellow	Viridian	Ivory Black	0.630%
Chinese Vermilion	Chrome Yellow	Lead White	Ivory Black	1.706%
Chinese Vermilion	Viridian	Lead White	Ivory Black	0.183%
Yellow Ochre	Chrome Yellow	Prussian Blue	Viridian	0.040%

Continued on next page

Table 4.7: Area identified per pigment mixture for painting 86P21. (Continued)

Pigment 1	Pigment 2	Pigment 3	Pigment 4	Area
Yellow Ochre	Chrome Yellow	Prussian Blue	Lead White	0.023%
Yellow Ochre	Chrome Yellow	Prussian Blue	Ivory Black	0.014%
Yellow Ochre	Chrome Yellow	Viridian	Lead White	1.475%
Yellow Ochre	Chrome Yellow	Viridian	Ivory Black	0.299%
Yellow Ochre	Chrome Yellow	Lead White	Ivory Black	0.052%
Yellow Ochre	Cobalt Blue	Cerulean Blue	Lead White	0.839%
Yellow Ochre	Cobalt Blue	Cerulean Blue	Ivory Black	0.002%
Yellow Ochre	Cerulean Blue	Lead White	Ivory Black	1.791%
Yellow Ochre	Prussian Blue	Viridian	Lead White	0.357%
Yellow Ochre	Prussian Blue	Viridian	Ivory Black	0.130%
Yellow Ochre	Prussian Blue	Lead White	Ivory Black	0.125%
Yellow Ochre	Viridian	Lead White	Ivory Black	1.959%
Chrome Yellow	Prussian Blue	Viridian	Lead White	0.011%
Chrome Yellow	Prussian Blue	Lead White	Ivory Black	0.017%
Cobalt Blue	Cerulean Blue	Lead White	Ivory Black	1.202%
Prussian Blue	Viridian	Lead White	Ivory Black	0.365%

For visualisation purposes, each point of the paintings analysed was assigned the reflectance of the matched pure pigment or pigment mixture. In the case of points marked as *Not Analysed* a reflectance corresponding to bright pink is used and for points marked as *Negative* a reflectance of bright purple is used. The resulting, estimated sRGB images are then estimated using the D65 illuminant. Figure 4.30 shows the resulting sRGB images from the assigned reflectances for painting 86P21 and the DCR Fake painting. Images from [171] are included for comparison as these could not be replicated using the supplied data. Unlike the resulting images obtained in [171] where only approximated sRGB values were used, our approach allows visualising truly reconstructed images from the predicted pigment assignments which allows visual correlation with the ground truth images.

For benchmarking and comparison, the use of SAM applied to the derivative of the smoothed reflectance for mixed pigment identification only as employed in the method from [171] instead of the RMSE function was evaluated. Similarly, the use of 3 and 4 pigments in the artificial mixtures as well as the exclusion of black and white, i.e. 14 pigments instead of 16 pigments in the artificial mixtures, was evaluated. To aid comparison, the reflectance reconstruction error was measured using RMSE and MRAE. The reconstruction error results are summarised in Table 4.8 and plotted in Figure 4.31

(a) 86P21 in [171]

(b) 86P21 by the proposed method

(c) Fake in [171]

(d) Fake by the proposed method

Figure 4.30: Comparison of results obtained in [171] and using the proposed method for painting 68P21 (top) and Fake (bottom).

where it can be seen that the proposed method using RMSE surpasses the performance using SAM as it produces the most accurate reconstruction while producing a good indicator of authenticity as shown in Table 4.9. Similarly, the use of 4-pigment mixtures including black and white generates a more accurate reconstruction of reflectances which are validated via XRF matching.

Table 4.8: Hyperspectral reconstruction error for the metric function and pigment combination used.

Painting	RMSE 3/16		RMSE 4/16		RMSE 3/14		SAM 3/14	
	RMSE	MRAE	RMSE	MRAE	RMSE	MRAE	RMSE	MRAE
68P11	0.0861	0.1706	0.0853	0.1563	0.1160	0.3436	0.1504	0.5815

Continued on next page

Table 4.8: Hyperspectral reconstruction error for the metric function and pigment combination used. (Continued)

Painting	**RMSE 3/16**		**RMSE 4/16**		**RMSE 3/14**		**SAM 3/14**	
	RMSE	**MRAE**	**RMSE**	**MRAE**	**RMSE**	**MRAE**	**RMSE**	**MRAE**
77P2	0.0895	0.2179	0.0882	0.2037	0.1243	0.3827	0.1674	0.6098
77P5	0.0878	0.2074	0.0868	0.1860	0.1191	0.3714	0.1638	0.5316
77P8	0.0711	0.2347	0.0700	0.2156	0.0978	0.4197	0.1379	0.5798
77P9	0.0931	0.2342	0.0927	0.2237	0.1082	0.3430	0.1308	0.5132
77P16	0.1198	0.2662	0.1191	0.2452	0.1452	0.3947	0.1624	0.5321
77P20	0.0931	0.2272	0.0926	0.2103	0.1110	0.3891	0.1395	0.6146
86P19	0.1235	0.3182	0.1231	0.3077	0.1353	0.4314	0.1483	0.6528
86P21	0.1168	0.3363	0.1146	0.3313	0.1335	0.3947	0.1576	0.5265
86P23	0.0475	0.3869	0.0464	0.3199	0.0607	0.5164	0.0938	0.7491
92P209	0.1107	0.2913	0.1107	0.2905	0.1475	0.3902	0.1618	0.4583
Fake	0.1697	0.3612	0.1697	0.3611	0.2182	0.3104	0.2191	0.3298

Table 4.9: Indicator of authenticity for the metric function and pigment combination used.

Painting	**RMSE 3/16**	**RMSE 4/16**	**RMSE 3/14**	**SAM 3/14**
68P11	90.06%	90.06%	90.02%	90.02%
77P2	84.86%	84.86%	82.99%	82.99%
77P5	92.68%	92.68%	90.70%	90.70%
77P8	64.91%	64.91%	63.68%	63.68%
77P9	84.33%	84.33%	80.32%	80.32%
77P16	74.89%	74.89%	72.50%	72.50%
77P20	78.78%	78.78%	76.58%	76.58%
86P19	42.43%	42.43%	38.83%	38.83%
86P21	69.85%	72.27%	66.54%	66.73%
86P23	63.99%	63.99%	59.71%	59.71%
92P209	82.54%	82.54%	52.72%	52.72%

Continued on next page

Table 4.9: Indicator of authenticity for the metric function and pigment combination used. (Continued)

Painting	RMSE 3/16	RMSE 4/16	RMSE 3/14	SAM 3/14
Fake	27.11%	27.11%	27.11%	27.11%

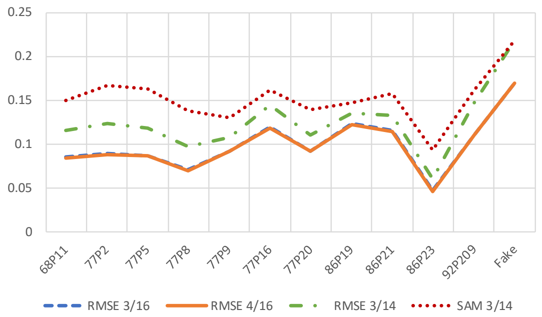

(a) RMSE

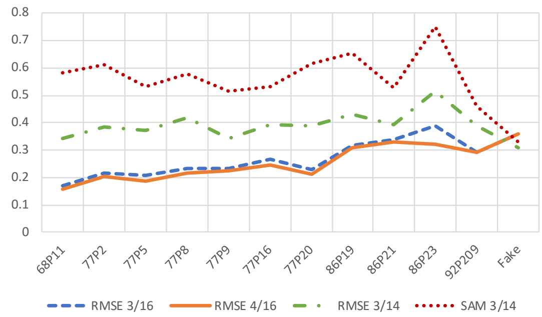

(b) MRAE

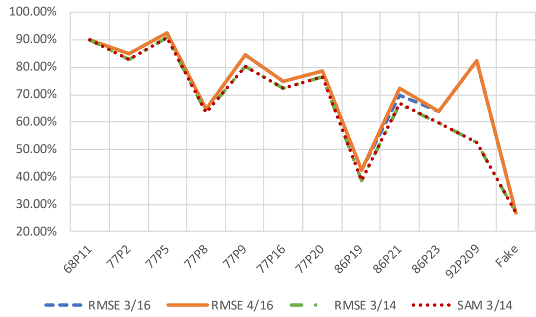

(c) Indicator of authenticity

Figure 4.31: Visualisation of measured results for the metric function and pigment combination used.

For visualisation only, the sRGB representation of the reconstructed hyperspectral image of painting 86P21 for the metric function and pigment combinations evaluated are shown in Figure 4.32.

4.4 Combined Authentication

As proposed in [171], the probability of a piece of artwork analysed being authentic can be estimated as the total indicator of authenticity I_A defined in Eq. 4.11, where I_{a_i} is the i^{th} indicator of authenticity calculated via a given analysis method, and α_i a weight assigned to the method.

$$I_A = \sum_{i=1}^{N} \alpha_i I_{a_i} \quad \{\alpha \in [0,1] \mid \sum_{i=1}^{N} \alpha_i = 1\} \tag{4.11}$$

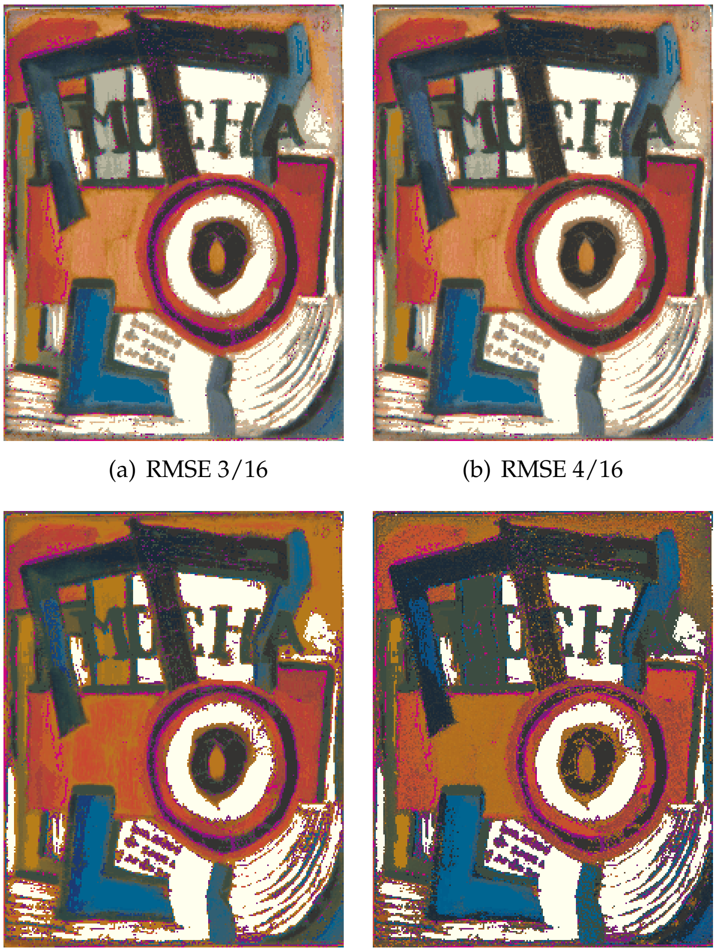

(a) RMSE 3/16 (b) RMSE 4/16

(c) RMSE 3/14 (d) SAM 3/14

Figure 4.32: sRGB representation of the reconstructed hyperspectral images for the metric function and pigment combination used for painting 68P21.

In this work, the indicator of authenticity for the brushstroke and pigment analysis are denoted as $I_a(B/Am)$ and $I_a(M/Am)$ respectively. The corresponding weights applied to each analysis method have been set to 0.5 to allow direct comparison with the values obtained in [171]. The values obtained via brushstroke analysis with the deep learning model proposed, the mixed-method proposed for pigment analysis and the values claimed in [171] are shown in Table 4.10 for each of the test images analysed.

Table 4.10: Comparison of indicator of authenticity in [171] and our method for all 12 test images analysed.

Painting	Method in [171]			Proposed method		
	$I_a(B/Am)$	$I_a(M/Am)$	I_A	$I_a(B/Am)$	$I_a(M/Am)$	I_A
68P11	89.00%	91.00%	90.00%	89.20%	90.06%	89.63%

Continued on next page

Table 4.10: Comparison of indicator of authenticity in [171] and our method for all 12 test images analysed. (Continued)

Painting	Method in [171]			Proposed method		
	$I_a(B/Am)$	$I_a(M/Am)$	I_A	$I_a(B/Am)$	$I_a(M/Am)$	I_A
77P2	80.00%	99.00%	89.50%	100.00%	84.86%	92.43%
77P5	95.00%	100.00%	97.50%	100.00%	92.68%	96.34%
77P8	82.00%	99.00%	90.50%	95.10%	64.91%	80.01%
77P9	35.00%	100.00%	67.50%	86.90%	84.33%	85.61%
77P16	99.00%	100.00%	99.50%	97.00%	74.89%	85.95%
77P20	71.00%	100.00%	85.50%	91.00%	78.78%	84.89%
86P19	73.00%	74.00%	73.50%	93.50%	42.43%	67.97%
86P21	70.00%	91.00%	80.50%	99.40%	72.27%	85.84%
86P23	98.00%	84.00%	91.00%	95.60%	63.99%	79.79%
92P209	98.00%	97.00%	97.50%	99.90%	82.54%	91.22%
Fake	42.00%	49.00%	45.50%	53.60%	27.11%	40.35%

The results obtained with the proposed methodology for authentication are encouraging and in agreement with those obtained by [171]. However, as discussed in section 2.6, the brushstroke results from [171] quoted are biased due to the handling of the test data in the KM clustering process. Furthermore, the values for pigment analysis reported by [171] were not repeatable with the data and code supplied.

In conclusion, the methodology proposed paves the path for further enhancements that can include results from other authentication methods or the same methods if further improvements in the deep learning models are implemented or if more data are made available for training.

4.5 Discussion

The use of deep learning for pure pigment prediction, i.e., image segmentation based on hyperspectral analysis was successfully implemented using three-dimensional convolutional neural networks. To train the model, a training methodology was devised where an artificial hyperspectral image containing pure pigments as well as artificial colour mixtures was generated. The spatial arrangement of the data within the training image was found to be of high importance for the performance of the model. The training image generated consisted of squares of areas of pure and mixed pigments randomly distributed within the image. Although this image produced better results than vertical or horizontal bars, the content of the image could be perhaps improved by the use of other geometrical features like circles. Such an image containing non-linear features could potentially improve the performance of the model if the features are closer to real-life features found in paintings and drawings. Alternatively, a truly generated group of paintings where the pigment content is known could be manually created and hyperspectral images obtained to generate a set of ground truth images to be used for training and validation. However, this process can be time-consuming and may not be able to reproduce the features of Souza-Cardoso or use the same pigments as used in his artwork.

Regarding the hyperspectral unmixing problem, a deep learning model was implemented to estimate the proportions of the pigments in the reference database required to reconstruct a reflectance. The model successfully approximated the reflectances of a painting. However, the reflectances generated did not necessarily contain the same pigment proportions used in real-life verified via μEDXRF analysis. This is because the model is unconstrained and will always aim to approximate any given reflectance using a combination of all pigments in the reference database. This resulted in a large number of points classified as *Negative* in the authentication process thereby limiting the use of the proposed model to the estimation of reflectances and colours for restoration purposes only. Further improvements could however be made to the model architecture or perhaps to the training data which also play an important role in the performance of the model. Additional training and validation could be achieved should further imagery be made available where the actual content of the pigment proportions is known.

The final approach used for the authentication of artwork is therefore a combination of deep learning for pure pigment prediction and hyperspectral metric functions for mixed pigment identification. Using the method proposed with the improvements added to the colour difference calculation and generation of artificial mixtures achieved a significant improvement of the previous work based on the use of SAM and manual thresholding. Future development of this could include the use of the numerical spectral information obtained with μEDXRF for processing via machine learning. This could potentially reduce human intervention required during the identification of associated chemical elements, thereby increasing the reliability of the authentication process.

5 Conversion of sRGB to Hyperspectral Images

5.1 Introduction

This chapter presents implementation and results obtained from the work on the estimation of hyperspectral images from sRGB images. This task is particularly important for researchers as it provides them with powerful information regarding the colour content of a painting. Such information can be used to highlight features or reveal details that to the naked eye are hard to identify or that other techniques might not be able to uncover. These details can be used for the purpose of conservation, authentication of artwork or for image retrieval systems in other contexts [128]. Nevertheless, in the art world the difficulty to perform analysis of cultural heritage artwork intensifies as the number of artworks for any given artist is limited and access to original items for data acquisition can be unattainable. Therefore, it is important to devise methods to estimate certain data, in this particular case, hyperspectral images from existing accessible information in the form or sRGB images.

The work reported in this chapter is a by-product of our primary interest; artwork authentication using deep learning methods. This work is motivated by the need for hyperspectral imagery of drawings and watercolour artwork by Souza-Cardoso for testing the authentication methods developed. The approach proposed differs from other work by providing a method that uses a reduced set of available data for training. The method developed includes an architecture based on two DNNs; one reconstructing the hyperspectral image while the other corrects for biases from the acquisition method.

5.2 Methodology

Hyperspectral imaging is usually obtained with hyperspectral cameras and with direct access to the original artwork of interest. This can be a particularly challenging and expensive process which is in many cases, prohibitive. One way to solve this is by estimating hyperspectral images from bitmap images of the artwork. More specifically, estimating the hyperspectral image $\mathbf{Z} \in \mathbb{R}^{W \times H \times B}$ where W, H and B are the width, height and number of spectral bands respectively, from the sRGB image of the same painting $\mathbf{I} \in \mathbb{R}^{W \times H \times 3}$.

To estimate the hyperspectral image $\mathbf{Z}$, two sets of data are available. The first dataset is a dictionary of N reference reflectances $\mathbf{P}_{i,\lambda}$, $i \in \{1...N\}$ corresponding to base pigments known to have been used in at least a painting. The second dataset is an exemplary group of hyperspectral signatures $\mathbf{S} \in \mathbb{R}^{B}$ from a painting obtained with a hyperspectral camera and B spectral bands. This is, an array of reflectances from a true hyperspectral image.

The proposed method to address the problem at hand, consists of a two-step process that implements DNNs to estimate the reflectance of each pixel in a bitmap image of heritage artwork. A block diagram of the proposed method is shown in Figure 5.1.

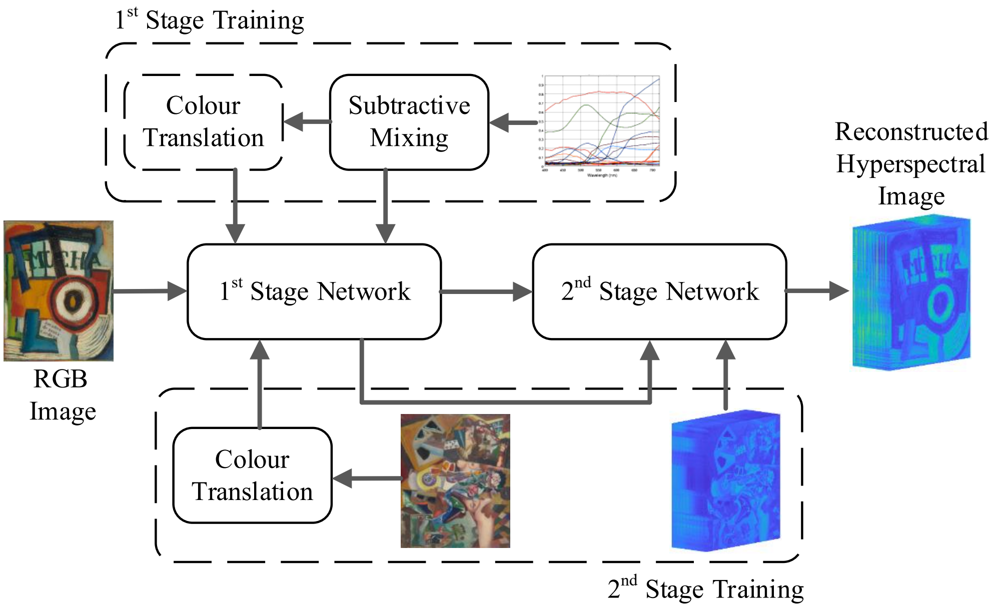

Figure 5.1: Block diagram of the proposed method for hyperspectral reconstruction from sRGB images.

In a first step, the preliminary hyperspectral image estimate is obtained by analysing the colour components of each pixel of the sRGB image with a DNN. More specifically, the CIELab colour components of a pixel in the sRGB image calculated using the D65 illuminant and CIE 1931 colour matching functions. The neural network proposed for this stage (1st Stage Network) is a 7-layer deep feed-forward, fully-connected network with 33, 35, 33, 30, 27, 25 and 20 neurons in each hidden layer respectively and a linear activation function. The training is performed by computing the mean squared error of the targets. This first network must be trained with a large dataset of reference reflectances and their corresponding CIELab colour components (Colour Translation).

The output of the first network can contain errors compared to a true hyperspectral image obtained with a camera due to the inherent effects of the camera itself or changes in illumination. Thus, a correction on the preliminary estimate is required and performed by the second stage network. This network is trained with the exemplary reflectance signatures $\mathbf{S} \in \mathbb{R}^B$ of a painting as labels and a first estimate of its corresponding sRGB image as input. The output of the second network therefore closely resembles the output of the hyperspectral camera if used on the same painting analysed. The network proposed for the second stage is a 4-layer deep feed-forward, fully-connected network with 33, 35, 35 and 33 neurons on each hidden layer respectively and with a linear activation function. The correction applied by this network is less complex than the initial colour to reflectance estimation which allows for a lower number of hidden layers required. The performance of the network is computed using the mean square error function.

5.2.1 Training and Test Data

The data used for this task are the set of reflectances previously collected at DCR of NOVA and used by [171]. These include the reflectances of the 16 pigments of appendix A as selected by [171] plus Cadmium Green. These reference reflectances are shown in Figure 5.2.

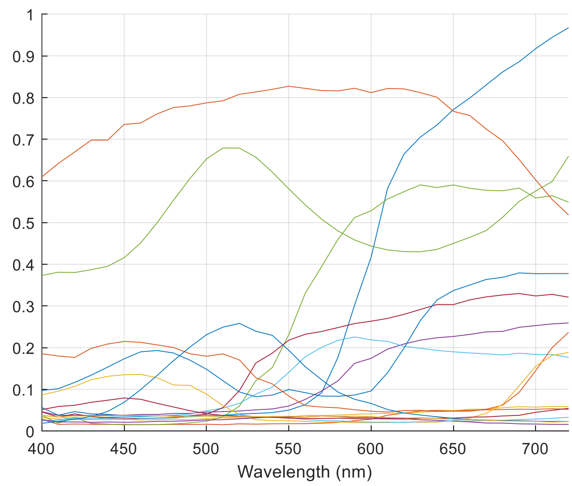

Figure 5.2: Reflectances in the reference database used as selected in [171].

Artificial mixtures using up to 3 pigments out of 17 in steps of 10% of the reference reflectance database were generated using the subtractive colour mixing model proposed in Eq. 4.5. The sRGB representation of the mixtures is shown in Figure 5.3. The corresponding CIELab colour components to be used in the first stage network were also computed for each artificial mixture generated using the D65 illuminant.

The test dataset includes a subset of the hyperspectral image database in appendix B as shown in Figure 5.4 corresponding to images of painting by Amadeo de Souza-Cardoso only.

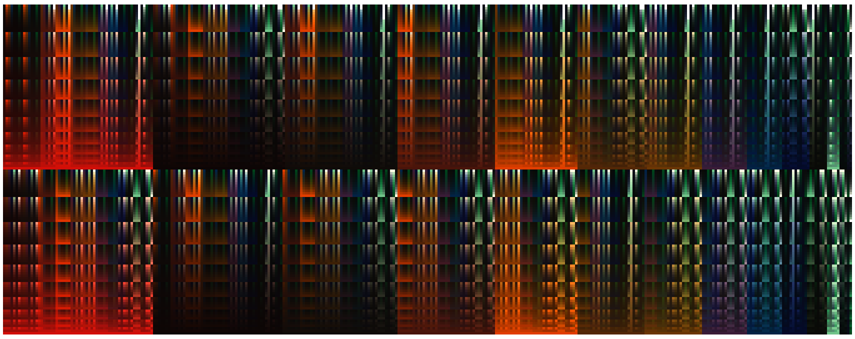

Figure 5.3: sRGB representation of the mixtures used for training of the first stage network.

Figure 5.4: sRGB representation of the hyperspectral image dataset used.

5.3 Test Results

Each of the 11 hyperspectral images in the test dataset was converted to sRGB and CIELab colour components which then were fed through the 2-stage process to estimate the hyperspectral cube. An example of a reconstructed reflectance obtained for a point of image 86P21 is shown in Figure 5.5 along with the ground truth version for comparison. As observed, the overall signature of the reconstructed reflectance shows a similar pattern as that of its ground truth version.

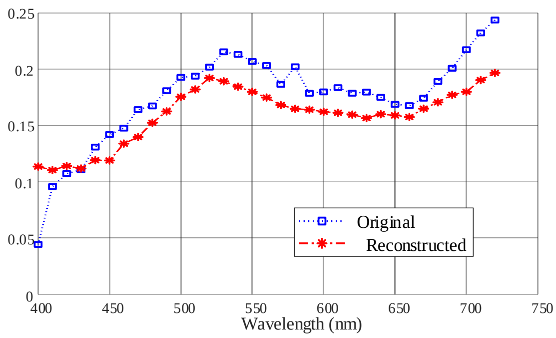

Figure 5.5: Ground truth and reconstructed reflectances for pixel 50,50 in painting 86P21.

To analyse the performance of the algorithm proposed the reconstruction error was calculated using MRAE as defined in Eq. 4.8. The second function to estimate the error is SAM averaged over the entire hyperspectral image as defined in Eq. 5.1 . The reconstruction error between original and reconstructed hyperspectral images is presented in Table 5.1.

$$SAM = \frac{1}{n}\sum_{i=1}^{n}\cos^{-1}\frac{\hat{z}_{ij}^{T}z_{ij}}{\|\hat{z}_{ij}\|_2\|z_{ij}\|_2} \tag{5.1}$$

Table 5.1: Reconstruction error measured using MRAE and SAM.

Painting	MRAE	SAM
68P11	0.0750	0.0815
77P2	0.1384	0.1737
77P5	0.1239	0.0929
77P8	0.1649	0.1473
77P9	0.1755	0.1603
77P16	0.4938	0.1220
77P20	0.9959	0.1155
86P19	0.2524	0.1293
86P21	0.2763	0.1670
86P23	0.7010	0.1685
92P209	0.4610	0.1695

For visual comparison of the results obtained, hyperspectral images at selected wavelengths are displayed in Figure 5.6 for painting 86P21; hyperspectral images are displayed in 8-bit greyscale for visualisation. The error map between the ground truth and the reconstruction highlights the regions where the largest discrepancy is found for the selected wavelengths; the error appears higher towards the upper end of the spectrum.

Finally, a comparison of the sRGB images generated from the original and reconstructed hyperspectral images is shown in Figure 5.7 with the colour difference measured as the ED of the CIELab colour components for each pixel.

5.4 Conclusion

The work achieved the development of a practical method where readily available hyperspectral signatures of reference oil paint pigments are used in conjunction with two

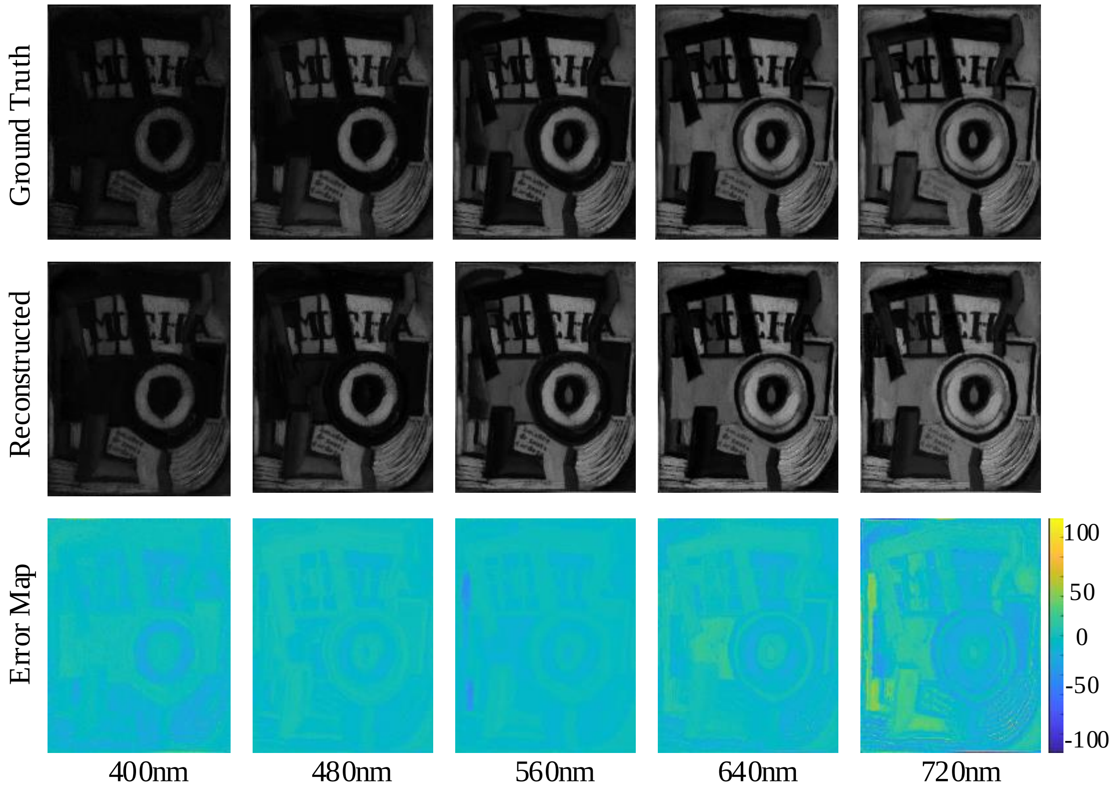

Figure 5.6: Reconstructed and ground truth reflectances at selected wavelengths of image 86P21. Error map on a scale of ±255 RGB.

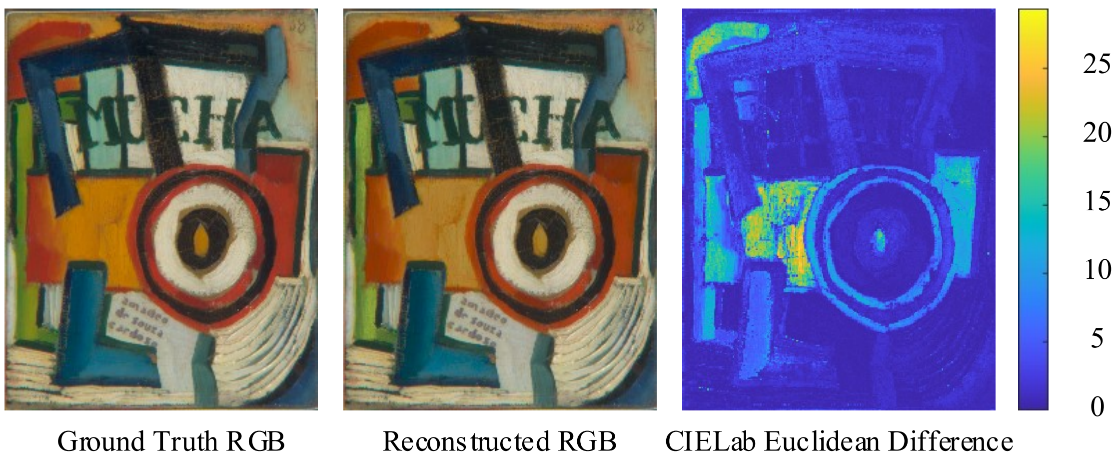

Figure 5.7: sRGB version of the ground truth and the reconstructed hyperspectral image of painting 86P21. Error map shown as the Euclidean difference of the CIELab values.

DNNs to reconstruct hyperspectral images of paintings. This is, for a new unseen sRGB image of a painting, its corresponding hyperspectral data can be reconstructed through the method proposed. The first network in the method is trained with the reflectance of artificial colour mixtures and their corresponding colour representation allowing reflectance prediction in the new unseen sRGB images. The second network serves as a regulator to learn and adjust the inherent characteristics such as illumination and camera properties. The results obtained however do not consider the effects of metamerism or that caused by layers on the paintings due to ageing, dirt or protective coatings. Despite the limitations and approximation error, in particular at higher wavelengths, the proposed method has achieved promising results for use in the analysis of heritage artwork, namely paintings by Souza-Cardoso.

Although the pigment mixtures in this case were limited to artificial mixtures of 3 pigments, it is recognised that in practice such a mixture rarely is limited in real life. On many occasions the mixtures might contain more pigments depending on the style of the artist. This aspect could be also a contributing factor to the errors measured. In other words, the artificial mixture can be generated by any chosen number of pigments with any arbitrary percentages. However, increasing the number of pigments in the mixture and the resolution of their concentrations, results in an increased computational load that grows exponentially potentially rendering the implementation prohibitive.

In conclusion, our approach successfully provides an alternative point of view in terms of spectral reconstruction and is interesting in the art field, when neither hyperspectral cubes of the artworks, nor high-resolution sRGB images are easily attainable, yet pre-acquired hyperspectral curves of base materials are available. If the reflectance data of known base pigments are unavailable, the proposed method could be used by building the dictionary of base reflectances from user-selected points of the hyperspectral image of a given painting. Artificial mixtures could then be generated from the selected reflectances thereby allowing to describe other paintings in terms of the chosen data. Thus, to reduce the reconstruction error, a wide selection of points with different colour would be required.

6 Analysis Tools

6.1 Introduction

In this section, the rationale and importance concerning the development of two applications are explained. First, an AR mobile application aiming for the general public, i.e., museum visitors, art enthusiasts, art lovers or art experts, to visualise the pigment of the artworks by Amadeo de Souza-Cardoso. Second, a desktop application aiming for art specialists, i.e., conservators and restorers, with multiple purposes, such as the visualisation of pigments and hyperspectral data.

6.1.1 Motivation

As we continue striding in the 21st century with the rapid advancement and innovation in multitudinous aspects, digitalisation is no longer a new concept referring to technological development, but more of a lifestyle. Society 5.0 is the very example of such a revolution in terms of digitalisation, where humans are deemed the centre of our society. This idea was first introduced in Japan, following a chronological definition of Hunting and Gathering Society (Society 1.0), Farming Society or Agricultural Society (Society 2.0), Industrial Society (Society 3.0), Information Society (Society 4.0), and Human-Centred Society (Society 5.0) [97, 220, 227].

Society 5.0 implements the most state-of-art technologies, such as AI and the Internet of Things (IoT) to facilitate human day-to-day life. The majority of these applications in Society 5.0 focus on public services such as healthcare and transportation, and daily activities like eating, shopping, and learning. Sometimes, it extends to broader services like disaster prediction and prevention, agriculture optimisation and logistics automation among others [97, 220, 227]. However, relatively less attention is paid to cultural heritage sectors in Society 5.0, to be more precise, the implementation of such high technology in artistic settings like galleries and museums.

The applications of AR and Virtual Reality (VR), that can provide an interactive and immersive experience for the users have been gradually introduced to visitors in so-called cultural heritage tourism just in the last few years [37]. Studies concerning AR and VR also have been slowly established to evaluate the impact on a user-centred experience. For instance, the work in [173] investigated the use of AR at a Jewish museum targeting mainly school children, and reported a more engaging and enhanced learning experience in an educational and cultural context, as well as a more sustainable museum infrastructure. The ArkaeVision project [37] introduced a game-like virtual environment to further motivate the users to have a more "culturally-qualified" immersion in a storytelling context to explore historical architectures; it was deemed to be very promising to provide a communicative and explorative approach to an educational and cultural heritage learning experience. The work in [238] created a large-scale VR experience juxtaposing the virtual and physical spaces making full use of the human physical, tactile and vestibular sensations via the stimulation from the visual and audio information of the VR. Such installations proved to be very convenient and re-applicable in different museums since they are scalable, tourable and can easily be moved around without conventional fixated installations. Although in the work of [257], the author intended to conduct a direct comparison of user experiences between these two types of technologies, the acquired results showed only positive feedback in areas including enjoyment, presence, cognitive, emotional and behaviour engagement in both, with slightly higher scores obtained for VR technology than AR technology in just a few aspects. The work in [75] confirmed the value of AR in various aspects such as economic, social, cultural and historical from the stakeholders' perspectives via a case study. The study published in [30] also reviewed different systems including AR, VR and mixed-reality systems in order to identify appropriate installation for specific cases in cultural heritage settings. Other examples include the work in [117], where two AR applications were tested and determined that active interactive participation improved participants' understanding of historical events. Or the work in [134], where experiments were performed on school children by integrating educational learning with AR games making understanding and learning more entertaining.

Despite the continuous advancement and emergence of AR, VR and mixed media systems, their use in cultural and historical environments is still sparse [22]. In Portugal, the use of these technologies in the areas of authentication, conservation and restoration remains limited. In pursuance of bridging the gap between cultural heritage and technology, an AR application and a desktop application are proposed based on research on the artworks done by late Portuguese artist Amadeo de Souza-Cardoso. The implementation and use of these is expected to help with the dissemination of information via a more engaging and captivating method for museum and gallery participants. Similarly, their use is intended to help connecting the collaborative networks concerning governmental entities, the scientific community and cultural institutions. This chapter elaborates on the details concerning the applications development by a successfully established collaborative network, and its application and benefit in the pursuit of a Society 5.0 environment.

6.1.2 Background

We present a case study that showcases some of the results collated from a long-term project established in the field of cultural heritage conservation and restoration. In particular, the work is focused on the artwork by the late Portuguese artist Amadeo de Souza-Cardoso. The work intends to analyse his artwork while creating tools that facilitate the scientific and forensic analysis of his creations. Through the project, it is expected that the results obtained will lead to a more thorough understanding of the artist's style and techniques as well as to the implementation of processes for art authentication and prevention of forgeries. The knowledge and information acquired will also contribute to the production of techniques and material for the dissemination of information and the inclusion of society in the preservation of cultural heritage.

The successful progress of the project to date has been achieved by the establishment of a network of organisations sharing a common objective: the study and dissemination of information related to cultural heritage. The structure of this collaborative network, as shown in Figure 6.1, contains a variety of entities including scientific researchers from multiple academic institutions, government departments, historians, curators and museums.

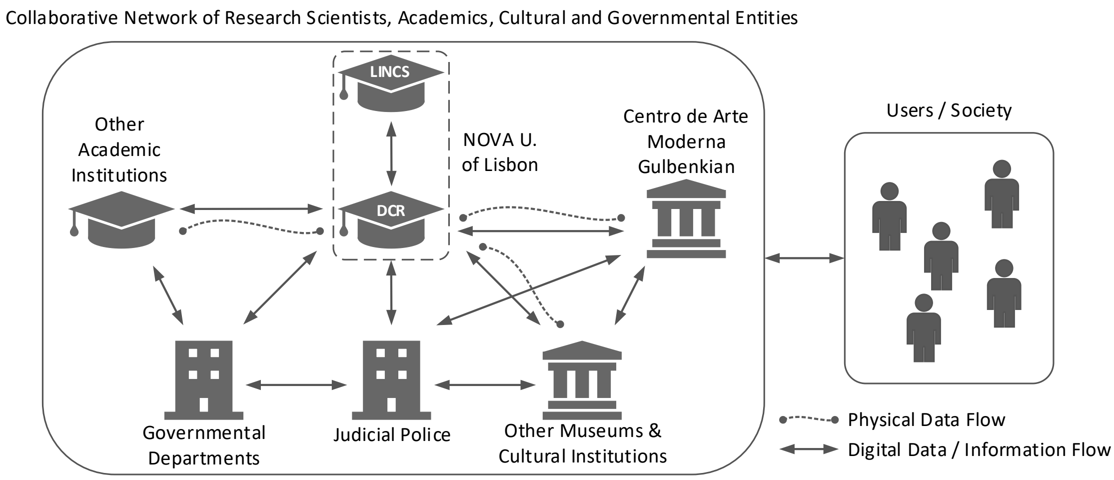

Figure 6.1: Block diagram of the collaborative network of the case study.

During the earlier stages of the project [10, 172], a dynamic team effort between entities was required to complete the data acquisition process. This included the invaluable assistance from museums for direct access to the artwork and the support of internal and external academic laboratories for access to specialised analytical and hyperspectral imaging equipment. Beyond the presential use of these temporary, virtual laboratories for physical data processing, the majority of the team interaction was conducted through the use of digital channels for sharing digital information, methodologies, results and organisation of other activities.

In subsequent stages of the project, researchers from different areas of specialisation turned their attention to the analysis of the data by employing analytical and digital processing techniques. This interdisciplinary work effectively resulted in the generation of algorithms to determine features of interest in the artwork; e.g., chemical composition, colour identification and degree of authenticity. These algorithms were implemented in a desktop application to facilitate the analysis of data, in particular, by government institutions to verify the authenticity of works of art.

With the information and progress attained, the focus of the research team turned to the next step where the following questions were considered: How can the knowledge and techniques developed be used for the benefit of society? Is it possible to increase awareness of the need to preserve cultural heritage while engaging society through the use of modern technology? To answer these questions, the team proposed the use of desktop and mobile applications for the analysis and visualisation of artwork that could be used by a wide variety of skilled and non-skilled individuals. The particular use case scenario targeted society, where it was envisaged that museum visitors could use an AR-enabled mobile application to enhance their visiting experience. The expected outcome of this solution was twofold; first, the mobile application would be used to disseminate results obtained by the research group and second, it would engage users with art through technology thereby fulfilling the objective of benefiting society with a step forward towards Society 5.0.

6.2 Amadeo AR

6.2.1 Overview

The applications covered in this study are focused on the artwork from Amadeo de Souza-Cardoso which is primarily on display at the Calouste Gulbenkian Museum in Lisbon. The artwork was limited initially to a group of 11 paintings of Souza-Cardoso (Figure 6.2) along with a selection of 16 pigments known to have been used by the artist. A group of individuals from different organisations were involved in the temporary acquisition of the original artwork from the Calouste Gulbenkian Museum for photography and digitisation. The hyperspectral images obtained were made available to the rest of the team members for analysis.

Prediction of features of interest was achieved through the analysis of the hyperspectral and analytical data using deep learning algorithms developed by the scientific team. These algorithms were implemented in a desktop application and included the following two main methods among others:

- The combination of numerical metric functions and convolutional neural networks for the identification of pure pigments [53].

- The estimation of the probability of artwork belonging to Souza-Cardoso based on brushstroke analysis using convolutional neural networks [54].

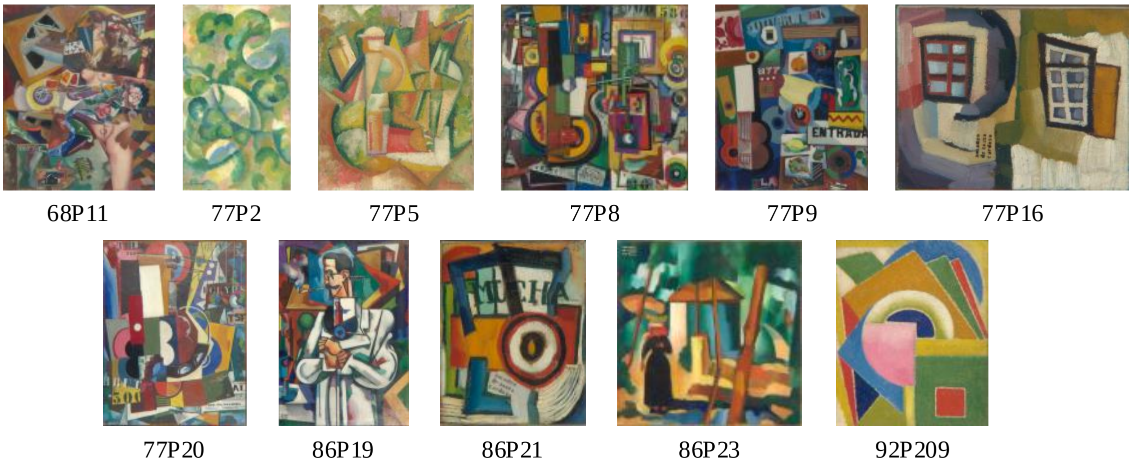

Figure 6.2: Overview of the 11 paintings by Amadeo de Souza-Cardoso evaluated.

Post-processing of the results generated images highlighting individual pigments of the artwork that were subsequently compiled into a database for ease of use. Finally, the results of the analyses using the desktop application can be then combined to obtain a statistical evaluation of the authenticity of the artwork evaluated.

The proof of concept of Amadeo AR was developed at the NOVA University of Lisbon using imagery obtained through painting analysis. To facilitate future access of the application to the wider society, the mobile application was developed using the Android operating system given the significant 71% worldwide market share compared to the 28% of its main competitor, iOS [231].

The functionality of the mobile application has been, in principle, constrained to the visualisation of previously identified features through the use of AR technology. Figure 6.3 shows the block diagram highlighting the data and functionality of Amadeo AR.

The Amadeo AR visualisation process includes the capture and real-time display of frames with the integrated device camera. The frames are evaluated using Google's ARCore technology to identify paintings from within a predefined reference database. The image is subsequently augmented by overlaying images containing features of interest, namely the presence of pigments in the reference database. The overlay images are stored locally and are the result of the analysis performed by the research team using machine learning algorithms and analysis of hyperspectral imagery.

Currently, the mobile application is constrained to the use of reference and overlay images derived from the 11 paintings analysed from the collection of Amadeo de Souza-Cardoso as seen in Figure 6.4. However, it is expected that future deployment of data through the use of cloud services will allow the visualisation of newly analysed images. This will allow the research team to further expand the dictionary of analysed artworks paving the road for the potential expansion to cover artwork from other artists and genres.

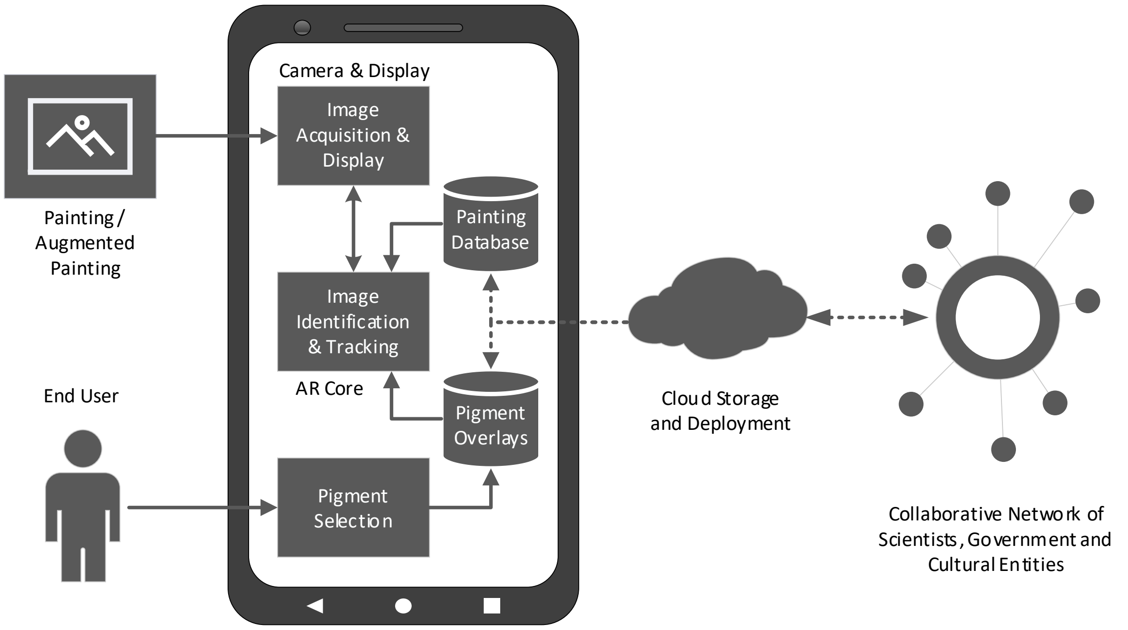

Figure 6.3: Block diagram of Amadeo AR. Dotted lines indicate proposed future development features.

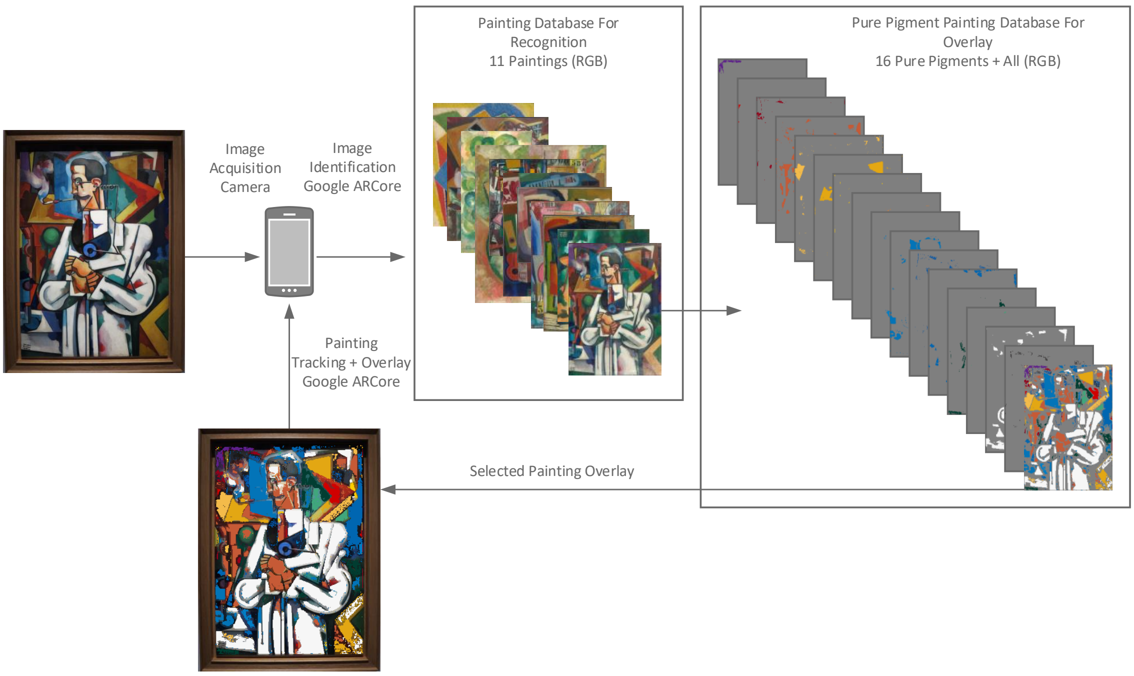

Figure 6.4: Detailed diagram of image data in Amadeo AR.

6.2.2 Usage

This section provides details of the use of the Amadeo AR application with images of paintings by Souza-Cardoso including examples and practical instructions for its use on a mobile phone.

After launching the application, the user is presented with a welcome screen (Figure 6.5(a)). A menu button is available to show the currently available activities: "*Home*", "*Pure Pigments*" and "*About*" (Figure 6.5(b)). By clicking "*Home*", the user is directed back to the "*Welcome*" page. By clicking "*About*", the user is directed to a page detailing basic information about the project and application including software version, sponsors and the associated museum, that is, Calouste Gulbenkian Museum (Figure 6.5(c)).

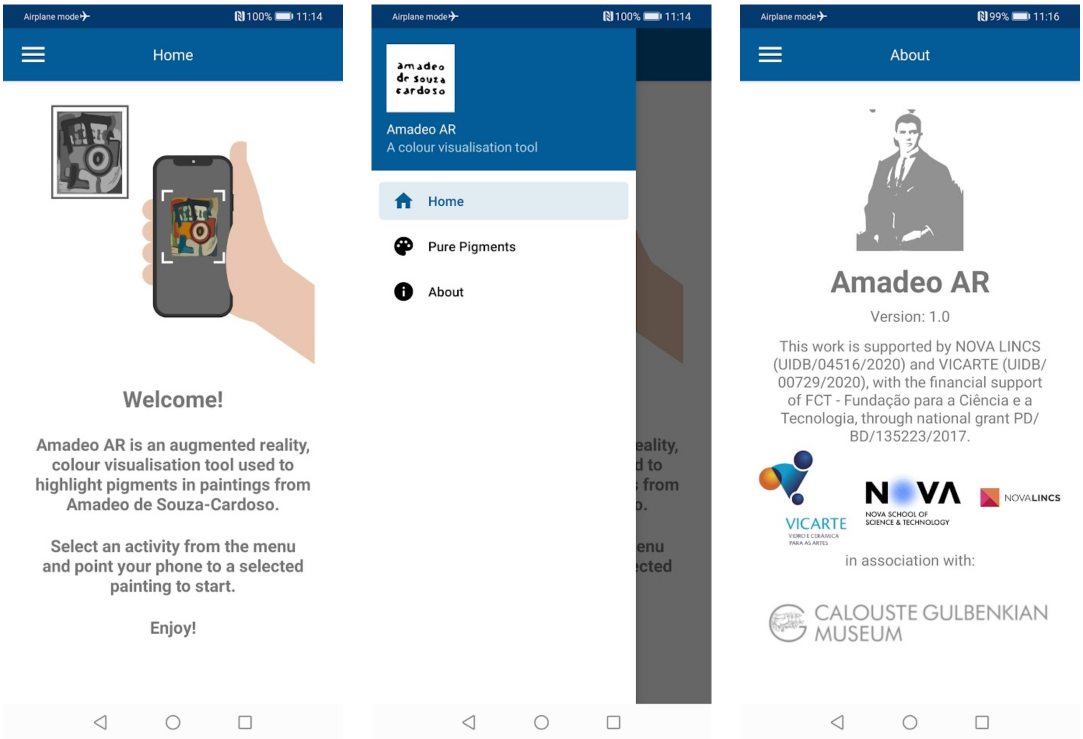

(a) Welcome (b) Menu (c) About

Figure 6.5: Amadeo AR main screens.

By clicking "*Pure Pigments*", the user is directed to the primary activity containing a live-camera screen where images of Souza-Cardoso's paintings can be scanned (Figure 6.6(a)). The user is required to point the camera towards a painting and keep the mobile steady to allow the software to scan and recognise the image successfully (Figure 6.6(b)). If the image of the painting is recognised, the predicted pure pigment overlay image will be displayed floating on top of the original image (Figure 6.6(c)). The user will then be presented with three buttons: a "*reload*" symbol, "*i*" and "+". The "+" button will show the list of all pure pigments available allowing the user to select a single or all pigments to highlight (Figure 6.6(d) and Figure 6.6(e)). The "*i*" button will bring up a screen with information related to the currently tracked painting (Figure 6.6(f)). Finally, the "*reload*" button will refresh the screen and clear the AR image so that the user can start afresh to scan a new painting image.

6.3 Amadeo Image Analysis Tool

6.3.1 Overview

The Amadeo Image Analysis Tool is a computer-based application that implements some of the algorithms developed during this research. Thus, the deep learning models and processing are tailored to suit the artwork from Amadeo de Souza-Cardoso. Yet, the tools included can be easily used or expanded to include analysis of the artwork of other artists.

Currently, the Amadeo Image Analysis Tool (Figure 6.7) includes the following functionality:

- Conversion from sRGB to hyperspectral image (Chapter 5)
- Hyperspectral data visualisation
- Pure pigment prediction and visualisation (Chapter 4)
- Reference pigment palette visualisation
- Brushstroke analysis (Chapter 3)

Conversion of sRGB images to hyperspectral images uses artificial neural networks to estimate the reflectance of an image on a pixel-by-pixel basis. Pure pigment identification from hyperspectral images is implemented through a deep learning model that predicts areas of the image that closely match those pigments in the reference palette. Alternative methods based on metric functions including RMSE, SAM and SCM are included for comparison. Brushstroke analysis calculates the probability of a bitmap image being one of Souza-Cardoso's artworks based on a deep learning model that analyses the features of the image.

6.3.2 Usage

This section provides basic instructions on the use of the Amadeo Image Analysis Tool software. Examples of the functionality implemented are provided with images of paintings of Amadeo de Souza-Cardoso.

The tool contains a menu that allows navigation between the multiple screens available as shown in Figure 6.8. These include: "*Home*", "*RGB To HS*", "*HS Viewer*", "*HS Pure Pigment Viewer*", "*Pure Pigment Palette Viewer*", "*Brushstroke Analysis*" and "*About*".

The "*RGB To HS*" screen (Figure 6.9) allows the user to load an sRGB image in BMP, PNG or JPG format by clicking the "*LOAD RGB*" button and convert it to hyperspectral

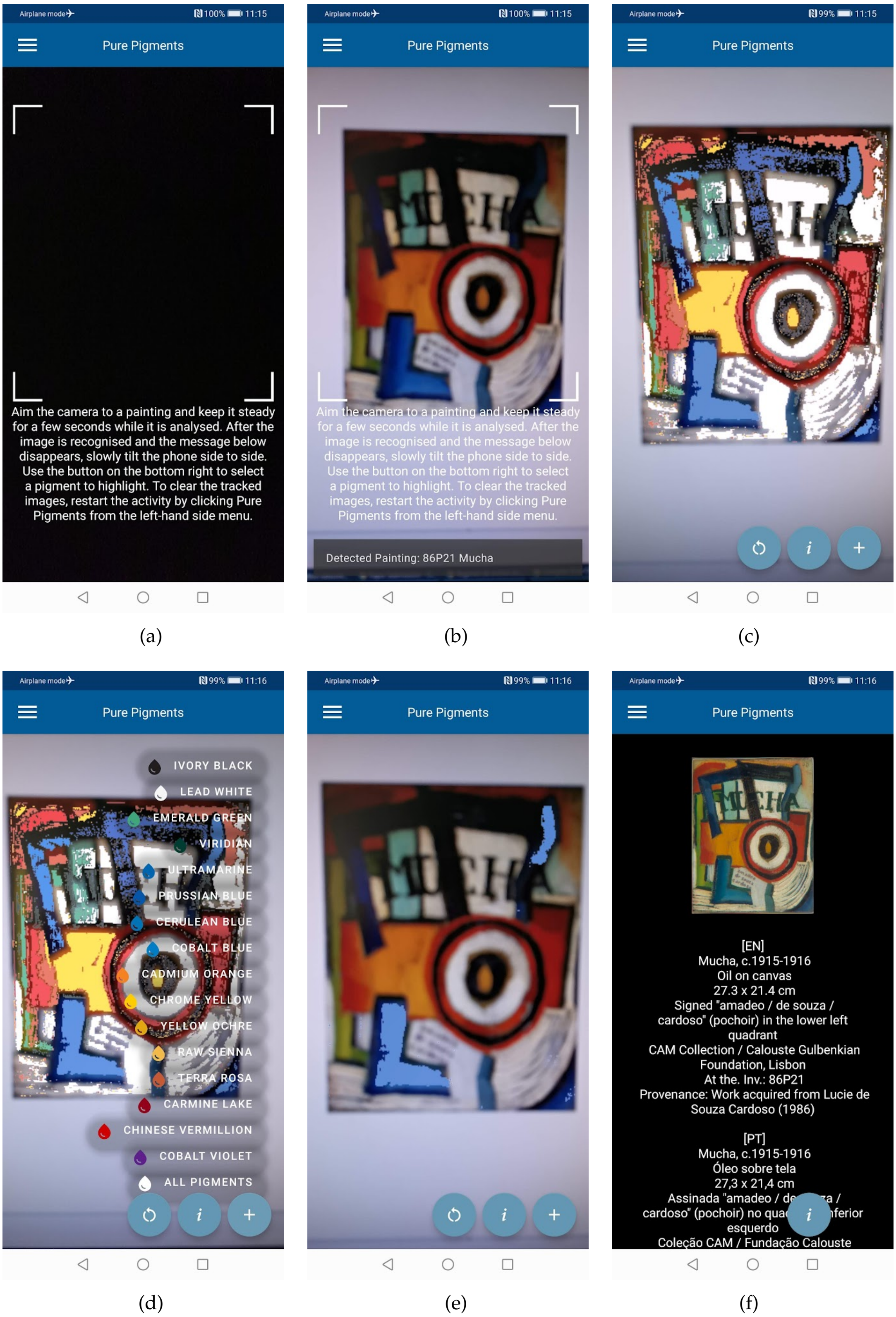

Figure 6.6: Amadeo AR "*Pure Pigments*" screens.

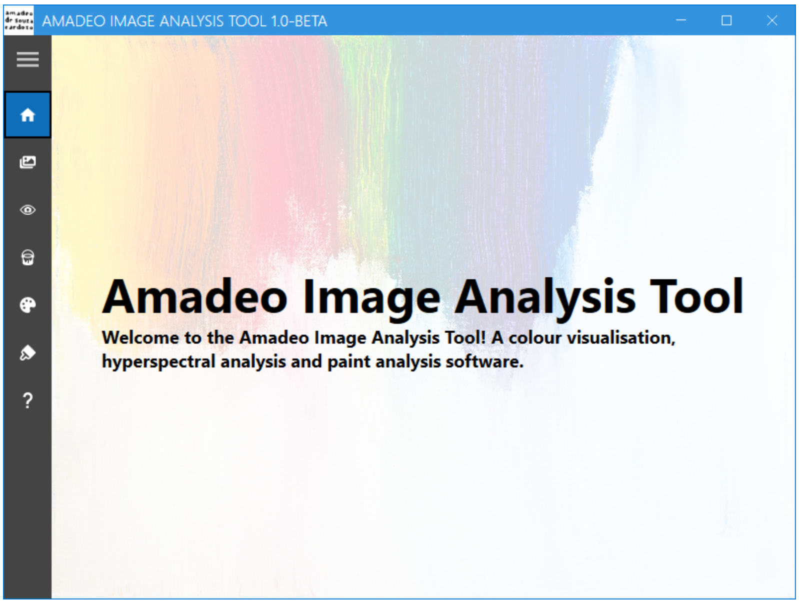

Figure 6.7: Amadeo Image Analysis Tool: *Home* screen.

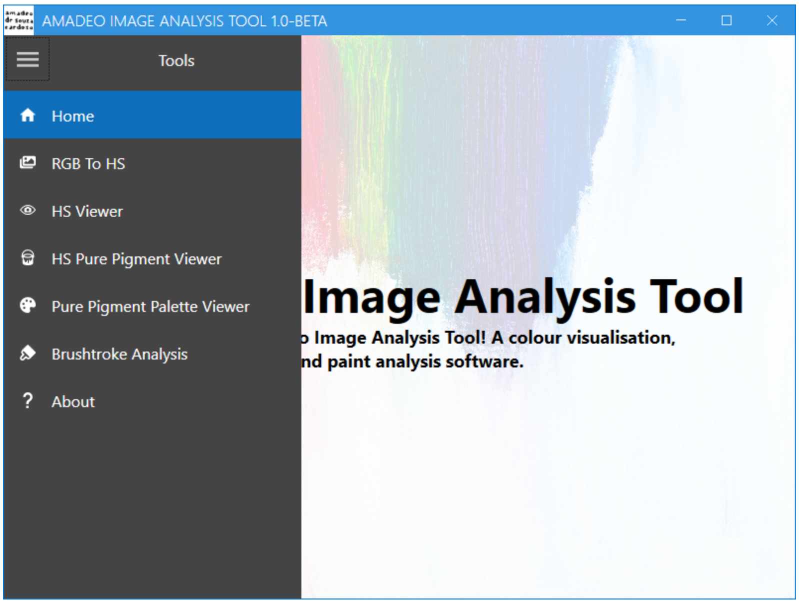

Figure 6.8: Amadeo Image Analysis Tool: menu.

data by clicking the "*CONVERT TO HS*" button using the supplied deep learning model. The user can then visualise the estimated hyperspectral image at multiple wavelengths using a variety of colour maps. The hyperspectral data can finally be exported as an image, an animated Graphics Interchange Format (GIF) file or Matlab data.

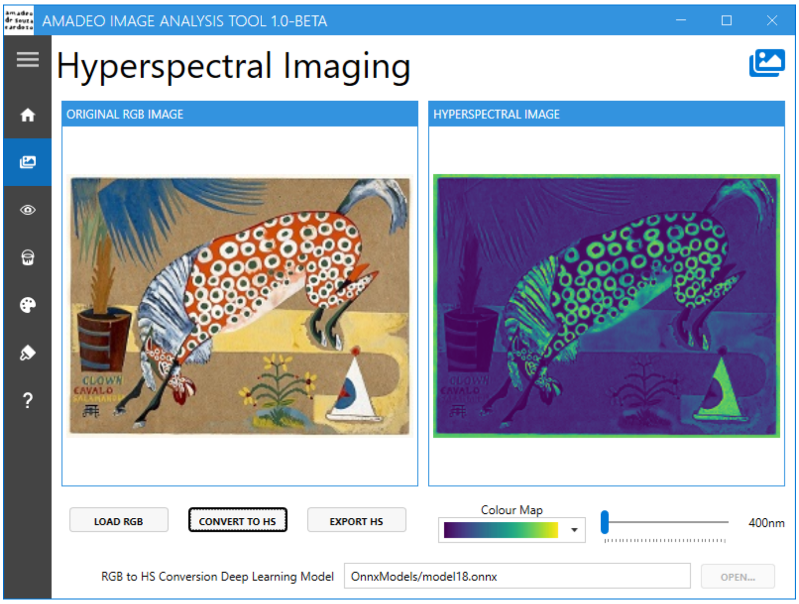

Figure 6.9: Amadeo Image Analysis Tool: *RGB to HS* screen.

In the "*HS Viewer*" screen (Figure 6.10), the user can visualise the reflectance of any point in a hyperspectral image by clicking on the image. This hyperspectral image can be the image estimated in the previous screen. Alternatively, the user can load a Matlab file containing the hyperspectral image. Zoom functionality is provided for ease of use.

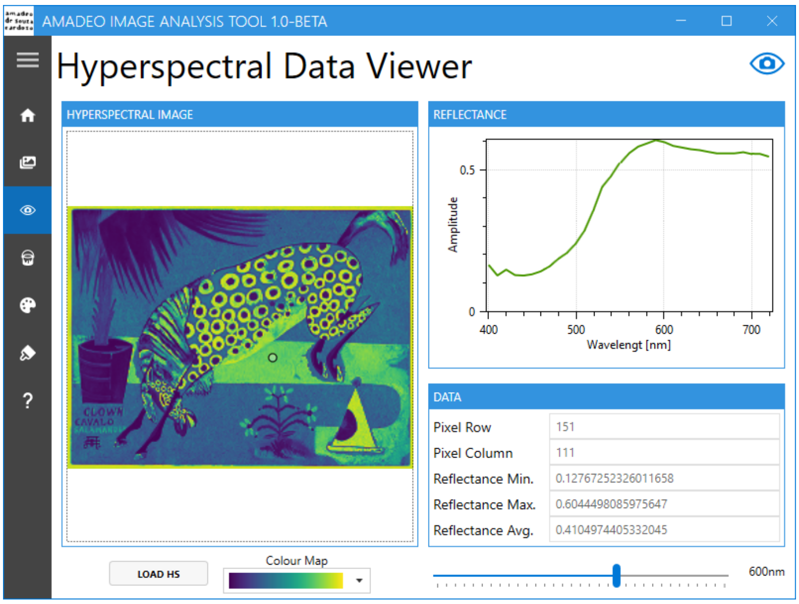

Figure 6.10: Amadeo Image Analysis Tool: *Hyperspectral Data Viewer* screen.

The "*HS Pure Pigment Viewer*" screen (Figure 6.11) allows the user to predict the pure pigments in the hyperspectral image currently loaded using a deep learning model (*DNN*) or one of the metric functions available (*SCM*, *SAM* or *RMSE*). On the right-hand side, information concerning the pure pigments detected is shown. At the bottom of the screen, the user can choose either opacity of the original image or the opacity of the predicted overlay to analyse in more detail the exact location of the detected pure pigments. When the user is satisfied with the comparison between the original sRGB image and the image with predicted pure pigments after having tweaked the opacity of each image, the user can use the "*EXPORT RESULTS*" button to export the results in a Comma Separated Values (CSV) file or the "*EXPORT IMAGE*" button to export the results to an image file.

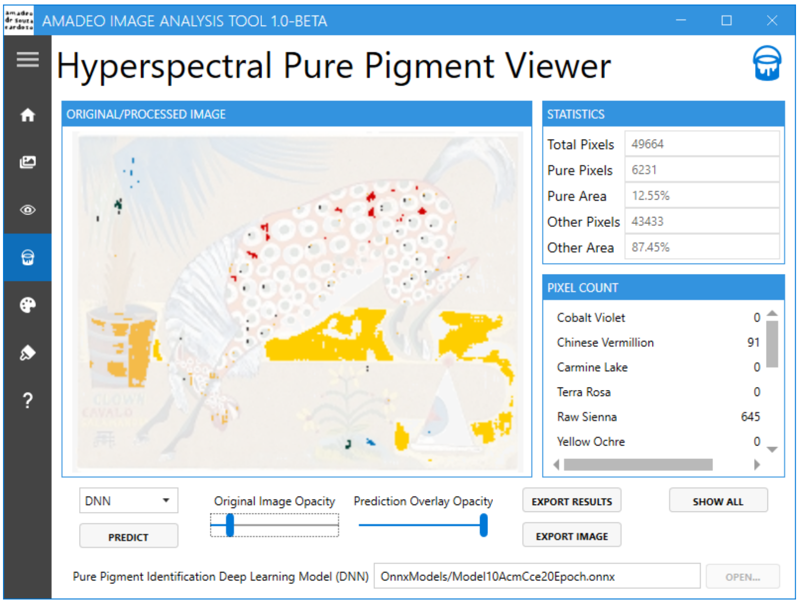

Figure 6.11: Amadeo Image Analysis Tool: *HS Pure Pigment Viewer* screen.

Choosing "*Pure Pigment Palette Viewer*" (Figure 6.12) allows the user to view the information about the pure pigments used in this project. The information available includes the spectral curve of each pigment, the colour coordinates in sRGB, CIE 1931 XYZ Colour Space (XYZ), CIELab colour components and the relevant chemical components associated with each pure pigment. The 16 default pure pigments are the pigments obtained directly from the paint tubes that Souza-Cardoso used during his lifetime. Theoretically, the user can also load other pure pigment database files if available.

In the "*Brushstroke Analysis*" screen (Figure 6.13), the user can analyse an sRGB image of a painting using a deep learning model to predict if the painting is an authentic artwork by Souza-Cardoso or not. First, the user must load the sRGB image of the painting to be analysed in BMP, PNG or JPG format, and then select the number of samples of the image to be used for analysis; the higher the number of samples, the more accurate the result will be. The size of the samples used in the algorithm is 227×227 pixels corresponding to randomly cropped images from the painting image; these samples are augmented as described in section 3.3. Upon clicking "*RUN ANALYSIS*", the progress and results will be displayed on the right-hand side of the screen, where individual samples will

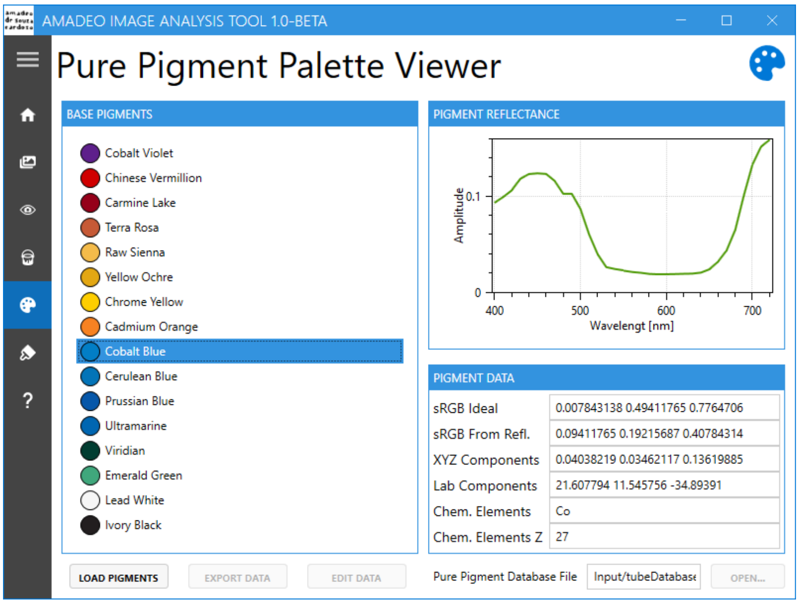

Figure 6.12: Amadeo Image Analysis Tool: *Pure Pigment Palette Viewer* screen.

be previewed. When the processing is finished, the final probability in terms of the authenticity of the processed painting belonging to Souza-Cardoso will be displayed at the bottom.

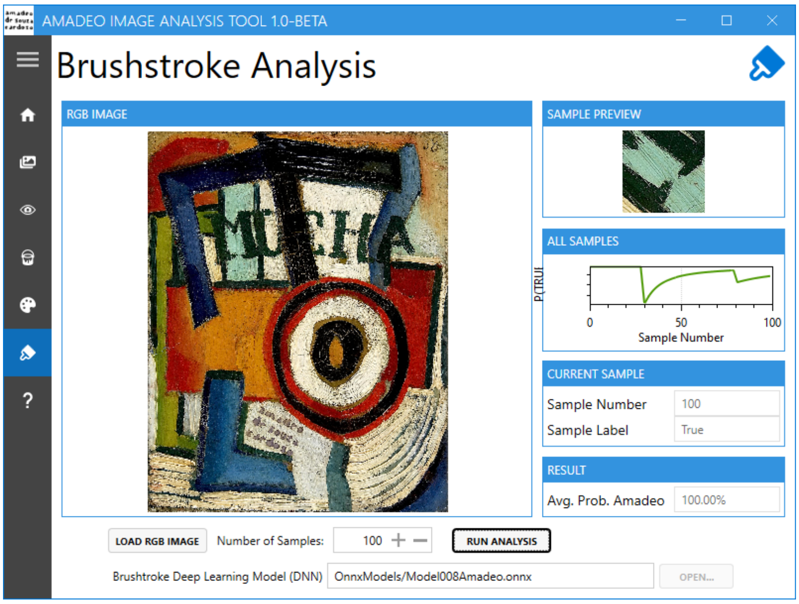

Figure 6.13: Amadeo Image Analysis Tool: *Brushstroke Analysis* screen.

Finally, the "*About*" screen (Figure 6.14)contains information regarding the sponsor of the work and application developed.

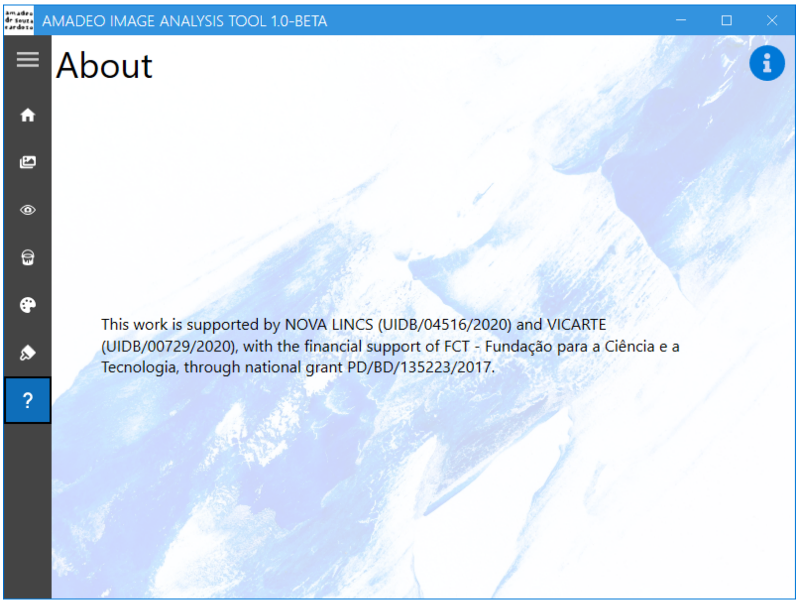

Figure 6.14: Amadeo Image Analysis Tool: *About* screen.

6.4 Usability Trial

Trials involving end-users were performed to evaluate both the desktop application and the Amadeo AR mobile application. The former was designed to be evaluated as a tool to be used by scientific researchers and government organisations while the latter was envisaged to be evaluated as a solution to the research questions proposed. Unfortunately, due to the unexpected circumstance of the pandemic, the trials on the usage of the two applications as well as questionnaires concerning their user experience could only be performed within the Department of Conservation and Restoration at NOVA University Lisbon (Figure 6.15).

To simplify and reduce the time of the trial and ensure that the subjects do not get disinterested easily, which would result in the inaccuracy of the feedback, the questionnaires were intentionally constructed short, and in a very simple and easy-to-answer manner in Google forms digitally. A copy of the questions and final responses obtained via Google forms can be found in Appendix C. The summary of the feedback obtained is as follows.

For the desktop application trial, a group of 17 participants from the scientific community were given access to the application and sample digital images of artwork for evaluation. The participants were then asked to provide feedback based on the user experience via a digital feedback questionnaire. The results, as shown in Figure 6.16, suggest that although the majority of the participants found the desktop application easy to use, some improvements to make the application more intuitive would be beneficial. These could be, for example, adding help buttons, descriptive text and tutorials. Overall, this application was received with positive feedback and encouragement by the academic society as indicated by one of the test users: "*Add another analysis like Raman, but it was perfect until now and I'm surprised*".

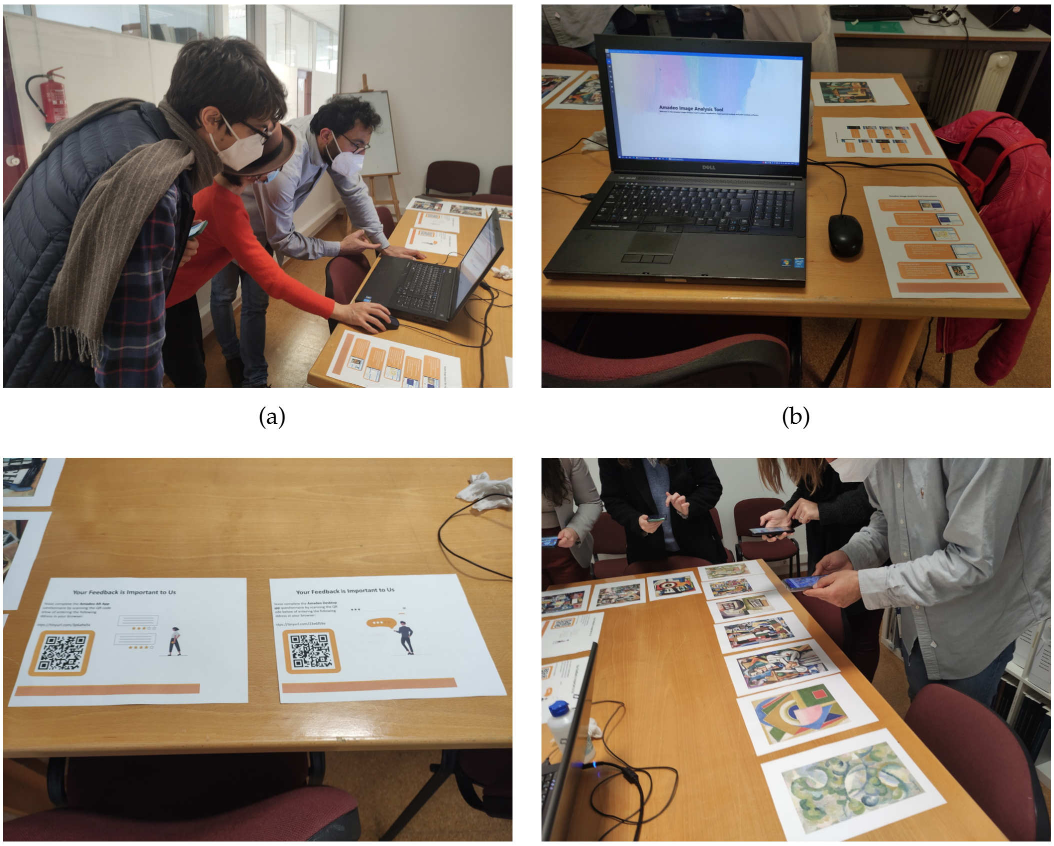

(a) (b) (c) (d)

Figure 6.15: Photos of the usability trial of Amadeo AR and Amadeo Image Analysis Tool at DCR of NOVA University Lisbon.

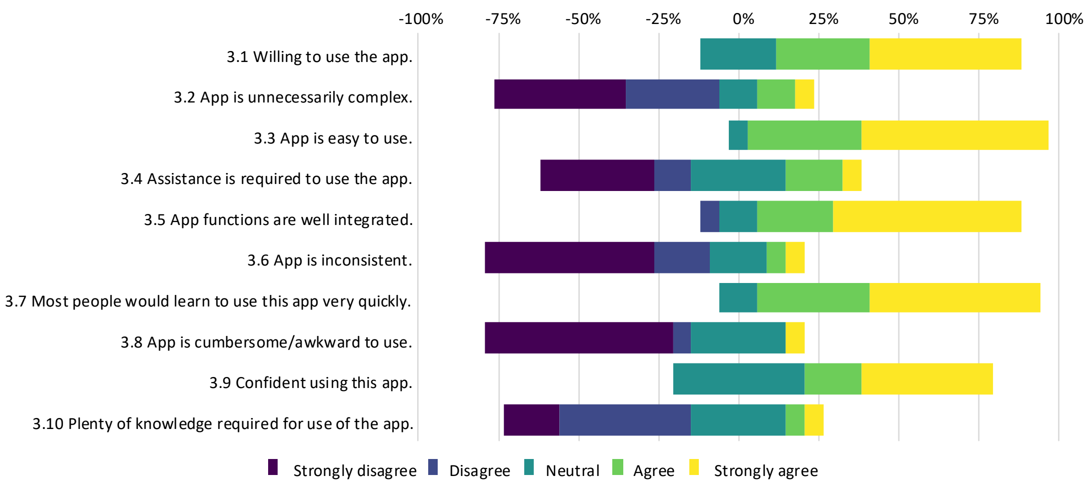

Figure 6.16: Survey results for questions 3.1 to 3.10 from the desktop application trial.

For the Amadeo AR application, trials involved direct use of the mobile application by a group of 24 volunteers of various backgrounds. The users tested the Amadeo AR functionality using printed copies of the artwork analysed and provided feedback on the overall user experience through a short online survey. The findings of the survey revealed that 79.2% of the participants were not familiar with Amadeo de Souza-Cardoso or his artwork despite him being a well-renowned modernist artist in Portugal. This strengthens the need for engagement of the society with local heritage and the requirement for further efforts to promote cultural activities. Regarding familiarity with AR applications, 91.7% of the participants indicated no previous user experience giving a good, unbiased indication of the overall satisfaction using Amadeo AR. In this case, the majority of participants indicated a good experience as shown in Figure 6.17. Finally, an indication of the success of the case study was obtained by asking the participants if the use of AR applications like Amadeo AR is important in a cultural setting like a museum, and whether an AR application would increase the likelihood to visit museum exhibits. In both cases, the overall majority of the participants supported the use of AR applications in a museum with less than 5% of the population sample indicating low importance. The findings of the trial in the case study, support the proposed solution to the need for bridging the gap between technology and cultural heritage. In particular, the mobile application Amadeo AR was found to have a positive impact on the population sample used. This marks a step forward toward the use of technology for the benefit of society and the art world.

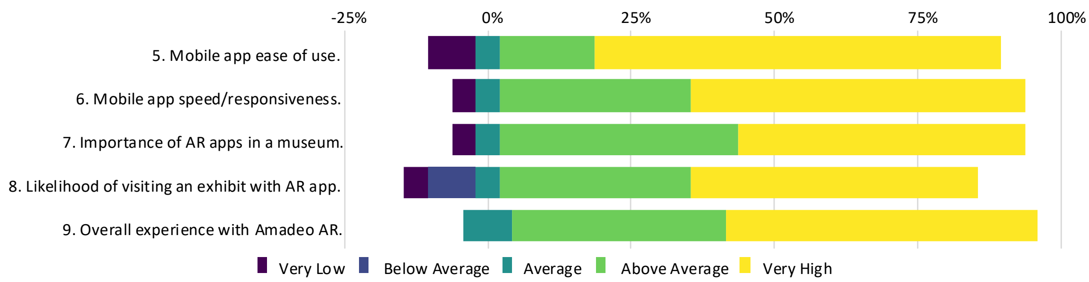

Figure 6.17: Survey results for questions 3.1 to 3.10 from the desktop application trial.

6.5 Conclusion and Further Work

The case study presented successfully implemented a solution to the need for information dissemination of cultural heritage and engagement of society in cultural activities. The success of the project was driven by the multidisciplinary collaboration network of research scientists, museums and governmental institutions established. Thanks to the expertise, knowledge and resources shared by the team it was possible to overcome the challenges faced in the collection and digitisation of data from its physical form, sharing of digital information, development of the processing algorithms software and the Amadeo AR mobile application.

The results of the trial confirmed the suitability of AR applications as a tool for the distribution of information and engagement of society in activities involving cultural heritage. Further work is planned to include the analysis of other artworks by Souza-Cardoso. In addition, it is envisaged that the existing methodology will be used to analyse more artists and genres. Therefore, further collaboration with other museums and research institutions will be established. Finally, future application development proposed includes the use of cloud services to store and deploy up-to-date information on the artwork analysed making the application an ideal point of access to information by the general public.

7

Conclusion and Future Work

This chapter concludes the PhD project, where the major outcome has been depicted in the previous sections of this dissertation. It will also discuss the limitations and barriers that this research has faced and the work that could be done in the future.

7.1 Conclusion

As the living standard of humankind improves in a general sense, more and more individuals start to practise spiritual fulfilment; one of the practices is artwork collection. Subsequently, the ever-growing interest in the commercial art market continues to flourish, and art forgers are also making use of this lucrative market. The demand for authentic artworks by renowned artists, especially by famous historical figures, also continues to prosper and not only individual art collectors but also museums and galleries are facing the likewise rampant art forgery problem. To combat the increasing problem of art forgery, and to protect the cultural heritage and artists' legacies, as well as the interest of the art market and the artists, the art authentication process is necessary and substantially important before artworks showcase to the public. This research contributed to solving the art authentication problem based on the paintings by Portuguese artist Amadeo de Souza-Cardoso. However, the algorithms were also tested wherever possible to ascertain their generalisation to paintings of other artists and genres. Some of the most advanced artificial machine learning algorithms, NNs, were actively applied in this research aiming to bridge the gap between computer science, more specifically artificial intelligence, and the art field.

Chapter 1 introduced briefly what the research and the dissertation entailed. Chapter 2 provided a detailed description of artwork analysis in relation to conservation and authentication. A comprehensive explanation concerning the principal research items in this PhD project, that is, brushstroke analysis and pigment analysis, is presented. Previous studies by other researchers are reviewed so that it is understandable that the implementation of NNs with the objective of artwork authentication is indeed still scarce. A brief presentation of the protagonist, whose paintings are examined in the research, that is, Amadeo de Souza-Cardoso is also given.

The original algorithm in [171] for both brushstroke and pigment analysis was carefully examined with the findings reported in section 2.6. Some flaws in the brushstroke analysis method were identified and the updated algorithm performance was evaluated showing a decrease in the classification accuracy. The pigment analysis review helped to evaluate improvements in pure and mixed pigment identification. Similarly, the review led to the successful implementation and generation of more accurate artificial mixed pigment reflectances using subtractive colour mixing. This proved useful later on in the development of deep learning models for pure and mixed pigment classification.

Chapter 3 and Chapter 4 explained in detail the deep learning models applied for brushstroke analysis and pigment analysis respectively. Concerning the brushstroke analysis in Chapter 3, after considerable research on different CNN architectures, the proposed model, based on the AlexNet architecture, was selected. After having compared artworks of different genres, that is, paintings by Souza-Cardoso, drawings by Souza-Cardoso, paintings by van Gogh, and paintings by Chinese painters, it was confirmed that the proposed model performed well in distinguishing the works by Souza-Cardoso. As with many deep learning problems, one of the biggest challenges faced in this project was the limited amount of data for training and testing. To solve this, a data augmentation process was necessary. This was successfully used to generate augmented data subsets for processing, including for example random rotation, random scaling, random reflection and random cropping. The proposed method was successfully applied and provided an improved set of results over the reviewed algorithm proposed in [171].

In Chapter 4, the proposed algorithms for both pure and mixed pigment identification were illustrated. To identify pure pigments, a deep learning model with three mix-data inputs was designed; the first input processes the reflectance hypercube of the analysed painting, the second input process the derivative of the smoothed reflectance hypercube of the same painting, and the third input processes the spectral correlation estimate via the SCM metric function between the individual pixel reflectance in the painting and the pure pigment reflectances obtained directly from the reference paint tubes. The calculated features were then examined via a series of other layers and functions, like MLP and Softmax, to predict the probabilities of the pure pigments in the painting. Similarly to the brushstroke analysis, the available reference data were not sufficient for a deep learning application and thus data augmentation was required. The use of subtractive mixing was used to generate a set of artificial reflectances from the 16 reference pure pigments acquired from the paint tubes. Since a ground truth hypercube was missing, an artificial training image was successfully constructed from the 16 pure pigments and artificial pigment mixtures. The proposed deep learning model and post-processing were successfully applied to segment the image into predicted pure pigment areas. The areas are comparable to those in [171] and exceed the performance of methods like FCLS. For mixed pigment identification, a regression deep learning model with a single input and multiple outputs was implemented to solve the hyperspectral unmixing problem. The model was successfully trained with augmented data from the reference database based on subtractive mixing. The proposed model and post-processing produced the fractions required per pigment to reconstruct a given reflectance. However, cross-examination of the chemical composition of the expected mixtures highlighted a disadvantage of the deep learning model. Although the model successfully generated reconstructed reflectances, these were made up of optimised mixtures of all pigments available. This meant that the predicted mixture did not necessarily match the true mixture but instead, it created the "best" approximation based on the training process (error minimisation). As a consequence, the model was replaced by the use of RMSE as a better function than SAM for mixed pigment matching. The results obtained were successfully verified with XRF data and the reconstructed hyperspectral and corresponding sRGB images accurately depicted the original images.

Next, a total estimation of authenticity was successfully calculated using the indicator of authenticity from brushstroke and pigment analysis. The tabulated and visual results are in line with those obtained in [171]. This confirms that the deep learning models used for the objective of the research are indeed useful for artwork authentication.

A by-product of this research was presented in chapter 5 where hyperspectral image reconstruction was achieved through a dual neural network architecture combined with colour analysis. The results show that the proposed algorithm is a suitable base for estimating hyperspectral data from paintings. In the case at hand, paintings from Souza-Cardoso as well as reference pigment data used by him were used in the training process. The algorithm however can be extended to the estimation of other types of artwork if a known database of base pigments or colours is available.

Chapter 6 described in detail the two applications that were developed as a proof of concept following the PhD research. First, Amadeo AR, a mobile application that was envisaged to serve mainly the general public in leisure and educational settings like museums and galleries. This AR application allows the user to visualise pure pigments identified in a set of Souza-Cardoso's paintings implementing Google's ARCore technology. Second, Amadeo Image Analysis Tool, a desktop application that was intended to serve principally experienced art experts in the settings of not only museums and galleries but also professional conservation and restoration departments, as well as potentially governmental institutions like the police, and forensic and judicial agencies. This desktop application includes multiple functions based on methods tested and developed during this research. For example, it allows art scientists to visualise various data like hyperspectral images and predicted pure pigment spectral data that could be used to estimate the authenticity of a painting. This chapter first explains the rationale behind the development of the two applications, followed by an illustration of the architecture and operation overview of both applications. Then, it continues with an explanation and feedback in terms of the trials on the user experience of the applications and ends with a short conclusion and future work.

7.2 Limitations and Constraints

The PhD project was proposed initially by the author with the support of the supervisors to cover multiple disciplines and to extend the project to various fields. For example, to maximise and comprehend fully the effect of real human brain responses towards artworks by individual artists in real-time, an experiment on human subjects applying Electroencephalogram (EEG) while visualising the artworks in real-time was proposed. In this way, distinguishing brain activities could be recorded during the visualisation of artworks by different artists. The rationale was that the collective human responses to artworks by a particular artist would be unique and exclusive to that individual artist, and it might be a gateway to understanding further how the human brain works. It was also hypothesised that it could also be a reliable channel to identify and determine if an artwork was authentic or not by that particular artist, and thus it could be used as an additional input variable for the indication of authenticity originally proposed in [171]. Thus, combining this channel of artwork authentication with other authentication techniques could further increase the accuracy of the artwork being authenticated correctly. The data obtained via the analysis of EEG were likewise presumed to be processed via deep learning algorithms; it would be interesting to discover what the results would look like and how they would affect the accuracy of art authentication. EEG experiments as well as other psychophysical experiments were proposed to be conducted not only with amateur art enthusiasts but also with art experts and scientists. The differences in the responses between amateurs and experts were pretended to be analysed and compared. However, as a result of the unexpected worldwide circumstances and restrictions in place at the time of this research, proposals involving any human interaction were not feasible and this part of the project could not be explored.

Additionally, further chemical data to be obtained by DCR on the drawings of Souza-Cardoso was also envisaged to be utilised and processed via deep learning models to test the algorithms devised originally for paintings. This would allow evaluating of the applicability and generalisation of the algorithms proposed in this thesis to other media. Information derived from chemical data from drawings could be added to the authentication estimate to maximise accuracy as well. Likewise, paintings of other Portuguese artists or other artists were considered to be acquired and analysed to determine the applicability and generality of the algorithms mentioned in the thesis. However, further data acquisition was not possible within the scope of the project.

Regarding the analysis methods developed, like in any other deep learning application, the performance of the models proposed heavily relies on the training data available. While significant efforts were made to generate artificial data for training and testing, increasing the performance of the models without further data is a very challenging task. Similarly, the quality of the data used is of particular importance for the performance of any method used. Should further hyperspectral data acquisition be possible, this should be performed ideally with the same equipment and following the same calibration and data normalisation as used during the acquisition of the data provided for this research.

The proposed models have been trained with a specific set of data based on reference pigments and reference images. Prediction of reflectances, pigment fractions or classification of authorship is thus limited to data akin to the training data. This is, for example, for authorship classification, images of similar size and resolution must be used. Similarly, as shown in Chapter 3, a model trained with paintings only, for example, cannot be expected to outperform other methods classifying drawings or other genres unless sample data of that particular type is included in the training process.

7.3 Future Work

As indicated in section 7.2, a series of proposals were made at the initial stage of the PhD project. It would be optimistic and ideal that all of the suggested ideas regarding psychophysical testing and EEG data collection could be put into practice. Several preprocessing techniques would be required to analyse the EEG numerical data collected for use with a deep learning model. This would likely include the use of statistical techniques like Principal Component Analysis to reduce dimensionality as well as frequency analysis with Fourier Transform or Wavelet Transform for example. These types of experiments are expected to be performed over a large population sample to ensure sufficient data are collected. This is required because deep learning requires a large training data set and data augmentation to generate human responses is not a suitable process. Therefore, careful planning for this task is required.

For brushstroke analysis, it would be ideal to evaluate the use of deeper architectures for better and more accurate classification of images and ultimately paintings. This requires exploring the use of pure residual networks or the addition of residual layers onto the currently proposed model to ensure the performance is not degraded as the network grows deeper.

One of the methods to identify art forgeries by curators and art experts is the analysis of the signature of an artist. This process is still highly subjective and requires thorough human expertise which, as history has proven, can lead to errors. Thus, the analysis of the signature of an artist on a painting using deep learning could be a new and better solution to the authentication problem. This would likely require the development and implementation of Generative Adversarial Network (GAN) for processing. This is, a pair of networks that compete against each other becoming more accurate in their predictions with each iteration. One of the networks, the generator, would be trained using a database of ground truth signature samples plus a function to generate artificial signatures. The second network, the discriminator, would be trained with the true signatures and the artificially generated signatures. With each iteration, the discriminator would make a prediction and the error would be minimised thus becoming better at identifying forgeries. On the other hand, with each iteration, the generator would be supplied with the result and thus it would improve itself generating signatures that are more real-life-like and harder to distinguish. The output of the GAN could thus be used as another input for the final indication of the authenticity of a painting.

Although the artificial mixtures generated served their purpose successfully, further enhancements could be made by using more complex colour mixing techniques other than subtractive mixing. For example, the Kubelka-Munk model could be used to generate more accurate artificial reflectances. This however requires access to the reference tube paint samples for further analysis to identify the absorption and backscattering of the pigments.

Other enhancements to the pure pigment identification model to be explored include the generation of different hyperspectral training images. Although the use of squares proved useful, it is believed that the use of different geometrical features including curves like circles could improve the image segmentation performance. This is because the model includes not only spectral analysis but also spatial analysis in the X-Y plane. Thus, identifying colour transitions in all directions could improve the accuracy of this model.

Finally, the software applications developed could be further improved. For example, the AR mobile application could benefit from accessing the database of paintings from a remote server in real time. This would allow easy and fast deployment of more augmented paintings without having to recompile and redeploy the mobile application. Furthermore, internet connectivity could be used to upload images to a remote server for processing with deep learning models if required. This would significantly improve processing times given the limited computing capabilities of mobile phones compared to powerful remote servers. For the desktop application, remote updates, new models and new data could also be deployed using could services effectively improving its capability and value for artwork analysis and authentication.

Bibliography

[1] *A Comprehensive Guide to Types of Neural Networks*. Accessed 22/08/2022. URL: https://www.digitalvidya.com/blog/types-of-neural-networks/ (cit. on pp. 42, 44, 46).

[2] F. M. Abed. "Pigment Identification of Paintings Based on Kubelka-Munk Theory and Spectral Images". In: 2014 (cit. on p. 20).

[3] P. Abry, H. Wendt, and S. Jaffard. "When Van Gogh meets Mandelbrot: Multifractal classification of painting's texture". In: *Signal Process.* 93 (2013), pp. 554–572 (cit. on p. 14).

[4] S. M. Adler-Golden et al. "Shadow-insensitive material detection/classification with atmospherically corrected hyperspectral imagery". In: *Algorithms for Multispectral, Hyperspectral, and Ultraspectral Imagery VII*. Ed. by S. S. Shen and M. R. Descour. Vol. 4381. Society of Photo-Optical Instrumentation Engineers (SPIE) Conference Series. 2001-08, pp. 460–469. DOI: 10.1117/12.437037 (cit. on p. 34).

[5] C. C. Aggarwal. *Neural Networks and Deep Learning. A Textbook*. Cham: Springer, 2018, p. 497. ISBN: 978-3-319-94462-3. DOI: 10.1007/978-3-319-94463-0 (cit. on pp. 42, 44–46).

[6] *AI vs. Deep Learning vs. Machine Learning: Everything You've Ever Wanted to Know*. Accessed 20/08/2022. URL: https://appen.com/blog/ai-vs-deep-learning-vs-machine-learning-everything-youve-ever-wanted-to-know/ (cit. on pp. 38, 41).

[7] *AI vs. Machine Learning vs. Deep Learning vs. Neural Networks: What's the Difference?* Accessed 20/08/2022. URL: https://www.ibm.com/cloud/blog/ai-vs-machine-learning-vs-deep-learning-vs-neural-networks (cit. on pp. 38, 41, 42).

[8] Y. Aksoy et al. "Semantic Soft Segmentation". In: *ACM Trans. Graph.* 37.4 (2018-07). ISSN: 0730-0301. DOI: 10.1145/3197517.3201275. URL: https://doi.org/10.1145/3197517.3201275 (cit. on p. 15).

[9] C. Alfaro. *"Amadeo de Souza-Cardoso: 1887-1918" in Catalogue Diálogo de Vanguardas-Avant-Garde Dialogues*. Assírio & Alvim and Fundação Calouste Gulbenkian, Lisbon, 2006 (cit. on p. 12).

[10] P. Almeida et al. "Analysis of paintings using multi-sensor data". In: *21st European Signal Processing Conference (EUSIPCO 2013)* (2013), pp. 1–5 (cit. on p. 109).

[11] E. Alpaydin. *Introduction to Machine Learning*. Cambridge, MA: The MIT Press, 2010 (cit. on pp. 39, 40).

[12] V. Antunes et al. "Calcium sulfate fillers and binders in Portuguese 15th and 16th centuries: Ground layers from a family painting workshop — Study by multianalytical spectroscopic techniques". In: *Microchemical Journal* 125 (2016), pp. 290–298 (cit. on p. 9).

[13] *ART CONSERVATION AND AUTHENTICATION*. Accessed 23/06/2022. URL: `https://www.redivivus.nl/post/art-conservation-and-authentication` (cit. on pp. 8, 9).

[14] *art conservation and restoration*. Accessed 24/06/2022. URL: `https://www.britannica.com/art/art-conservation-and-restoration` (cit. on p. 7).

[15] *Art forger finds Hollywood fame*. Accessed 15/07/2022. URL: `https://www.theguardian.com/uk/2007/jul/15/artnews.film` (cit. on p. 23).

[16] *Art Fraud*. Accessed 15/07/2022. URL: `https://www.britannica.com/topic/art-fraud/Smuggling-and-provenance` (cit. on p. 23).

[17] *Art Provenance: What It Is and How to Verify It*. Accessed 15/07/2022. URL: `https://www.artbusiness.com/provwarn.html` (cit. on p. 23).

[18] *Art restoration: Saving cultural heritage*. Accessed 16/06/2022. URL: `https://www.thejakartapost.com/life/2017/07/27/art-restoration-saving-cultural-heritage.html` (cit. on p. 7).

[19] D. Arthur and S. Vassilvitskii. "k-means++: the advantages of careful seeding". In: *SODA '07: Proceedings of the eighteenth annual ACM-SIAM symposium on Discrete algorithms*. Philadelphia, PA, USA: Society for Industrial and Applied Mathematics, 2007, pp. 1027–1035. ISBN: 978-0-898716-24-5 (cit. on p. 30).

[20] *Artificial Intelligence (AI) vs. Machine Learning vs. Deep Learning*. Accessed 20/08/2022. URL: `https://wiki.pathmind.com/ai-vs-machine-learning-vs-deep-learning` (cit. on pp. 38, 41).

[21] *Artificial Intelligence vs. Machine Learning vs. Deep Learning: Essentials*. Accessed 20/08/2022. URL: `https://serokell.io/blog/ai-ml-dl-difference` (cit. on pp. 38, 41).

[22] M. Atzeni, G. del Chiappa, and J. M. Pung. “Enhancing visit intention in heritage tourism: The role of object-based and existential authenticity in non-immersive virtual reality heritage experiences”. In: *International Journal of Tourism Research* (2021) (cit. on p. 108).

[23] B. Bahmani et al. “Scalable K-Means++.” In: *Proc. VLDB Endow.* 5.7 (2012), pp. 622–633. URL: `http://dblp.uni-trier.de/db/journals/pvldb/pvldb5.html#BahmaniMVKV12` (cit. on p. 30).

[24] D. Bai, D. W. Messinger, and D. Howell. “Hyperspectral analysis of cultural heritage artifacts: pigment material diversity in the Gough Map of Britain”. In: *Optical Engineering* 56 (2017), pp. 081805–081805 (cit. on p. 17).

[25] D. Bai, D. W. Messinger, and D. Howell. “Pigment diversity estimation for hyperspectral images of the Selden map of China”. In: *Defense + Security*. 2018 (cit. on p. 20).

[26] D. Bai, D. W. Messinger, and D. Howell. “A hyperspectral imaging spectral unmixing and classification approach to pigment mapping in the Gough & Selden Maps”. In: *Journal of the American Institute for Conservation* 58 (2019), pp. 69 –89 (cit. on p. 19).

[27] H. Balard and E. Papirer. “Characterization and modification of fillers for paints and coatings”. In: *Progress in Organic Coatings* 22.1 (1993), pp. 1–17. ISSN: 0300-9440. DOI: `https://doi.org/10.1016/0033-0655(93)80011-X`. URL: `https://www.sciencedirect.com/science/article/pii/003306559380011X` (cit. on p. 8).

[28] C. Balas et al. “Hyperspectral imaging and spectral classification for pigment identification and mapping in paintings by El Greco and his workshop”. In: *Multimedia Tools and Applications* 77 (2017), pp. 9737–9751 (cit. on p. 20).

[29] L. S. Bauman. “Legal Control of the Fabrication and Marketing of Fake Paintings”. In: *Stanford Law Review* 24 (1972), p. 930 (cit. on p. 23).

[30] M. K. Bekele et al. “A Survey of Augmented, Virtual, and Mixed Reality for Cultural Heritage”. In: *Journal on Computing and Cultural Heritage (JOCCH)* 11 (2018), pp. 1 –36 (cit. on p. 108).

[31] T. J. Benoy, W. Edwards, and H. G. M. Edwards. “CHAPTER 3:Evidence of Pentimenti for the Authentication of Paintings: A Challenge for Analytical Science at the Interface with Art History”. In: 2018 (cit. on p. 10).

[32] I. J. Berezhnoy, E. O. Postma, and H. J. van den Herik. “Authentic: Computerized Brushstroke Analysis”. In: *2005 IEEE International Conference on Multimedia and Expo* (2005), pp. 1586–1588 (cit. on p. 16).

[33] I. J. Berezhnoy, E. O. Postma, and H. J. van den Herik. "Automatic extraction of brushstroke orientation from paintings". In: *Machine Vision and Applications* 20 (2007), pp. 1–9 (cit. on p. 16).

[34] *Biggest Art Fakes and Forgeries Revealed in 2018*. Accessed 15/07/2022. URL: https://www.artworkarchive.com/blog/biggest-art-fakes-and-forgeries-revealed-in-2018 (cit. on pp. 1, 23).

[35] L. Bonizzoni et al. "In situ non-invasive EDXRF analysis to reconstruct stratigraphy and thickness of Renaissance pictorial multilayers". In: *X-Ray Spectrometry* 36 (2007), pp. 55–61 (cit. on p. 2).

[36] L. Bonizzoni et al. "Micro-invasive approach for non-destructive XRF analysis on light matrix: Inside the Opus Lemovicense". In: *X-Ray Spectrometry* 44 (2015), pp. 169–176 (cit. on p. 2).

[37] G. Bozzelli et al. "An integrated VR/AR framework for user-centric interactive experience of cultural heritage: The ArkaeVision project". In: *Digit. Appl. Archaeol. Cult. Heritage* 15 (2019), p. 00124 (cit. on pp. 107, 108).

[38] *Brush technique: types of brush strokes and pictorial styles*. URL: https://www.paintingandartists.com/brush-technique-types-of-brush-strokes-and-pictorial-styles (cit. on p. 13).

[39] *brushstroke*. Accessed 28/06/2022. URL: https://www.merriam-webster.com/dictionary/brushstroke (cit. on p. 13).

[40] *Brushstrokes Styles and Techniques of Chinese Painting*. Accessed 28/06/2022. URL: https://education.asianart.org/wp-content/uploads/sites/6/2019/09/Brushstrokes.pdf (cit. on p. 13).

[41] L. Burgio, R. J. H. Clark, and R. R. Hark. "Spectroscopic investigation of modern pigments on purportedly medieval miniatures by the 'Spanish Forger'". In: *Journal of Raman Spectroscopy* 40 (2009), pp. 2031–2036 (cit. on p. 18).

[42] A. Burmester. In: *Studies in Conservation* 45.1 (2000), pp. 68–71. ISSN: 00393630. URL: http://www.jstor.org/stable/1506685 (visited on 2023-04-13) (cit. on p. 18).

[43] M. Caccia et al. "Behind the Scene of "The Holy Family with St. Anne and the Young St. John" by Bernardino Luini: A Computer-Assisted Method to Unveil the Underdrawings". In: *Applied Spectroscopy* 75 (2020), pp. 274 –286 (cit. on p. 10).

[44] O. A. Carvalho and P. R. Meneses. "Spectral Correlation Mapper (SCM) : An Improvement on the Spectral Angle Mapper (SAM)". In: 2000 (cit. on p. 63).

[45] O. A. Carvalho et al. "A New Approach to Change Vector Analysis Using Distance and Similarity Measures". In: *Remote Sensing* 3.11 (2011), pp. 2473–2493. ISSN: 2072-4292. DOI: 10.3390/rs3112473. URL: https://www.mdpi.com/2072-4292/3/11/2473 (cit. on p. 63).

[46] L. Catterson. “Michelangelo’s "Laocoön?"” In: *Artibus et Historiae* 26.52 (2005), pp. 29–56. ISSN: 03919064. URL: http://www.jstor.org/stable/20067096 (visited on 2023-03-29) (cit. on p. 1).

[47] *Catálogo Raisonné - Amadeo de Souza Cardoso - Fotobiografia*. Vol. 1. Assírio & Alvim and Fundação Calouste Gulbenkian, Lisbon, 2007 (cit. on pp. 13, 54).

[48] *Catálogo Raisonné - Amadeo de Souza Cardoso - Pintura*. Vol. 2. Assírio & Alvim and Fundação Calouste Gulbenkian, Lisbon, 2008 (cit. on pp. 13, 54).

[49] S. Ceccarelli et al. “Remote and contactless infrared imaging techniques for stratigraphical investigations in paintings on canvas”. In: *Applied Physics B* (2021) (cit. on p. 11).

[50] T. D. Chaplin and R. J. H. Clark. “Identification by Raman microscopy of anachronistic pigments on a purported Chagall nude: conservation consequences”. In: *Applied Physics A* 122 (2016), pp. 1–5 (cit. on p. 18).

[51] T. D. Chaplin et al. “Pigment analysis by Raman microscopy and portable X-ray fluorescence (pXRF) of thirteenth to fourteenth century illuminations and cuttings from Bologna”. In: *Philosophical Transactions of the Royal Society A: Mathematical, Physical and Engineering Sciences* 374 (2016) (cit. on pp. 17, 18).

[52] H. P. Chapman and T. Weststeijn. “Connoisseurship as knowledge. An introduction”. In: 2020 (cit. on p. 22).

[53] A. Chen, R. Jesus, and M. Vilarigues. “Convolutional Neural Network-Based Pure Paint Pigment Identification Using Hyperspectral Images”. In: *ACM Multimedia Asia*. MMAsia ’21. Gold Coast, Australia: Association for Computing Machinery, 2021. ISBN: 9781450386074. DOI: 10.1145/3469877.3495641. URL: https://doi.org/10.1145/3469877.3495641 (cit. on pp. 62, 110).

[54] A. Chen, R. Jesus, and M. Villarigues. “Using Deep Learning Techniques for Authentication of Amadeo de Souza Cardoso Paintings and Drawings”. In: *Progress in Artificial Intelligence*. Ed. by P. Moura Oliveira, P. Novais, and L. P. Reis. Cham: Springer International Publishing, 2019, pp. 172–183. ISBN: 978-3-030-30244-3 (cit. on pp. 53, 56, 110).

[55] C. Y. Cheung, A. Mohan, and J. Tumblin. “Revealing Pentimenti Through Raking Angle Photography”. In: *Eurographics*. 2008 (cit. on p. 10).

[56] R. M. Christie and A. G. M. Abel. “Phthalocyanine pigments: general principles”. In: *Physical Sciences Reviews* 0 (2021) (cit. on p. 18).

[57] W.-T. Chu and Y.-C. Chao. “Line-Based Drawing Style Description for Manga Classification”. In: *Proceedings of the 22nd ACM international conference on Multimedia* (2014) (cit. on p. 16).

[58] M. J. Clark. “The Perfect Fake: Creativity, Forgery, Art and the Law”. In: *DePaul Journal of Art, Technology & Intellectual Property Law* 15 (2016), p. 1 (cit. on p. 23).

[59] *Clearing the Confusion: AI vs Machine Learning vs Deep Learning Differences*. Accessed 20/08/2022. URL: https://towardsdatascience.com/clearing-the-confusion-ai-vs-machine-learning-vs-deep-learning-differences-fce69b21d5eb (cit. on p. 38).

[60] *CNN vs. RNN vs. ANN – Analyzing 3 Types of Neural Networks in Deep Learning*. Accessed 22/08/2022. URL: https://www.analyticsvidhya.com/blog/2020/02/cnn-vs-rnn-vs-mlp-analyzing-3-types-of-neural-networks-in-deep-learning/ (cit. on pp. 42, 44, 46).

[61] *connoisseur*. Accessed 08/07/2022. URL: https://www.oxfordlearnersdictionaries.com/definition/english/connoisseur?q=connoisseur (cit. on p. 14).

[62] *connoisseurship*. Accessed 08/07/2022. URL: https://www.oxfordreference.com/view/10.1093/oi/authority.20110803095632669 (cit. on p. 14).

[63] *Cultural Heritage*. Accessed 16/06/2022. URL: https://en.unesco.org/fieldoffice/santiago/cultura/patrimonio (cit. on p. 7).

[64] S. Dasgupta and M. A. Hossain. "Pattern recognition through brushstroke analysis: an inspection to classify van Gogh from others". In: 2017 (cit. on p. 14).

[65] S. Davies et al. *A Companion to Aesthetics*. Wiley, 2009 (cit. on p. 21).

[66] H. Deborah. "Pigment Mapping of Cultural Heritage Paintings Based on Hyperspectral Imaging". PhD thesis. Gjøvik University College, 2013 (cit. on pp. 17, 19).

[67] H. Deborah, S. George, and J. Y. Hardeberg. "Pigment mapping of the scream (1893) based on hyperspectral imaging". In: *Image and Signal Processing (ICISP 2014)* 85009 (2014). DOI: 10.1007/978-3-319-07998-1_28. URL: https://doi.org/10.1007/978-3-319-07998-1_28 (cit. on p. 19).

[68] H. Deborah, S. George, and J. Y. Hardeberg. "Spectral-divergence based pigment discrimination and mapping: A case study on The Scream (1893) by Edvard Munch". In: *Journal of the American Institute for Conservation* 58 (2019), pp. 90 –107 (cit. on p. 20).

[69] H. Deborah, M. O. Ulfarsson, and J. Sigurdsson. "Fully Constrained Least Squares Linear Spectral Unmixing of The Scream (Verso, 1893)". In: *2021 11th Workshop on Hyperspectral Imaging and Signal Processing: Evolution in Remote Sensing (WHISPERS)* (2021), pp. 1–5 (cit. on p. 19).

[70] *Deep Learning vs. Machine Learning: Beginner's Guide*. Accessed 20/08/2022. URL: https://www.coursera.org/articles/ai-vs-deep-learning-vs-machine-learning-beginners-guide (cit. on p. 38).

[71] *Deep Learning vs Machine Learning vs Neural Network*. Accessed 20/08/2022. URL: https://www.xenonstack.com/blog/deep-learning-vs-ml-vs-neural-network (cit. on pp. 42, 44, 46).

[72] *Deep Learning vs. Machine Learning – What's The Difference?* Accessed 20/08/2022. URL: https://levity.ai/blog/difference-machine-learning-deep-learning (cit. on p. 38).

[73] *Demystifying the Mathematics Behind Convolutional Neural Networks (CNNs).* Accessed 22/08/2022. URL: https://www.analyticsvidhya.com/blog/2020/02/mathematics-behind-convolutional-neural-network/ (cit. on p. 46).

[74] *Detecting Art Forgeries: What Scientific Methods Can We Use?* Accessed 24/06/2022. URL: https://www.futurelearn.com/info/courses/art-crime/0/steps/11884 (cit. on p. 11).

[75] M. C. tom Dieck and T. H. Jung. "Value of Augmented Reality at Cultural Heritage Sites: A Stakeholder Approach". In: *Journal of Destination Marketing and Management* 6 (2017), pp. 110–117 (cit. on p. 108).

[76] *Discover the Differences Between AI vs. Machine Learning vs. Deep Learning*. Accessed 20/08/2022. URL: https://www.simplilearn.com/tutorials/artificial-intelligence-tutorial/ai-vs-machine-learning-vs-deep-learning (cit. on p. 38).

[77] V. Dumoulin and F. Visin. "A guide to convolution arithmetic for deep learning". In: *ArXiv e-prints* (2016-03). eprint: 1603.07285 (cit. on p. 46).

[78] *Dutch Master: The art forger who became a national hero*. Accessed 14/07/2022. URL: https://www.newyorker.com/magazine/2008/10/27/dutch-master (cit. on p. 22).

[79] J. K. (ed.) *Perspectives on Connoisseurship of Chinese Painting*. Washington, D.C.: New Academia Publishing, 2008 (cit. on p. 22).

[80] J. L. (Ed.). *The Oxford Handbook of Aesthetics (Oxford Handbooks)*. OUP UK, 2005 (cit. on p. 21).

[81] "Editorial: Art history, connoisseurship and scientific literacy". In: *International Journal of Museum Management and Curatorship* 7.1 (1988), pp. 5–10. DOI: 10.1080/09647778809515098. eprint: https://doi.org/10.1080/09647778809515098. URL: https://doi.org/10.1080/09647778809515098 (cit. on p. 22).

[82] A. Elgammal, Y. Kang, and M. D. Leeuw. "Picasso, Matisse, or a Fake? Automated Analysis of Drawings at the Stroke Level for Attribution and Authentication". In: *AAAI*. 2018 (cit. on p. 15).

[83] *Fakes And Forgeries*. Accessed 11/07/2022. URL: https://cen.acs.org/articles/85/i37/Fakes-Forgeries.html (cit. on p. 18).

[84] S. G. Federico Grillini Jean-Baptiste Thomas. "Mixing models in close-range spectral imaging for pigment mapping in Cultural Heritage". In: *AIC2020 Symposium Natural Colours - Digital Colours 20* (2020) (cit. on p. 19).

[85] W. Feng-qian. "Research on Art Painting Pigment Composition Recognition Based on Spectra Feature Fitting". In: *The Journal of Light Scattering* (2014) (cit. on p. 20).

[86] *Fillers and Pigment Extenders for Paints*. Accessed 01/10/2022. URL: https://feltmagnet.com/painting/Fillers-and-Pigment-Extenders-for-Paints (cit. on p. 8).

[87] L. Fiske et al. "Investigation of reflectance-based pigment classification in layered media (Conference Presentation)". In: *Optics for Arts, Architecture, and Archaeology VII* (2019) (cit. on p. 18).

[88] S. J. Fleming and E. P. Hall. "Authenticity in Art: The Scientific Detection of Forgery". In: *American Journal of Physics* 54 (1976), pp. 572–572 (cit. on p. 18).

[89] G. Folego, O. Gomes, and A. Rocha. "From impressionism to expressionism: Automatically identifying van Gogh's paintings". In: *2016 IEEE International Conference on Image Processing (ICIP)* (2016), pp. 141–145 (cit. on p. 15).

[90] *Forging Papers to Sell Fake Art*. Accessed 15/07/2022. URL: https://www.fbi.gov/news/stories/forging-papers-to-sell-fake-art (cit. on p. 23).

[91] S. Frank and A. M. Frank. "Rembrandts and Robots: Using Neural Networks to Explore Authorship in Painting". In: *ArXiv* abs/2002.05107 (2020) (cit. on p. 14).

[92] J. França. *"A Febre da vida Moderna" in Amadeo & Almada*. Venda Nova:Bertand, Lisbon, 1986 (cit. on p. 12).

[93] J. França. *"As últimas pinturas de Amadeo de Souza-Cardoso" in Amadeo de Souza-Cardoso 1887-1918*. Porto Ed. Fundação de Serralves, 1992 (cit. on p. 12).

[94] H. Freitas. "Amadeo de Souza-Cardoso 1887-1918". In: *Catálogo Raisonné - Amadeo de Souza Cardoso - Fotobiografia.* Vol 1 (2007) (cit. on pp. 11–13).

[95] *French museum discovers more than half of its paintings are fakes*. Accessed 15/06/2022. URL: https://edition.cnn.com/style/article/french-museum-half-paintings-fake-intl/index.html (cit. on p. 1).

[96] Y. Fu et al. "Fast Accurate and Automatic Brushstroke Extraction". In: *ACM Trans. Multimedia Comput. Commun. Appl.* 17.2 (2021-05). ISSN: 1551-6857. DOI: 10.1145/3429742. URL: https://doi.org/10.1145/3429742 (cit. on pp. 13, 15).

[97] M. Fukuyama. "Society 5.0: Aiming for a New Human-Centered Society". In: *Japan Spotlight, Japan Economic Foundation* (2018) (cit. on p. 107).

[98] M. Gelzo et al. "Comparison of binder compositions in Pompeian wall painting styles from Insula Occidentalis". In: *Chemistry Central Journal* 8 (2014) (cit. on p. 9).

[99] P. Gerstenblith. "Provenances: Real, Fake, and Questionable". In: *International Journal of Cultural Property* 26 (2019), pp. 285 –304 (cit. on p. 23).

[100] M. Gifford. In: *Studies in Conservation* 52.3 (2007), pp. 238–240. ISSN: 00393630. URL: http://www.jstor.org/stable/20619509 (visited on 2023-04-13) (cit. on p. 18).

[101] V. Ginsburgh and J. C. van Ours. "Expert opinion and compensation: evidence from a musical competition". In: *The American Economic Review* 93 (2003), pp. 289–296 (cit. on p. 22).

[102] *Glossary: Craquelure*. Accessed 24/06/2022. URL: https://www.nationalgallery.org.uk/paintings/glossary/craquelure (cit. on p. 11).

[103] M. S. Gomes. "Investigating surface treatments and coatings, their history, application and detection on selected pigments: Lead White, Zinc White and Titanium White". In: 2018 (cit. on p. 18).

[104] A. A. Gooch. "Revealing pentimenti: the hidden history in a painting". In: *Electronic Imaging*. 2007 (cit. on p. 10).

[105] A. A. Gooch and J. Tumblin. "Visualizing pentimenti : revealing the hidden history of paintings". In: *Journal of Mathematics and the Arts* 1 (2007), pp. 133 –142 (cit. on p. 10).

[106] I. J. Goodfellow, Y. Bengio, and A. Courville. *Deep Learning*. http://www.deeplearningbook.org. Cambridge, MA, USA: MIT Press, 2016 (cit. on pp. 42, 44–46).

[107] N. Goodman. *Art and Authenticity*. Hackett Publishing, 1976 (cit. on p. 23).

[108] F. Grillini, J.-B. Thomas, and S. George. "Linear, Subtractive and Logarithmic Optical Mixing Models in Oil Painting". In: *CVCS*. 2020 (cit. on p. 20).

[109] F. Grillini, J.-B. Thomas, and S. George. "Comparison of Imaging Models for Spectral Unmixing in Oil Painting". In: *Sensors (Basel, Switzerland)* 21 (2021) (cit. on p. 20).

[110] D. Gysau. *FILLERS FOR PAINTS*. Vincentz Network GmbH & Co. KG, Hanover, 2017 (cit. on p. 8).

[111] *Han van Meegeren's Fake Vermeers*. Accessed 14/07/2022. URL: http://www.essentialvermeer.com/misc/van_meegeren.html (cit. on p. 22).

[112] D. C. Heinz and Chein-I-Chang. "Fully constrained least squares linear spectral mixture analysis method for material quantification in hyperspectral imagery". In: *IEEE Transactions on Geoscience and Remote Sensing* 39.3 (2001). DOI: 10.1109/36.911111. URL: https://doi.org/10.1109/36.911111 (cit. on p. 73).

[113] J. D. Herbert. *Brushstroke and Emergence: Courbet, Impressionism, Picasso*. University of Chicago Press, 2015 (cit. on pp. 13, 14).

[114] *Hidden Artwork Revealed by X-Ray Appears to Be Van Gogh Self-Portrait, Experts Say*. Accessed 15/07/2022. URL: https://www.nytimes.com/2022/07/14/arts/design/van-gogh-self-portrait-x-ray.html (cit. on p. 10).

[115] C. Hill. "Art crime and the Wealth of Nations". In: *Journal of Financial Crime* 15 (2008), pp. 444–448 (cit. on p. 23).

[116] G. Hinton and T. Sejnowski. *Unsupervised Learning: Foundations of Neural Computation*. MIT Press, 1999 (cit. on p. 39).

[117] L. Hirsch et al. "Embedded AR Storytelling Supports Active Indexing at Historical Places". In: *Sixteenth International Conference on Tangible, Embedded, and Embodied Interaction* (2022) (cit. on p. 108).

[118] K. Holmberg. "Review of the book The Scientist and the Forger: Probing a Turbulent Art World by Jehane Ragai". In: 2018 (cit. on p. 18).

[119] P. Hook. *Breakfast at Sotheby's: An A–Z of the art world*. London: Penguin Books, 2013 (cit. on p. 22).

[120] *How Beltracchi, the world's most famous art forger, plays with the market*. Accessed 15/06/2022. URL: https://www.dw.com/cda/en/how-beltracchi-the-worlds-most-famous-art-forger-plays-with-the-market/a-18436266 (cit. on p. 1).

[121] *How to spot a perfect fake: the world's top art forgery detective*. Accessed 11/07/2022. URL: https://www.theguardian.com/news/2018/jun/15/how-to-spot-a-perfect-fake-the-worlds-top-art-forgery-detective (cit. on p. 18).

[122] J. Hughes, D. Graham, and D. Rockmore. "Quantification of artistic style through sparse coding analysis in the drawings of pieter bruegel the elder". In: *Proceedings of the National Academy of Sciences* 107.4 (2010) (cit. on p. 14).

[123] L. Ibrahim. "Design and Implementation an Automated System for Analyzing Brushstrokes to Distinguish between Van Gogh and his Contemporaries by using Swarm Intelligent Method". In: *International Journal of Computer Applications* 179 (2018), pp. 5–14 (cit. on p. 14).

[124] *Ideal Filler Properties in Paint Formulations*. Accessed 01/10/2022. URL: https://www.turkchem.net/ideal-filler-properties-in-paint-formulations-2.html (cit. on p. 8).

[125] *Is this Monet real or fake—and who gets to decide?* Accessed 15/06/2022. URL: https://qz.com/588932/is-this-monet-real-or-fake-and-who-gets-to-decide/ (cit. on p. 2).

[126] P. Isola et al. "Image-to-Image Translation with Conditional Adversarial Networks". In: *2017 IEEE Conference on Computer Vision and Pattern Recognition (CVPR)*. 2017, pp. 5967–5976. DOI: 10.1109/CVPR.2017.632 (cit. on p. 15).

[127] K. Janssens et al. "Non-Invasive and Non-Destructive Examination of Artistic Pigments, Paints, and Paintings by Means of X-Ray Methods". In: *Topics in Current Chemistry* 374 (2016), pp. 1–52 (cit. on p. 2).

[128] R. M. Jesus, A. J. Abrantes, and N. Correia. "Photo Retrieval from Personal Memories Using Generic Concepts". In: *Proceedings of the 7th Pacific Rim Conference on Advances in Multimedia Information Processing*. PCM'06. Berlin, Heidelberg: Springer-Verlag, 2006, 633–640. ISBN: 3540487662. DOI: 10.1007/11922162_73. URL: https://doi.org/10.1007/11922162_73 (cit. on p. 100).

[129] F. Ji et al. "Discerning the painter's hand: machine learning on surface topography". In: *Heritage Science* 9.152 (2021). DOI: 10.1186/s40494-021-00618-w (cit. on p. 13).

[130] C. R. Johnson et al. "Image Processing for Artist Identification – Computerized Analysis of Vincent van Gogh's Painting Brushstrokes". In: *IEEE Signal Processing Magazine* 25.4 (2008-07), pp. 37 –48 (cit. on pp. 13, 14).

[131] *K-means Clustering Algorithm: Applications, Types, and How Does It Work?* Accessed 20/08/2022. URL: https://www.simplilearn.com/tutorials/machine-learning-tutorial/k-means-clustering-algorithm (cit. on p. 39).

[132] K. Kale et al. "A Research Review on Hyperspectral Data Processing and Analysis Algorithms". In: *Proceedings of the National Academy of Sciences, India Section A: Physical Sciences* 87 (2017-11). DOI: 10.1007/s40010-017-0433-y (cit. on p. 34).

[133] R. Karki et al. "A Novel Algorithm based on Contourlet Transform for Extracting Paint Features to Determine Drawing Style and Authorship". In: *Indian journal of science and technology* 10 (2017), pp. 1–11 (cit. on p. 16).

[134] P. Kiefer, S. Matyas, and C. Schlieder. "Learning About Cultural Heritage by Playing Geogames". In: *ICEC*. 2006 (cit. on p. 108).

[135] A. Kirsh and R. S. Levenson. *Seeing Through Paintings: Physical Examination in Art Historical Studies*. Yale University Press, 2000 (cit. on p. 8).

[136] T. Kleynhans. "Automatic Pigment Classification in Painted Works of Art from Diffuse Reflectance Image Data". PhD thesis. Rochester Institute of Technology, 2020 (cit. on p. 20).

[137] T. Kleynhans, J. K. Delaney, and D. W. Messinger. "Automatic material classification of paintings in illuminated manuscripts from VNIR reflectance hyperspectral data cubes". In: *Defense + Commercial Sensing*. 2020 (cit. on p. 20).

[138] T. Kleynhans et al. "An alternative approach to mapping pigments in paintings with hyperspectral reflectance image cubes using artificial intelligence". In: *Heritage Science* 8 (2020-08). DOI: 10.1186/s40494-020-00427-7. URL: https://doi.org/10.1186/s40494-020-00427-7 (cit. on p. 20).

[139] A. Koestler. *The Act of Creation*. Hutchinson, 1964 (cit. on p. 23).

[140] D. Kotovenko et al. "Rethinking Style Transfer: From Pixels to Parameterized Brushstrokes". In: *2021 IEEE/CVF Conference on Computer Vision and Pattern Recognition (CVPR)* (2021), pp. 12191–12200 (cit. on p. 15).

[141] L. Krippahl. *Aprendizagem Automática (Machine Learning) Lecture Notes*. NOVA University Lisbon, 2018 (cit. on p. 41).

[142] A. Krizhevsky, I. Sutskever, and G. E. Hinton. "ImageNet Classification with Deep Convolutional Neural Networks". In: *Advances in Neural Information Processing Systems*. Ed. by F. Pereira et al. Vol. 25. Curran Associates, Inc., 2012. URL: https://proceedings.neurips.cc/paper/2012/file/c399862d3b9d6b76c8436e924a68c45b-Paper.pdf (cit. on pp. 48, 49).

[143] A. Krizhevsky, I. Sutskever, and G. E. Hinton. "ImageNet classification with deep convolutional neural networks". In: *Communications of the ACM* 60 (2012), pp. 84 –90 (cit. on p. 46).

[144] A. Kriznar et al. "Scientific study of the bozzetto of Murillo's painting "Moses and the water from the rock of Horeb"". In: *Rendiconti Lincei. Scienze Fisiche e Naturali* 31 (2020), pp. 795 –805 (cit. on p. 11).

[145] P. kubelka and F. Munk. "An article on optics of paint layers". In: *Fuer Tekn. Physik* 12 (1931), pp. 593–609 (cit. on p. 66).

[146] K. M. Kuenzli. *Henry Van de Velde: Designing Modernism*. Yale University Press, 2019 (cit. on p. 14).

[147] F. Lamberti, A. Sanna, and G. Paravati. "Computer-assisted analysis of painting brushstrokes: digital image processing for unsupervised extraction of visible features from van Gogh's works". In: *EURASIP Journal on Image and Video Processing* 2014 (2014), pp. 1–17 (cit. on p. 14).

[148] M. Latasa. "A simple method to increase sensitivity for RP-HPLC phytoplankton pigment analysis". In: *Limnology and Oceanography: Methods* 12 (2014) (cit. on p. 17).

[149] Y. Lee et al. "Application of Photosynthetic Pigment Analysis Using a HPLC and CHEMTAX Program to Studies of Phytoplankton Community Composition". In: 2011 (cit. on p. 17).

[150] A. Lessing. "What Is Wrong with a Forgery". In: *The Journal of Aesthetics and Art Criticism* 23 (1965), pp. 105–117 (cit. on p. 23).

[151] B. Lewis. *The last Leonardo*. London: William Collins, 2019 (cit. on p. 22).

[152] B. Li et al. "Pigments identification of paintings using subspace distance unmixing algorithm". In: *International Conference on Graphic and Image Processing*. 2018 (cit. on p. 20).

[153] J. Li et al. "Rhythmic Brushstrokes Distinguish van Gogh from His Contemporaries: Findings via Automated Brushstroke Extraction". In: *IEEE Transactions on Pattern Analysis and Machine Intelligence* 34.6 (2012), pp. 1159–1176. DOI: 10.1109/TPAMI.2011.203 (cit. on p. 14).

[154] B. Liss and S. Stout. "Materials Characterization for Cultural Heritage: XRF Case Studies in Archaeology and Art". In: *Heritage and Archaeology in the Digital Age: Acquisition, Curation, and Dissemination of Spatial Cultural Heritage Data*. Ed. by M. L. Vincent et al. Cham: Springer International Publishing, 2017, pp. 49–65. ISBN: 978-3-319-65370-9. DOI: 10.1007/978-3-319-65370-9_3. URL: https://doi.org/10.1007/978-3-319-65370-9_3 (cit. on p. 8).

[155] H. Liu, R. H. Chan, and Y. Yao. "Geometric Tight Frame based Stylometry for Art Authentication of van Gogh paintings". In: *ArXiv* abs/1407.0439 (2014) (cit. on p. 14).

[156] H. Liu et al. "Mesozooplankton selective feeding in subtropical coastal waters as revealed by HPLC pigment analysis". In: *Marine Ecology Progress Series* 407 (2010), pp. 111–123 (cit. on p. 17).

[157] M. Liu, Y. Xie, and Y. L. Zhang. "Research on Ceramic Artworks' Anti-Counterfeiting and Authentication Based on Two-Dimensional Code". In: *Advanced Materials Research* 791-793 (2013), pp. 2096 –2099 (cit. on p. 24).

[158] Y. Liu et al. "A Novel Spectral Matching Approach for Pigment: Spectral Subsection Identification Considering Ion Absorption Characteristics". In: *Remote. Sens.* 12 (2020), p. 3415 (cit. on p. 20).

[159] M. R. Lopez-Ramirez et al. "Study of modern artistic materials using combined spectroscopic and chromatographic techniques. Case study: painting with the signature "Picasso"". In: *Analytical Methods* 7 (2015), pp. 1499–1508 (cit. on p. 18).

[160] J. M. Lourenço. *The NOVAthesis LaTeX Template User's Manual*. NOVA University Lisbon. 2021. URL: https://github.com/joaomlourenco/novathesis/raw/master/template.pdf (cit. on p. ii).

[161] X. Lu et al. "Hyperspectral Image Super-Resolution Based on Spatial Correlation-Regularized Unmixing Convolutional Neural Network". In: *Remote. Sens.* 13 (2021), p. 4074 (cit. on p. 20).

[162] S. Lyu et al. "Quantitative analysis of mixed pigments for Chinese paintings using the improved method of ratio spectra derivative spectrophotometry based on mode". In: *Heritage Science* 8 (2020), pp. 1–21 (cit. on p. 19).

[163] S. Lyu, D. N. Rockmore, and H. Farid. "A digital technique for art authentication". In: *Proceedings of the National Academy of Sciences of the United States of America* 101 49 (2004), pp. 17006–10 (cit. on p. 24).

[164] K. C. M. Perez-Alonso and J. M. Madariaga. "Investigation of degradation mechanisms by portable Raman spectroscopy and thermodynamic speciation: The wall painting of Santa Maria de Lemoniz (Basque Country, North of Spain)". In: *Analytica Chimica Acta* 571 (2006) (cit. on p. 11).

[165] E. P. Laurens van der Maaten. "Identifying the Real Van Gogh with Brushstroke Textons". In: *Tilburg centre for Creative Computing, Tilburg University, The Netherlands* (2009) (cit. on pp. 13, 14).

[166] D. J. Mandal et al. "Influence of Acquisition Parameters on Pigment Classification using Hyperspectral Imaging". In: *Journal of Imaging Science and Technology* (2021) (cit. on p. 20).

[167] E. Manzano et al. "A combination of invasive and non-invasive techniques for the study of the palette and painting structure of a copy of Raphael's Transfiguration of Christ". In: *Heritage Science* 9 (2021), pp. 1–14 (cit. on p. 17).

[168] R. J. Meilunas, J. G. Bentsen, and A. Steinberg. "Analysis of aged paint binders by FTIR spectroscopy". In: *Studies in Conservation* 35 (1990), pp. 33–51 (cit. on p. 9).

[169] J. Min et al. "Digital imaging methods for painting analysis: the application of RTI and 3D scanning to the study of brushstrokes and paintings". In: *Multimedia Tools and Applications* (2020), pp. 1–13 (cit. on p. 16).

[170] M. M. Mochizuki, A. Golahny, and L. Vergara. "In his milieu : essays on Netherlandish art in memory of John Michael Montias". In: 2007 (cit. on p. 22).

[171] C. Montagner. "The brushstroke and materials of Amadeo de Souza-Cardoso combined in an authentication tool". PhD thesis. Departamento de Conservação e Restauro, Faculdade de Ciências e Tecnologia: Universidade NOVA de Lisboa, 2015 (cit. on pp. 2, 8, 16, 20, 24, 26, 27, 29–32, 34, 35, 37, 38, 47, 49, 51, 53, 54, 56–59, 61, 63, 65, 72–76, 83, 84, 86, 90, 93, 94, 96–98, 102, 125–127, 152, 153, 155–160, 164, 173, 174, 181–183).

[172] C. Montagner et al. "Features Combination for Art Authentication Studies: Brushstroke and Materials Analysis of Amadeo de Souza-Cardoso". In: *Multimedia Tools Appl.* 75.7 (2016-04), pp. 4039–4063. DOI: `10.1007/s11042-015-3197-x`. URL: `https://doi.org/10.1007/s11042-015-3197-x` (cit. on pp. 2, 16, 20, 109).

[173] N. Moorhouse, M. C. tom Dieck, and T. H. Jung. "Augmented Reality to enhance the Learning Experience in Cultural Heritage Tourism: An Experiential Learning Cycle Perspective". In: 2017 (cit. on p. 108).

[174] A. A. Morden, R. Sloggett, and N. Tse. "Authentication in a legal framework: Methodologies that underscore art authentication in practice". In: 2014 (cit. on p. 21).

[175] D. M. Murashov, A. Berezin, and E. Y. Ivanova. "A Technique for Computerised Brushwork Analysis". In: *VISAPP*. 2015 (cit. on p. 16).

[176] A. Murphy. "Aura, Provenance, Fakes & Forgeries. Exploring the Pitfalls of Provenance and how this Can Enhance the Agenda of Fakes and Forgeries in the Art World". In: 2021 (cit. on p. 23).

[177] R. Nakano. "Neural Painters: A learned differentiable constraint for generating brushstroke paintings". In: *ArXiv* abs/1904.08410 (2019) (cit. on p. 16).

[178] *Neural Network Models Explained*. Accessed 22/08/2022. URL: https://www.seldon.io/neural-network-models-explained (cit. on pp. 42, 44).

[179] *Neural Networks*. Accessed 22/08/2022. URL: https://www.ibm.com/cloud/learn/neural-networks (cit. on pp. 42, 44, 46).

[180] K. Nicolas and C. Westphal. *The Restoration of Paintings*. Konemann, 1998 (cit. on p. 8).

[181] *No One Could Beat Rembrandt at This*. URL: https://www.artistsnetwork.com/art-history/no-one-could-beat-rembrandt/ (cit. on p. 14).

[182] L. Nodari and P. Ricciardi. "Non-invasive identification of paint binders in illuminated manuscripts by ER-FTIR spectroscopy: a systematic study of the influence of different pigments on the binders' characteristic spectral features". In: *Heritage Science* 7 (2019), pp. 1–13 (cit. on p. 9).

[183] A. M. Obeso et al. "Connoisseur: classification of styles of Mexican architectural heritage with deep learning and visual attention prediction". In: *Proceedings of the 15th International Workshop on Content-Based Multimedia Indexing* (2017) (cit. on p. 22).

[184] N. Odegaard, S. Carroll, and W. S. Zimmt. *Material Characterization Tests for Objects of Art and Archaeology*. Archetype Publications Ltd., 2000. ISBN: 1909492205 (cit. on p. 8).

[185] E. O'Donnell and N. Tse. "Authentication, Attribution and the Art Market: Understanding Issues of Attribution in Contemporary Indonesia". In: 2018 (cit. on p. 21).

[186] *On connoisseurship*. Accessed 14/07/2022. URL: https://www.arthistorynews.com/articles/1101_On_connoisseurship (cit. on p. 22).

[187] H. N. Opperman. "The Thinking Eye, the Mind That Sees: The Art Historian as Connoisseur". In: *Artibus et Historiae* 11 (1990), pp. 9–13 (cit. on p. 22).

[188] *Organic vs Inorganic Pigments*. Accessed 01/10/2022. URL: https://www.meghmaniglobal.com/organic-vs-inorganic-pigments/ (cit. on p. 8).

[189] J. Orsilli et al. "More than XRF Mapping: STEAM (Statistically Tailored Elemental Angle Mapper) a Pioneering Analysis Protocol for Pigment Studies". In: *Applied Sciences* (2021) (cit. on p. 20).

[190] *Over 50 Percent of Art is Fake*. Accessed 15/07/2022. URL: https://news.artnet.com/market/over-50-percent-of-art-is-fake-130821 (cit. on p. 1).

[191] Y. Pan et al. "Network Inference Analysis Identifies an APRR2-Like Gene Linked to Pigment Accumulation in Tomato and Pepper Fruits1[W][OA]". In: *Plant Physiology* 161 (2013), pp. 1476 –1485 (cit. on p. 17).

[192] E. Panofsky. *Meaning in the Visual Arts*. University of Chicago Press; Phoenix edition, 1983 (cit. on p. 22).

[193] L. Peti et al. "Itrax μ-XRF core scanning for rapid tephrostratigraphic analysis: a case study from the Auckland Volcanic Field maar lakes". In: *Journal of Quaternary Science* 35 (2019) (cit. on p. 2).

[194] *Pigment analysis*. Accessed 09/07/2021. URL: https://arts.unimelb.edu.au/grimwade-centre-for-cultural-materials-conservation/conservation-services/services-support/technical-analysis/pigment-analysis (cit. on p. 17).

[195] K. Polk and D. Chappell. "Examining Art Fraud". In: *The Palgrave Handbook on Art Crime* (2019) (cit. on pp. 22, 23).

[196] R. S. Popelka-Filcoff. "Pigment Analysis in Archaeology". In: *Encyclopedia of Global Archaeology* (2020) (cit. on p. 17).

[197] *Portable X-Ray Fluorescence (PXRF)*. Accessed 23/06/2022. URL: http://fieldmuseum.org/portable-x-ray-fluorescence-pxrf (cit. on p. 10).

[198] A. Potter. *The Authenticity Hoax: How We Get Lost Finding Ourselves*. McClelland & Stewart, 2010 (cit. on pp. 22, 23).

[199] E. Pouyet et al. "Artificial Intelligence for Pigment Classification Task in the Short-Wave Infrared Range". In: *Sensors (Basel, Switzerland)* 21 (2021) (cit. on p. 20).

[200] *Preserving Cultural Heritage, an IFLA guide*. Accessed 16/06/2022. URL: www.ifla.org/cultural-heritage (cit. on p. 7).

[201] S. W. T. Price et al. "Unravelling the spatial dependency of the complex solid-state chemistry of Pb in a paint micro-sample from Rembrandt's Homer using XRD-CT." In: *Chemical communications* 55 (2019), pp. 1931–1934 (cit. on pp. 8, 11).

[202] L. Pronti et al. "Optimized Method for Mapping Inorganic Pigments by Means of Multispectral Imaging Combined with Hyperspectral Spectroscopy for the Study of Vincenzo Pasqualoni's Wall Painting at the Basilica of S. Nicola in Carcere in Rome". In: *Minerals* (2021) (cit. on p. 20).

[203] *Provenance*. Accessed 15/07/2022. URL: https://www.nationalgallery.org.uk/paintings/glossary/provenance (cit. on p. 23).

[204] T. Putri, R. Mukundan, and K. Neshatian. "Artistic Style Characterization of Vincent Van Gogh's Paintings using Extracted Features from Visible Brush Strokes". In: *Proceedings of the 6th International Conference on Pattern Recognition Applications and Methods (ICPRAM 2017)* (2017). DOI: 10.5220/0006188303780385 (cit. on p. 14).

[205] T. Putri. "Artistic Style Characterization of Vincent van Gogh's Brushstrokes". PhD thesis. University of Canterbury, 2019 (cit. on p. 14).

[206] A.-S. V. Radermecker. "The Art Market Facing New Connoisseurship: The Reception of Pieter Brueghel the Younger at Auction". In: 2020 (cit. on p. 22).

[207] A.-S. V. Radermecker. "The market reception of 'new connoisseurship'". In: 2020 (cit. on p. 22).

[208] *Researching the Provenance of a Work of Art*. Accessed 15/07/2022. URL: https://www.artic.edu/library/discover-our-collections/research-guides/researching-the-provenance-of-a-work-of-art (cit. on p. 22).

[209] *Restored Vermeer painting finally reveals hidden Cupid in background*. Accessed 15/07/2022. URL: https://arstechnica.com/science/2021/09/restored-vermeer-painting-finally-reveals-hidden-cupid-in-background/ (cit. on p. 10).

[210] *Revealing Paintings' Secrets with Scientific Technology*. Accessed 24/06/2022. URL: https://www.forbes.com/sites/evaamsen/2019/03/19/revealing-paintings-secrets-with-scientific-technology/ (cit. on p. 11).

[211] N. Rohani et al. "Automatic pigment identification on roman Egyptian paintings by using sparse modeling of hyperspectral images". In: *2016 24th European Signal Processing Conference (EUSIPCO)* (2016), pp. 2111–2115 (cit. on p. 20).

[212] N. Rohani et al. "Nonlinear Unmixing of Hyperspectral Datasets for the Study of Painted Works of Art." In: *Angewandte Chemie* 57 34 (2018), pp. 10910–10914 (cit. on p. 19).

[213] N. Rohani et al. "Pigment unmixing of hyperspectral images of paintings using deep neural networks". In: *ICASSP 2019 - 2019 IEEE International Conference on Acoustics, Speech and Signal Processing (ICASSP)*. Brighton, UK: IEEE, 2019-04, pp. 3217–3221. DOI: 10.1109/ICASSP.2019.8682838. URL: http://doi.org/10.1109/ICASSP.2019.8682838 (cit. on p. 19).

[214] R. Russell. *Machine Learning: Step-by-Step Guide To Implement Machine Learning Algorithms with Python*. CreateSpace Independent Publishing Platform; Illustrated edition (22 May 2018), 2018 (cit. on pp. 39, 40).

[215] S. J. Russell and P. Norvig. *Artificial Intelligence: A Modern Approach*. Prentice Hall, 2010 (cit. on p. 39).

[216] L. Schlüter, F. Møhlenberg, and H. Kaas. "Temporal and spatial variability of phytoplankton monitored by a combination of monitoring buoys, pigment analysis and fast screening microscopy in the Fehmarn Belt Estuary". In: *Environmental Monitoring and Assessment* 186 (2014), pp. 5167–5184 (cit. on p. 17).

[217] L. Schlüter et al. "Characterization of phytoplankton by pigment analysis and the detection of toxic cyanobacteria in reservoirs with aquaculture production". In: *Aquaculture Environment Interactions* 10 (2018), pp. 35–48 (cit. on p. 17).

[218] *Scientific Analysis of Fine Art with FTIR*. Accessed 01/10/2022. URL: https://www.thermofisher.com/blog/materials/scientific-analysis-of-fine-art-with-ftir/ (cit. on p. 9).

[219] J. Searle. *The Mystery of Consciousness*. New York Review Books, 1997 (cit. on p. 38).

[220] P. A. Setiawan. "Delivering cultural heritage and historical events to people through virtual reality". In: *IOP Conference Series: Earth and Environmental Science* 729 (2021) (cit. on p. 107).

[221] G. Sharma. *Digital Color Imaging Handbook*. USA: CRC Press, Inc., 2002. ISBN: 084930900X (cit. on p. 85).

[222] B. R. Shivakumar and S. V. Rajashekararadhya. "Performance évaluation of spectral angle mapper and spectral correlation mapper classifiers over multiple remote sensor data". In: *2017 Second International Conference on Electrical, Computer and Communication Technologies (ICECCT)*. 2017, pp. 1–6. DOI: 10.1109/ICECCT.2017.8117946 (cit. on p. 63).

[223] C. Shorten and T. M. Khoshgoftaar. "A survey on Image Data Augmentation for Deep Learning". In: *Journal of Big Data* 6.1 (2019-07), p. 60. ISSN: 2196-1115. DOI: 10.1186/s40537-019-0197-0. URL: https://doi.org/10.1186/s40537-019-0197-0 (cit. on p. 50).

[224] A. Shortland and A. Shortland. "Governance under the shadow of the law: trading high value fine art". In: *Public Choice* 184 (2019), pp. 157–174 (cit. on pp. 2, 22).

[225] R. H. Silva. *"Os anos do Orpheus e de Portugal futurista", in História da Arte Portuguesa*. Círculo de Leitores, Lisbon, 1995 (cit. on p. 12).

[226] L. Simonot and M. Hébert. "Between additive and subtractive color mixings: intermediate mixing models". In: *J. Opt. Soc. Am. A* 31.1 (2014-01), pp. 58–66. DOI: 10.1364/JOSAA.31.000058. URL: http://opg.optica.org/josaa/abstract.cfm?URI=josaa-31-1-58 (cit. on p. 66).

[227] *Society 5.0*. Accessed 17/07/2022. URL: https://www8.cao.go.jp/cstp/english/society5_0/index.html (cit. on p. 107).

[228] G. S. Spagnolo et al. "Painting authentication by means of a biometric-like approach". In: 2015 (cit. on p. 24).

[229] R. D. E. Spencer. *The expert vs. the object. Judging fakes and false attributions in the visual arts.* Oxford and New York: Oxford University Press, 2004 (cit. on pp. 21, 22).

[230] R. D. E. Spencer. "Spencer's Art Law Journal". In: *Spencer's Art Law Journal* 1 (2010) (cit. on pp. 21, 22).

[231] *statcounter*. Accessed 17/07/2022. URL: https://gs.statcounter.com/os-market-share/mobile/worldwide (cit. on p. 111).

[232] I. Steinwart and A. Christmann. *Support Vector Machines*. 1st. Springer Publishing Company, Incorporated, 2008. ISBN: 0387772413 (cit. on p. 39).

[233] W. F. Steven Saverwyns. "Genuine or fake: a micro-raman spectroscopy study of an abstract painting attributed to Vasily Kandinsky." In: *Conference: Art'11, 10th International Conference on non-destructive investigations and microanalysis for the diagnostics and conservation of cultural and environmental heritage* (2011) (cit. on p. 18).

[234] J. Striová et al. "Synchronized Hardware-Registered VIS-NIR Imaging Spectroscopy and 3D Sensing on a Fresco by Botticelli". In: *Sensors (Basel, Switzerland)* 21 (2021) (cit. on p. 10).

[235] M. Sun et al. "Brushstroke based sparse hybrid convolutional neural networks for author classification of Chinese ink-wash paintings". In: *2015 IEEE International Conference on Image Processing (ICIP)* (2015), pp. 626–630 (cit. on p. 16).

[236] X. Tang et al. "Painting and calligraphy identification method based on hyperspectral imaging and convolution neural network". In: *Spectroscopy Letters* 54 (2021), pp. 645 –664 (cit. on p. 20).

[237] A. M. N. Taufique and D. W. Messinger. "Hyperspectral pigment analysis of cultural heritage artifacts using the opaque form of Kubelka-Munk theory". In: *Defense + Commercial Sensing*. 2019 (cit. on p. 20).

[238] S. Tennent Pauland Martindale et al. "Thresholds: Embedding Virtual Reality in the Museum". In: *ACM Journal on Computing and Cultural Heritage* 13 (2020), 12:1–12:35 (cit. on p. 108).

[239] *The Beauty of a Brushstroke*. URL: https://medium.com/thinksheet/the-beauty-of-a-brushstroke-82cf759adc15 (cit. on p. 13).

[240] *The Big Question: How many of the paintings in our public museums are fakes?* Accessed 15/06/2022. URL: https://www.independent.co.uk/arts-entertainment/art/news/the-big-question-how-many-of-the-paintings-in-our-public-museums-are-fakes-1946264.html (cit. on p. 1).

[241] *the brush and brushstrokes*. Accessed 28/06/2022. URL: https://www.handprint.com/HP/WCL/tech18.html (cit. on p. 13).

[242] *The Enduring Challenges of Authenticating Art*. Accessed 24/06/2022. URL: https://www.art-critique.com/en/2020/03/art-authentication-today/ (cit. on p. 9).

[243] *The master forger*. Accessed 15/06/2022. URL: https://www.theguardian.com/artanddesign/2005/dec/08/art (cit. on p. 1).

[244] *The mostly complete chart of Neural Networks, explained*. Accessed 22/08/2022. URL: https://towardsdatascience.com/the-mostly-complete-chart-of-neural-networks-explained-3fb6f2367464 (cit. on p. 44).

[245] *The Science of Art Authentication*. Accessed 24/06/2022. URL: https://medium.com/lantern-theater-company-searchlight/the-science-of-art-authentication-308714906b2d (cit. on p. 11).

[246] *The Ten Most Notorious Art Forgers Of All Time*. Accessed 15/06/2022. URL: https://www.sleek-mag.com/article/art-forgers/ (cit. on p. 1).

[247] E. L. Thompson. *The Curious History of Private Collectors*. Yale University Press, 2016 (cit. on p. 1).

[248] *Types of Neural Networks and Definition of Neural Network*. Accessed 22/08/2022. URL: https://www.mygreatlearning.com/blog/types-of-neural-networks/ (cit. on pp. 42, 44, 46).

[249] O. Uncu, B. Ozen, and F. Tokatli. "Authentication of Turkish olive oils by using detailed pigment profile and spectroscopic techniques." In: *Journal of the science of food and agriculture* (2020) (cit. on p. 17).

[250] *Understanding Support Vector Machine(SVM) algorithm from examples (along with code)*. Accessed 18/08/2022. URL: https://www.analyticsvidhya.com/blog/2017/09/understaing-support-vector-machine-example-code/ (cit. on p. 39).

[251] *Unknown Modigliani sketches found hidden beneath Nude with Hat*. Accessed 15/07/2022. URL: https://www.theguardian.com/artanddesign/2022/jul/13/unknown-modigliani-sketches-found-hidden-beneath-nude-with-hat (cit. on p. 10).

[252] *Unlawful Appropriation of Objects During the Nazi Era*. Accessed 15/07/2022. URL: https://www.aam-us.org/programs/ethics-standards-and-professional-practices/unlawful-appropriation-of-objects-during-the-nazi-era/ (cit. on p. 22).

[253] G. Vaggelli et al. "Islamic glass weights from Egypt: A systematic study by non-destructive μ-XRF technique". In: *Journal of Non-Crystalline Solids* 363 (2013), pp. 96–102. ISSN: 0022-3093. DOI: https://doi.org/10.1016/j.jnoncrysol.2012.12.003. URL: https://www.sciencedirect.com/science/article/pii/S0022309312007119 (cit. on p. 2).

[254] J. C. Valdiviezo-N., G. Urcid, and E. Lechuga. "Digital restoration of damaged color documents based on hyperspectral imaging and lattice associative memories". In: *Signal, Image and Video Processing* 11 (2017), pp. 937–944 (cit. on p. 20).

[255] P. Vandenabeele and L. Moens. "The application of Raman Spectroscopy for the Non-destructive Analysis of Art Objects". In: *Roma 2000 15th WCNDT* (2013). URL: https://www.ndt.net/article/wcndt00/papers/idn163/idn163.htm (cit. on p. 11).

[256] F. Ventrella. "Constance Jocelyn Ffoulkes and the Modernization of Scientific Connoisseurship". In: *Visual Resources* 33 (2017), pp. 117 –139 (cit. on p. 22).

[257] I. Verhulst et al. "Do VR and AR versions of an immersive cultural experience engender different user experiences?" In: *Comput. Hum. Behav.* 125 (2021), p. 106951 (cit. on p. 108).

[258] M. Vilarigues et al. "Uma mão cheia de cores, o século XX e o nascimento da arte moderna". In: *Catálogo Raisonné - Amadeo de Souza Cardoso - Pintura.* Vol 2 (2008) (cit. on p. 13).

[259] *Vincent van Gogh: Hidden self-portrait discovered by X-ray.* Accessed 17/07/2022. URL: https://www.bbc.co.uk/news/uk-scotland-62135891 (cit. on p. 10).

[260] J. Z. Wang. "Computerized Comparison and Analysis of Vincent van Gogh's Painting Brushstrokes". In: *Bulletin of the American Physical Society* (2009) (cit. on p. 14).

[261] J. Z. Wang. "Modeling Aesthetics and Emotions in Visual Content: From Vincent van Gogh to Robotics and Vision". In: *Joint Workshop on Aesthetic and Technical Quality Assessment of Multimedia and Media Analytics for Societal Trends* (2020) (cit. on p. 14).

[262] *When fakes and false provenance go hand in hand.* Accessed 15/07/2022. URL: https://art-crime.blogspot.com/2020/01/when-fakes-and-false-provenance-go-hand.html (cit. on p. 23).

[263] *When is a fake not a fake? When it's a genuine forgery.* Accessed 15/06/2022. URL: https://www.theguardian.com/money/2005/jul/02/alternativeinvestment.jobsandmoney (cit. on p. 1).

[264] *Why Heritage Preservation Is Way More Important Than You Thought.* Accessed 16/06/2022. URL: https://sites.utm.utoronto.ca/historyinternships/blog/10252015-2300/why-heritage-preservation-way-more-important-you-thought (cit. on p. 7).

[265] *Why is Conservation in Art Important.* Accessed 24/06/2022. URL: https://www.oilpaintingrestorations.co.uk/why-is-conservation-in-art-important (cit. on p. 7).

[266] *Why Post-Impressionist Painter Paul Cézanne Is Known as the "Father of Modern Art".* URL: https://mymodernmet.com/paul-cezanne-paintings/ (cit. on pp. 11, 14).

[267] *Wikimedia Commons.* Accessed 08/07/2022. URL: https://commons.wikimedia.org/wiki/Main_Page (cit. on p. 15).

[268] *World Heritage -Why preserve, conserve and protect?* Accessed 16/06/2022. URL: https://www.flame.edu.in/in-the-media/world-heritage-why-preserve-conserve-and-protect (cit. on p. 7).

[269] *X-Ray Reveals Hidden van Gogh Self-Portrait.* Accessed 17/07/2022. URL: https://www.artnews.com/art-news/news/van-gogh-hidden-self-portrait-barkley-hendricks-frick-morning-links-1234634148/ (cit. on p. 10).

[270] H. Yamanaka and S. Kondo. "In vitro analysis suggests that difference in cell movement during direct interaction can generate various pigment patterns in vivo". In: *Proceedings of the National Academy of Sciences* 111 (2014), pp. 1867 –1872 (cit. on p. 17).

[271] Q. Yin and S. Lv. "Spectral unmixing of mineral pigment mixture by using derivative of ratio spectroscopy". In: *2016 4th International Workshop on Earth Observation and Remote Sensing Applications (EORSA)* (2016), pp. 174–178 (cit. on p. 19).

[272] Y. Zang, H. Huang, and C. Li. "Stroke style analysis for painterly rendering". In: *Journal of Computer Science and Technology* 28.5 (2013) (cit. on p. 13).

[273] Y. Zhao, R. S. Berns, and L. A. Taplin. "Image Segmentation and Pigment Mapping in Spectral Imaging". In: 2006 (cit. on p. 20).

[274] Y. Zhu et al. "Machine: The New Art Connoisseur". In: *ArXiv* abs/1911.10091 (2019) (cit. on p. 22).

[275] B. Łydżba-Kopczyńska and J. Szwabiński. "Attribution Markers and Data Mining in Art Authentication". In: *Molecules* 27 (2021) (cit. on p. 24).

A

Appendix 1 Pure Pigment Database

The reference pigment database comprises the reflectances and representative sRGB and CIELab colour components obtained from oil paint samples known to have been used by Amadeo de Souza-Cardoso in his artwork. These samples were stored in paint tubes at the Casa de Manhufe and provided for digitisation with a hyperspectral camera [171]; the hyperspectral data contain spectral information in the 400nm to 720nm range in steps of 10nm. No data were acquired in the work presented here and therefore validation and verification of the data supplied have not been possible. An sRGB representation of the hyperspectral image of the samples is presented in Figure A.1.

The 16 pigments selected for analysis include the following which correspond exactly to those used in [171] for direct comparison:

- Cobalt Violet
- Chinese Vermilion
- Carmine Lake
- Terra Rosa
- Raw Sienna
- Yellow Ochre
- Chrome Yellow
- Cadmium Orange
- Cobalt Blue
- Cerulean Blue
- Prussian Blue
- Ultramarine

- Viridian
- Emerald Green
- Lead White
- Ivory Black

Figure A.1: sRGB representation of the hyperspectral image of the paint tube samples obtained in [171].

The reflectances in the pure pigments database of [171] were acquired by averaging manually-selected areas of the spectral data. The areas selected are reported to be of size

5 pixels by 5 pixels for all pigments used but the location of these on the hyperspectral image is not documented. Therefore, new, carefully selected areas of varying sizes have been manually chosen to maximise the quality of the hyperspectral data from the paint samples while providing a reproducible data set. The areas selected for each pigment are summarised by the coordinates in Table A.1.

Table A.1: Coordinates of areas selected in file *ref_amostras_a.mat* for the reference pigment database.

Pigment	X Coord.	Y Coord.	Size Sq. Px.
ASC13 Cobalt Violet	647	350	3
	623	345	3
MG6 Chinese Vermilion	231	84	10
ASC5 Carmine Lake	644	55	3
	664	70	2
	660	91	1
	656	79	1
	622	96	1
MG18 Terra Rosa	654	717	8
MG7 Raw Sienna	899	661	3
	899	661	1
	905	630	3
	900	658	3
MG11 Yellow Ochre	895	999	4
	916	1041	3
	914	1020	5
ASC17 Chrome Yellow	254	994	3
	255	985	5
MG2 Cadmium Orange	646	845	7
	644	854	6
	637	866	4
MG4 Cobalt Blue	627	1114	4
	626	1119	5
	644	1104	3

Continued on next page

Table A.1: Coordinates of areas selected in file *ref_amostras_a.mat* for the reference pigment database. (Continued)

Pigment	X Coord.	Y Coord.	Size Sq. Px.
ASC7 Cerulean Blue	619	211	4
	644	193	5
	641	209	3
	639	236	2
	655	214	1
	643	207	2
ASC19 Prussian Blue	647	495	3
	659	469	3
	644	449	1
	624	493	1
	625	500	1
35_3128 Ultramarine	255	1134	5
	250	1138	3
	243	1128	3
	273	1120	4
ASC20 Viridian	654	572	3
	658	611	3
	646	587	3
	670	607	2
	653	571	5
18_3130 Emerald Green	260	737	8
	288	731	4
	268	727	5
	268	736	4
13_3130 Lead White	645	1297	3
	637	1245	1
	655	1228	1
	636	1244	3
	645	1260	1
MG17 Ivory Black	286	587	5

For each selected pigment, the representative reflectance is finally obtained as the average reflectance of all pixels within the specified areas. The resulting reflectances are shown in Figure A.2 along with the reflectances used in [171] and the reflectances obtained using Fibre Optic Reflectance Spectroscopy (FORS) scaled to the same range as those from the hyperspectral camera for comparison purposes. As observed, the new reflectances obtained show smoother curves that closely follow those obtained via FORS suggesting our reference data are appropriate for the analyses presented in our work. In particular, the new reflectance for Prussian Blue is significantly closer to that obtained using FORS while the one obtained in [171] is more representative of green colour. Finally, Table A.2 shows the CIELab colour components and associated chemical elements as indicated in [171].

Table A.2: Colour and chemical information per pigment.

Pigment	**CIELab**			
	L	**a**	**b**	**Elements**
Cobalt Violet	38.8817	324674	-29.5958	Co, As
Chinese Vermilion	46.4914	57.8106	39.9008	Hg
Carmine Lake	16.3068	19.6592	8.6145	Sr
Terra Rosa	40.2390	26.3825	24.7961	Fe, As
Raw Sienna	19.2523	8.6073	9.9969	Fe, Mn
Yellow Ochre	43.2626	19.0897	43.7410	Fe
Chrome Yellow	57.8149	14.1569	58.4063	Cr
Cadmium Orange	66.8529	36.6389	85.4719	Cd
Cobalt Blue	21.6078	11.5458	-34.8939	Co
Cerulean Blue	37.4715	-9.6289	-33.7333	Co, Sn, Ni
Prussian Blue	13.1717	1.6187	-11.5084	Fe, S
Ultramarine	24.2362	8.8241	-23.3787	Al, Si
Viridian	29.0161	-11.1832	1.3616	Cr
Emerald Green	48.5845	-45.8146	16.6973	Cu, As
Lead White	96.8866	-2.4818	8.3296	Pb
Ivory Black	20.2192	0.1607	1.0307	

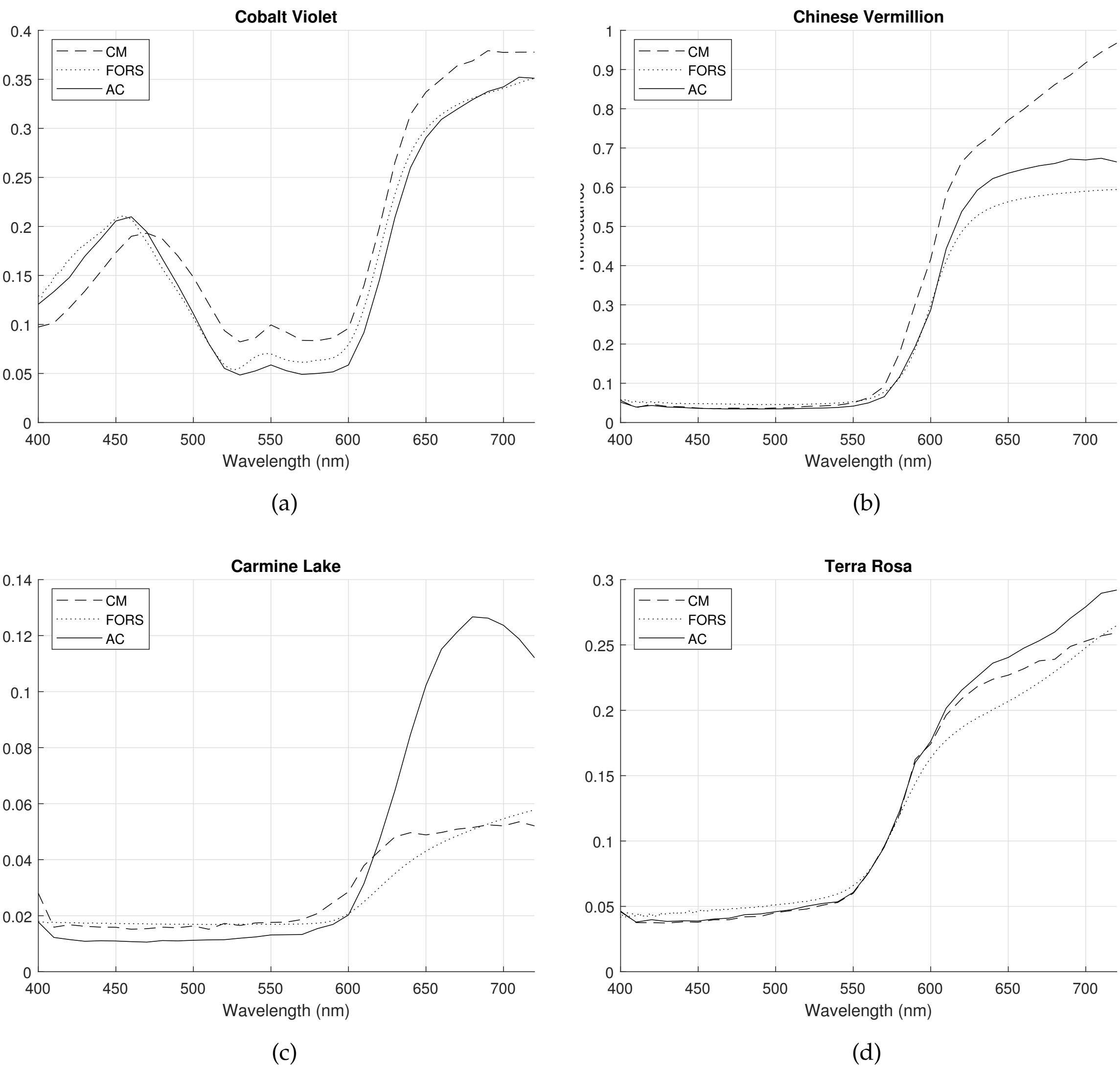

Figure A.2: Pure pigment reflectance database used in [171] (CM), ours (AC) and FORS.

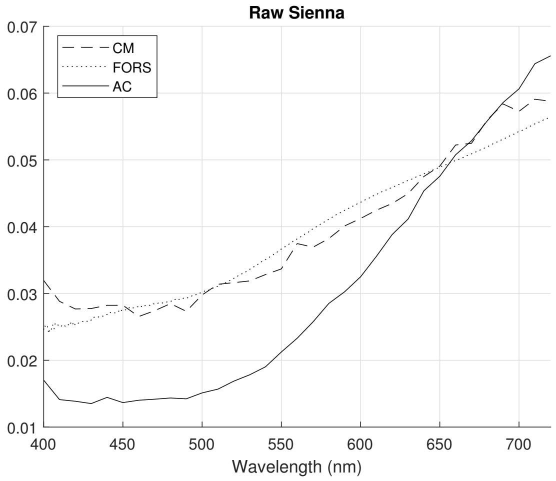

(e)

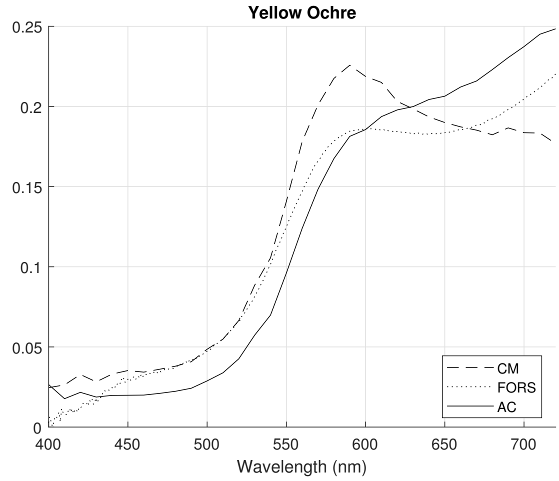

(f)

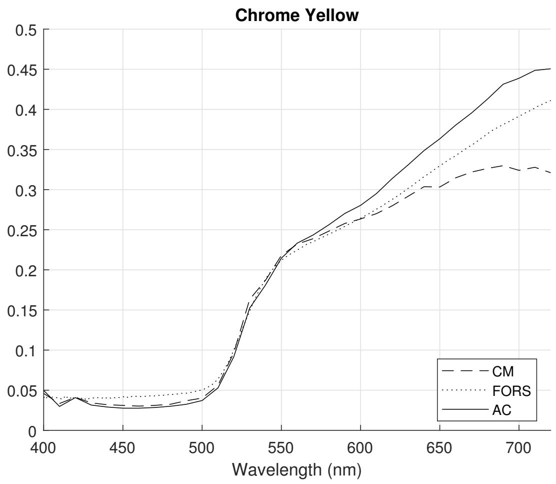

(g)

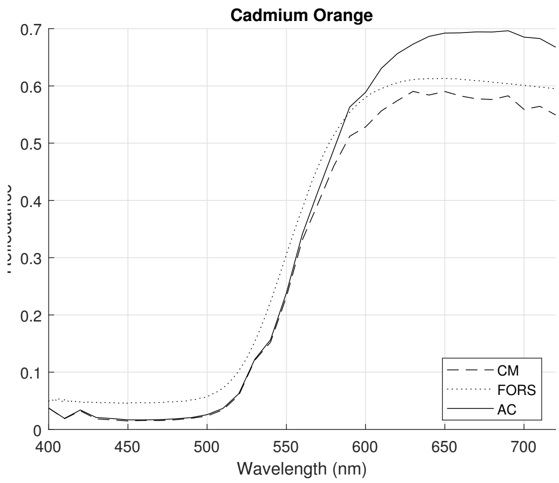

(h)

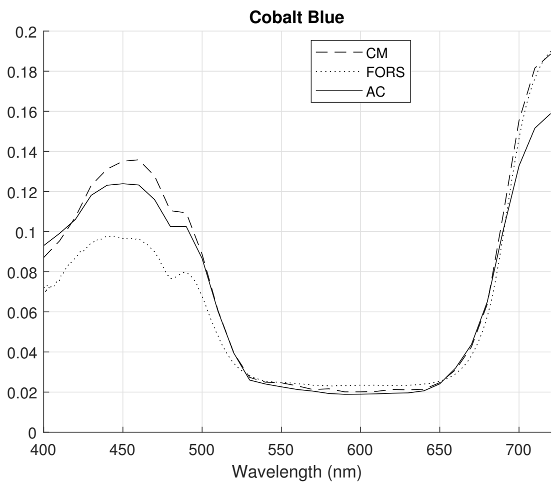

(i)

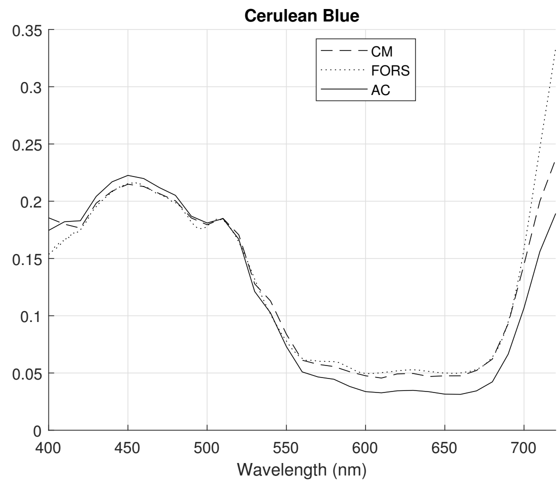

(j)

Figure A.2: Pure pigment reflectance database used in [171] (CM), ours (AC) and FORS.

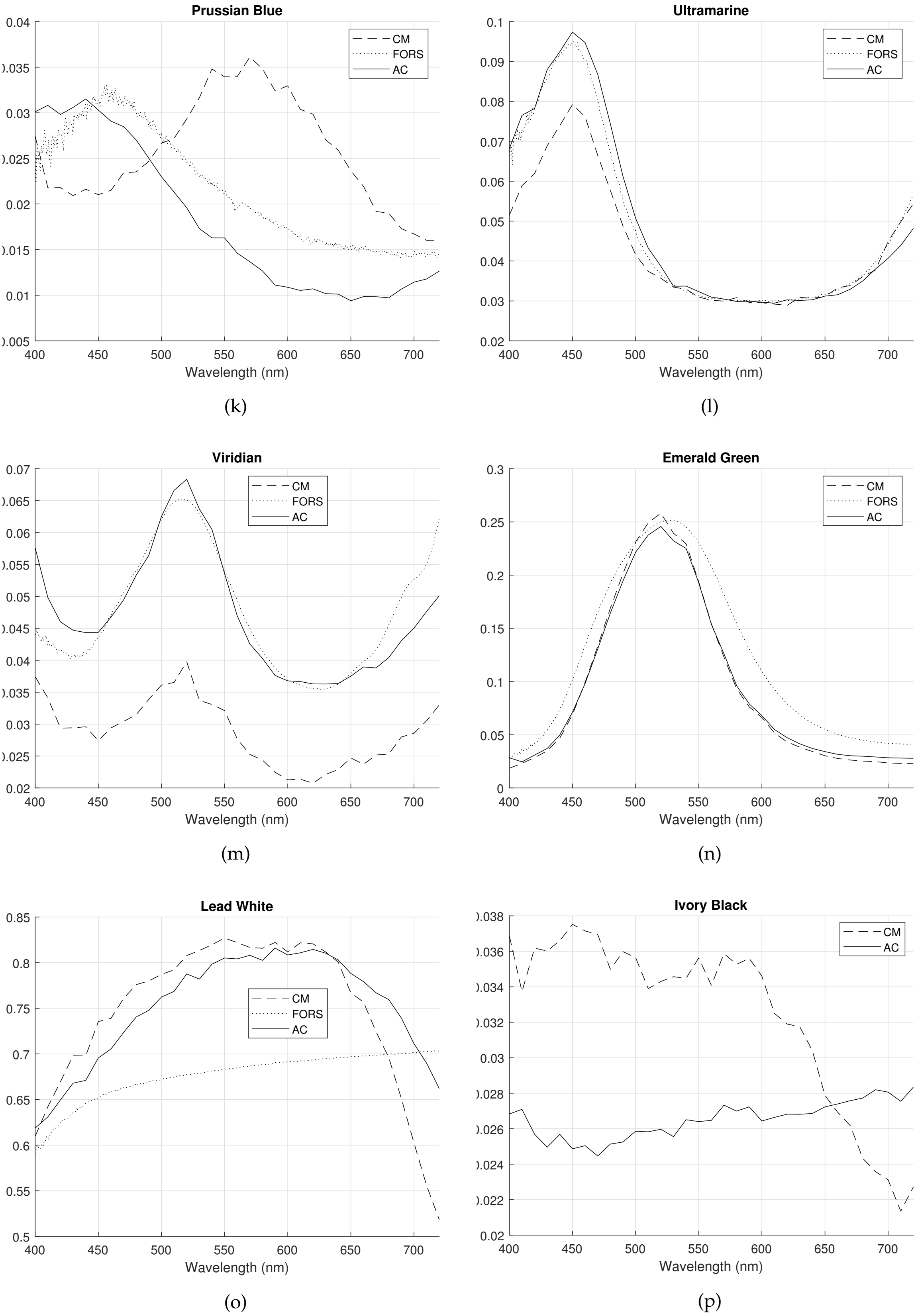

(k) (l)

(m) (n)

(o) (p)

Figure A.2: Pure pigment reflectance database used in [171] (CM), ours (AC) and FORS.

B

Appendix 2 Image Database

B.1 sRGB Image Database

This section contains the list of sRGB images used for training and testing. The images and training/testing list were provided by [171]. No further images were acquired during this research.

Table B.1: List of training dataset files: positive class.

File Name	File Name	File Name	File Name
Amadeo_P100.jpg	Amadeo_P150.jpg	Amadeo_P192.jpg	Amadeo_P61.jpg
Amadeo_P101.jpg	Amadeo_P151.jpg	Amadeo_P193.jpg	Amadeo_P63.jpg
Amadeo_P104.jpg	Amadeo_P152.jpg	Amadeo_P195.jpg	Amadeo_P66.jpg
Amadeo_P106.jpg	Amadeo_P153.jpg	Amadeo_P196.jpg	Amadeo_P67.jpg
Amadeo_P107.jpg	Amadeo_P155.jpg	Amadeo_P198.jpg	Amadeo_P69.jpg
Amadeo_P114.jpg	Amadeo_P156.jpg	Amadeo_P199.jpg	Amadeo_P70.jpg
Amadeo_P116.jpg	Amadeo_P159.jpg	Amadeo_P1b.jpg	Amadeo_P71.jpg
Amadeo_P117.jpg	Amadeo_P16.jpg	Amadeo_P20.jpg	Amadeo_P72.jpg
Amadeo_P121.jpg	Amadeo_P167.jpg	Amadeo_P26.jpg	Amadeo_P73.jpg
Amadeo_P124.jpg	Amadeo_P168.jpg	Amadeo_P28.jpg	Amadeo_P74.jpg
Amadeo_P125.jpg	Amadeo_P169.jpg	Amadeo_P30.jpg	Amadeo_P75.jpg
Amadeo_P128.jpg	Amadeo_P17.jpg	Amadeo_P32.jpg	Amadeo_P76.jpg
Amadeo_P13.jpg	Amadeo_P171.jpg	Amadeo_P34.jpg	Amadeo_P77.jpg
Amadeo_P131.jpg	Amadeo_P172.jpg	Amadeo_P35.jpg	Amadeo_P78.jpg
Amadeo_P132.jpg	Amadeo_P173.jpg	Amadeo_P36.jpg	Amadeo_P82.jpg
Amadeo_P133.jpg	Amadeo_P175.jpg	Amadeo_P37.jpg	Amadeo_P83.jpg

Continued on next page

Table B.1: List of training dataset files: positive class. (Continued)

File Name	File Name	File Name	File Name
Amadeo_P135.jpg	Amadeo_P177.jpg	Amadeo_P42.jpg	Amadeo_P87.jpg
Amadeo_P137.jpg	Amadeo_P178.jpg	Amadeo_P47.jpg	Amadeo_P88.jpg
Amadeo_P138.jpg	Amadeo_P179.jpg	Amadeo_P48.jpg	Amadeo_P9.jpg
Amadeo_P139.jpg	Amadeo_P18.jpg	Amadeo_P49.jpg	Amadeo_P90.jpg
Amadeo_P140.jpg	Amadeo_P182.jpg	Amadeo_P50.jpg	Amadeo_P91.jpg
Amadeo_P141.jpg	Amadeo_P187.jpg	Amadeo_P51.jpg	Amadeo_P92.jpg
Amadeo_P143.jpg	Amadeo_P188.jpg	Amadeo_P52.jpg	Amadeo_P98.jpg
Amadeo_P146.jpg	Amadeo_P189.jpg	Amadeo_P55.jpg	Amadeo_P99.jpg
Amadeo_P147.jpg	Amadeo_P19.jpg	Amadeo_P57.jpg	
Amadeo_P149.jpg	Amadeo_P190.jpg	Amadeo_P58.jpg	
Amadeo_P15.jpg	Amadeo_P191.jpg	Amadeo_P60.jpg	

Table B.2: List of training dataset files: negative class.

File Name	File Name
AvonJawlenski_cabeca.jpg	MDuchamp_Landscape.jpg
Derain_Paisagem.jpg	Macke_Farbige.jpg
Eloy_04P1268.jpg	Macke_Rotes Haus.jpg
Eloy_83P200.jpg	Modigliani_sem titulo.jpg
Eloy_83P202.jpg	Nalmada_62P260.jpg
Eloy_83P204.jpg	Nalmada_83P1424.jpg
Eloy_83P315.jpg	Nalmada_83P55.jpg
Eloy_83P316.jpg	Nalmada_83P57.jpg
Eloy_83P317.jpg	Nalmada_83P60.jpg
Eloy_83P318.jpg	OFreundlich_Sem titulo.jpg
Eloy_83P81.jpg	ORozanova_boutique.jpg
Eloy_84P80.jpg	ORozanova_homen.jpg
Exter_dinamica.jpg	PPicasso_cabeca.jpg
FLeger_horloge.jpg	RDelaunay_Janela.jpg

Continued on next page

Table B.2: List of training dataset files: negative class. (Continued)

File Name	File Name
FMarc_ImagemcomGadoI.jpg	RDelaunay_SCloud.jpg
FMarc_zinnobergruss.jpg	SDelaunay_marche.jpg
GSeverini_ritmo.jpg	Severini_ballerina.jpg
Gleizes_Homen.jpg	Viana_61P781.jpg
Gleizes_Paisagem.jpg	Viana_69P38.jpg
HCamarasa_interior.jpg	Viana_83P37.jpg
IPuni_Nowoie.jpg	Viana_83P40.jpg
IPuni_lavagem.jpg	Viana_83P41.jpg
JGris_violino.jpg	Viana_83P423.jpg
JMetzinger_barcos.jpg	Viana_83P669.jpg
KMalevich_O Amolador.jpg	Viana_83P782.jpg
KMalevitch_Cow.jpg	Viana_83P787.jpg
KMalevitch_Portait.jpg	Viana_83P788.jpg
LFeininger_corrida.jpg	Viana_99P832.jpg
LPopova_Composicao3.jpg	robert delaunay PE113.jpg
LPopova_Nu Feminino.jpg	sonia delaunay_PE114.jpg

Table B.3: List of testing dataset files: positive class.

File Name	File Name	File Name	File Name
Amadeo_P120.jpg	Amadeo_P110.jpg	Amadeo_P53.jpg	Amadeo_P127.jpg
Amadeo_P123.jpg	Amadeo_P174.jpg	Amadeo_P109.jpg	Amadeo_P144.jpg
Amadeo_P62.jpg	Amadeo_P103.jpg	Amadeo_P118.jpg	Amadeo_P14.jpg
Amadeo_P79.jpg	Amadeo_P108.jpg	Amadeo_P130.jpg	Amadeo_P122.jpg
Amadeo_P105.jpg	Amadeo_P111.jpg	Amadeo_P97.jpg	Amadeo_P95.jpg
Amadeo_P160.jpg	Amadeo_P112.jpg	Amadeo_P10.jpg	Amadeo_P65.jpg
Amadeo_P134.jpg	Amadeo_P157.jpg	Amadeo_P45.jpg	Amadeo_P89.jpg
Amadeo_P145.jpg	Amadeo_P158.jpg	Amadeo_P86.jpg	Amadeo_P102.jpg

Continued on next page

Table B.3: List of testing dataset files: positive class. (Continued)

File Name	File Name	File Name	File Name
Amadeo_P165.jpg	Amadeo_P161.jpg	Amadeo_P94.jpg	Amadeo_P136.jpg
Amadeo_P23.jpg	Amadeo_P176.jpg	Amadeo_P44.jpg	Amadeo_P6.jpg
Amadeo_P29.jpg	Amadeo_P185.jpg	Amadeo_P25.jpg	Amadeo_P113.jpg
Amadeo_P4.jpg	Amadeo_P194.jpg	Amadeo_P2.jpg	Amadeo_P27.jpg
Amadeo_P1a.jpg	Amadeo_P31.jpg	Amadeo_P180.jpg	Amadeo_P96.jpg
Amadeo_P164.jpg	Amadeo_P54.jpg	Amadeo_P56.jpg	Amadeo_P129.jpg
Amadeo_P201.jpg	Amadeo_P80.jpg	Amadeo_P85.jpg	Amadeo_P148.jpg
Amadeo_P33.jpg	Amadeo_P64.jpg	Amadeo_P81.jpg	Amadeo_P166.jpg
Amadeo_P59.jpg	Amadeo_P21.jpg	Amadeo_P38.jpg	Amadeo_P162.jpg
Amadeo_P170.jpg	Amadeo_P43.jpg	Amadeo_P197.jpg	Amadeo_P154.jpg
Amadeo_P5.jpg	Amadeo_P12.jpg	Amadeo_P24.jpg	Amadeo_P183.jpg
Amadeo_P11.jpg	Amadeo_P142.jpg	Amadeo_P46.jpg	Amadeo_P200.jpg
Amadeo_P3.jpg	Amadeo_P8.jpg	Amadeo_P22.jpg	Amadeo_P68.jpg
Amadeo_P39.jpg	Amadeo_P186.jpg	Amadeo_P119.jpg	Amadeo_P93.jpg
Amadeo_P40.jpg	Amadeo_P41.jpg	Amadeo_P184.jpg	Amadeo_P7.jpg
Amadeo_P84.jpg	Amadeo_P163.jpg	Amadeo_P126.jpg	

Table B.4: List of testing dataset files: negative class.

File Name	File Name
AvonJawlenski_cabeca mistica.jpg	Modigliani_Gris.jpg
CP0146.jpg	Modigliani_cariatide2.jpg
CP0158.JPG	NUdaltsova_guitare.jpg
Derain_Pears.jpg	Nalmada_83P56.jpg
Eloy_83P198.jpg	Nalmada_83P58.jpg
Eloy_83P199.jpg	Nalmada_83P59.jpg
Eloy_83P203.jpg	NÂ°19.jpg
Eloy_83P314.jpg	NÂ°20.jpg
Eloy_83P79.jpg	NÂ°21.jpg

Continued on next page

Table B.4: List of testing dataset files: negative class. (Continued)

File Name	**File Name**
FLeger_Factories.jpg	ORozanova_metronome.jpg
FMarc_cow.jpg	RDelaunay PE126 V.jpg
FMarc_foxes.jpg	RDelaunay_Champ de Mars.jpg
FMarc_horses.jpg	RDelaunay_cardiff team.jpg
GMunter_Herbstlich.jpg	SDelaunay_Sem titulo.jpg
GSeverini_centrifuga.jpg	SDelaunay_marchÃ minho.jpg
IPopova_Architectonic.jpg	SDelaunay_prospectus.jpg
JGris_Bottle.jpg	VPestel_Nature.jpg
JMetzinger_Life.jpg	Viana_83P382.jpg
KMalevitch_Headgirl.jpg	Viana_83P39.jpg
KMalevitch_ingles.jpg	Viana_83P783.jpg
LPopova_Composicao1.jpg	Viana_83P784.jpg
LPopova_Composicao2.jpg	Viana_83P785.jpg
MFranz_Animal.jpg	Viana_83P786.jpg
MOrtiz_portrait.jpg	Viana_83P789.jpg
MWerefkin_corpus.jpg	

B.2 Hyperspectral Image Database

The following are the sRGB representations of the hyperspectral images used for testing. The images were acquired and provided by [171]. No further images were acquired during this research.

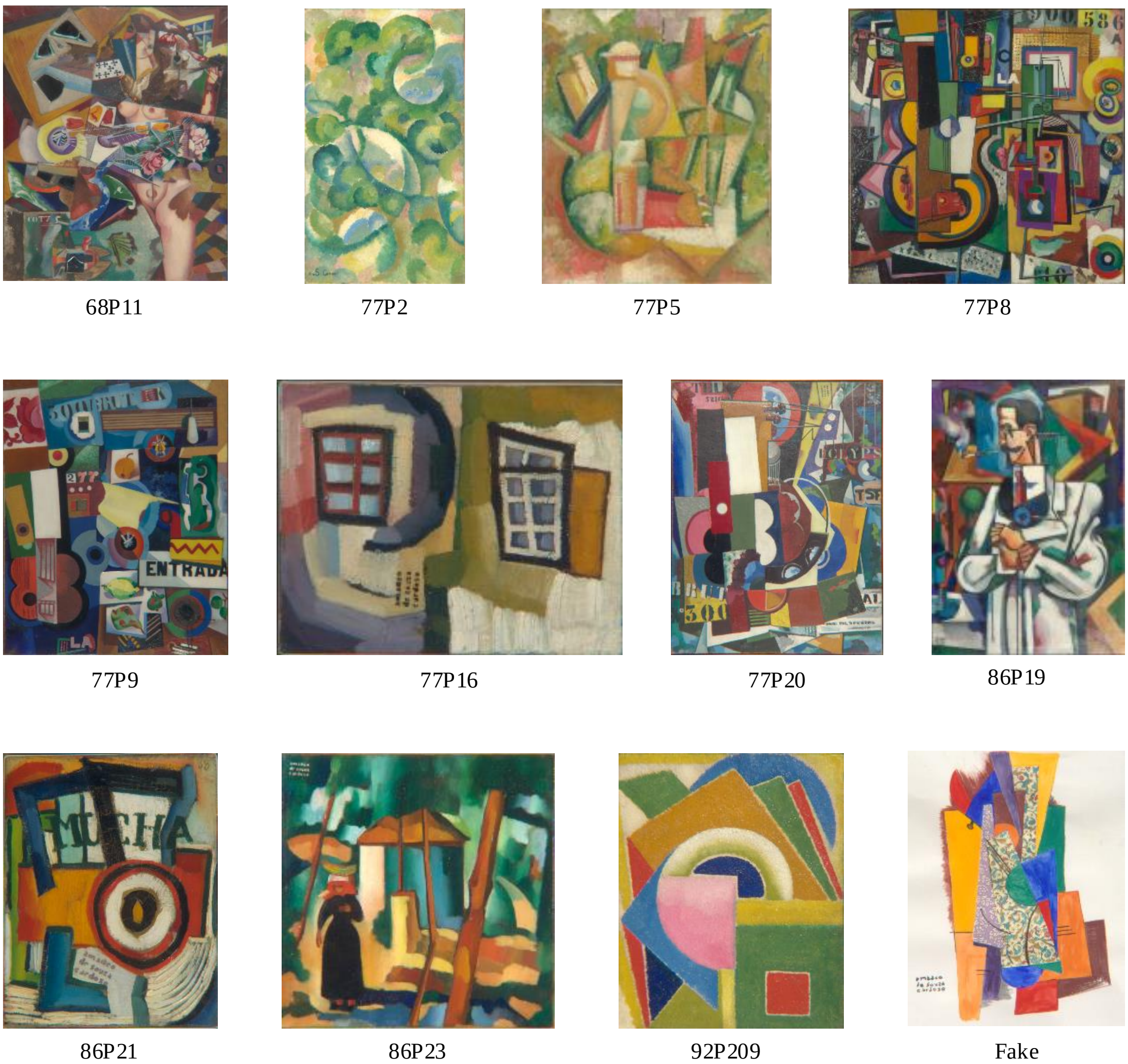

Figure B.1: Hyperspectral test images.

C

Appendix 3 Application Supplementary Data

C.1 Amadeo AR

C.1.1 Questionnaire

This quick questionnaire intends to collect feedback regarding the usability and performance of the Amadeo AR (Augmented Reality) App.

1. Gender
   - Male
   - Female
   - Other
   - Prefer not to say
2. Age
   - Below 15 years old
   - 16-25 years old
   - 26-35 years old
   - 36-45 years old
   - 46-55 years old
   - Over 55 years old
3. Do you know the Portuguese artist Amadeo de Souza-Cardoso or his paintings?
   - Yes
   - No

4. Have you used AR (Augmented Reality) App before? If yes, what App was it? Please specify it.
   - Yes
   - No

After having tried the Amadeo AR App, please answer the following questions:

5. On a scale of 1 (very difficult) to 5 (very easy), how difficult or easy do you find this App?
6. On a scale of 1 (very slow) to 5 (very fast), how fast or slow do you find this App?
7. On a scale of 1 (very unimportant) to 5 (very important), how important is the use of AR (Augmented Reality) Apps like this in a museum?
8. On a scale of 1 (less likely) to 5 (more likely), if an exhibit has an AR (Augmented Reality) App like this, would you be more willing to visit it?
9. On a scale of 1 (very bad) to 5 (very good), what is the overall experience of this AR (Augmented Reality) App?
10. What more would you want to see or add to this App? Do you have any other suggestions?

C.1.2 Questionnaire Results

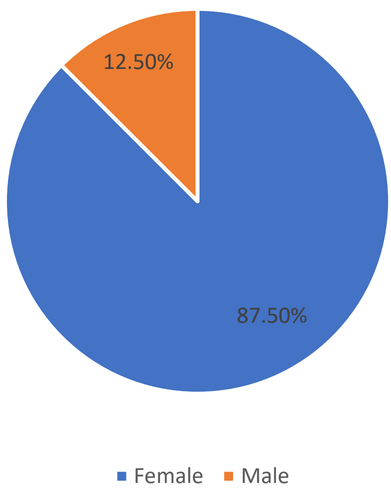

(a) Q1

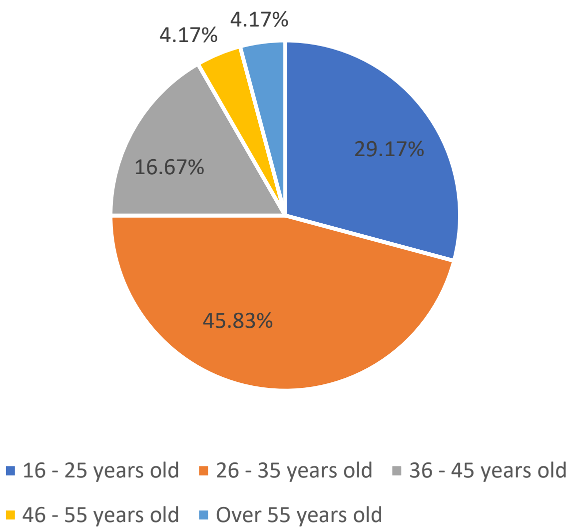

(b) Q2

Figure C.1: Amadeo AR results of questions 1 to 2.

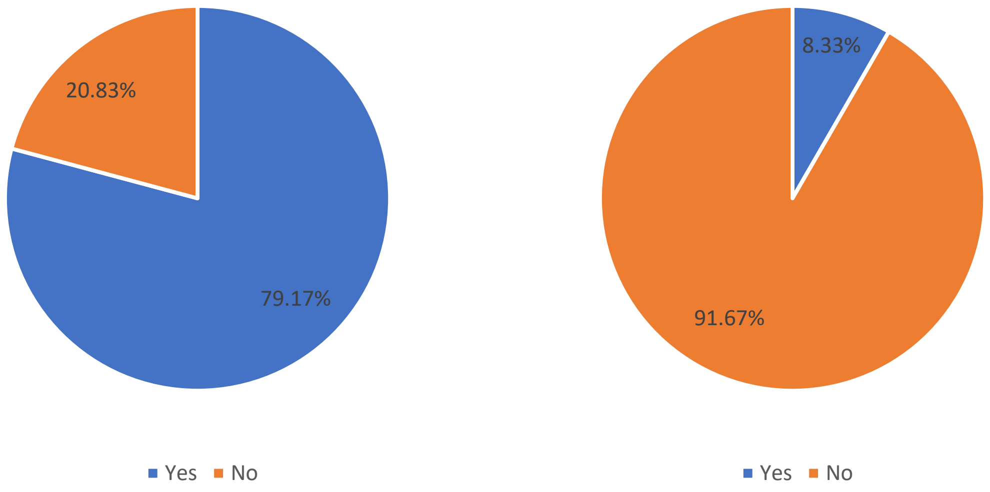

(a) Q3

(b) Q4

Figure C.2: Amadeo AR results of questions 3 to 4.

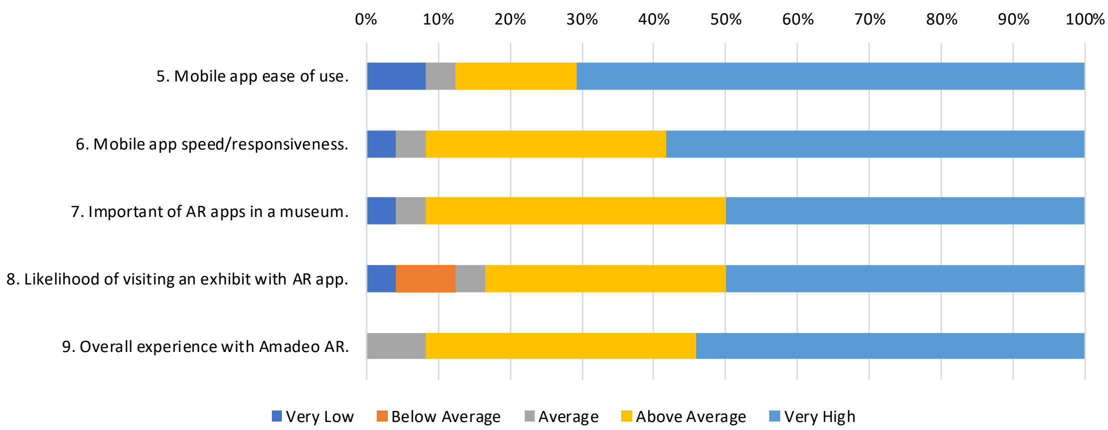

Figure C.3: Amadeo AR results of questions 5 to 9.

Question 10:

- *Maybe some general information on the pigments identified*
- *From the very brief use I've done in the trial I have no specific suggestions to make*
- *Also the binders (if they are different)*
- *I suggest you add the possibility to scroll the list of pure pigments because in some phones the list does not appear complete due to resolution.*
- *I think that it would be interesting to include information about the pigments when choosing a specific color.*
- *Perhaps it would be interesting a short explanation on how you produced this information or the basic knowledge of your PhD, so the public becomes aware of the research behind this app (separate tab perhaps?).*
- *I would do click on a colour and have the pigment dentification*
- *Maybe showing the material*
- *The black pigment is difficult to see. The option of being able to see more than one pigment at a time to understand layers would be very interesting.*
- *The app worked well when I first used it, but when I tried to see other paintings it would only show the pigments from Cerulean Blue downwards (it would not let me see the green pigments, or any other above Cerulean Blue on the list). My phone is a Motorola Moto g(7) play. Otherwise, very easy to use.*
- *development for iOS*

C.2 Amadeo Image Analysis Tool

C.2.1 Questionnaire

This quick questionnaire intends to collect feedback regarding the usability and performance of the Amadeo Desktop Application.

1 Gender

- Male
- Female
- Other
- Prefer not to say

2 Age

- Below 15 years old
- 16-25 years old
- 26-35 years old
- 36-45 years old
- 46-55 years old
- Over 55 years old

3 After having tried the application, for each of the following statements, mark what best describes your reactions to the application.

3.1 I think that I would like to use this application frequently. 1=Strongly disagree, 5=Strongly agree

3.2 I found this application unnecessarily complex. 1=Strongly disagree, 5=Strongly agree

3.3 I thought this application was easy to use. 1=Strongly disagree, 5=Strongly agree

3.4 I think that I would need assistance to be able to use this application. 1=Strongly disagree, 5=Strongly agree

3.5 I found the various functions in this application were well integrated. 1=Strongly disagree, 5=Strongly agree

3.6 I thought there was too much inconsistency in this application. 1=Strongly disagree, 5=Strongly agree

3.7 I would imagine that most people would learn to use this application very quickly. 1=Strongly disagree, 5=Strongly agree

3.8 I found this application very cumbersome/awkward to use. 1=Strongly disagree, 5=Strongly agree

3.9 I felt very confident using this application. 1=Strongly disagree, 5=Strongly agree

3.10 I needed to learn a lot of things before I could get going with this application. 1=Strongly disagree, 5=Strongly agree

4 What more would you want to see or add to this software? Do you have any other suggestions?

C.2.2 Questionnaire Results

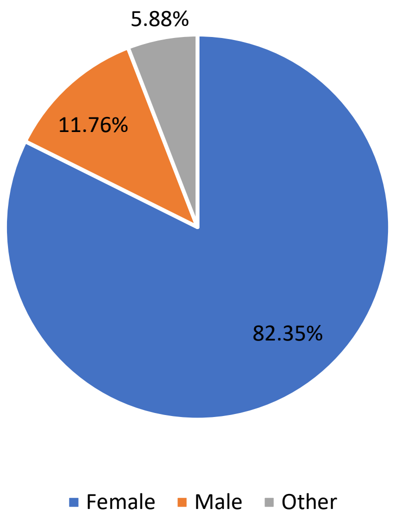

(a) Q1

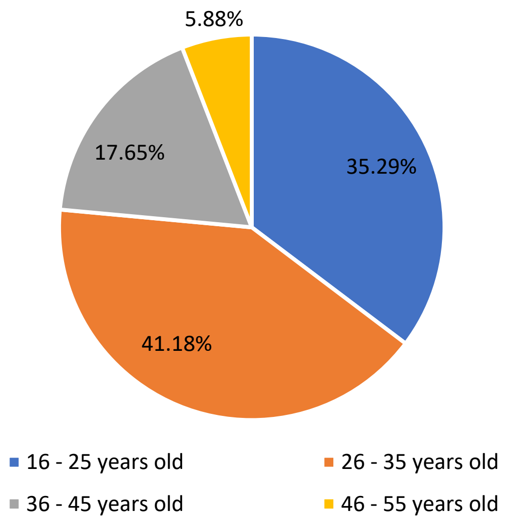

(b) Q2

Figure C.4: Amadeo Image Analysis Tool results of questions 1 to 2.

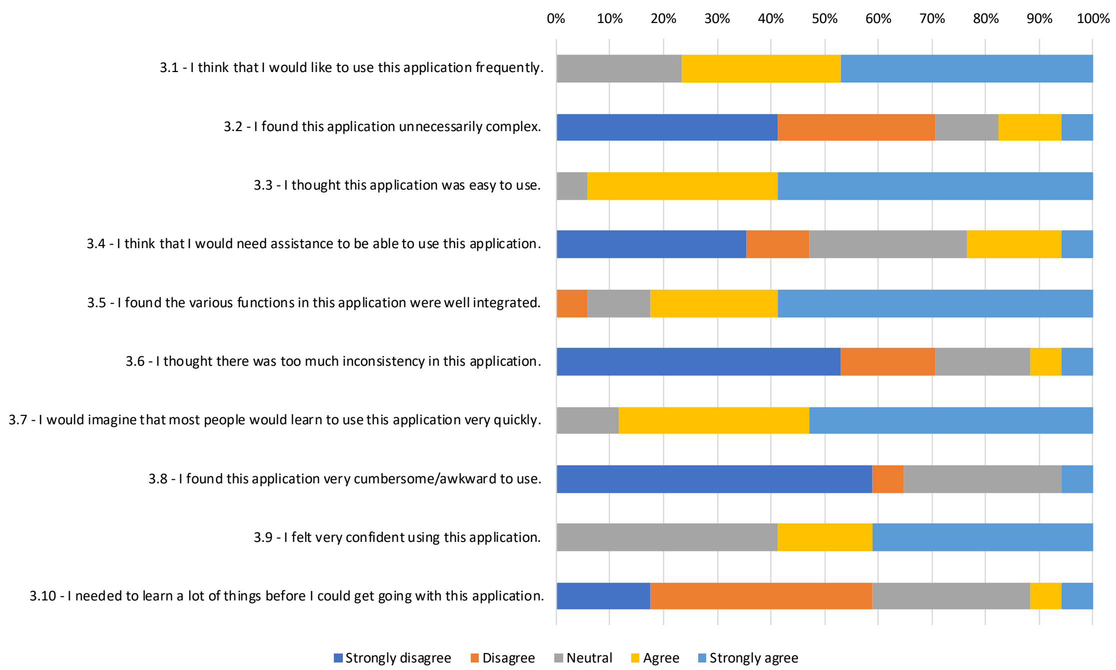

Figure C.5: Amadeo AR results of questions 3.1 to 3.10.

Question 4:

- *I think it could become more intuitive for a first-time user, maybe by adding a tutorial as video or on the side bar or as balloons.*
- *A tutorial for starters would be useful. Information on the creation of this app could also be added as a plus in a separated tab or in the menu (by click, only for users that want to go there read it).*
- *I think it would be interesting to add buttons to stop an action. Regarding the spectrum identification part from the spectral image, it would be interesting to include the color image or the information of the identical color.*
- *Add another analysis like Raman, but it was perfect until now and I'm surprised*

D

Appendix 4 Additional Test Results

D.1 Brushstroke Analysis

The results presented here have been produced using the original brushstroke analysis method in [171] modified to include parallel processing wherever possible. In the interest of making a better comparison with previous results and those listed in [171], the number of images in the training and testing sets has been kept the same for all tests. This is, the training set is composed of 165 images (60 negative, 105 positive) and the testing set is composed of 144 images (49 negative, 95 positive). Similarly, the number of centroids used in the clustering process has been set to match the number of visual words used in [171]; the number of words is 100, 200, 400, 1000, 1200, 1400, 1600 and 2000 where the number of words is effectively composed of the sum of negative and positive centroids. For example, for 100 visual words, 50 negative centroids and 50 positive centroids are used.

For the tests performed, the threshold value used to generate the bag of features has been kept constant. While this is not ideal, this has been done to facilitate a comparison with the published results in [171]. However, for a better understanding of the importance of carefully choosing this parameter some tests have been performed where the value of the threshold is evaluated. Gabor Regular and SIFT+Gabor methods are used to generate results; Gabor Regular as the initial testing point whilst SIFT+Gabor, the method reported to have the best results in [171], as the comparison medium here.

D.1.1 K-Means with Pre-Selected Set of Seeds

This test corresponds to the original method in [171] and the results are shown in Figure D.1. Including the testing images in the clustering process affects the output significantly as it pulls the centroids to a position closer to the features of the testing data hence biasing the results of the classifier. Using this approach is therefore not recommended.

D.1.2 K-Means with Random Seeds

This test aims at showing the importance of selecting the correct initial centroids (seeds) when using KM. This is because incorrect resulting centroids can have a significant effect on

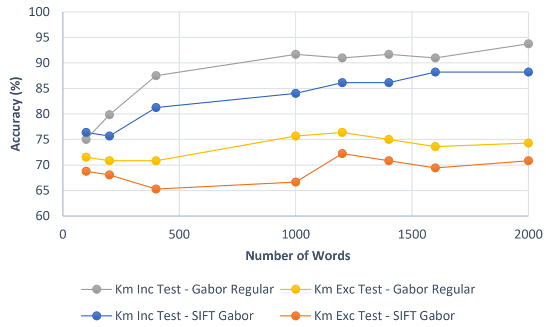

Figure D.1: KM with pre-selected set of seeds [171].

the overall results. The results in Figure D.2, Figure D.3, Figure D.4 and Figure D.5 indeed show a general trend confirming that this algorithm tends to generate better accuracy with a higher number of words when the testing data are included. However, when the testing data are excluded from the clustering process the improvement is minimal.

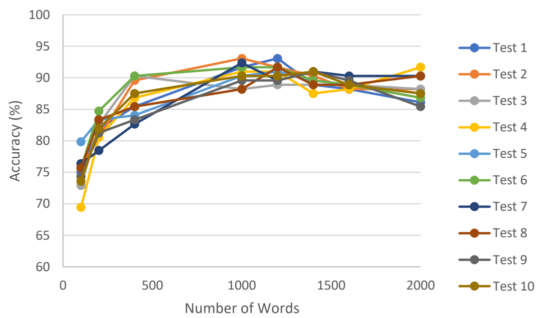

Figure D.2: KM with random seeds with testing data included in clustering – Gabor Regular.

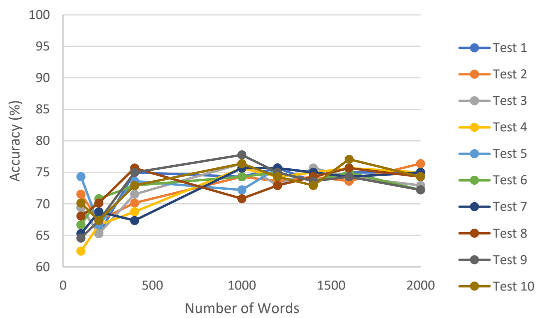

Figure D.3: KM with random seeds with testing data excluded from clustering – Gabor Regular.

D.1.3 K-Means++

As shown with KM and random seeds, it is important to choose carefully the initial centroids. Therefore KM++ has been evaluated as a better alternative to KM as this algorithm uses a better initial selection of centroids. In addition to that, KM++ was found to be around 150% faster than standard KM. The results with KM++ shown in Figure

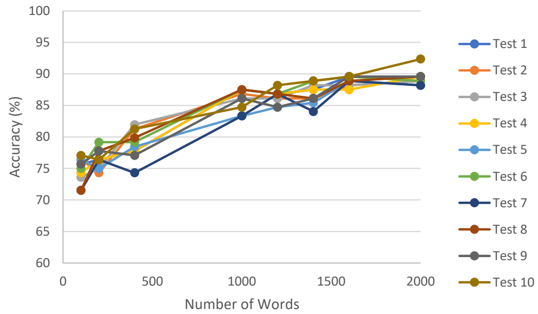

Figure D.4: KM with random seeds with testing data included in clustering - SIFT+Gabor.

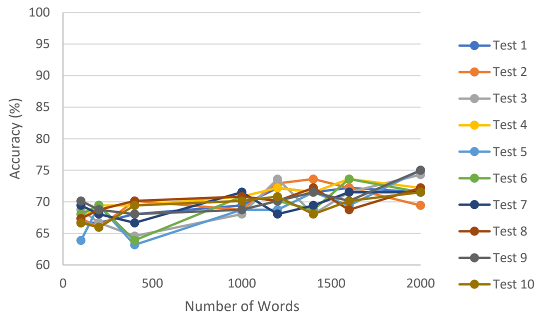

Figure D.5: KM with random seeds with testing data excluded from clustering - SIFT+Gabor.

D.6, Figure D.7, Figure D.8 and Figure D.9 exhibit the same trend as those obtained with standard KM.

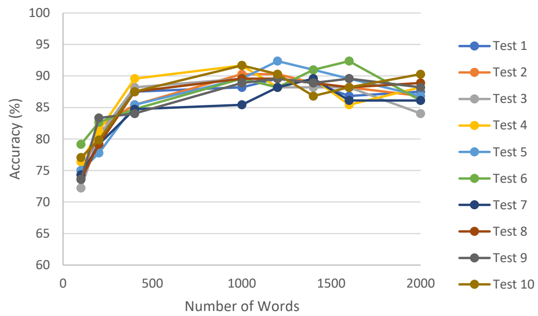

Figure D.6: KM++ with testing data included in clustering – Gabor Regular.

D.1.4 K-Means vs K-Means++

When comparing the results of KM vs KM++, as shown in Figure D.10 and Figure D.11, the standard deviation of KM++ seemed lower than that of KM suggesting an increased confidence factor on the results produced by KM++.

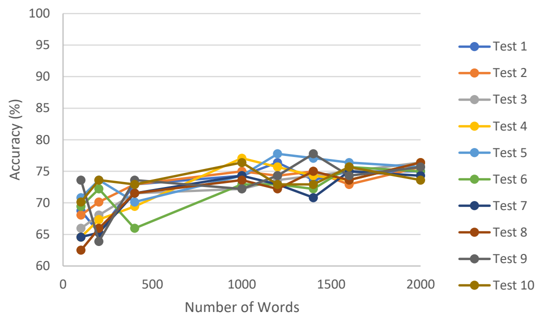

Figure D.7: KM++ with testing data excluded from clustering – Gabor Regular.

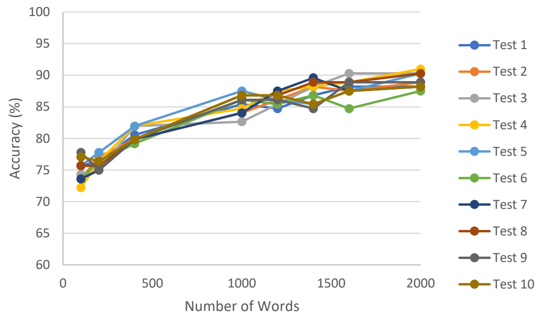

Figure D.8: KM++ with testing data included in clustering – SIFT+Gabor.

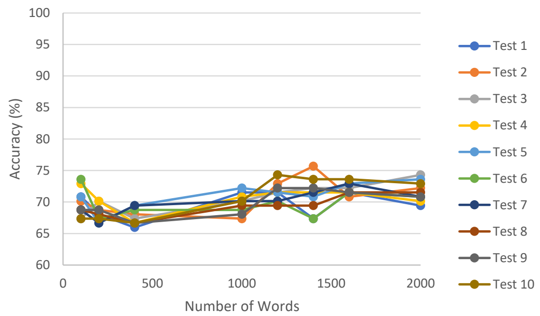

Figure D.9: KM++ with testing data excluded from clustering – SIFT+Gabor.

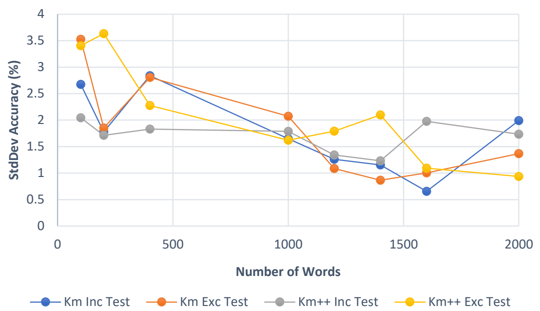

Figure D.10: Standard Deviation KM vs KM++ – Gabor Regular.

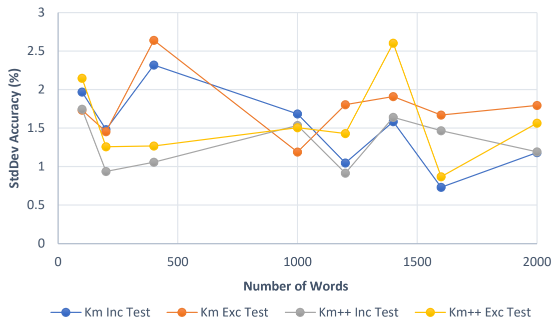

Figure D.11: Standard Deviation KM vs KM++ – SIFT+Gabor.

D.1.5 Random Training and Test Data

This test was performed to evaluate the effect of selecting the right data for the training and testing datasets. To help compare the results of this test with previous results, the number of elements in the training and testing datasets was kept constant, i.e., training set of 165 images (60 negative, 105 positive) and testing set of 144 images (49 negative, 95 positive). The images of each set were selected using a random permutation function to avoid duplicates. Both algorithms KM and KM++ were evaluated with results shown in Figure D.12, Figure D.13 and Figure D.14. For both algorithms, the results show a wide accuracy spread in excess of 13% depending on the datasets. This strongly indicates the importance of ensuring the right training set is selected. The criteria to select the best images is yet to be specified but it could be based on results from the algorithm or the use of the "most representative" samples based on human observations. From the results to date, it is understood that the former method can guarantee better results for the existing testing data but the performance of both methods on new samples is yet to be investigated. Additionally, the results tend not to differ significantly applying pre-selected seeds and random seeds with KM.

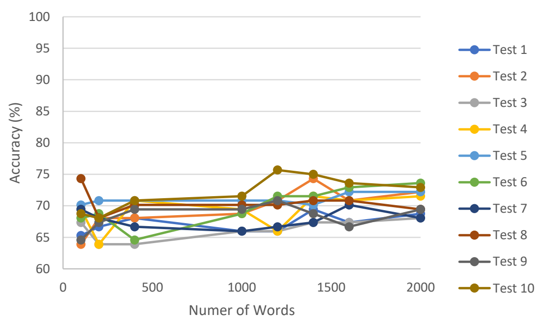

Figure D.12: KM with pre-selected seeds, random training/testing data, and testing data excluded from clustering – SIFT+Gabor.

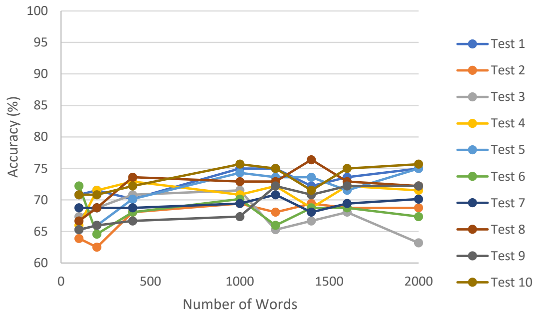

Figure D.13: KM with random seeds, random training/testing data, and testing data excluded from clustering – SIFT+Gabor.

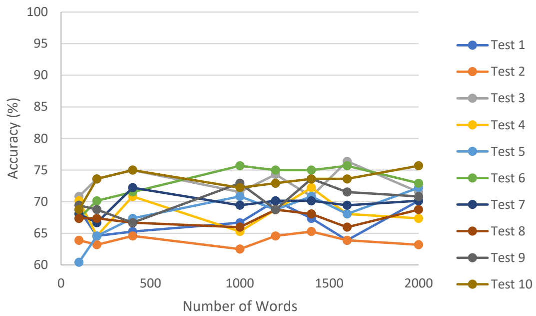

Figure D.14: KM++ with random training/testing data, and testing data excluded from clustering – SIFT+Gabor.

D.1.6 Best Centroids

An attempt was made to select the best centroids obtained by each method KM and KM++. This was based on executing each one up to ten times and removing outliers, i.e., centroids whose distance to others was greater than 2 times the scaled median absolute deviation away from the median. The coordinates of the remaining centroids were then averaged to generate an "average" centroid. This method did not produce better results. In fact, this method did not enhance the location of the centroids but instead, moved the centroids to a location that generated a "constant", average-like accuracy regardless of the number of centroids. The results of this are shown in Figure D.15 for Gabor Regular only. Note that this method was initially tested using Gabor Regular. Based on the results obtained which did not show any improvement and based on the long computation time of SIFT+Gabor (more than 7 days per 10 runs) it was decided not to perform this operation on the SIFT+Gabor algorithm.

D.1.7 Bag of Features Thresholding

The following tests intend to establish the effect on overall accuracy that different thresholds have when generating the bag of features (Figure D.16). It is noted previously that the trend of the results generated from KM appear to be similar applying either pre-selected seeds in the original method or random seeds. Subsequently, the comparison is made

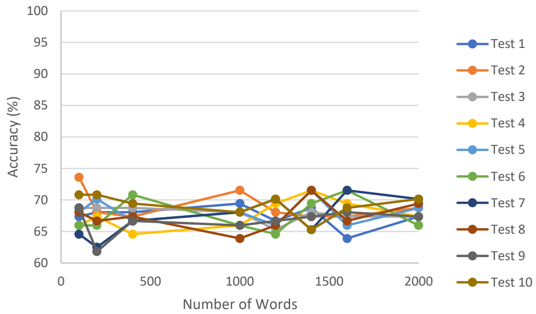

Figure D.15: KM++ with random seed with testing data excluded from clustering intending to select the best centroid – Gabor Regular.

mainly based on the results produced by applying KM with a pre-selected set of seeds. Figures generated implementing KM as well as KM++ with random training and testing image data are shown in Figure D.17, Figure D.18 and Figure D.19 for reference.

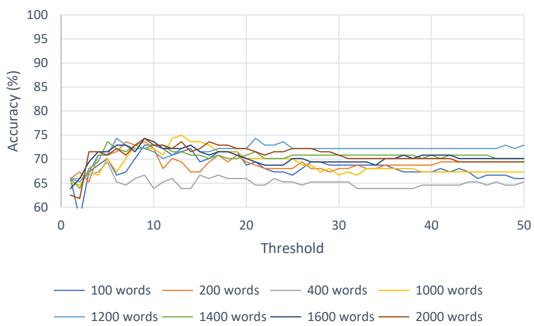

Figure D.16: SIFT-Gabor using original KM centroids excluding testing data. Threshold tested from 1 to 50 in increments of 1.

As stated earlier, when the testing data are included in the clustering there is a tendency for the accuracy to increase as the number of words increases for both Gabor Regular and SIFT+Gabor methods. Interestingly, when the threshold value is greater than 10, the accuracy tends to remain more or less stable. The accuracy of Gabor Regular reported earlier also appears to be higher than its counterpart of SIFT+Gabor when the threshold is increased. This highlights the importance of choosing the threshold for the bag of features correctly. When the testing data are excluded from the clustering, the accuracy seems to be the highest when the number of words is 1200 instead of 2000. However, this inclination will again diverge when other algorithms (KM or KM++ with or without random training/testing images) are applied which are shown in the following figures.

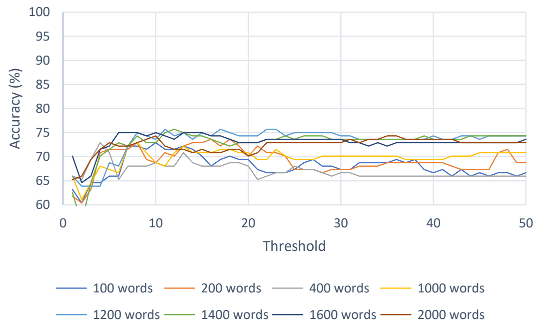

Figure D.17: SIFT+Gabor using KM++ centroids including testing data. Threshold tested from 1 to 50 in increments of 1.

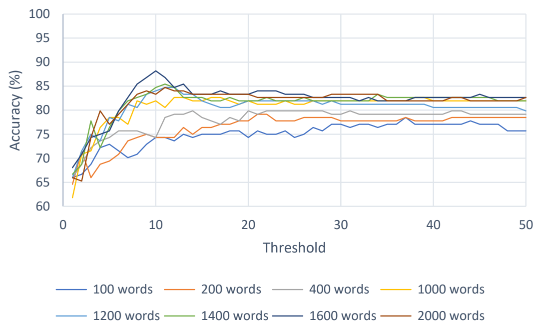

Figure D.18: SIFT+Gabor using KM centroids excluding testing data with random images. Threshold tested from 1 to 50 in increments of 1.

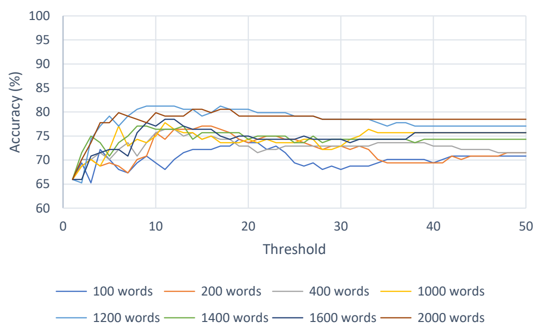

Figure D.19: SIFT+Gabor using KM++ centroids excluding testing data with random images. Threshold tested from 1 to 50 in increments of 1.

D.2 Pigment Analysis

D.2.1 Black and White Identification

For this test, the objective was to identify the black and white pixels of a painting. This effectively requires identifying three classes: black, white or colour. To achieve this, a simple neural network consisting of an input layer with 33 elements corresponding to a pixel reflectance, a hidden layer of 1 neuron and a single output. The training set consisted of the following:

- 30000 samples of augmented white reflectance labelled as 1
- 30000 samples of augmented black reflectance labelled as 0
- 30030 artificial mixtures generated with 15 pigments in the reference database selected by [171] in steps of 10% all labelled as 0.5

The neural network was trained to produce a numerical prediction based on the reflectances provided and a threshold was applied to the output to classify the prediction as black (prediction < 0.1), white (prediction > 0.9) or colour otherwise.

The result of the classification is shown in Table D.1 where the values obtained with the method in [171] are shown for comparison. Figure D.20 highlights the classified pixels where a good similarity is found between the neural network approach and the original method. This result shows that neural networks could be a potential candidate for pixel classification.

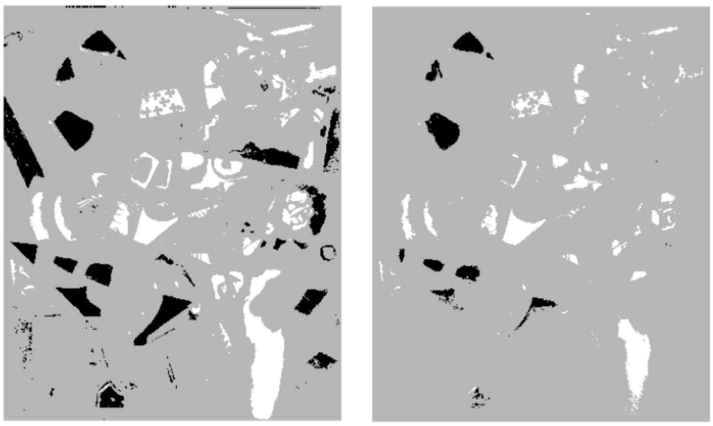

(a) (b)

Figure D.20: Results of black/white/colour identification using (a) the original method and (b) a neural network.

Table D.1: Comparison of results from NN for black/white/colour identification.

Method	White Area	Black Area	Colour Area
Neural Network	3.68%	1.68%	94.64%
Method in [171]	7.59%	6.78%	85.63%

D.2.2 Pure Pigment Identification Using Decision Trees

Another ML evaluated for pure pigment identification is decision trees. Four different trees were evaluated: fine, medium and coarse. As opposed to the neural network in the previous section, the trees were trained and tested with reflectance of pixels of image 68P11 classified with the method of [171]. The training set, therefore, consisted of pure pigments whose label corresponds to the index in the reference pigment database and all other mixed/negative pixels labelled as class 0. The evaluation was performed using k-fold and the results are summarised in Table D.2.

Table D.2: Results of pure pigment identification using decision trees.

Tree Topology	Accuracy
Fine	96.5%
Medium	95.2%
Coarse	98.8%

Although the results obtained seemed to show a high accuracy, the training and testing data are highly imbalanced and therefore the accuracy is driven by the correct classification of mixed pigments rather than pure pigments as shown in the confusion matrix of the fine tree shown in Figure D.21; the grey diagonal represents the accurate classifications. The high accuracy is driven by the correct classification of non-pure pixels (class 0).

True Class \ Predicted Class	0	3	5	6	7	8	9	15
0	275311	5	174	267	1115	233	1493	212
3	1979							
5	341		909					
6	1184			418	1			
7	2297				18138			
8	622					1862		
9	959						5059	
15	190							331

Figure D.21: Confusion matrix for a fine tree classifier with 15 outputs (pure pigments) and non-pure pigments (class 0).

D.2.3 Pure Pigment Identification Using Support Vector Machine Classifiers

A fine Gaussian SVM classifier was designed to identify 18 classes: any of the 17 pure pigments (including black and white) in the reference pigment database or a non-pure colour. For this particular test, the use of true data in the training process was evaluated. To achieve this, the pixels of all 11 images available were classified using the improved method proposed in [171] using RMSE and raw reflectance values. The results of the classification showed that the number of pure pigment pixels is highly imbalanced with some pigments not present in any of the images analysed regardless of the method used. For example, the total number of pixels per pigment in all 11 painting images are: Black - 166014; White Pb - 163165; Emerald - 23909; Ultramarine - 0; Viridian - 0; Green Cd - 0; Prussian B. - 0; Cobalt B. - 5614; Cerulean B. - 47170; Violet Cd - 5732; Yellow Cr - 83046; Y. Ochre - 4576; Orange Cd - 11624; T. Rossa - 0; R. Sienna - 2875; Carmine - 0; Vermilion - 43. To overcome this problem the following approach was used:

- Set the number of samples to 3000 (average number of reflectances per pure pigment found)
- If the number of pure reflectances is less than 3000, balance the number using data augmentation
- If the number of pure reflectances is greater than 3000, randomly select 3000
- Randomly select 3000 samples from the non-pure reflectances

A total of 54000 samples were compiled. For the calculation of the confusion matrix, the number of folds was set to 5. The confusion matrix is shown in Figure D.22. The results show that the fine Gaussian SVM classifier accurately distinguishes pure from non-pure pigments.

The selected SVM classifier was evaluated using the data from painting 68P11. This is, the reflectance of each pixel was fed into the classifier to predict whether the reflectance belonged to one of the 17 pure pigments or to a non-pure pigment. To reduce computation time the hyperspectral images were downsized to ensure the maximum number of total reflectances per painting did not exceed 130000. To enhance the visualisation of the results, the non-pure pixels were coloured with grey to allow white and black to be identified (Figure D.23). For a true comparison, the images were also re-analysed using the original method but downsized to match the size of the images tested with the classifier.

The results of the processing show a good correlation of pigments identified by the SVM suggesting that this SVM model generated is adequate for the identification of pure pixels including black and white.

True Class \ Predicted Class	0	1	2	3	4	5	6	7	8	9	10	11	12	13	14	15	16	17
0	2719	21		4	10	37	15	68	20	36	26					17	22	5
1		3000																
2			2983															17
3	134			2824														42
4	213				2787													
5	59	168				2772											1	
6	205	3					2792											
7	200	2						2798										
8	77	8							2915									
9	50	12								2938								
10	116										2884							
11												2872						128
12		1											2999					
13														2640				360
14															2884			116
15	172	3														2825		
16	5	37											6				2952	
17	47	2		16											1			2934

Figure D.22: Confusion matrix for SVM classifier. Accuracy 95.40%.

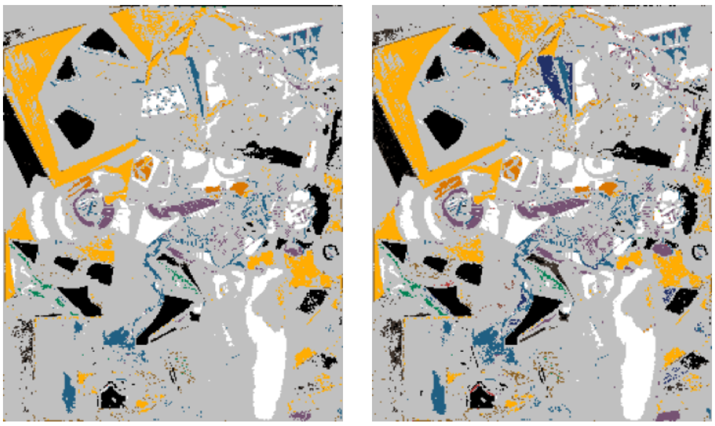

(a) (b)

Figure D.23: Comparison of pure pigments identified in 68P11 with (a) original improved method and (b) SVM classifier.

2022 Authentication of Amadeo de Souza-Cardoso Paintings and Drawings With Deep Learning Ailin Chen